UNIVERSITY OF SOUTHAMPTON

FACULTY OF PHYSICAL SCIENCES AND ENGINEERING

DEPARTMENT OF ELECTRONICS AND COMPUTER SCIENCE

Classification and Localisation of Multiple Partial Discharge Sources within High Voltage Transformer Windings

by

Nik Hakimi Bin Nik Ali

Thesis for the degree of Doctor of Philosophy

July 2017

ABSTRACT

UNIVERSITY OF SOUTHAMPTON

FACULTY OF PHYSICAL SCIENCES AND ENGINEERING

DEPARTMENT OF ELECTRONICS AND COMPUTER SCIENCE

Doctor of Philosophy

by Nik Hakimi Bin Nik Ali

Partial discharge (PD) analysis is a common method for condition monitoring and diagnostics of power transformers, which can be used as a tool for assessing the lifespan of transformers and can detect insulation malfunctions before they lead to failure. This report describes the development of analytical tools for PD activities within HV transformer windings. In most cases, PD will occur in transformer windings due to ageing processes, operational over stressing or defects introduced during manufacture, and different PD sources have different effects on the condition and performance of power equipment insulation system. Therefore, for further analyses, the ability to accurately distinguish between the PD signals generated from different sources is seen as a critical function for future diagnostic systems. Under realistic field conditions, multiple PD sources may be activated simultaneously within the transformer winding. An experiment has been designed to assess different methodologies for the identification and localisation of multiple PD sources within a HV transformer winding. Previous work at Southampton developed a non-linear based technique that facilitates identification of the location of a single PD source within an interleaved winding. It is assumed that any discharge occurring at any point along a winding will produce an electrical signal that will propagate as a travelling wave towards both ends of the winding. This project is concerned with the feasibility of locating several sources simultaneously based only on measurement data from wideband radio frequency current transformers (RFCTs) placed at the neutral to earth point and the bushing tap-point to earth. The proposed processing technique relies on the assumption that the PD pulses generated from different sources exhibit unique waveform characteristics. Due to termination and path taken characteristics, the PD signals will suffer attenuation and distortion during the

propagation of the PD signals along transformer windings. Therefore, it will cause changes in the energy characteristics of the PD pulses at both measurement points, which can be used to separate, identify and locate the multiple PDs within an HV transformer winding. Based on analysis of the captured data from experiment, various approaches for identifying multiple PD sources have been assessed. Obtained results indicate that the analysis of absolute energy distributions determined using Mathematical Morphology and the use of OPTICS for clustering will reliably separate PD data from two sources that are simultaneously active within a distributed winding.

Contents

DECLARATION OF AUTHORSHIP

I, N. H. Nik Ali, declare that the thesis entitled *Classification and Localisation of Multiple Partial Discharge Sources within High Voltage Transformer Windings* and the work presented in the thesis are both my own, and have been generated by me as the result of my own original research. I confirm that:

- this work was done wholly or mainly while in candidature for a research degree at this University;
- any part of this thesis has previously been submitted for a degree or any other at this University or any other institution, this has been clearly stated;
- where I have consulted the published work of others, this is always clearly attributed;
- where I have quoted from the work of others, the source is always given. With the exception of such quotations, this thesis is entirely my own work;
- I have acknowledged all main sources of help;
- where the thesis is based on work done by myself jointly with others, I have made clear exactly what was done by others and what I have contributed myself;
- parts of this work have been published as:

Refereed Conference papers;

- Nik Ali, N. H., J. Hunter, P. Rapisarda and P. Lewin, "Identification of multiple partial discharge sources in high voltage transformer windings," in IEEE Conference on Electrical Insulation and Dielectric Phenomena (CEIDP), 2014, Des Moines, IA, 19-22 Oct. 2014.
- Nik Ali, N. H., Abd Rahman, M.S.; J. Hunter, P. Rapisarda and P. Lewin, "Wavelet and Mathematical Morphology as the De-Noising Methods for PD Analysis of High Voltage Transformer Windings," in IEEE Electrical Insulation Conference (EIC), 2015, Seattle, Washington, 7-10 June 2015

- Nik Ali, N. H.; W. H. Goldsmith, J. Hunter, P. Rapisarda and P. Lewin, "Comparison of Clustering Techniques of Multiple Partial Discharge Sources in High Voltage Transformer Windings" in IEEE 11th International Conference on the Properties and Applications of Dielectric Materials (ICPADM), 2015, Sydney, Australia, 19-22 July 2015
- Nik Ali, N. H., Michalis Giannakou, R D Nimmo, P. Rapisarda and P. Lewin, "Classification and Localisation of Multiple Partial Discharge Sources Within a High Voltage Transformer Winding," in IEEE Electrical Insulation Conference (EIC), 2016, Montreal, QC, Canada, 19 - 22 June 2016.
- Nik Ali, N. H., P. Rapisarda and P. Lewin, " Separation of Multiple Partial Discharge Sources Within a High Voltage Transformer Winding using Time Frequency Sparsity Roughness Mapping," in IEEE Condition Monitoring and Diagnosis (CMD), 2016, Xi'an, China, 25 - 28 September 2016.
- Nik Ali, N. H., P. Rapisarda and P. Lewin, " Multiple Partial Discharge Sources Discrimination In A High Voltage Transformer Winding" in 13th International Electrical Insulation Conference (INSUCON), 2017, Birmingham, United Kingdom, 16 – 18 May 2017.

Journal Papers;

- Nik Ali, N. H., P. Rapisarda and P. Lewin, "Identification and Localisation of Multiple Partial Discharge Sources within High Voltage Transformer Windings", submitted to IEEE Transactions on Dielectrics and Electrical Insulation.
- Nik Ali, N. H., P. Rapisarda and P. Lewin, "Comparison of Multiple Partial Discharge Clustering Techniques within High Voltage Transformer Windings", in preparation for submission to IEEE Transactions on Dielectrics and Electrical Insulation.

Signed: .....

Date: .....

NOMENCLATURE

cA	Approximation coefficients
cD	Detail coefficients
C_m	Covariance matrix
d	Separation distance
D(x,y,z)	Distance in x, y and z axes
E_{abs_B}	Energy for bushing tap point to earth
E_{abs_N}	Energy for neutral tap to earth point
E_A	Approximation energy
E_D	Details energy
ε	Radius of points of data
I_s	Input signal
ø	Phase angle
ø-q-n	Phi-q-n
p_n	A certain point of data
q	charge
λ	Eigenvalues
υ	eigenvectors
φ	Scaling function
ψ	Wavelet function

ABBREVIATIONS

CAD	Computer aided design
CBM	Condition based maintenance
CD	Core distance
CWT	Continuous Wavelet transforms
DBSCAN	Density-based spatial clustering of applications with noise
DDF	Dielectric dissipation factor
DDR	Directly density reachable
DGA	Dissolve gas analysis
DR	Density reachable
DWT	Discrete Wavelet transform
EMI	Electromagnetic interference
FFT	Fast Fourier Transform
FSVM	Fuzzy support vector machine
HPF	High pass filter
HV	High voltage
IEC	International Electro-technical Commision
KNN	K-nearest neighbour
KPCA	Kernel principle component analysis
LPF	Low pass filter
MLP	Multi-layer perceptron
MM	Mathematical morphology
MTLM	Multi conductor transmission line model
OPTICS	Ordering points to identify clustering structure
PCA	Principle component analysis
PD	Partial discharge
PDE	Partial differential equation
PRPD	Phase resolved partial discharge
PSD	Power spectral density
RBF	Radial basis function
RD	Reachability distance

RFCT	Radio frequency current transducer
SE	Structure elements
TF	Time frequency
t-SNE	t-Distributed stochastic neighbour embedding
UHF	Ultra high frequency

ACKNOWLEDGEMENTS

First and foremost, I would like to thank to Allah for giving me health and blessing in completing this report. Without HIS blessing, I would never manage to complete this report.

Secondly, I would also like to express my deepest gratitude and appreciation to my first supervisor, Professor Paul Leonard Lewin, for his attention, professional guidance and assistance, continues comments, support, valuable advices and friendship throughout preparing this report, which I consider all that as something beyond repayment. Thank you for believing in me and molding me into a better person with your continuous guidance in every single day. I really appreciate the time he had spent in order to guide me towards the goal. My thanks also goes to his wife Mrs Nicki Lewin for her indirect support given during my study. Not to forget Professor Paolo Rapisarda as my second supervisor for his guidance, valuable suggestions and encouragement that have substantially helped in my work.

To my respected parents, Mr. Nik Ali Bin Tuan Kadir and Mrs. Rokhiah Binti Abdul Rahman and my lovely wife, Nurul Wahida Binti Mohamad, thank you for their continuous prayers and support for me in whatever I do especially for my studies. Without the prayers from both of you, I would never get this far in my life. To all my sisters, Nik Arlina Binti Nik Ali and Nik Azlida Binti Nik Ali, thanks for caring and loving me so much.

My special thanks to Dr. Jack A. Hunter, Dr. Safwan Abd Rahman, Dr. Hidayat Zainuddin and Dr. Demetres Evagorou for the helps, supports, and motivations that they gave me throughout the process of completing this report. It really means a lot to me and unforgettable. I would also like to express my sincere gratitude to the University of Southampton, Tony Davies High Voltage Laboratory and its members especially Neil L Palmer, Liz Tillotson, Michael A J Smith, Brian Rogers, Ernest Asiedu, Michael Hickey and Ian Virtanen and to those who are involved directly and indirectly in completing this report. They are highly appreciated and forever will be honoured.

To my parents, my dearest wife, Nurul Wahida, my two little daughters, Nik Fatimah Az Zahra' and Nik Maream Yusayrah, family, colleagues and friends

CHAPTER 1

INTRODUCTION

A power transmission system consists of many assets that are very expensive and their reliabilities are important for the industrial, commercial and residential sectors. High voltage power transformers are one of the most important and critical components in the electrical power system network. They are used to change voltages to meet requirements of the transmission and distribution power systems. The majority of them have been in service for many years under different environmental, electrical and mechanical conditions [1]–[4].

The main components of a transformer are a magnetic core, which plays an important role in a transformer, the windings; primary and secondary windings, insulation components and ancillary equipment such as insulated bushings, the tap changer and oil conservator. Although the transformer has been designed in order to withstand a severe environment and extreme operational conditions, as the transformer ages, the condition of its components and insulation material may suffer degradation, thus may reduce the capability of the transformer to withstand events such as switching transients, short circuits, lightning strikes without increased risk of failure [2]. One of the main reasons for transformer failure is due to problems associated with its insulation [1][5].

Hence, before a transformer reaches the point of failure, the use of appropriate and proper condition monitoring techniques are important. Condition monitoring of electrical equipment, such as power transformers, benefits both manufacturers and operators in many ways, for example obtaining information of the health of equipment, estimating the remaining service life of equipment, increasing plant availability and planning of maintenance schedules [6]. There a number of condition monitoring techniques for transformers such as Dissolved Gas Analysis (DGA), Thermal Analysis, Vibration Analysis, Frequency Response Analysis and also the preventive maintenance technique, PD Analysis [7]–[9].

Even though the approaches are different, they have similar objectives; which is to obtain information at an early stage before catastrophic failure occurs. This project is primarily concerned with PD analysis within a high voltage transformer winding. Partial discharge analysis is an important technique for diagnosis and online monitoring of transformer insulation systems. PD within transformer windings may be due to several causes such as manufacturing defects, degradation of the primary insulation or contamination of the oil. The degradation processes occurring in dielectric insulation components can lead to development of different types of PD sources [10][11].

Multiple PD sources induced by different defects can be simultaneously present within the transformer winding [12]–[14]. Therefore, it is necessary to develop tools to separate measurement data from multiple PD sources in order to facilitate PD source identification and location to allow accurate condition assessment of the winding. An experiment has been designed at the Tony Davies High Voltage Laboratory, University of Southampton in order to access the methodologies for identification and localisation of multiple PD sources within a HV transformer winding. The experiment facilitates the testing of transformer winding under conditions similar to those found in a large power transformer.

This project is concerned with the feasibility of locating several PD sources simultaneously based only on measurement data from a pair of wideband radio frequency current transducers (RFCTs). The RFCTS were positioned at the neutral to earth point and the bushing tap-point to earth due to the fact that any discharge occurring at any point along a winding produces an electrical signal that will propagate as a travelling wave towards both ends of the winding [15].

1.1 RESEARCH MOTIVATION

A power transformer outage would cause significant affects to either a large number of the residential consumers or impact on industrial plant [7]. Therefore, it is necessary to develop methodologies for detecting the early signs of a developing incipient fault and provide the network operator with useful information. It is no longer sufficient to just confirm the presence of a problem, additional diagnosis is required as well as some indication of the likelihood of failure in the short, medium or long term. This is because in many cases, the original redundancy built into the network no longer exists and key components such as HV transformers are not straightforward to repair or replace.

One of the common causes of transformer failure is due to degradation and ageing of the insulation in the transformer windings. According to D. J. Allan and A. White [17], based on the CIGRE Working Group Study Committee (WG SC) 12, in terms of individual components, 29% of the failures in transformer were found to be due to issues with the windings. This survey covers 47000 transformers-years in 13 countries over a 10-year period. In another survey by Commonwealth of Independent States (CIS) it was reported that 10% of transformer failures were caused by problems associated with the windings. Additionally, according to [18], a few failure surveys by IEEE (1986), Australia-New Zealand (1985 – 1995) and India Power Grid found respectively 41%, 30% and 73.3% failure of transformers were due to winding failures.

Generally, degradation within transformer windings is caused by partial discharge activity. PD is a dangerous degradation and ageing mechanism in the solid insulation system, which can be considered as a precursor of transformer failure that leads to eventual failures. In PD diagnosis and prognosis studies, one of the important issues that needs to be addressed is the ability to locate the affected PD location accurately in order to assess a suitable maintenance process effectively. Hence, techniques that have the ability to locate PD activity within transformer windings are very useful.

It is difficult to access the internal condition of the winding from outside of the transformer. Access is very limited due to the structure of transformer windings; they are very complicated and physically sealed within a closed enclosure of a tank immersed in insulation media. PD

activities within a power transformer can be detected by various techniques and the common techniques are centered on the use of electrical, acoustical and optical detection. Any discharges that occur within the windings produce signals that will propagate towards both end of the transformer windings. Based on fundamental theory of travelling waves along passive transmission lines by L.V. Bewley [15], the discharges that occur inside a transformer winding are in the forms of electrical signals that can be considered as travelling waves. Therefore, in this work, an electrical measurement technique is used based the captured current signals produced by PD activities from two radio frequency current transducers (RFCTs) which are positioned at both ends of the transformer winding.

1.2 RESEARCH OBJECTIVES AND SCOPE

The main objectives of the research are to detect, measure, identify and locate multiple PD sources within a HV transformer winding. A previous project [16], at The Tony Davies High Voltage Laboratory, University of Southampton, has developed non-linear based techniques that facilitate identification of the location of a single PD source within an interleaved windings. This work is concerned with the feasibility of locating several sources simultaneously. An experiment using a transformer winding model consisting of a plain disc and interleaved disc windings has been developed in The Tony Davies High Voltage Laboratory, University of Southampton. The transformer winding model is filled with transformer mineral oil and was built at Alstom T&D Transformer Limited and has been incorporated into an experimental arrangement that includes a core, tank and bushing.

Several artificial PD sources have been generated and signals can be injected simultaneously via an external connection at different tap points along the transformer winding model in order to simulate PD activities using different artificial PD sources. The signals captured by RFCTs at both ends of the transformer winding are extracted using advanced signal processing techniques in order to study PD propagation behaviour and distribution of energy patterns with the aim of source localisation. Therefore, this research has developed a new approach based on the distribution of energy of measured PD pulses in order to separate, identify and estimate the location of multiple PD sources within a transformer winding.

1.3 PUBLICATIONS RESULTING FROM THIS RESEARCH

The works in this thesis have contributed to the following publications:

Refereed Conference papers;

- Nik Ali, N. H., J. Hunter, P. Rapisarda and P. Lewin, "Identification of multiple partial discharge sources in high voltage transformer windings," in IEEE Conference on Electrical Insulation and Dielectric Phenomena (CEIDP), 2014, Des Moines, IA, 19-22 Oct. 2014.
- Nik Ali, N. H., Abd Rahman, M.S.; J. Hunter, P. Rapisarda and P. Lewin, "Wavelet and Mathematical Morphology as the De-Noising Methods for PD Analysis of High Voltage Transformer Windings," in IEEE Electrical Insulation Conference (EIC), 2015, Seattle, Washington, 7-10 June 2015.
- Nik Ali, N. H.; W. H. Goldsmith, J. Hunter, P. Rapisarda and P. Lewin, "Comparison of Clustering Techniques of Multiple Partial Discharge Sources in High Voltage Transformer Windings" in IEEE 11th International Conference on the Properties and Applications of Dielectric Materials (ICPADM), 2015, Sydney, Australia, 19-22 July 2015.
- Nik Ali, N. H., Michalis Giannakou, R D Nimmo, P. Rapisarda and P. Lewin, "Classification and Localisation of Multiple Partial Discharge Sources Within a High Voltage Transformer Winding," in IEEE Electrical Insulation Conference (EIC), 2016, Montreal, QC, Canada, 19 - 22 June 2016.
- Nik Ali, N. H., P. Rapisarda and P. Lewin, " Separation of Multiple Partial Discharge Sources Within a High Voltage Transformer Winding using Time Frequency Sparsity Roughness Mapping," in IEEE Condition Monitoring and Diagnosis (CMD), 2016, Xi'an, China, 25 - 28 September 2016.
- Nik Ali, N. H., P. Rapisarda and P. Lewin, " Multiple Partial Discharge Sources Discrimination In A High Voltage Transformer Winding" in 13th International Electrical Insulation Conference (INSUCON), 2017, Birmingham, United Kingdom, 16 – 18 May 2017.

Journal Papers;

- Nik Ali, N. H., P. Rapisarda and P. Lewin, “Identification and Localisation of Multiple Partial Discharge Sources within High Voltage Transformer Windings”, submitted to IEEE Transactions on Dielectrics and Electrical Insulation in August 2017.
- Nik Ali, N. H., P. Rapisarda and P. Lewin, “Comparison of Multiple Partial Discharge Clustering Techniques within High Voltage Transformer Windings”, in preparation for submission to IEEE Transactions on Dielectrics and Electrical Insulation in 2017.

1.4 REPORT ORGANIZATION

An overview of the composition of this thesis is provided here:

- **Chapter 1** – An introduction to this report consists of an overview, research motivation, research objectives and scopes, research contributions and report organization.
- **Chapter 2** – Literature review of the background studies regarding high voltage power transformers, power transformer condition monitoring techniques and partial discharge phenomena including its measurement as a condition monitoring tool, behaviour within transformer windings, identification and localisation.
- **Chapter 3** – The generation of artificial PD sources, arrangements and measurement system regarding the experiments setup for the identification and localisation of multiple PD sources in a high voltage transformer winding.
- **Chapter 4** – Describes several of the signal processing techniques that have been used in partial discharge data analysis in order to produce distributions of energy which then lead to a technique to identify the location of multiple partial discharge sources within a high voltage transformer winding.
- **Chapter 5** – Discuss the decomposition techniques used to decompose original signals into different levels based on their frequency ranges. Two techniques, which are wavelet analysis and mathematical morphology decomposition, were employed to generate a representation of an original measured PD signals into different components.
- **Chapter 6** – Illustrates the clustering of results obtained from the decomposition techniques using Principle Component Analysis (PCA), t-distributed Stocastic Neighbour Embedding (t-SNE) and Time Frequency Mapping with the application of Density based Spatial Clustering of Applications with Noise (DBSCAN).
- **Chapter 7** – Demonstrates the clustering of results obtained from the decomposition techniques using Principle Component Analysis (PCA), t-distributed Stocastic Neighbour Embedding (t-SNE) and Time Frequency Mapping with the application of Ordering Points to Identify Clustering Structure (OPTICS).

- **Chapter 8** – Discusses the approaches that have been developed for localisation of multiple partial discharge sources within a high voltage transformer winding.
- **Chapter 9** – Discussion, conclusions and future works are presented in this chapter.

CHAPTER 2

HIGH VOLTAGE TRANSFORMER CONDITION MONITORING

2.1 INTRODUCTION

Power system networks consist of three basic stages, which are generation, transmission and distribution. One of the most important components of the transmission and distribution stages of the electrical power system network are HV power transformers. Figure 2.1.1 shows a typical example of an oil-filled power transformer.

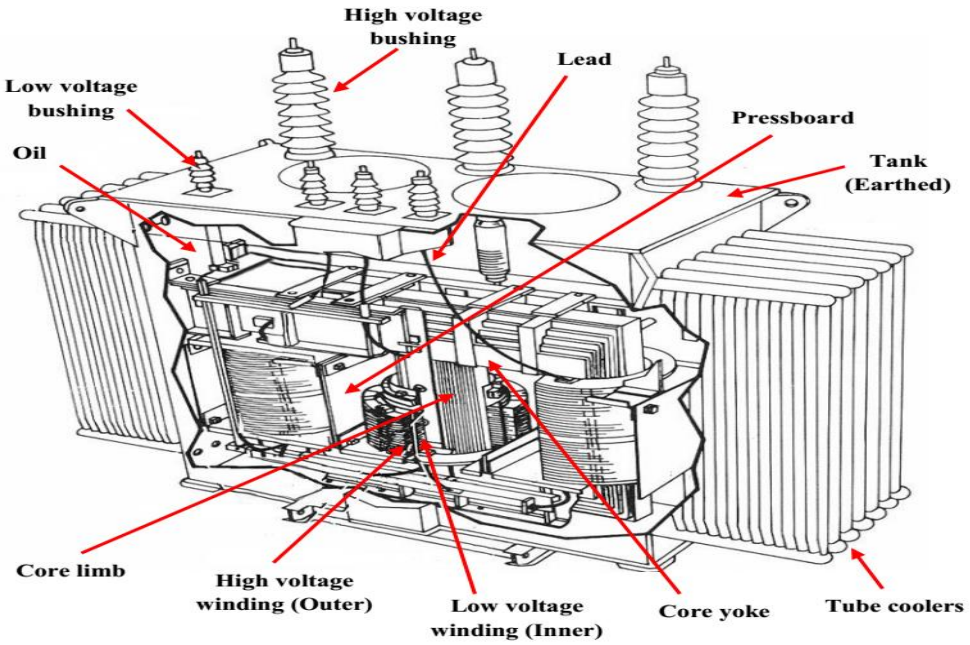

Figure 2.1.1 Oil-filled power transformer arrangement [17]

The majority of power transformers along with other power system grid infrastructure have been in service for many years and have experienced different environments and conditions

that can be considered to directly affect their several health. Unexpected failure or the need to replace unreliable units or undertake major maintenance procedures for ageing transformers may cause interruption of supply and have high financial impact to the national economy and business [18]. Therefore, HV power transformers are widely regarded as key critical components of a power system that require continuous monitoring and health assessment.

There are many possible factors related to transformers ageing, one of them is partial discharge. Partial discharge can cause the insulation strength of the transformer to degrade which then lead to transformer failure. Statistics have shown that a fairly high proportion of transformer failures (up to 50%) are linked to failure of the insulation systems [19][20]. A study in [21] about transformer failures of transformers rated at 25 MVA or above over the period 1997 – 2001 reveals that insulation failure is the leading cause of transformer failure. Another report [22], categorizes transformer failure with respect to its components and reports that the tap changer (41%), winding (19%), tank leakage (13%) and bushing (12%) are responsible for a significant majority of transformer failures. Figure 2.1.2 shows an example of a transformer winding that has suffered catastrophic failure due to damaged insulating paper.

Figure 2.1.2 A transformer winding that has suffered catastrophic failure [26]

Although, faults that cause transformer failures can be detected during planned routine maintenance, there are some faults for example internal partial discharge, that may develop

rapidly before the planned maintenance take place. Therefore, before a transformer reaches the point of failure, diagnosis using an on-line condition monitoring system is required in order to detect incipient faults which may develop from the beginning of a transformer's service. Condition monitoring offers benefits in terms of increasing both reliability and efficiency, and benefits manufacturers and operators in obtaining information of the health of the transformer over its operational life [6].

2.2 CONDITION MONITORING TECHNIQUES FOR POWER TRANSFORMERS

According to E. Gockenbach, and H. Borsi, condition monitoring has the advantages of extension of remaining life, improvement of overloading possibility, higher availability and service reliability, condition-based maintenance and repair and prevention of loss and destruction [6].

Ahmed E. B. Abu-Elanien, and M. M. A. Salama state that by using condition monitoring, the trends of the equipment can be verified and also the unknown faults can be diagnosed. Moreover, man power, down time, and repair costs can be optimized using condition monitoring. As a result, the lifetime of the equipment can be extended with acceptable performance guaranteed [7]. Apart from that, condition monitoring is able to ensure the plant availability, allow for planned operation beyond continuous design limits and detect incipient faults [23].

Most monitoring techniques are based on classical methodologies that be divided into two main modes of failure; internal and external causes [2], [5] [24]. Internal failures commonly occur within the insulation and winding system of the transformer which are caused by internal factors for example partial discharge.

Meanwhile, external failures happen at the point when the insulation system is no longer able to withstand severe conditions by external factors such as lightning strikes or short circuits. Table 2.2.1 shows the overall internal and external causes of the transformer failure.

Table 2.2.1 Causes of transformer failure.

Internal	**External**
Insulation deterioration	Lightning strikes
Loss of winding clamping	System switching operations
Overheating	System overload
Oxygen (from oil oxidation)	System faults (short circuit)
Moisture (i.e. high level of water content in oil or insulation paper)	
Solid contamination in the insulating oil	
Partial discharge	
Design and manufacture defects	

The classic techniques of condition monitoring are mainly focused on the insulation and winding systems. These techniques are still developing and are continually being improved [24]–[27]. However, in order for condition monitoring to be successfully deployed, there are some characteristics that need to be fulfilled, which are [28][23], the condition monitoring system must be:

1. self-sufficient and not require manual intervention or detailed analysis.
2. capable of detecting gradual or sudden deterioration and trends and have predictive capabilities to permit alarming in sufficient time to allow appropriate action to be taken and avoid major failure.
3. reliable and not reduce the integrity of the system
4. not require undue maintenance itself.
5. cost effective.

There are two types of condition monitoring; off-line and on-line condition monitoring. Considering the limitation of off-line condition monitoring techniques, nowadays power utilities tend to employ the on-line condition monitoring techniques in order to avoid the cost of traditional maintenance procedures and unnecessary service outages [5][29]. There are several techniques that are offered by manufacturers and also maintenance companies [23] which allow the monitoring of various aspects of the transformer.

Traditionally, high voltage power transformer condition monitoring may be undertaken using chemical analysis; Dissolved Gas Analysis (DGA), senses the changes in physical conditions of transformers and produces a relation between faults using measurement analysis. A comprehensive review of chemical and also electrical diagnostic methods can be found in [9]. Generally, transformer condition monitoring can be divided into several categories as shown in the Figure 2.2.1.

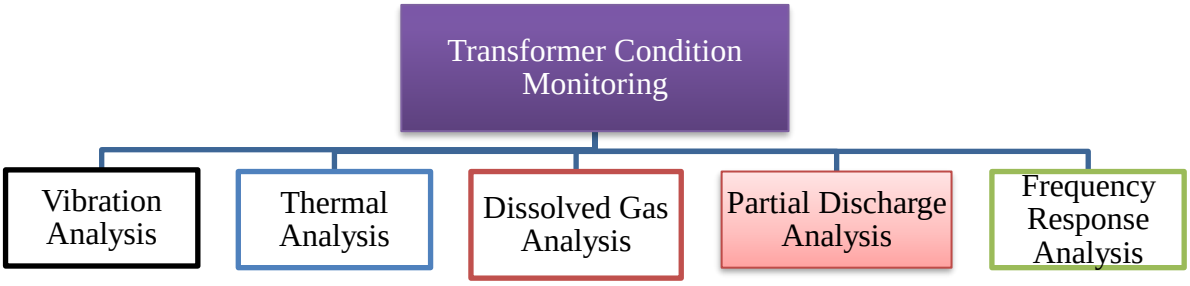

Figure 2.2.1 Transformer Condition Monitoring Techniques

Further details regarding Vibration Analysis, Thermal Analysis, DGA, PD Analysis and Frequency Response Analysis have been discussed in [7][30], [31]. Some of those techniques can be combined together when necessary for more accuracy, for example, when condition monitoring is involved in monitoring the condition of insulation properties of transformer windings.

2.2.1 OFF-LINE TRANSFORMER CONDITION MONITORING

Condition monitoring can be defined as a technique or method for monitoring the operating characteristics of a component in such a way that changes and trends of the monitored characteristics can be used to predict the need for maintenance before serious deterioration or breakdown occurs. Condition monitoring is the technique that facilitates Condition-Based Maintenance (CBM) which is sometimes referred to as predictive maintenance.

Previously, time based maintenance had been used as the maintenance strategy within electrical power transmission and distribution companies. Basically, time based maintenance are undertaken to examine and repair components offline either according to a time schedule or running hours. Therefore, there are possibility for unnecessary shutdowns and unexpected accidents may happen between maintenance intervals [32].

Time based maintenance processes are generally manual and require observations that include the levels and types of dissolved gases in oil-filled equipment, mechanical routine checks or gas pressure checks [6]. Off-line condition monitoring means that transformers are taken out of service to perform analysis. Therefore, manpower, time and money can be wasted because the maintenance assessment is blindly performed with little prior information of the current condition of the transformer [32]. Thus, off-line condition monitoring does not give an instantaneous condition assessment of the transformer and at best it provides a lagging indication of failure.

However, condition monitoring techniques as part of CBM will provide engineers or operators with more information about the condition of the transformer and indicate clearly when and what maintenance is needed. This automatically reduces the manpower, time and expense. Therefore, in order to meet the modern requirements of asset management in power networks [7][33], significant research is currently being conducted to identify new techniques for transformer on-line condition monitoring.

2.2.2 ON-LINE TRANSFORMER CONDITION MONITORING

As the power transformers is a key element of energy transmission and distribution, on-line condition monitoring is widely used on large autotransformers, as ideally it should allow undisturbed operation of power transformers. Nevertheless, it is often discarded because of the required investment costs. There are a few published examples that illustrate on-line condition monitoring for high voltage transformers.

According to [18], there are three major measurements for on-line condition monitoring and these are centred on DGA [34], Dielectric Dissipation Factor (DDF) measurements [35] and PD measurements. DGA is routinely employed to detect internal electrical discharging in power transformers which can only provide information about the nature and severity of the PD [2]. However, the location of the PD events cannot be obtained by using DGA which is very important to the engineering specialist who must make decisions about remedial action.

Using PD measurements techniques, should enable the detection, location, analysis and monitoring of PD in transformers. There are a few examples of on-line condition monitoring techniques based on PD measurements, for example, by using ultra high frequency (UHF) sensors [36]. Additionally, if the DGA and DDF methods are employed the related accurate measurement devices are relatively expensive. While PD measurement does not have these limitations and there is a good economic balance between measuring equipment cost and its accuracy [37].

There are a few more examples of on-line condition monitoring such as by using MIT's model-based system [38], Alstom T&D MS 2000 monitoring system [39] and SIEMENS power transformer monitoring system [40]. However, this thesis is only concerned with transformer condition monitoring techniques based on PD phenomenon and particularly on the localisation of partial discharge sources within transformer windings.

2.3 PARTIAL DISCHARGE ANALYSIS AS A CONDITION MONITORING TOOL

PD analysis as a condition monitoring tool is used to provide condition monitoring information in this research. The term partial discharge is defined in the international standard IEC (International Electro-technical Commission) 60270 as, “a localized electrical discharge that only partially bridges the insulation between conductors and which can or cannot occur adjacent to a conductor” [41]. There are two necessary conditions for PD to occur. The first condition is that, the electric field has to be above the PD inception field or in other words, the inception voltage should be higher than the threshold voltage. Secondly, electrons need to be available in order to trigger any discharge processes [10], [42].

Generally, PD is a consequence of local electrical stress concentrations in the insulation itself or just on the surface of the insulation. The insulation may consist of solid, liquid or gaseous materials or any combination of them. Usually, the discharge appears as pulses which have duration of much less than 1 micro seconds (μs). The term PD itself covers a wide group of discharge phenomena [41], such as:

i. Internal discharges occurring in voids or cavities within solid or liquid dielectrics
ii. Surface discharges appearing at the boundary of different insulation materials
iii. Corona discharges occurring in gaseous dielectrics in the presence of inhomogeneous fields
iv. Continuous impact of discharges in solid dielectrics forming discharge channels (treeing and/or surface tracking).

During PD on the surface or inside electrical insulation, high energy electrons or ions cause deterioration of the insulation material. This bombardment may cause changes in chemical decomposition in the insulation material which then lead to complete breakdown. Additionally, PD often occur accompanied by emission of sound, light, heat and chemical reactions. Thus, it is essential to monitor as well as to measure partial discharge activities in order to slow down or stop degradation processes which would affect the performance and lifetime of a transformer.

2.3.1 PARTIAL DISCHARGE MEASUREMENT

There is on-going research into on-line condition monitoring using PD detection and measurement for high voltage transformers. However, there a few issues to be considered before PD detection and measurement can be undertaken. In [10], a few considerations that need to be considered during PD measurements have been identified, they are:

i. The apparent charges of PD signals maybe small in magnitude, where they usually superimposed by interferences and disturbances therefore it is necessary to distinguish the actual PD signals.
ii. In three-phase systems such as real transformers, PD sources can be present in all three phases and the PD signals can crosstalk from one phase to another, so it is also necessary to distinguish PD from different phases.
iii. Measuring and acquisition systems can distort characteristics of PD signals i.e. the signals are not captured totally or two signals are measured as one if the acquisition system comes with a low sampling rate or resolution time.

Additionally, there is a lot of interference or noise during the measurement on site. Consequently, PD signals can be swamped with noise signals. Therefore, it is important to distinguish between a real PD and noise signals in order to obtain accurate measurements. PD signal de-noising can be achieved by using either wavelet de-noising, Fast Fourier Transform (FFT) based de-noising or low pass filtering [16], [43]–[46].

Generally, noise will reduce the quality of measurement as it masks the presence of small PD signals or noise signals also can be mistaken for PD signals themselves. Typically, noise can be divided into two types, which are white noise and impulse-like noise. White noise is usually observed as randomly distributed pulses that have similar magnitude and occur within the entire power cycle and possess wide-band frequency characteristics. Therefore, in a laboratory environment, by using appropriate electromagnetic shielding such as a Faraday cage can reduce the white noise level. This approach is not possible when measuring PD on-line in the field, so additional signal processing is required before analysis can be performed.

Impulse-like noise usually appear in bursts at a magnitude significantly higher than white background noise. It can sometimes be observed to possess a fixed phase relationship and tends to have a consistent frequency signature from pulse to pulse. This type of noise can be reduced by employing hardware such as power frequency filters to reduce the noise levels introduced by the mains power supply.

There are several techniques which have been implemented in order to measure PD activity inside high voltage plant (e.g. transformers). The measurements are based on sensing of changes of energy that take place during the PD events. These changes include:

i. electrical pulse currents
ii. dielectric losses
iii. electromagnetic radiation (including light)
iv. sound waves
v. increased gas temperature and pressure
vi. chemical reactions

According to [47], partial discharge activity can cause changes in the chemical and physical nature of a system while it is assumed that the actual process may involve generation of an electrical, thermal, gas pressure, light or sound emission or a combination of these parameters. As the propagating PD pulse must travel an arbitrary distance through a distributed impedance from the site of the PD to the PD sensor, there are further energy transfers and loss of information in the form of signal dissipation and attenuation.

There are two main classes of PD detection; non-conventional (acoustic, UHF detection and optical) and conventional (electrical) detection approaches [48]. PD activity can be monitored by simply listening to the hissing noise associated with PD activity in air (corona). However, this method has low sensitivity and difficultly in differentiating PD from other noise. While, by using optical techniques, detection is limited to discharge sites located at the edges of bulk materials and surfaces of non-transparent media.

Basically, PDs are pulses of current that occur in a transformer when the electric field strength exceeds the dielectric breakdown strength of the insulation material. This results in high

frequency transient signals that propagate within transformer windings in all directions; towards bushing tap points and neutral to ground terminals. However, the PD radiation, radiates towards the transformer tank wall via the surrounding oil. Therefore, PDs in transformers can also be detected using non-conventional techniques [47], [48].

The acoustic method is the detection of acoustic emission of partial discharges. The sensors used can be placed in a safe way (assuming that the transformer tank is grounded) at any point on the wall of transformer tank [51]. Acoustic emission detection has been successfully used in order to localize the PD sources due to the fact that acoustic signal is strongly dependent upon the geometry of the test object [48]. However, it was reported in [52] that the sensitivity and reliability of this technique is reduced in a high noise environment and also if the insulation damping is high. Additionally, it has also been found that this method does not work well in dealing with both direct and indirect acoustic waves produced by PD due to the interference of both waves and also the impedance transfer function of propagation path is complicated as acoustic waves tend to propagate along multiple pathways.

UHF sensors of detection bandwidths of 500 MHz – 2 GHz can be mounted outside the transformer tank providing the tank has been fitted with dielectric windows and are able to detect the wave radiation from any PDs events within transformers. Although this kind of sensor is found to be more sensitive than acoustic sensors, it is also found that these sensors are unable to tolerate high levels of interference from other sources [53].

Many researchers have been developed methods using UHF signals, for example in [36][53]–[55], multiple UHF sensors are fitted to the transformer tank to locate multiple PDs events within transformer. However, the UHF sensors are not suitable for detecting and locating PDs events within a transformer winding due to the geometrical complexity of the transformer winding. Additionally, during the measurement UHF sensors will also capture other PD events at different locations within a transformer.

Therefore, it can be difficult to distinguish between PDs inside a winding and PDs from another part of a transformer. Figure 2.3.1 (a) shows an example of UHF coupler for external mounting and Figure 2.3.1 (b) shows an example of installed UHF coupler on a transformer tank.

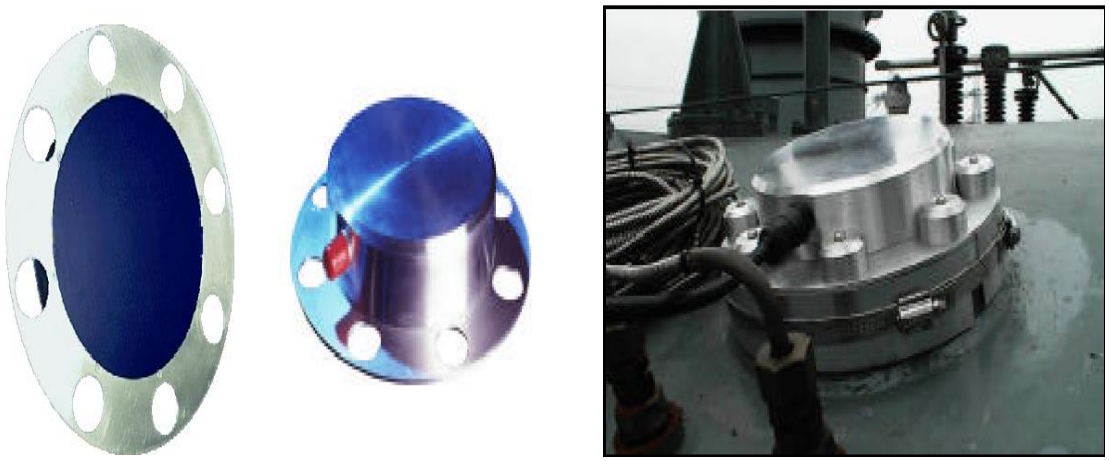

(a) (b)

Figure 2.3.1 a) UHF transformer coupler for external mounting [56]
b) Installed UHF coupler on a transformer tank [56]

PDs also can be detected via optical detection methods. Optical emission from PD can be detected using optical sensors. The system requires a sensor probe, an optical fiber linked to the sensor and high end signal processing unit [24]. This technique is reported to be immune to electromagnetic interference (EMI) which allow them to perform in noisy environments. They are also flexible, small and easy to install [16][24]. However, by only using this method, there is no information about PD severity [48].

Most common methods used to investigate PD activity use electrical techniques, by using capacitively or inductively coupled transducers which capture the high frequency voltage and current pulses that propagate away from the PD site. Current transformers based on inductive coupling such as RFCT and HFCT are usually used for detecting PD current signals within transformers [24][57]. The use of current coupling sensors like RFCT or HFCT is because

the sensors have a large impedance against power frequency but have a low impedance against high frequency components. Therefore, the sensors will eliminate power frequency components and detect discharge currents which contain high frequency components flowing to the ground [16]. Figure 2.3.2 shows an example of RFCT sensor installed on the earth conductor of single-core cables.

Figure 2.3.2 A RFCT sensor installed on the earth conductor of single-core cables [58]

The widespread use of electrical techniques for the task of PD measurement is due to the associated advantages such as: sensitivity, reliability and feasibility for the given application [59]. However, the use of electrical techniques, for example in this investigation, by using RFCTs have limitations such as low noise immunity. Therefore, nowadays, in modern technology, these techniques mentioned above are combined as a system monitoring tool where the use of electrical detection has the advantage of allowing the application of digital signal processing techniques. There is a study that has compared several PD measurement techniques based on electrical, chemical and acoustical techniques and concludes that each technique come with their own advantages and drawbacks [60].

2.4 PARTIAL DISCHARGE WITHIN TRANSFORMER WINDINGS

Typically, PDs within the insulation of high voltage transformers can arise from a single or multiple defects. PDs that occurs in high voltage transformers may come from different defects, for examples voids inside dielectric material, sharp point electrodes, discharges in oil or surface discharges in oil, gas bubble discharges in oil and discharges in indeterminate-potential particles moving in oil. Formation of partial discharges inside transformer windings is due to several causes such as manufactured defects or contamination during manufacture processes. However, the main factor may be due to degradation processes occurring in dielectric insulation components of high voltage transformers which then lead to development of different types of PD source [10], [11][16].

The following typical scenarios of an insulation failure model are presented on the basis of historical cases analysis (summary of over 200 failures) [20]:

1. Critical contamination of oil (typically presence of free water) + rapid change of temperature → PD appearance at rated voltage → breakdown.
2. Surface contamination + water + rapid change of temperature → PD appearance → flashover.
3. Particles contamination + switching surge → critical PD → breakdown.
4. Water + particles contamination (or bubble present in oil) → critical PD → creeping discharge progressing → breakdown
5. Surface contamination + lightning impulse → surface discharge → flashover.
6. Distortion of winding geometry → PD appearance → creeping discharge progressing → breakdown.
7. Distortion of winding geometry + switching surge → flashover between coils (sometimes with restoring withstand strength) → gas evolution.

In a report titled “Characteristics of PD during its evolution in transformer winding” [61], it states that during the development of PD within transformer winding, there are only two different phenomena involved in the development of discharge activities inside transformer windings. The phenomena are surface discharge at inception followed by internal discharge which then leads to breakdown.

In another report investigating the PD development within transformer winding [62], it is stated that once PDs occurred inside a transformer winding, the discharge was sustained and stable from the initial stage to the finally insulation breakdown, and the whole development process could be divided into four descriptive stages: initial, development, severe and dangerous.

PD activity within high voltage transformer windings can be visualised as a very short duration of electrical pulses that propagate from PD sources locations along the winding towards the measurement points. In terms of magnitude, it was found in [63], that the minimum and maximum PDs magnitude that could be reliably detected over the range of injection points was 100 pC and 2.5 nC. While the duration and shape of PD pulses depend on the type of PDs and also the system where the PDs occurred. In [26] reported that the PDs pulses are determined by the nature, form and the extent of the discharge severity. However, measurements of magnitude should be treated with some caution, as there is likely to be significant differences between real and apparent charge and this will be dependent on the propagation pathways from the source to sensor.

PDs can occur anywhere within the transformer winding and are described as stochastic in nature (there is a variation in the time interval between discharge events and magnitude of discharges) [16][64]. However, according to original work by L. V. Bewley in [15], based on the fundamental theory using the theory of travelling waves along passive transmission lines, PDs pulses change their shape, steepness becomes reduced, becoming elongated and the propagating waves are no longer similar because PD pulses will suffer distortion and attenuation during travelling from discharge locations to measuring points. The attenuation and distortion occur because of energy losses due to resistances and by variations in the inductances and capacitances caused by frequency and position in transformer windings

where usually at the end of the winding some of the parameter values can be higher compared to others based on arrangements [16].

Under realistic field conditions, PDs not only occur due to a single source, but PDs may occur from multiple sources which can be activated simultaneously within a transformer winding at different locations along a HV transformer winding [65], [66]. These PDs might occur in the high voltage leads of windings, within pressboard, near the high voltage winding ends, clamps of windings, inter-sections of windings, inside the winding and within the transformer oil [67]. Therefore, in the presence of multiple PD sources, the ability to accurately discriminate and locate between PD signals generated is required.

2.5 PARTIAL DISCHARGE IDENTIFICATION

Over the last few decades, the PD phenomenon has attracted extensive investigations not just related to its mechanisms and detection techniques, but also related to its identification and localisation. It is well-known that different types of PD sources can produce different discharge characteristics. Consequently, different PD sources may have different effects on the condition and performance of the power equipment insulation system. Therefore, identification of PD sources is of great interest to both systems, utilities and equipment manufacturers.

Traditionally, phi-q-n (ø-q-n) or phase resolved partial discharge (PRPD) plots are the most popular method for PD diagnostics which can provide important information as well as identification of PD sources. The ø-q-n plots consist of three parameters relating to the time domain properties of a single PD pulse. The relative phase angle (ø) relates the applied voltage and the pulse peak occurrence and have a value between $0^o – 360^o$. While the apparent charge (q) of the pulse is calculated by integrating the associated current pulse which usually expressed in Pico-coulombs (pC). However, the calculated apparent charge is not equal to the amount of charge locally involved at the source of the discharge but is an estimated of amount of charge that, if injected into the terminals of the test object, would lead to the same reading on the PD measurement setup. The number of PD pulses (n) with similar ø and q values for a given test sample period makes up the third dimension of the plots. Analysis then

can be completed by plotting the discharge quantity such as the apparent charge or the number of PD pulses against the ac phase (in 2-dimensions) or all three parameters can be plotted together (in three dimensions). The success of such plots to represent different types of PD can be attributed to the fact that they can be related to parameters physically describing the PD process [68]. However, this approach has the limitation when used for on-line measurements. The measurements data may be corrupted by multiple sources that can discharge near simultaneously. Figure 2.5.1 shows an example of a PRPD plot of multiple sources (in this case surface and void discharge) that occur simultaneously. With reference to Figure 2.5.1, the captured pulses are superimposed over a 20ms period and the intensity scale represents the total number of PDs with the same magnitude and phase occurrence captured over the duration of the experiment. In this case, the plot is produced using the Mtronix PD measurement software.

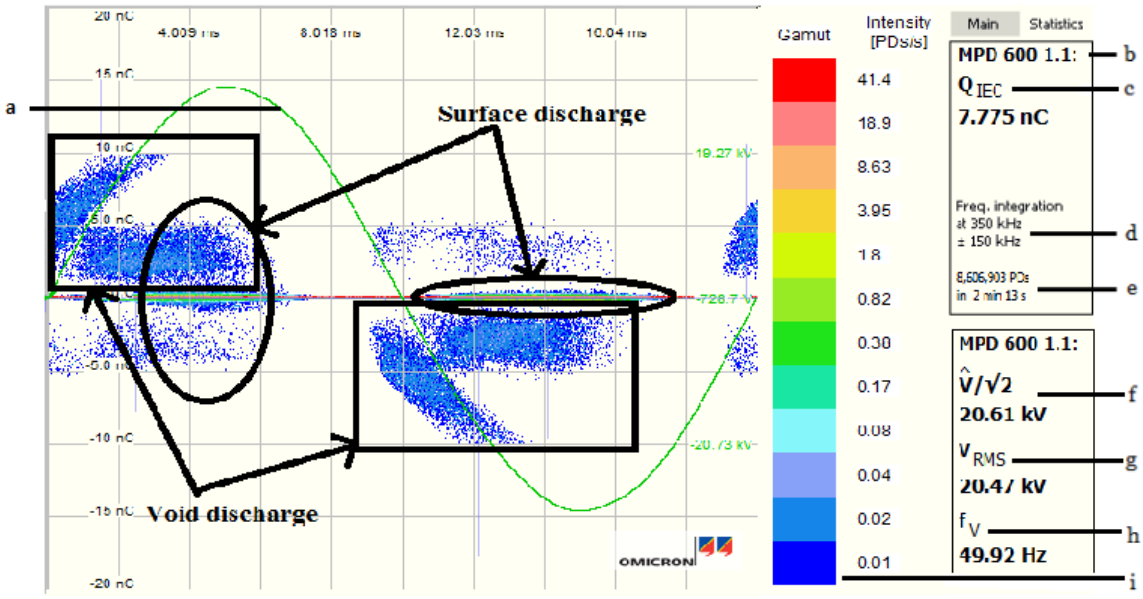

Figure 2.5.1: PRPD plot. a) Applied voltage waveform. b) Test unit designator. c) Average charge calculation across a single power cycle. d) PD calibration bandwidth and centre frequency. e) PD number and test period. f) Applied voltage magnitude estimation. g) Applied voltage RMS calculation. h) Applied voltage waveform frequency. i) Histogram legend.

Most of the PD source separation and classification techniques are based on the assumptions that the PD signals generated by the same PD source have similar characteristics. In [69], a comprehensive study of applying pattern recognition techniques to automatic PD source classification has been presented. Three issues have been investigated; firstly, feature extraction for obtaining representative attributes from original PD measurement data. Several approaches are adopted as the feature extraction including Principle Component Analysis (PCA), Stochastic Neighbour Embedding (SNE), discrete wavelet transform (DWT), kernel principle component analysis (KPCA) and conventional statistic operators. Secondly, pattern recognition algorithms for identifying different types of PD sources. Several techniques such as K-nearest neighbour (KNN), two-layer (input and output) network, multi-layer perceptron (MLP), radial basis function (RBF) network, Bayesian classifier and fuzzy support vector machine (FSVM) have been applied as the pattern recognition algorithm. Thirdly, the identification of multiple PD sources which may occur in high voltage equipment simultaneously. Although there are two approaches used in the report that can recognize multiple PD sources, it was reported that further research is still required due to the complexity of multiple PD source classification.

In [70], the recognition of single and multiple PD sources in transformer insulation has been discussed. The PD pulses were captured using an UHF sensor and then recorded via a spectrum analyser and an oscilloscope. As the presence of noise will affect the analysis results, it is important to de-noise the recorded signals before further analyses can be carried out. Wavelet multivariate de-noising was utilised to de-noise the PD signals. In order to recognise the different types of PD sources, three features of decomposed signal components were extracted from the PD signals and used as inputs into a neural network. It was demonstrated that by using the proposed method, that single and multiple PD sources could be classified. However, in the neural network, the training data must be sufficient enough to describe all sources. Another limitation on the neural network is the inability to use linguistics to describe an output, since it is difficult to understand the content of a network [71].

Identifying multiple PD sources provides additional information that could enable more accurate decisions concerning the integrity of the insulation to be made. The presence of different types of PD sources as well as the interferences that can be activated simultaneously in on-line environment, will complicate the identification process. In [72], it was shown that

by utilising the Wavelet Packet Transform and Higher Order Statistics, together with the Density-based Spatial Clustering of Applications with Noise (DBSCAN) algorithm and the Principle Component Analysis (PCA) only around 70 % identification was successful on experimental data to identify multiple PD sources and at the same time reject interference.

There are various pattern identification techniques that have been extensively used in PD identification such as fuzzy clustering [73], [74], mixed Weibull model [75], auto-correlation function [13], equivalent time and bandwidth computation of the acquired PD signal [76] and density based spatial clustering [12]. These approaches are mostly based on the assumptions that the PD signals generated from the same sources will have similar characteristics.

2.6 PARTIAL DISCHARGE LOCALISATION

Important tools for quality assessment of power transformers are detection, measurement and classification. However, for maintenance and repair of transformers, the most important tool is determination of the location of PD sources. The main reason of transformer failure is due to failure in its insulation either within a bushing or the windings [5]. Therefore, in order to provide cost benefit and effective solutions, not only to detect, measure and classify the PDs, it is also important to determine the location of PDs inside transformer windings, which should be considered as a part of a condition monitoring and maintenance strategy. A suitable and appropriate decision can then be made with respect to any corrective action by knowing the location of PDs inside the transformer.

Localisation of PDs is one of the important aspects in the condition monitoring process when applied to HV transformers. It can be a complicated process when a winding is involved if the discharge occurs deep inside a transformer winding. Additionally, there is no access for utility engineers into the transformer winding. There are a few more problems when involve the localisation within transformer winding for example the problem due to the complexity of the transformer winding itself which affects the propagation of signals in terms of attenuation and distortion from location of the discharge to the measurement points. On top of that, there may be a lot of additive interference and disturbances during on-line measurement such as noise from internal or external sources which are not related to any

detected PD signals. Therefore, it is also important to distinguish the actual PD signals in order to locate the PD sources inside the transformer winding accurately.

There are various techniques to localise PDs occurrence which can provide utility engineers an advanced on-line condition monitoring techniques for HV transformers. Many researchers have proposed methods in the literature for PD localisation based on analysis of different types and the analysis processes for localisation which may involve additional mathematical solutions and advanced signal processing techniques [24], [63].

The localisation process can be based on various methodologies. For example in [3] and [77], the localisation of the PD inside transformer winding was measured by using the winding transform function. However, this technique has limitations especially for old transformers, where the design data such as winding number, type, and type of disks, turn number in each disk and dimension of the winding do not exist. These parameters of the transformer are required in order to model the winding transfer function [1].

Alternatively, other works have also shown that multi-conductor transmission-line model (MTLM) can be used to locate PD sources within transformer winding [78]. Through this model, two methods for calculation of model parameters were used in order to decrease computational complexity of the model. A comparison between the measured and calculated transfer function of a 132 kV/20 kV transformer allows the best model parameters to be obtained. PD pulses generated by a calibrator were injected into different points of a research 20 kV/0.4 kV transformer and measured at both ends of the winding in order to investigate the accuracy of MTLM in PD localisation. The sectional winding transfer functions computed by the model were used to refer measured PD signals to possible PD locations. Then PD location in the transformer winding can be estimated by comparison of referred signals.

In another paper [54], UHF sensors are used to localise the PDs inside a transformer. This technique is based on detecting electromagnetic radiation in UHF ranges (300 MHz – 2 GHz). Usually there are three or more UHF sensors are installed on the transformer tank to detect PDs signals that occur inside a transformer. Basically, this technique locates the PD source by measuring the shortest time of arrival of the PDs signals to the UHF sensors which are mounted on the transformer tank. This technique has a high sensitivity, is robust and

successfully detects PDs. A complete procedure of PDs localisation using electromagnetic radiation was reported in [79]. However, this technique may be disrupted by attenuation and scattering of electromagnetic waves which are caused by the transformer structure. Therefore, it may cause some errors of the actual arrival time due to the energy losses during the radiation process [80], [81].

On the other hand, the location of a PD source can also be established using power spectral density (PSD) estimation [82]. The PSD estimated was processed, then a distance classifier was employed to determine the location of PD based on the periodogram (spectral estimation method) features. The authors reported that this method does have capability to work on-line and can estimate the PD location even in noisy (white noise) environments as the periodogram has the ability to reduce the effect of the noise. However, this technique needs installation of extra equipment.

Another method to locate PD in transformer winding was reported in [1] by using a neuro-fuzzy technique. This technique adapted a neuro –fuzzy system that uses unsupervised pattern recognition, based on the changes in the shape of PD signals. PD signals were injected into 30 points of a medium-voltage transformer winding and detected at both ends of the winding (bushing and neutral ends). In this paper, a comparison between the proposed neuro-fuzzy technique with other two techniques; using orthogonal transform and calibration line was compared to evaluate the advantages of the proposed technique. The results show a significant improvement in localising PD by using this technique, however the methodology for locations of multiple PD sources occurring at the same time by using this technique is still under investigation.

As far as localisation of PD are concerned, this thesis aims to develop an alternative method to locate multiple PD sources in a high voltage transformer winding only based on measurement data i.e. PD signals from two measurement points; bushing tap point to earth and neutral to earth point of the transformer. This investigation originates from the original analysis completed by L.V. Bewley [15], when he investigated travelling waves inside transmission systems represented as lumped parameters networks, and hence based on this, he introduced a split winding analysis where a partial differential equation (PDE) is used to define a travelling wave moving from PD sites towards the winding ends. Based on the

fundamental theory using the theory of travelling waves along passive transmission lines by Bewley, PD produces a signal that will propagate towards both ends of the transformer winding bushing and neutral to earth connection point from the sources. However, PD sources may be distorted and attenuated during the propagation process from the discharge location to the measurement sensors. PD sources from different locations will suffer different distortion and attenuation which may then be used to inform PD source location.

2.7 SUMMARY

An overview of high voltage transformer condition monitoring has been presented in this chapter. It is important to monitor the condition of high voltage power transformers including its windings before the transformer reaches the point of failure. Basically, condition monitoring of transformers provides important and beneficial information for both manufacturers and operators.

There are two types of condition monitoring; off-line and on-line transformer condition monitoring. Historically, the condition of a transformer was monitored using time based maintenance. However, in order to avoid unnecessary costs of routine maintenance, many power utilities nowadays tend to use on-line condition monitoring.

On-line condition monitoring is widely used for high voltage power transformers as it reduces the number of planned outages. There are several examples of on-line condition monitoring applications for transformers and these have been summarized.

Condition monitoring of power transformers can prevent catastrophic transformer failure which has unwanted social and economic impacts. There are many possible factors related to the transformer failure, one of them is partial discharge. Therefore, it is important to detect, measure, identify and locate any internal partial discharges. However, this investigation is only concerned with identifying and locating the partial discharge sources that can be activated simultaneously within a high voltage transformer winding. Partial discharge behaviour within transformer winding, identification and its localisation have been briefly discussed in this chapter and are further investigated throughout this thesis.

CHAPTER 3

PARTIAL DISCHARGE EXPERIMENTS

This chapter details the PD sources that were generated artificially and also the experimental arrangement used in order to investigate activities and propagation characteristics of multiple PD sources within a HV transformer winding from discharge source locations towards points of measurements connected at both ends of the winding namely, the bushing tap point to earth and neutral tap point to earth. The measured PD signals by two RFCTs at both ends of the transformer winding are used for further analysis to test and validate the proposed method on identification and localisation of multiple PD sources within a HV transformer winding.

3.1 PARTIAL DISCHARGE SOURCES

Three model PD sources were generated in the laboratory which are surface, void and floating discharge which were then used to inject into the winding sections at different locations along the winding as input data. They are among of the common types of discharge events that may occur within HV transformer windings. Different arrangements need to be set up to generate different discharge according to a specific type of PD source. All arrangements were placed in a bath of transformer oil to replicate the conditions inside a real transformer and remove the likelihood of corona discharge also occurring.

3.1.1 SURFACE DISCHARGE

Surface discharge occurs along the surface or interface of solid insulation. Pressboard is frequently used inside power transformers as insulation. The combination of oil and pressboards inside a power transformer gives a higher dielectric strength. However, due to complications in the transformer design, there are places where the field component is parallel to the insulation surface. This reduces the strength and surface discharges may occur along the pressboard insulation surface [83].

Generally, surface discharge in oil has been investigated by using a point-plane method as shown in Figure 3.1.1.

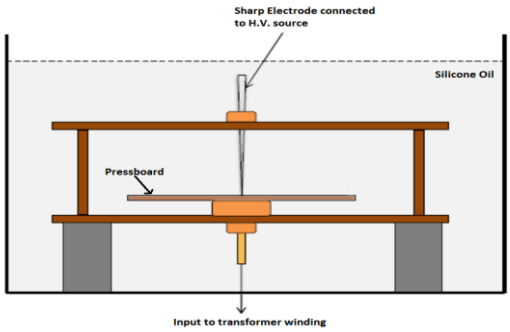

Figure 3.1.1 Point-plane surface discharge arrangement.

This method has been widely used to study surface discharge phenomena on various types of solid materials [84][85][86]. However, this method produces a more directional and intense electric field towards the solid surface from localised and inhomogeneous electric field at the edge of the needle. It has recognised that the pressboard can get punctured under AC [17] and impulse voltages [87]. Therefore, in this study the needle-bar electrode configuration has been used to promote surface discharge at the oil-pressboard interface as shown in Figure 3.1.2. The needle discharge source is placed at an angle close to horizontal on the pressboard and at distance of 35 mm from an earthed conductor bar which is also placed on the pressboard surface. This configuration also significantly reduces the possibility of the pressboard being punctured compared to a more traditional point-plane electrode configuration as shown in Figure 3.1.1.

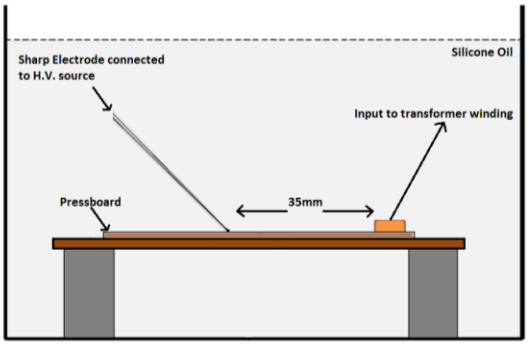

Figure 3.1.2 Needle-bar surface discharge arrangement.

Inception voltage for this type of surface discharge on the pressboard is around 14 kV. Figure 3.1.3 shows the ø-q-n plots for surface discharge for configuration in Figure 3.1.2 with three applied voltages; 18 kV, 20 kV and 23 kV respectively.

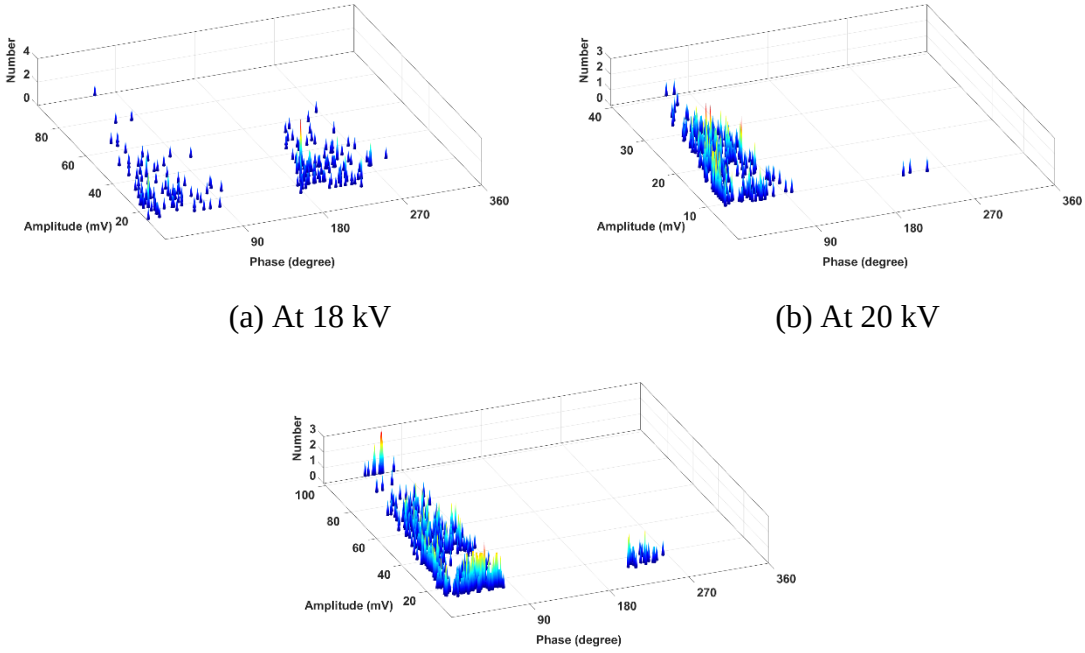

(a) At 18 kV

(b) At 20 kV

(c) At 23 kV

Figure 3.1.3 ø-q-n plots for surface discharge.

The discharges occur in the positive half cycle between the phase angle of 0° – 90° and negative half cycle between the phase angle of 180° – 270°. In the positive half cycle the magnitude and the number of PD events is bigger than the magnitude in the negative half cycle. Increased applied voltage results in a higher average magnitude of discharge.

3.1.2 VOID DISCHARGE

Void discharge are normally due to cavities inside an electrical insulation. Cavities inside HV transformer could be because of bad manufacturing or improper transportation of the transformer. To develop a suitable void source, a new method was devised utilising computer aided design (CAD) and 3-D printing technology. The design incorporates a cylindrical void with diameter of 12 mm and depth of 2 mm within a larger cylinder of resin with diameter of 4 mm and depth of 0.5 mm. The sample was designed using Solid Works CAD modelling

software as in Figure 3.1.4 (b) and then printed in two halves in a UV-cured resin. The same resin used from printing was then applied between the two halves and the sample was cured in a UV light box for 50 seconds. The result is as shown in Figure 3.1.4 (c). The 3-D printed sample was then mounted between a plane of electrodes with a diameter of 24.43 mm and the whole set of artificial PD source arrangement was immersed in transformer oil. A schematic diagram is shown in Figure 3.1.4 (a).

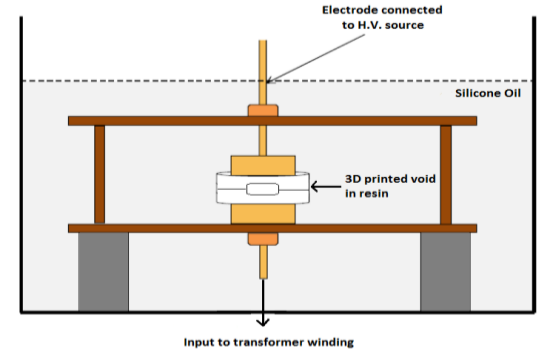

(a)

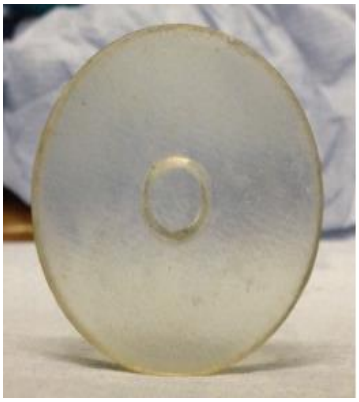

(b) (c)

Figure 3.1.4 (a) Void discharge arrangement (b) 3-D CAD model in Solid Works (c) 3-D cured printed sample.

The upper electrode was connected to the HV source; meanwhile the bottom electrode was connected at various points along the winding section. The PD inception voltage for this type of material and void dimensions was found to be approximately 16 kV. Three separate tests also have been done at increasing applied voltage which are 18 kV, 20 kV and 22 kV

respectively. Figure 3.1.5 shows the ø-q-n plots of discharge event using the cylindrical void of applied voltage at voltage 18 kV, 20 kV and 22 kV respectively.

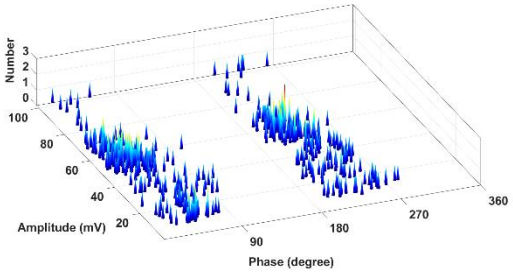

(a) At 18 kV

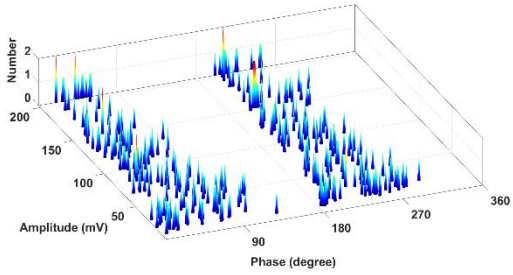

(b) At 20 kV

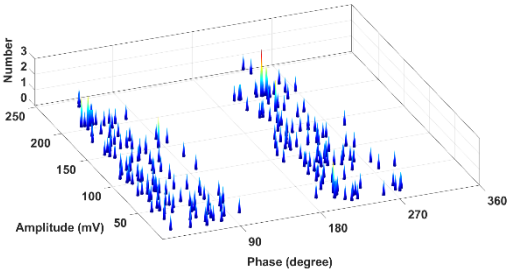

(c) At 22 kV

Figure 3.1.5 ø-q-n plots for void discharge.

The void discharges occur at the beginning of each half cycle where the magnitudes of the discharge is almost the same in positive and negative half cycles for each voltage level. It is also noticeable that the patterns of the discharge remain unchanged as the applied voltage is increased. As the applied voltage increased from 18 kV to 22 kV, the magnitude of discharge becomes greater, from 100 mV to 250 mV respectively.

3.1.3 FLOATING DISCHARGE

Floating discharge may be introduced during manufacturing or maintenance of a high voltage transformer. These unwanted particles reduce the electric strength of its insulation system [88]. In order to generate an artificial floating discharge signal, a few thin layers of copper strips were placed on the interface of pressboard and immersed inside the transformer oil. A plane to plane electrode was used in order to have a uniform field that will interact with

the copper strips on the pressboard. The schematic diagram for this type of discharge is shown in Figure 3.1.6.

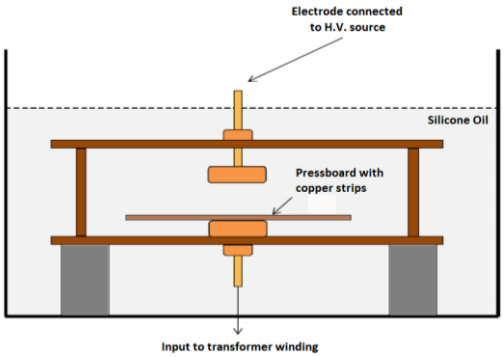

Figure 3.1.6 Floating discharge arrangement.

Inception voltage of this type of discharge activity is around 15 kV. Three different voltages have been applied to the source, 18 kV, 20 kV and 22 kV. Figure 3.1.7 shows ø-q-n plots for floating source discharge at three different voltages levels.

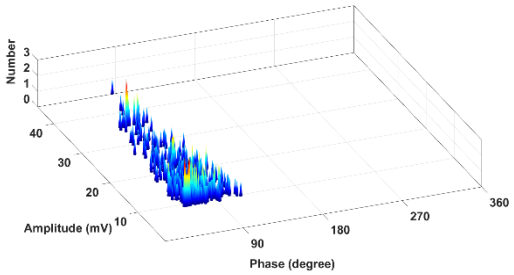

(a) At 18 kV

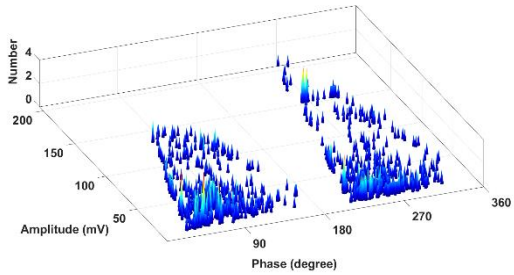

(b) At 20 kV

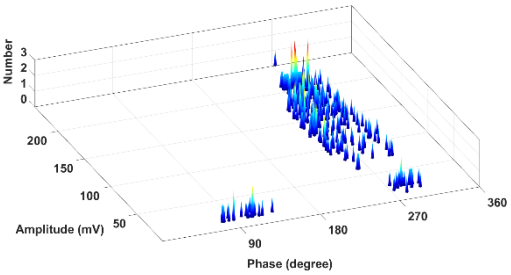

(c) At 22 kV

Figure 3.1.7 ø-q-n plots for floating discharge.

The ø-q-n plots for this type of discharge shows that the patterns of discharge events are different from each other. The possible reason is probably due to the unstable characteristics of floating discharge. At 18 kV, the discharge event only occurs in the positive half cycle, while at 20 kV and 22 kV the discharge occurs in both positive and negative half cycles around 45° - 180° and 225° – 315° respectively. At 20 kV and 22 kV, the magnitude of discharge in the negative half cycle is larger compared to the positive half cycle. It also shows that as the applied voltage increase, the magnitude of discharge increase accordingly.

3.2 EXPERIMENTAL ARRANGEMENT

Three different experimental arrangements have been designed and constructed in the Tony Davies High Voltage Laboratory, University of Southampton to simulate multiple PD pulses inside a transformer winding. The produced measurement data were used to assess different approaches to HV transformer condition monitoring, which involve PD measurement and localisation within HV transformer windings.

3.2.1 EXPERIMENT SENSITIVITY

Before setting up the experimental arrangement, a frequency response measurement of the RFCTs was undertaken in order to investigate the sensor responses at high frequency. The measurement of the frequency response was obtained using an Agilent network analyser. In order to validate the accuracy and the offset level of gain measurement, self-calibration of the analyser was performed using an impedance reflector in transmission and reflection mode. During the test, the measurement frequency range was set from 100 Hz to 500 MHz, with a sample bandwidth of 30 Hz. It is necessary to measure the frequency response over the large range in order to represent the total system response. In order to stabilize the trace of the measurement and improve the measurement data quality, the response was measured using the averaging function which was set to 300 times.

The captured frequency response is in the form of a complex coefficient, which is then used to calculate the response on terms of dB gain and phase angle. Figure 3.2.1 shows the measured frequency response data in dB magnitude and its corresponding phase response in

radian of the two RFCTs used in this investigation with the secondary conductor wrapped three times around the RFCT core. The Figures show that both RFCTs used in this investigation are very similar and have a close magnitude and phase frequency response. All the measurement data used in this investigation where measured using RFCTs with the frequency response shown in Figure 3.2.1.

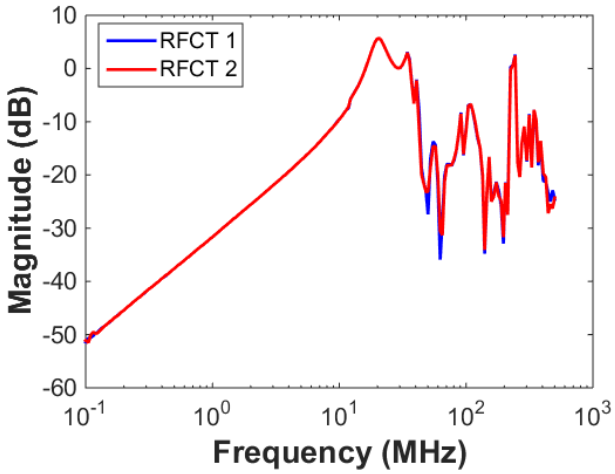

(a)Magnitude of frequency response

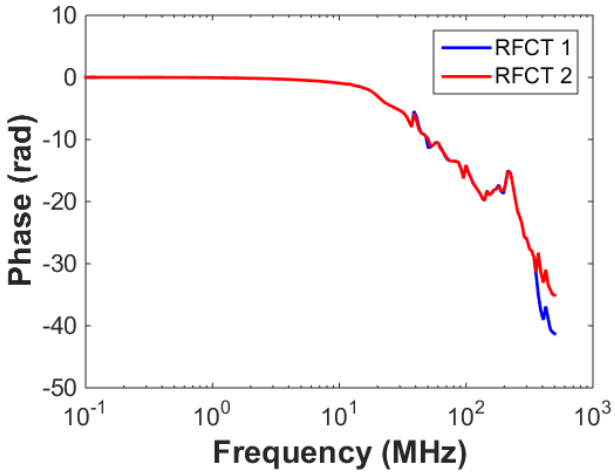

(b) Phase of frequency response

Figure 3.2.1 Frequency response of the RFCTs

In an industrial environment, the sensitivity of PD measurement is often limited by the levels of electrical interference experienced under practical conditions. Large noise levels can reduce the quality of the measurement as they can mask the presence of small PD signals or they can be mistaken counted as the PD signals themselves.

Therefore, it is very important to measure the background noise of the experiments. The background noise was measured for all the experiments undertaken in this investigation. Figure 3.2.2 shows the background noise measured using a commercial PD detector from OMICRON Mtronix with a MPD600 acquisition unit. The Figure shows that the background noise was only around 627 fC under an applied voltage of 21 kV.

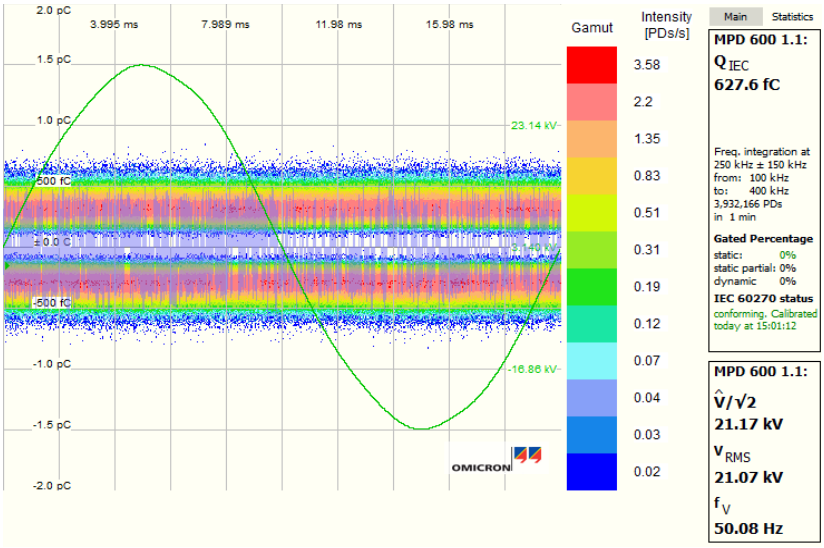

Figure 3.2.2 Background noise.

3.2.2 PULSE GENERATOR SOURCE INJECTION

In order to fulfil the requirement of practically modelling a high voltage transformer and standard PD condition monitoring, the experiments consist of a HV transformer winding model with eight injection terminals, a 60 kV transformer bushing, two measurement sensors and an oscilloscope as shown in Figure 3.2.3. In this test, a signal generator was used as a source to inject pulse shaped signals into terminals along the transformer winding sections. The signal generator was set to have a rise time of 8 ns and amplitude of 1.5 V.

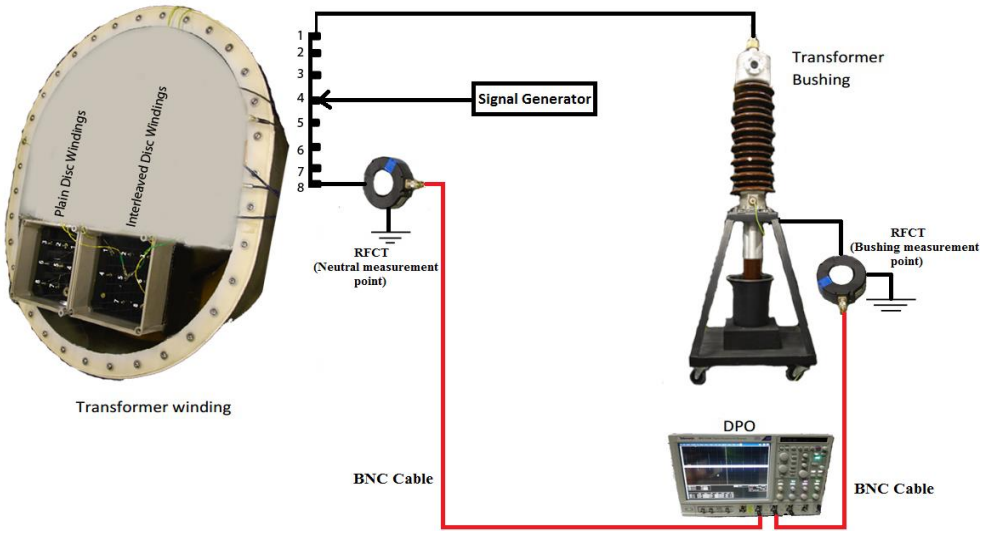

Figure 3.2.3 Experimental arrangement for pulse generator source injection.

The HV transformer winding model was used to study PD signal propagation inside a transformer winding. The model consists of two sections; an interleaved winding located at the top and the bottom part of the winding section consists of a plain disc winding. The entire winding section is immersed in an oil filled tank filled with oil specification of BS148:1998 class 1, which is discharge-free up to the 30 kV test voltage [16]. In this report, only PD activity along the interleaved disc type winding has been studied.

The 60 kV transformer bushing is included to be more representative of transformers and account for any attenuation or distortion of higher frequency components of a discharge that

are detected via the measurement sensor at the bushing tap point. A high performance digital oscilloscope used in this experiment was a Tektronix DPO 7254C with a sampling rate set to 500 MSs^{-1} and a bandwidth of 2.5 GHz respectively for real time visualisation and data recording.

Two RFCTs were used as the measurement sensors to capture the propagated PD pulses from the sources in the winding and were placed at the neutral to earth point (terminal 1) and the bushing tap-point to earth (terminal 8). The use of an RFCT has been demonstrated to be able to capture high frequency transient signals that are proportional to the time derivative of current in a conductor. Hence the RFCT is an ideal sensor to monitor high frequency discharge currents. In order to increase the sensitivity of each RFCT, both RFCTs were wrapped with three turns of wire conductor which also has been done in previous research at University of Southampton [16], [24].

During the experiment, the pulse generated from the signal generator was injected into different terminals along the transformer winding through 50 Ω BNC cable to maintain the impedance value from the signal generator output in order to reduce the reflection of the signal at the terminals connections. The signal generator was setup to generate a controllable pulse which then was injected into different terminals of the transformer winding.

3.2.3 INDIVIDUAL SOURCE INJECTION

In this experiment, artificial PD sources were used to inject pulses into different terminals along the transformer winding. In order to stimulate the artificial PD sources, a HV power supply along with a HV transformer is incorporated with the test arrangement in order to step up the voltage and is connected to a PD sources during the measurement process. A commercial PD measurement system is included in the experiment and it is incorporated with the coupling capacitor. The schematic diagram for the experiment is shown in Figure 3.2.4.

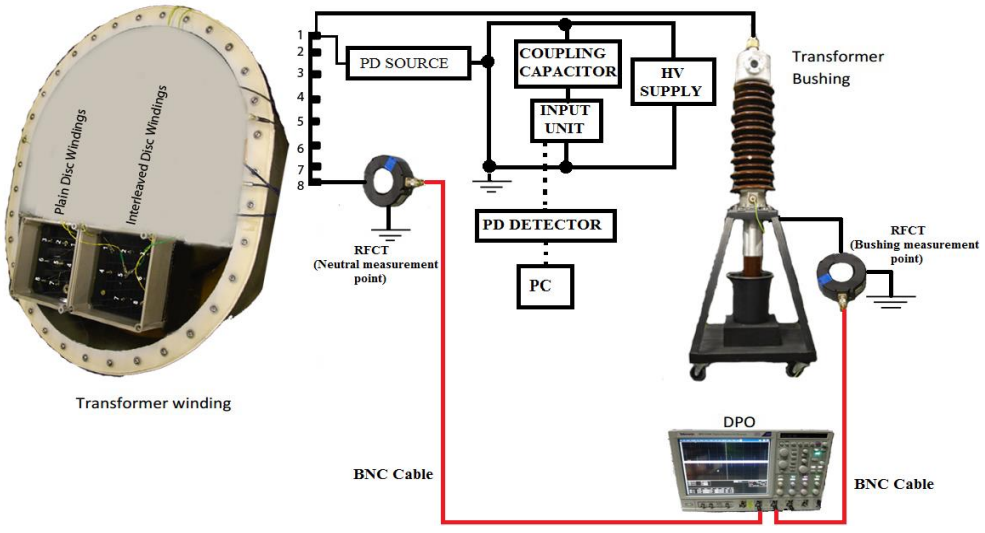

Figure 3.2.4 Experimental arrangement for single source injection.

In this experiment, PD pulses from different discharge sources as described in Section 3.1 were injected individually along a transformer winding via external terminals. During the PD measurement process, a 50 Hz applied voltage is connected to the PD sample via the needle or upper electrode which is interconnected with a high voltage transformer and coupling capacitor. When the voltage is applied up to the inception voltage for each type of PD source, discharge start to occur within the dielectric material. The PD signal then propagates to the earth electrode connected to the terminals of the transformer winding.

Based on the theory of travelling waves by L.V. Bewley [15], the resultant PD signal splits and propagates from a source location towards both ends of the winding. The PD signals travel via the RFCT to the HV ground at the neutral to earth measurement point, meanwhile only high frequency components of the discharge signals are able to pass to the bushing to earth measurement point due to the bushing core bar which acts as a capacitor. Both RFCTs captures the signals which eventually connected to the common HV earthing system.

On the oscilloscope, Channel 1 is connected to the voltage output of Quadripole unit of the MPD 600 Partial Discharge Analysis System. While RFCTs at the neutral to earth point measurement and bushing tap point measurement were connected to the Channel 2 and Channel 3 respectively. Channel 1 was set as a reference so that the RFCTs were triggered on the oscilloscope in phase to the applied voltage.

In order to quantify the apparent charge in terms of mV when the measurement was recorded using RFCTs, a sensitivity process using the Mtronix CAL542 charge calibrator was used. It was found that 1 mV of output signal was equal to 10 pC which is maintained for all the experiments to produce consistent measurements data in this investigation.

The measurement data from this experiment were used for comparison with the experiment using the signal generator and also as a reference for subsequent experiments where multiple PD sources were injected along the transformer winding simultaneously. When multiple PD sources were injected simultaneously into the transformer winding, a question arises either characteristics of the pulse propagation within the transformer winding will be the same as single source injection or not.

3.2.4 MULTIPLE SOURCE INJECTION

In this experiment, the basic arrangement remained unaltered except, two of the artificial PD sources discussed previously were generated using a 20 kV AC voltage and then injected into the transformer winding sections simultaneously. The arrangement for this experiment is shown in Figure 3.2.5.

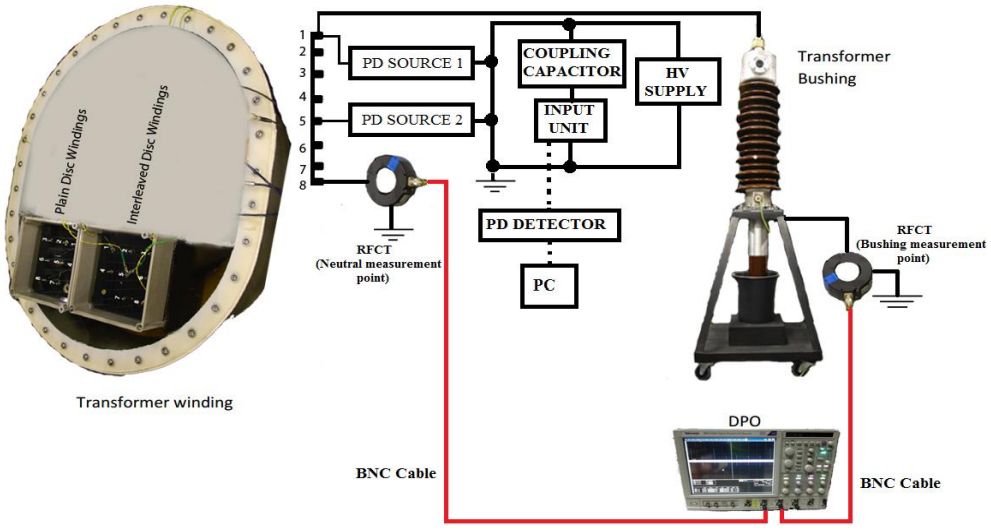

Figure 3.2.5 Experimental arrangement for multiple sources injection.

During the experiment, PD source 1 was injected into Terminal 1 to Terminal 8 while PD source 2 was only injected into Terminal 5. There are three combination of the sources as shown in Table 3.2.1.

Table 3.2.1 Multiple sources combination.

Combination	Terminal 1 – Terminal 8	Terminal 5
1	Floating discharge	Surface discharge
2	Surface discharge	Void discharge
3	Void discharge	Floating discharge

3.3 PARTIAL DISCHARGE MEASUREMENT SYSTEM

The MPD 600 Partial Discharge Analysis System was used in this investigation to detect, record and analyse any discharge activities that occurred in the oil bath. Before any measurements were undertaken, the system was calibrated using a charge calibrator to provide a measurement of the apparent charge that was injected to the sample under test in order to verify that the measurement system would be able to quantify the size of PD and hence obtain an accurate PD pattern.

The centre frequency and bandwidth used for PD measurement in this investigation are set to 350 kHz and 300 kHz which is fully compliant with the IEC 60270 standard. Figure 3.3.1 shows the schematic representation of the measurement circuit.

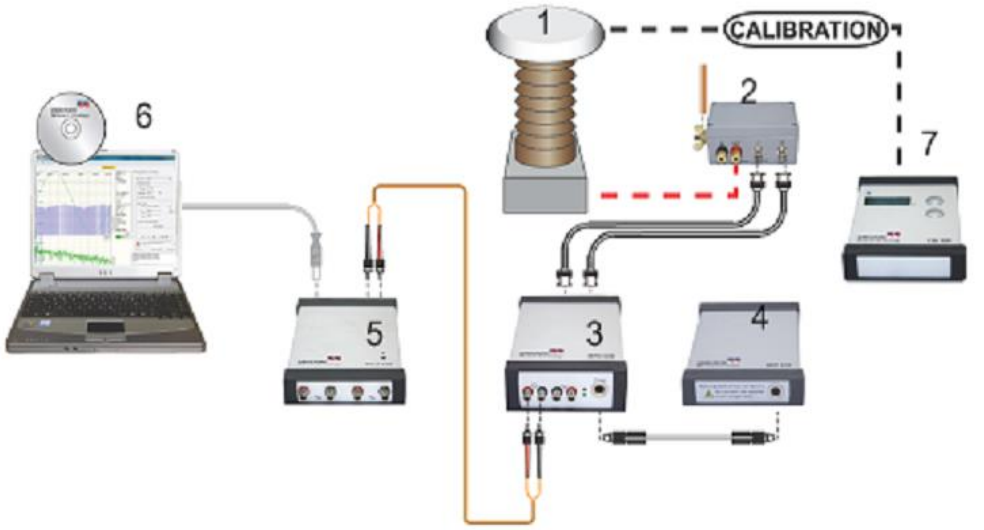

Figure 3.3.1 Mtronix MPD 600 PD measurement circuit [16], [59].

The HV coupling capacitor (1) blocks the 50 Hz network frequency voltage and transfers the high frequency PD signal to a Quadripole unit (2) which acts as the measuring impedance for the PD detector (3). The PD acquisition unit (3) functions not only as a PD detector but also a digital signal processing (DSP) based A/D converter and an electro-optic converter. It can be powered by a rechargeable Lithium-ion battery (4) or an 8-12 V DC power supply. The acquisition unit is fully controlled by a computer (6) via a USB interface (5) and optic fibre.

The captured PD signal is recorded on the computer for post-processing, replay and subsequent analysis. The amount of data that can be stored is limited by the operating system and the size of the PC's hard drive. The system is calibrated by a charge calibrator, pulses with a known apparent charge level are injected into the sample under test. The Mtronix CAL542 charge calibrator (7) can provide a 300 Hz pulse train with a pulse rise time of less than 4 ns. The system has a measurement frequency of up to 32 MHz and a variable bandwidth from 9 kHz to 3 MHz [59].

Figure 3.3.2 (a) and Figure 3.3.2 (b) show the example of PRPD plots for surface discharge and void discharge detected using Mtronix detection system. As multiple PD sources are concerned in this investigation, Figure 3.3.2 (c) shows an example of ø-q-n plot when surface discharge and void discharge were generated simultaneously. It is clearly shown that the generated ø-q-n patterns from both sources overlap each other.

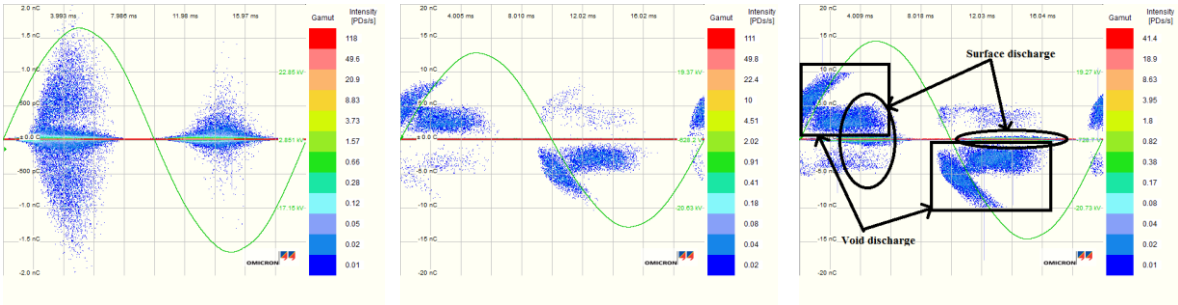

(a) (b) (c)

Figure 3.3.2 Example of ø-q-n plots using Mtronix MPD 600 system.
(a) surface discharge, (b) void discharge and (c) surface and void discharge.

From the PRPD plots, types of PD source that occur within the transformer winding can be recognised. Moreover, important information such as the measurement of apparent charge and applied voltage are known which can be used as an indicator of the energy transfer involved with any recorded PD activity. However, if two or more PD sources are co-generated in a system, the pattern of PRPD plots are too complicated to analyse.

3.4 PARTIAL DISCHARGE SIGNALS EXTRACTION

The PD signals are measured electrically using two RFCTs positioned at the bushing tap-point to earth and the neutral to earth tap point. 50 Ω BNC cables were used to interconnect the RFCT sensors to the Tektronix oscilloscope to displayed, analysed and stored in appropriate waveform format (.WFM). Then for further investigation the measured PD signals generated from the experiment, a method to discriminate between different PD pulses has been developed. The initial pre-processing stage was the use of a converter to convert the stored data into appropriate format, in this case is Matlab files format (.mat) for further analyses.

Due to the operation of the pulse generation hardware, a DC offset was produced in the measured signals. Therefore, the DC offset need to be removed from the raw data to allow further processing. This was completed by subtracting the mean amplitude of the entire cycle from each individual sample to ensure it exhibits a zero mean. Another challenge during the measurement was the background noise. It is important to remove the noise in order to extract PD pulses with confidence. As this investigation have been carried out in a controlled laboratory conditions which have a low noise level, a method known as hard-thresholding was used in this investigation for de-noising the raw signals as well as to extract PD pulses.

The extraction process was done by applying a peak detection technique to the raw data, transferring each pulse into a new variable matrix, replacing the removed pulse with a zero vector. This process was repeated until the peak magnitude of the remaining pulses within the raw data is smaller than a pre-defined threshold value. By doing this process, the significant PD pulses can be isolated from background noise.

Before setting a threshold value, it is important to identify the value of background noise via the signal plot of raw data which clearly show off the noise level. The threshold value must be set carefully, because if the threshold value was set too high, there are possibility of loss of PD pulse information. Otherwise, if the value was too low, noise pulses might be interpreted as PD events. For some cases, the threshold value can be differed according to particular conditions. For example, in Figure 3.4.1 shows that the threshold value was set

to 0.1 mV for bushing tap point to earth measurement while Figure 3.4.2 shows that the threshold value was set to 0.05 mV for neutral to earth measurement.

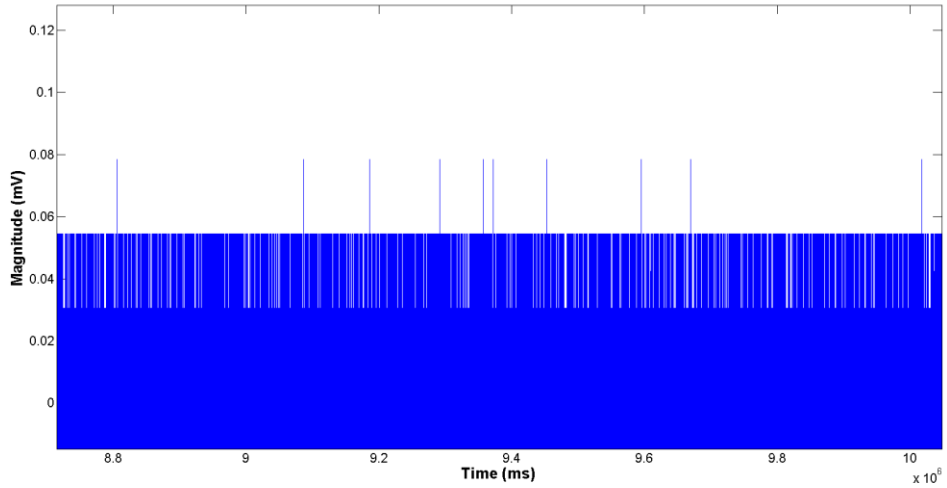

Figure 3.4.1 Noise level for bushing tap point to earth measurement

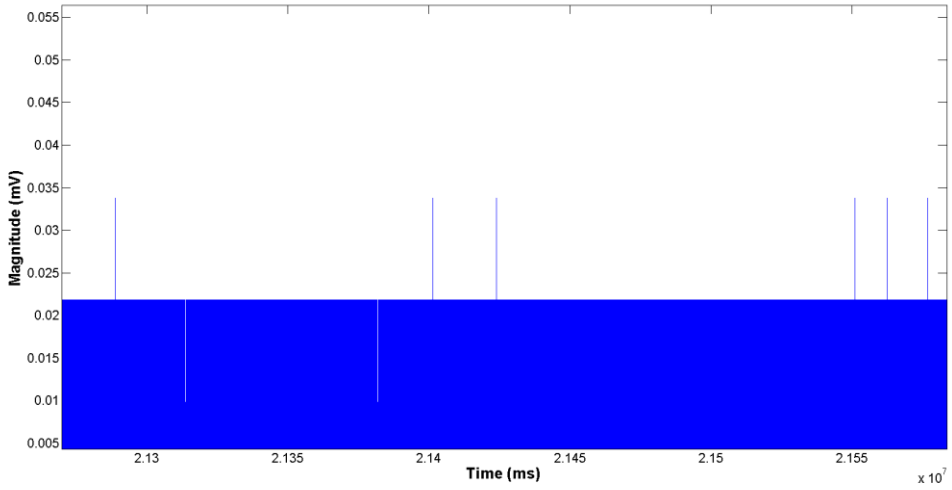

Figure 3.4.2 Noise level for neutral to earth measurement

After removing the DC offset and background noise, the raw signal at both measurement points can be assumed to only contain PD pulses of interest. In the literature, there are also a lot of de-noising techniques that can be carried out for the task of noise suppression within PD data such as Wavelet de-noising, Fast Fourier Transform (FFT) based de-noising and low pass filtering [43]–[45].

3.5 SIGNALS PROPAGATIONS FROM A PULSE GENERATOR

It is assumed that the signals may vary in term of propagation behaviour especially the magnitude of the signals. During the signal propagation process, there are attenuation and distortion processes occurring which affect signal behaviour. The attenuation process depends on where the signal occurs and the effective distance the signal needs to propagate to the measurement points. This will provide a variation in measurement data. Figure 3.5.1 shows the average of peak magnitude of the pulse measured from terminal 1 to terminal 8.

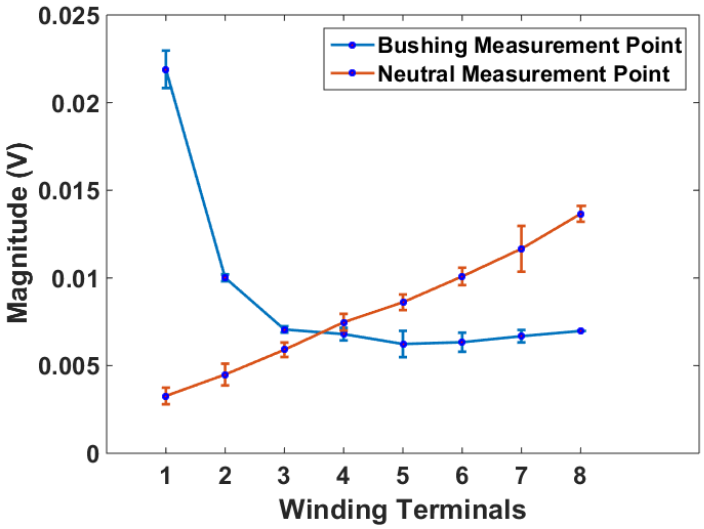

Figure 3.5.1 Average peak magnitude at all terminals.

In Figure 3.5.1, it can be seen that when the source signals are injected into Terminal 1 to Terminal 3, the peak magnitude of the signals are bigger at bushing tap point measurement than the signals measured at neutral to earth point measurement. However, when the source signals are injected into Terminal 4 onwards, the opposite effect starts to take place where the peak magnitude of the signals are smaller at bushing tap point measurement than the signals measured at neutral to earth point measurement. The peak magnitude of the signals is seen to be similar at Terminal 4. The variation in peak magnitude of the signals is due to the attenuation process during propagation from a location of signal origin towards measurement points.

However, when real PD source signals were injected into the transformer winding, the peak magnitudes of the measured signal from a location is not as constant as the pulses generated using a signal generator. As discussed in Chapter 2, PD events is known as stochastic in nature, meaning there is a variation in the time interval between discharge events and magnitude of discharges. Therefore, by use of the peak magnitude of the signal is not an ideal parameter to use for this investigation. Thus, instead of peak magnitude, the energy of the pulse has been considered. It is assumed that, during the propagation of the signals along transformer windings, the response with respect to the propagation path taken and termination characteristics will cause attenuation and distortion to the waveforms, thus produced changes in the energy characteristics of the signals when they reach both measurement sensors. The energy of the signals can be calculated using:

$$E = \sum_{i=1}^{N} |S_i|^2 \tag{3.1}$$

where N is the number of PD and S is the PD signals.

Figure 3.5.2 shows the average of energy content of the signals for Terminal 1 to Terminal 8.

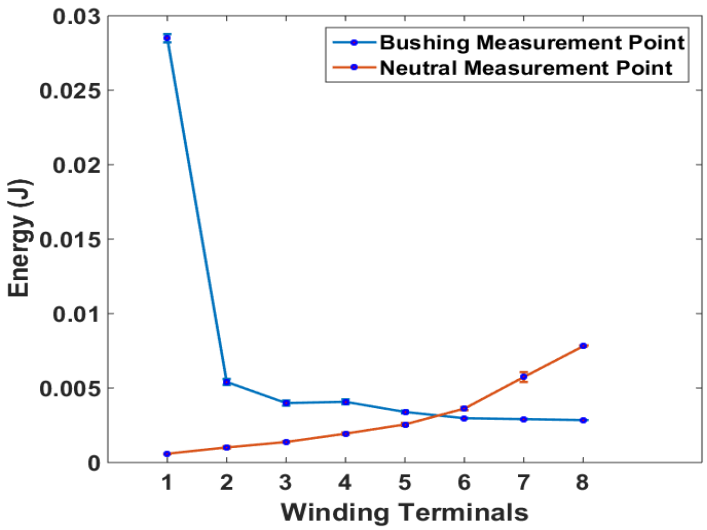

Figure 3.5.2 Average of energy content.

Comparing Figure 3.5.1 to Figure 3.5.2, the pattern of the average of energy content is different where the energy content is bigger at bushing tap point measurement than the signals measured at neutral to earth point measurement at Terminal 1 to Terminal 5. While the opposite effect starts to take place at Terminal 6 to Terminal 8. The energy content is seen to be closest matched at Terminal 6. Therefore, from both Figures, it is not necessary that larger PD magnitudes produce larger energy content. The Figures show that there are attenuation and distortion processes occurring during signal propagation which affect signal magnitude, oscillation patterns and energy content. These features ultimately can be exploited in order to estimate the location of a PD source. Therefore, this experiment supports the hypothesis that use of signal energy distributions can provide useful information with respect to the identification and localisation of multiple PD sources within a transformer winding. The result of this experiment was then compared to the experiments when artificial PD sources signal were injected into the terminals of the transformer winding. It is assumed that the characteristics of the signals propagation from pulse generator which have constant rise times, amplitudes and pulse duration are similar to the characteristics of the signal from artificial discharge sources that produce non-uniform signals amplitudes and frequencies.

3.6 SIGNALS PROPAGATION FROM ARTIFICIAL PD SOURCES

RFCTs that were connected to both measurement points; bushing tap point and neutral to earth connection are used to measure the PD current propagating along the winding. Therefore, any current generated from PD sources that reached measurement points can be measured and recorded using an oscilloscope. A comparison in time domain of measured PD pulses from both measurement points have been done as a preliminary analysis to investigate the changes of the signals for both signals from all injection points of the winding. This analysis is taken based on two assumptions, firstly is that each injection point does associate with the individual characteristic which may cause changes in the measured PD pulses. Second assumption is different injection points, will cause different propagation path that PD pulses need to go through from where it is located to the measurement sensors. Figures 3.6.1 – Figure 3.6.8 show the comparison of individual measured PD pulses for both measurement points for all types of discharge under an applied voltage of 20 kV.

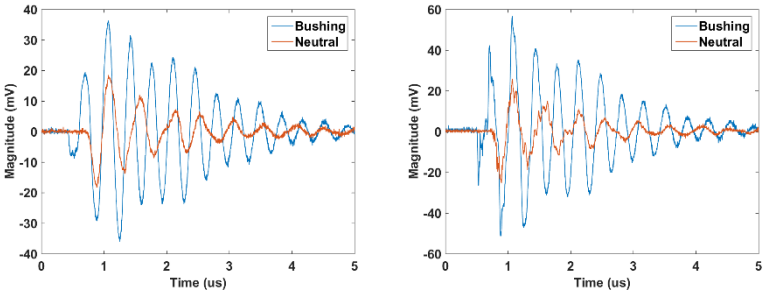

(a)

(b)

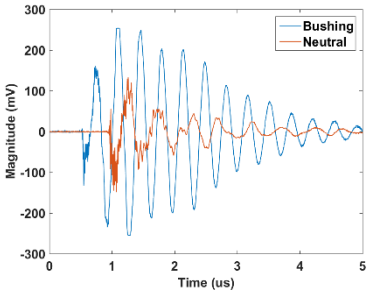

(c)

Figure 3.6.1. PD pulses plots for injection at Terminal 1 for: (a) Surface discharge, (b) Void discharge and (c) Floating discharge.

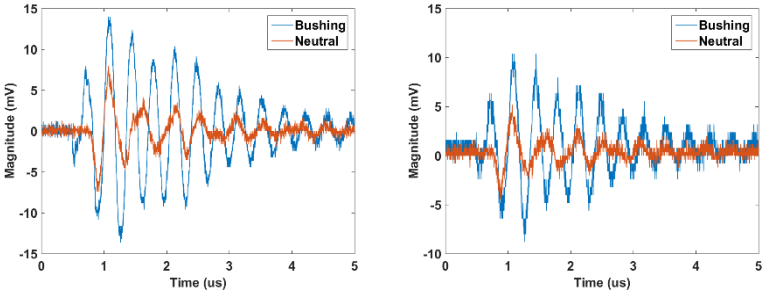

(a)

(b)

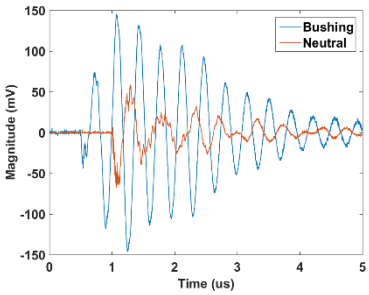

(c)

Figure 3.6.2. PD pulses plots for injection at Terminal 2 for: (a) Surface discharge, (b) Void discharge and (c) Floating discharge.

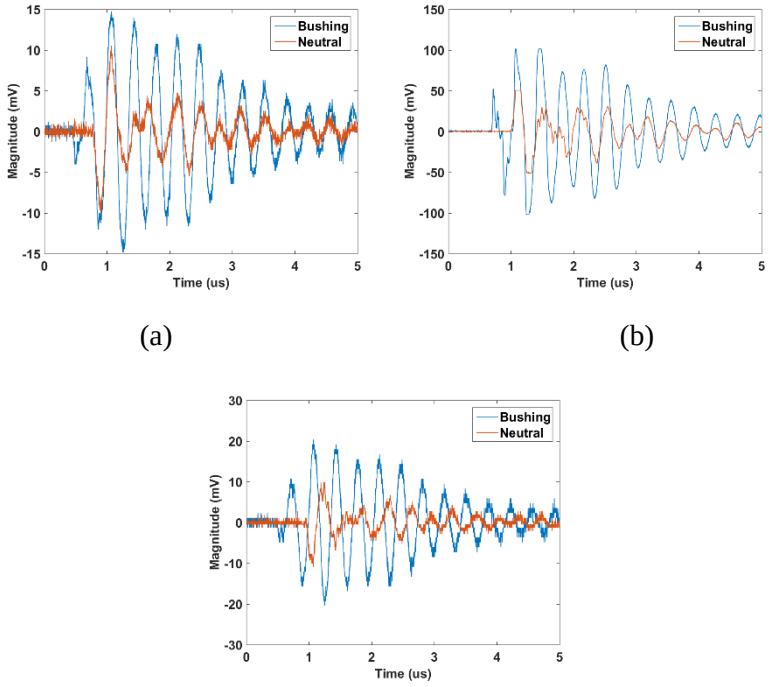

(a) (b)

(c)

Figure 3.6.3. PD pulses plots for injection at Terminal 3 for: (a) Surface discharge, (b) Void discharge and (c) Floating discharge.

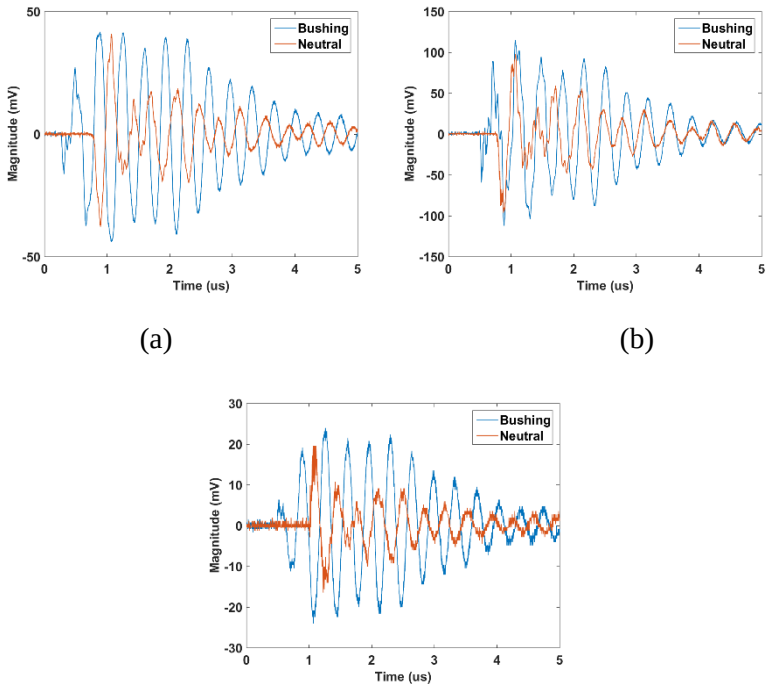

(a) (b)

(c)

Figure 3.6.4. PD pulses plots for injection at Terminal 4 for: (a) Surface discharge, (b) Void discharge and (c) Floating discharge.

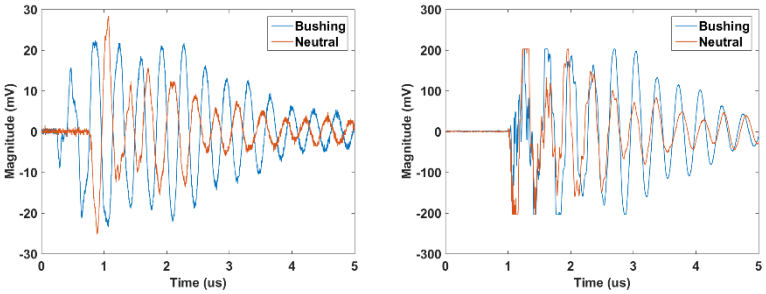

(a)

(b)

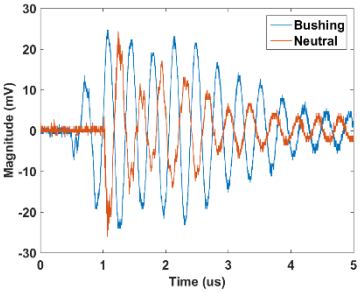

(c)

Figure 3.6.5. PD pulses plots for injection at Terminal 5 for: (a) Surface discharge, (b) Void discharge and (c) Floating discharge.

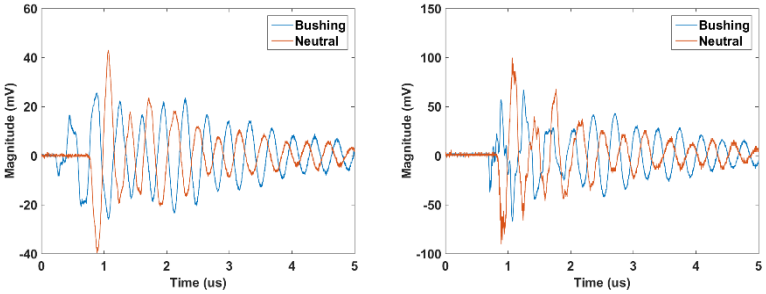

(a)

(b)

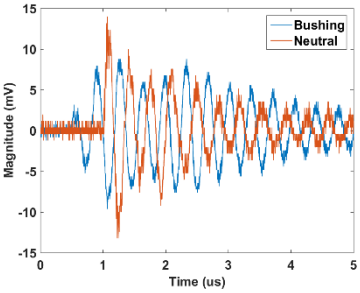

(c)

Figure 3.6.6. PD pulses plots for injection at Terminal 6 for: (a) Surface discharge, (b) Void discharge and (c) Floating discharge

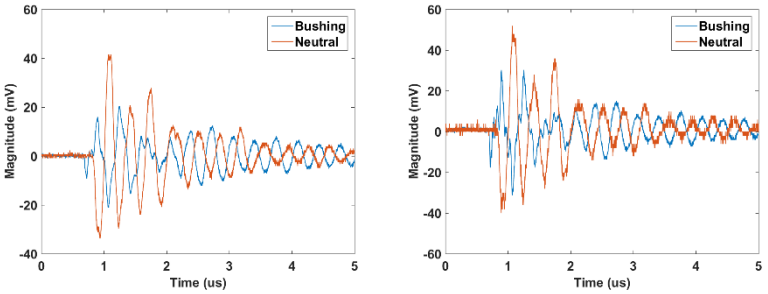

(a) (b)

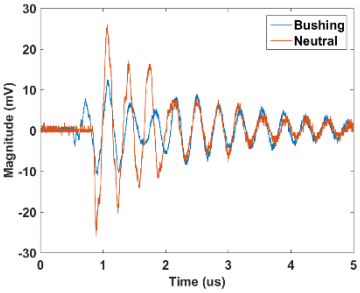

(c)

Figure 3.6.7. PD pulses plots for injection at Terminal 7 for: (a) Surface discharge, (b) Void discharge and (c) Floating discharge.

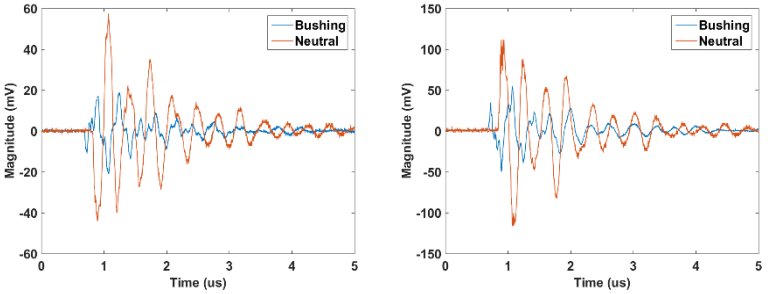

(a) (b)

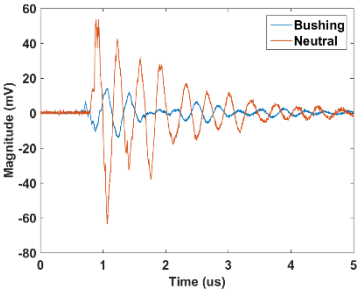

(c) .

Figure 3.6.8. PD pulses plots for injection at Terminal 8 for: (a) Surface discharge, (b) Void discharge and (c) Floating discharge.

Figure 3.6.1 highlight that the magnitude of measured PD signals at bushing tap measurement point is significantly greater than the magnitude of pulses measured at neutral to earth measurement point when the PD signals are injected into terminal 1. However, from Figure 3.6.2 to Figure 3.6.4, when the injection point moves along from terminal 2 to terminal 4 of the transformer winding, the difference between magnitude of pulses from bushing measurement point and neutral to earth measurement point decreases. The magnitudes from both measurement points are almost the same when PD signals are injected into terminal 5 and beyond that point, the magnitudes of pulses from bushing measurement point become smaller than the magnitudes of pulses measured at neutral to earth measurement point which can be seen from Figure 3.6.5 to Figure 3.6.8.

The variation in term of magnitude of pulses from both measurement points is due to the length of propagation path that the pulses needed to travel from injection points to the measurement points. PD signals suffer attenuation and distortion before reaching the measurement point and different injection points have different propagation path, therefore have different level of attenuation and distortion. Hence, comparison with the data obtained using the signal generator reveals that the characteristics of signals propagation from artificial PD sources are similar to the characteristics of signal propagation when using signal generator. However, solely focusing on the variation of the magnitude is not an ideal parameter in order to determine sources location within a transformer winding because the initial discharging magnitudes of PD signals at discharge location is unknown. Hence, advanced signal processing techniques are required in order to analyse the measured data to produce derivation of energy vectors associated with the signals.

3.7 SUMMARY

This chapter introduces the development of artificial PD sources that were used in this investigation. These sources were created in order to produce PD measurement data which was ultimately used to study the multiple PD sources identification and localisation approaches for a transformer winding. Three different applied voltages were used to simulate PD activity at different voltages. The purpose of the undertaken test is to provide information

regarding PD activity and whether it is influenced by applied voltages in terms of numbers and intensity of events. It is shown that increased voltage results in a greater magnitude of discharge as well as a higher number of discharges. When the applied voltage is increased, the electric field is enhanced and the electron generation rate is increased. Therefore, initial free electrons will be larger which then resulting in more PDs occurring.

A number of preliminary experiments were undertaken. The initial experiment involved quantifying the sensitivity and background noise of the experiment with regard to the PD measurement. Various experiment arrangements and developments employed within this research are also explained in this chapter.

An initial pulse generator source injection experiment was used to develop a preliminary understanding of the characteristics of the PD source signals propagation within the transformer winding. Two RFCTs were used as the measurement sensors to capture the propagated PD pulses. The sensors were placed at both ends of the winding which were at bushing tap point to earth and neutral to earth point. This is due to the fact that discharges occurring inside transformer windings can be considered as travelling waves which will propagate from a source location towards both ends of the transformer winding that have connection to earth.

The plotted signals at the bushing tap point and neutral to earth measurements show that there are attenuation and distortion processes during the signal propagation which affect the signal characteristics; magnitude and energy content. The attenuation process depends on path taken from the source injection location to the measurement points. These features can be exploited in order to identify and estimate the PD sources within a transformer winding. These findings were used to compare with experiment data obtained using artificial PD sources. There are two experiments involving the artificial PD sources; single source injection and multiple sources injection experiments. The captured signals will be analysed using signal processing techniques which are discussed in the next chapter.

CHAPTER 4

PARTIAL DISCHARGE SIGNAL PROCESSING

As has already been discussed, measurement data was obtained from two RFCT sensors located at the bushing tap point and neutral to earth point. It is assumed that, during the propagation of the signals along transformer windings, the response is attenuated and distorted by the propagation path taken and termination characteristics altering the output waveforms. This produces changes in the energy characteristics of the signals when they reach both measurement sensors. Advanced signal processing techniques are required in order to analyse the measured data and to produce energy vectors associated with the signals.

4.1 PARTIAL DISCHARGE SIGNAL DECOMPOSITION

The purpose of signal decomposition is to reveal intrinsic components which are representative of the measured PD pulses related to the corresponding PD sources in decomposed signals. In this thesis, two decomposition techniques used in order to decompose the measured PD signals from both measurement points. The details of both techniques are discussed in this chapter.

4.1.1 WAVELET ANALYSIS

Wavelet analysis has been widely used in the area of frequency analysis within signal processing for both research and practical applications. In the field of PD analysis, wavelet analysis is gaining increasing interest. Its ability to extract information from transient signals in both the time and frequency domain makes wavelet analysis a powerful tool for signal processing, especially in the analysis of PD in HV power transformers [54], [89]. In this research, wavelet analysis is used to analyse PD signals in the time and frequency domains. Hence, the PD signals can be described as components in different frequency ranges.

Wavelet analysis is a time-frequency analysis method, making it more suitable than the Fourier transform which is only a frequency analysis method. Wavelet analysis has been applied not only in detecting fault location [90], but also in analysing of power system transients [91] and power quality [92]. The operation of both wavelet and Fourier transform is similar though they both represent the original signal in a different form.

There are differences between those techniques, wavelet analysis retains signal information in both the time and frequency domain while Fourier transform retains signal information in just the frequency domain. The biggest difference between wavelet analysis and Fourier transform is that Fourier Transform employs a sine wave as its base function, while Wavelet Transform, employs a user-defined Mother wavelet [16], [59].

There are several families of mother wavelets, such as Harr, Daubechies, Coiflet and Symlet [93]. In PD analysis, the choice of the mother wavelet plays a significant role. In previous research [16], a comparison of mother wavelets was made and suitable mother wavelets were chosen. The Symlet and Daubechies wavelet families have been identified as suitable for PD analysis.

The study used different types of wavelet families and orders. There was some similarity in the results produced from different wavelets. The study showed that wavelet families ‘db9’ and ‘sym6’ produced the best results according to the separation distance plots for Daubenchies and Symlet families.

Another study, showed that among the available wavelets families, the Daubenchies wavelet family has several desirable properties such as limited duration, compactness, asymmetry and orthogonality for analysis of fast transient and irregular pulses [43]. The key concept behind wavelet analysis is that a given signal can be decomposed into a series of scaled and time shifted forms of mother wavelet producing a time-scale view of a signal from which the original signal can be recovered.

Wavelets can be divided into two groups; Continuous Wavelet Transforms (CWT) and Discrete Wavelet Transforms (DWT). The CWT of a time-dependent signal f(t) can be expressed as:

$$W_{\psi}f(a,b) = |a|^{-\frac{1}{2}} \int f(t)\,\psi\left(\frac{t-b}{a}\right) dt \qquad (4.1)$$

The wavelet coefficients of CWT are calculated at every possible scale and for every time instant. The value of $W_{\psi}f(a,b)$ represents the similarity between the examined section of f(t) and the scaled and shifted wavelets. While the DWT is realized by characterizing the scale variable a in $a = 2^m$ and assuming that the time variable b as $b = n2^m$ at a given scale m where m and n being integer values. Thus avoiding time consumed by coefficient calculation and at the same time eliminating wavelet coefficient redundancy [16], [43].

The individual PD pulses have been processed via DWT which involves a multi resolution algorithm. At this stage, a PD signal is decomposed into different scales of different time and frequency resolutions which provides good frequency resolutions with poor time resolution at low frequency and vice versa. The process is performed by passing the PD signal through a series of a quadrature filters. The filters consist of a pair of complementary high-pass (HPF) and low-pass filters (LPF), which divide up of the original signal (S), into a series of approximation coefficients (cA1) and detail coefficients (cD1) at the 1st level.

The process is performed iteratively on the approximation coeeficients of the previous iteration, with each iteration producing another set of approximate (cA) and detailed (cD) coefficients. The first approximate coefficients (cA1) which are decomposed from the original signal (S) will again decompose into the next level, producing a new set of approximate coefficients (cA2) and a new set of detailed coefficients (cD2) at the 2nd level. This process is repeated up to a pre-determined number of times (n-level).

Figure 4.1.1 shows the iterative decomposition process of the wavelet transform where (cA) and (cD) represent the approximate and detailed coefficients of the Wavelet filter.

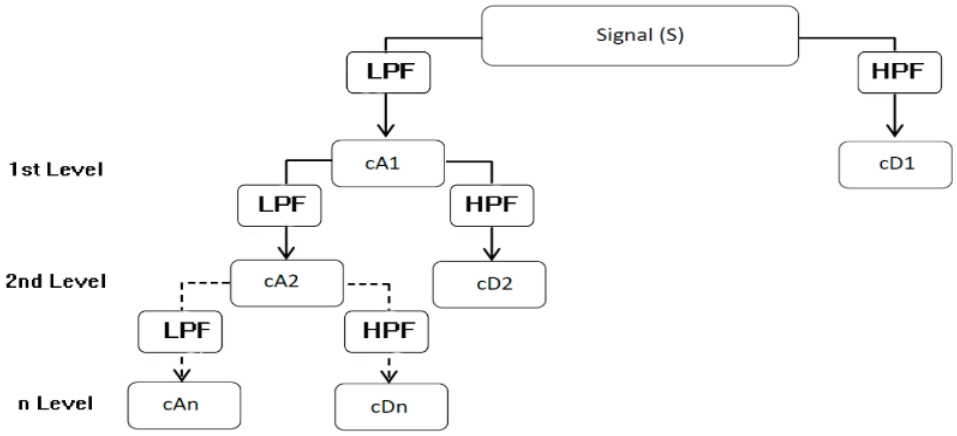

Figure 4.1.1 An iterative Wavelet decomposition process

The decomposition levels need to be carefully chosen as it can be useful to prevent unwanted loss of any PD signal in the frequency region of interest. The decomposition level needs to fulfil the condition of the Wavelet function (ψ) and scaling function (φ) in terms of its support length. This is unique based on the number of the order. Apart from that, the maximum decomposition level also depends on the number of data points and the length of the filters. This is due to the sample being down-sampled by a factor of 2 from one level to the next level. The relationship between a LPF with the scaling function and a HPF with the Wavelet function can be mathematically defined as:

$$\varphi(\mathrm{n}) = \sum_{m=0}^{N} g(m)\Phi(2\mathrm{n} - \mathrm{m}) \tag{4.2}$$

$$\psi(\mathrm{n}) = \sum_{m=0}^{N} \mathrm{h}(m)\Phi(2\mathrm{n} - \mathrm{m}) \tag{4.3}$$

where g and h represent a LPF and a HPF respectively.

If a PD input signal I_s is applied to Equation 4.2 and Equation 4.3, the output of the first decomposition level of wavelet analysis can be calculated using [94]:

$$A_1(t) = I_s(t)\ \varphi(\mathrm{n}) \tag{4.4}$$

$$D_1(t) = I_s(t)\psi(\mathrm{n}) \tag{4.5}$$

where A and D are the approximate and detailed coefficients of the wavelet analysis iteration.

4.1.1.1 **Wavelet energy distribution**

In this investigation, wavelet analysis is used to decompose the measured PD signals in both the time and frequency domains and then identify the distribution of signal energies from the wavelet approximation and details coefficients as feature vectors. This approach has been successfully applied in PD classification technique [12]. The measured PD signals can be described by components in the different frequency ranges.

A mother wavelet of Daubechies order 9 (db9) was applied to each of PD pulse to decompose the signal into nine levels, presented in the form of a ten dimensional vector which consist of the detailed and the approximate coefficient of the original signal. Figure 4.1.2 and Figure 4.1.3 show an example of wavelet decomposition coefficients for all detail and approximation of ninth level for a PD pulse that has been measured from the bushing tap point to earth and neutral to earth connection measurement points of a transformer.

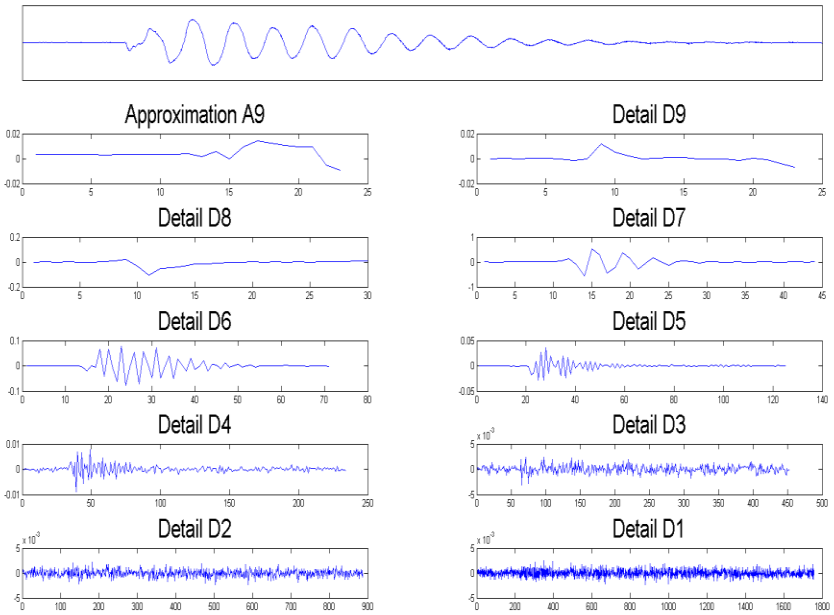

Figure 4.1.2 A PD pulse with its associated Wavelet decomposition coefficients - measured at the bushing tap point to earth.

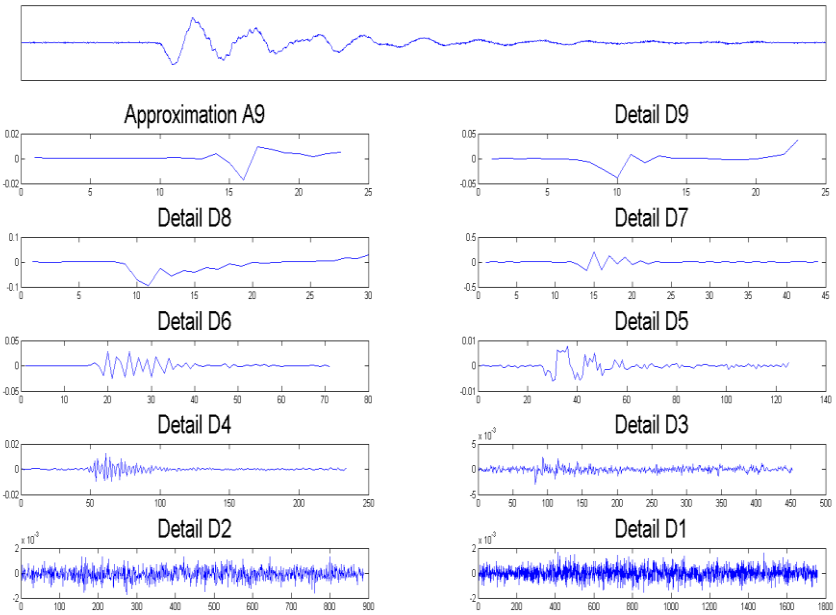

Figure 4.1.3 A PD pulse with its associated Wavelet decomposition coefficients - measured at the neutral to earth point.

By using the series of approximate coefficients (cA) and detailed coefficients (cD) for n-levels (in this case 9 levels), the distribution of signal energy in each decomposition level which is the percentage of energy corresponding to the details energy (E_D) and approximation energy (E_A) can be calculated using:

$$E_{Di} = \frac{\sum_{j=1}^{Nci} Cd_{i_j}^2(t)}{\sum_{i=1}^{n}\sum_{j=1}^{Nci} Cd_{i_j}^2(t) + \sum_{j=1}^{Ncn} Ca_n^2(t)} \times 100\% \quad (4.6)$$

$$E_{An} = \frac{\sum_{j=1}^{Ncn} Ca_n^2(t)}{\sum_{i=1}^{n}\sum_{j=1}^{Nci} Cd_{i_j}^2(t) + \sum_{j=1}^{Ncn} Ca_n^2(t)} \times 100\% \quad (4.7)$$

Where n, Cd and Ca are the decomposition level, detail decomposition coefficients and approximate decomposition coefficients respectively. In term of data dimensionality reduction, these energy levels were found to be more effective at representing the PD pulse compared to just using wavelet decomposition coefficients [12].

However, in order to differentiate which measured signals either measured at the bushing tap point or neutral to earth point contain greater total energy, this wavelet energy distribution is not practical. This is because the wavelet energy distribution has been scaled to give 100 percent for both measurement points.

The use of absolute energy distribution (total energy of the generated signal) is found to be more useful rather than the individual wavelet energy for each measured signal. This is because the use of absolute energy revealed the variation of energy at different measurement points as well as at different injection terminals [16].

The percentage of energy contained in each decomposition level for both measurement points can be represented as a fraction of each decomposition level energy to the generated PD signal and can be calculated using:

$$E_A = \frac{\sum_{j=1}^{N_C} Ca_j^2}{\sum_{i=1}^{D_L}\sum_{j=1}^{N_c} Cd_{b_j}{}^2 + \sum_{i=1}^{D_L}\sum_{j=1}^{N_c} Cd_{n_j}{}^2 + \sum_{j=1}^{N_c} Ca_{b_j}{}^2 + \sum_{j=1}^{N_c} Ca_{n_j}{}^2} \tag{4.8}$$

$$E_{D_i} = \frac{\sum_{j=1}^{N_C} Cd_i^2}{\sum_{i=1}^{D_L}\sum_{j=1}^{N_c} Cd_{b_j}{}^2 + \sum_{i=1}^{D_L}\sum_{j=1}^{N_c} Cd_{n_j}{}^2 + \sum_{j=1}^{N_c} Ca_{b_j}{}^2 + \sum_{j=1}^{N_c} Ca_{n_j}{}^2} \tag{4.9}$$

where N_c is the number of coefficients, D_L is the number of decomposition level, Ca_b and Ca_n are approximate coefficients for bushing tap point and the neutral to earth connection, while Cd_b and Cd_n are the coefficients for the detail levels.

4.1.2 MATHEMATICAL MORPHOLOGY

Mathematical Morphology (MM) was originally introduced as an image processing technique by Matheron and Serra. Later, the application of MM has been extended into feature extraction and machine fault diagnosis [95]–[98]. The concept of signal processing using MM is to modify the shape of a signal by transforming it through the interaction with another object. Recently, it has been used in other areas such as signal processing. In signal processing, the only determinative factor is the information of local morphological features of the signals. A complex signal can be separated from the background and decomposed into several components while the morphological features of the signal are still preserved [99].

The operation of MM is based on mathematical operators, which are applied to the captured PD signals using structure elements (SE). SE is a pre-defined geometric shape with finite length used to interact with a given signal, with the purpose of determining how this shape fits the shape of the signal [100], [101]. There are two types of SE; non-flat and flat structuring elements. In this paper, flat structuring elements are chosen due to their simplicity and their ability to detect positive and negative peaks of any signals [95][102]. When a flat

structuring element is used, it will not consider its amplitude since the flat structuring element is a straight line and its amplitude in the vertical direction is zero. Since only a single parameter (flat structuring element) is considered in the operation of MM decomposition, it does not need a user to choose an appropriate parameter or function as in the case for wavelet-based analysis. Additionally, according to [98], the shapes of the SE only have little effect on the analysis.

Two basic set operations used in MM are the Minkowski set addition and the Minkowski set subtraction. The Minkowski set addition between two sets A and B of numbers can be defined as:

$$A \oplus \mathrm{B} = \{\alpha + b, a \in A, b \in B\} = \bigcup_{b \epsilon B} A_b \tag{4.10}$$

where ϵ represents the set inclusion, $\cup$ represents the set union and A_b is a set obtained by shifting the origin of the set A at distances determined by the elements b of the set B. Then the Minkowski subtraction can be calculated using:

$$A \ominus B = (A^c \oplus \mathrm{B})^c = \bigcap_{b \epsilon B} A_b \tag{4.11}$$

where A^c represents the complement of the set A and $\cap$ represents the set intersection. The subtraction of the two sets A and B is a set consisting of the common elements of the sets A_b, which are obtained by shifting the origin of the set A at distances determined by the elements of the set B. Based on the Minkowski addition and subtraction, two morphological operations called as dilation and erosion operators can be defined as:

$$dil(A, B) = A \oplus B^r = \{x, B_x \cap A = \varnothing\} = \bigcup_{b \epsilon B} A_{-b} \tag{4.12}$$

$$er(A, B) = A \ominus B^r = \{x, B_x \subseteq A\} = \bigcap_{b \epsilon B} A_{-b} \tag{4.13}$$

where $\subseteq$ represents the set inclusion and B_r represents the set obtained by reflecting the set of B with respect to the origin.

From dilation and erosion operation definitions, another morphological operation called closing and opening operation can be defined:

$$cl(A,B) = A \bullet \mathrm{B} = (\mathrm{A} \oplus B^r) \ominus B \tag{4.14}$$

$$op(A,B) = A \circ \mathrm{B} = (\mathrm{A} \ominus B^r) \oplus B \tag{4.14}$$

In order to account for multilevel signals defined by a discrete or a continuous function, MM provides two different and equivalent approaches in representing functions by sets. The first approach uses the concept of the cross-section of a function and the second approach uses the umbra of the function. The details of both approaches are explained in [97]. After some mathematical derivations from both approaches, the four basic mathematical morphological operations are achieved. For a signal f(k), defined over a domain D_f, and for a function g(u) of length L over a domain D_g, called the structuring element (SE), the dilation, erosion, opening and closing operations of the signal f(k) by element g(u) can be defined as:

$$dil(k) = (f \oplus \mathrm{g})(\mathrm{k}) = \ max_{y \epsilon Dg}\{f(k+u) + g(u)\} \tag{4.15}$$

$$er(k) = (f \ominus \mathrm{g})(\mathrm{k}) = \ min_{u \epsilon Dg}\{f(k+u) - g(u)\} \tag{4.15}$$

$$cl(k) = (f \bullet \mathrm{g})(\mathrm{k}) = er\big(dil(k)\big) \tag{4.16}$$

$$op(k) = (f \circ \mathrm{g})(\mathrm{k}) = dil\big(er(k)\big) \tag{4.17}$$

Different mathematical operators in MM give different extracted shapes. The effects of each operator in MM are shown in Figure 4.1.4.

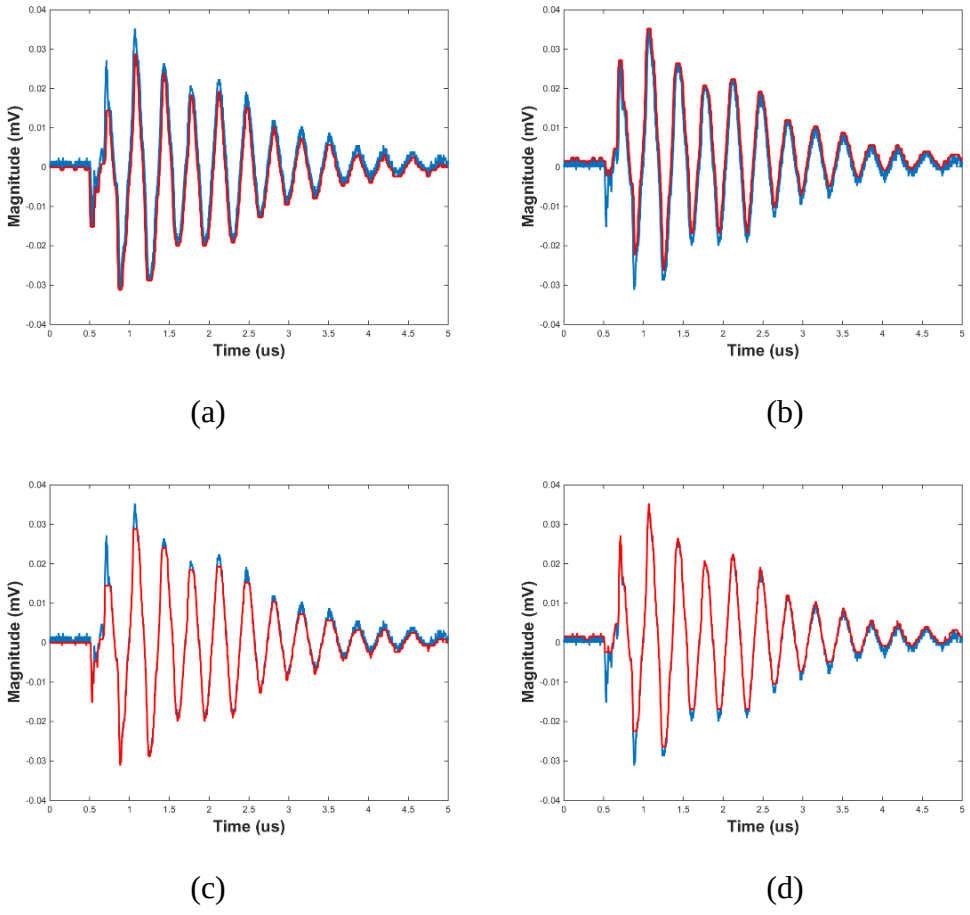

Figure 4.1.4. Effects of mathematical morphology operators (red lines) on original signal (blue lines). (a) Erosion, (b) Dilation, (c) Opening and (d) Closing.

Figure 4.1.4 highlight that the Erosion operator minimizes positive peaks while the Dilation operator enlarges positive peaks. On the other hand, the Closing operator maintains positive peaks and cuts negative peaks while the Opening operator maintains negative peaks and cuts positive peaks. However, in this research, opening and closing operators were used as they preserve negative and positive peaks in the data. When opening and closing operators were used, the amplitudes of positive and negative peaks of the original PD signals will be unchanged before and after execution of opening and closing operation. In order to maintain integrity of decomposed PD signals in this research, opening and closing operators were chosen. Based on [102], changing the lengths of SE allows investigation of different

frequency ranges within the PD signal. Therefore, the decomposed signal in this work is obtained by increasing the length of SE incrementally to analyse different frequency bands of the captured PD pulse.

4.2 PARTIAL DISCHARGE DATA MINING

The role of data mining for this application involves identifying, extracting and visually representing key information from a large data-set. A key requirement of a data-mining technique is to reduce the computational requirement for a given process. In the context of this work, data mining is employed to identify specific features of individual PD pulses with the aim of identifying pulses with similar characteristics that can be attributed to individual sources.

4.2.1 PRINCIPLE COMPONENT ANALYSIS (PCA)

There are a lot of linear transformation analyses like factor analysis, linear discriminant analysis and projection pursuit analysis that have been used in pattern recognition for feature extraction and dimensionality reduction [103]. However, in this work, in order to reduce the dimensionality from decomposition techniques data down to lower dimensions and allow for visualisation, Principle Components Analysis (PCA) which is a non-parametric linear method has been applied. PCA is one of important techniques in PD analysis. PCA can be applied as a data mining tool in order to reveal or extract any hidden patterns inside raw data as known as feature extraction as well as PD classification [19]. This technique relies on the assumption that pulses exhibiting similar energy-frequency characteristics that have been generated by the same source will occupy a localized region of 3-D space. By using this technique, the extracted PD pulses could be represented in 3-D space whilst minimizing the information lost during the dimension reduction process [12].

Generally, PCA transforms the original variables based on an orthogonal linear transformation in the direction of the greatest variance in the variables [16][104]. As a result, the new principal component values represent the original data and the original information can be retained as much as possible whilst removing any redundancy. The data first is

standardized by subtracting the mean value for each dimension to provide zero mean and unity variance. The covariance matrix (C_m) can be obtained using:

$$C_m = \frac{M.M^T}{N-1} \tag{4.14}$$

where the WE distribution data is M and N is the processed PD pulses. From the covariance matrix, the eigenvalues (λ) and eigenvectors (υ) are obtained and the eigenvalues are arranged in descending order. The matrix (C_m) is transposed into a projection, Pi using the eigenvectors (υ) such that:

$$P_i = \upsilon^T \times M \tag{4.15}$$

Therefore, each row of the projection, P_i represents principal components, with decreasing significance. The new representation of the data in 3-D feature space can be plotted using the three lower order principal components [12], [16], [59].

4.2.2 t-Distributed stochastic neighbour embedding (t-SNE)

Instead of using PCA, t-SNE has also been used in this investigation as a dimensional reduction technique in order to compare performance in terms of reducing the dimensionality of the distributions of the PD data. The aim of t-SNE as well as PCA is to preserve as much as possible of the significant structure in a lower dimensional space from the high-dimensional data. t-SNE [105] is a highly flexible dimensionality reduction technique. The concept of the algorithms is based on a probabilistic modelling of points in the original space and the projection space. It tries to preserve the probabilities as much as possible as measured by the Kullback-Leibler distance [106]. t-SNE is a variation of stochastic neighbour embedding that is simpler in terms of optimization, and by reducing the tendency to crowd points together in the centre of the map, it produces much better visualizations. Additionally, t-SNE has improved performance compared to existing techniques in creating a single map that reveals data structure at many different scales. This is very important for high dimensional data that lie on several different, but related, low-dimensional manifolds, such as images of objects from multiple classes seen from multiple viewpoints, which is similar

to the situation of PD pulses generated from multiple PD sources within a system measured by an ultra-wide bandwidth PD sensor [105]. SNE transforms the Euclidean distances between data points in the high dimensional space into conditional probabilities $p_{j|i}$ which represent similarities. The conditional probability $p_{j|i}$ is given by:

$$P_{(j|i)} = \frac{\exp\left(-\frac{\|x_i - x_j\|^2}{2\sigma_i^2}\right)}{\sum_{k \neq i} \exp\left(-\frac{\|x_i - x_j\|^2}{2\sigma_i^2}\right)} \tag{4.16}$$

Where ∂_i is the variance of the Gaussian distribution that is centred on data point x_i.

Similarly, for the low dimensional counter parts y_i and y_j of the high dimensional data point x_i and x_j, its conditional probability $q_{j|i}$ is calculated using:

$$q_{(j|i)} = \frac{\exp\left(-\|y_i - y_j\|^2\right)}{\sum_{k \neq i} \exp(-\|y_i - y_j\|^2)} \tag{4.17}$$

For highly similar pairwise data points and correct mapping, $p_{j|i} = q_{j|i} = 0$. Therefore, the SNE aims to find a low dimensional data representation that minimizes the mismatch between $p_{j|I}$ and $q_{j|i}$ [69].

The t-SNE then improved performances of SNE by using a different cost function. The cost function used in t-SNE is different from cost function used in SNE. In t-SNE uses a symmetrized version of the SNE cost function which have simpler gradients. It also uses a Student-t distribution rather than a Gaussian used in SNE to compute the similarity between two objects in the low dimensional space. Additionally, in order to overcome the crowding and optimization problems created by SNE, t-SNE employs a heavy-tailed distribution in the low dimensional space [105]. The application of t-SNE as a dimensional reduction technique in this investigation is mainly based on the local properties of the captured PD data whereas some important global structures are also retained and revealed.

4.2.3 TIME-FREQUENCY SPARSITY ROUGHNESS MAPPING

In feature extraction and classification, the time or frequency domain descriptions of a signal alone do not provide comprehensive information. In the time domain, the frequency descriptions of the signals are not provided. While in frequency domain, it cannot depict how the spectral content of the signal changes with time. Hence, in order to overcome this problem, the time variable is introduced in the frequency domain which provide a proper description of the spectral content changes as a function of time. To visualise the changes of spectral content as a function of time, a time frequency (TF) map is introduced.

TF mapping is widely used in separation of multiple PD sources. This technique is based on the assumption that different shapes of PD pulses are characterized by different types of PD sources [14], [76], [107], [108]. For a PD pulse, p, with N samples, a time reference is defined as:

$$t_o = \frac{\sum_{i=0}^{N} t_i p_i(t_i)^2}{\sum_{i=0}^{N} p_i(t_i)^2} \tag{4.18}$$

where t_i represents the time instant of acquiring the i^{th} sample. The equivalent time length of a PD pulse is defined as:

$$T^2 = \frac{\sum_{i=0}^{N} (t_i - t_o)^2 \, p_i(t_i)^2}{\sum_{i=0}^{N} p_i(t_i)^2} \tag{4.19}$$

If P is the frequency value obtained from Fourier transform, the equivalent bandwidth of a PD pulse is defined as:

$$F^2 = \frac{\sum_{i=0}^{\frac{N}{2}} {f_i}^2 \, |P_i(f_i)|^2}{\sum_{i=0}^{\frac{N}{2}} \; |P_i(f_i)|^2} \tag{4.20}$$

where f_i represents the frequency at the i^{th} sample [109].

Then, the TF map is obtained by projecting T^2 and F^2 of each PD pulse onto a two dimensional space. In this space, the projected objects which belong to PD pulses having similar shape, will merge together to form a distinct group. However, PD pulses generated from the same

PD source, which are supposed to have similar values of T^2 and F^2 and locate closely on the TF plane, can be scattered into different groups. Therefore, (see Chapter 5), TF sparsity roughness map is used instead of TF map itself. It is constructed based on calculated sparsity and its roughness values in decomposed signals in both time and frequency domains with multi resolutions. This TF sparsity roughness map can provide improved accuracy in terms of representing PD pulses compared to the TF map [109].

4.3 PARTIAL DISCHARGE CLUSTERING

Partial discharge clustering techniques were employed to identify subsets within the experiment data automatically. This technique relies on the assumption that different PD pulse waveforms produced by different source will contain different characteristics and subsequently occupy different localised region of a feature space. Two density based clustering techniques have been identified as being suitable for this task.

4.3.1 DENSITY-BASED SPATIAL CLUSTERING OF APPLICATIONS WITH NOISE (DBSCAN)

DBSCAN was used to assign the clustered data into specific classes based on the variation of point density in a set volume as defined by the minimum number of data point and neighbourhood radius. DBSCAN clustering algorithm has the ability to discover clusters of arbitrary shape in n-dimensional space as well as distinguishes noise. DBSCAN is one of the promising techniques of data clustering, which was applied to the data in a specific space to group the data into specific classes or clusters accordingly based on the concept of density. Theoretically, the density of any clusters is higher than the density of the noise and for each cluster, it has different value of density. Therefore, DBSCAN is a method to separate regions of high density and low density.

The DBSCAN algorithm uses three important parameters which are Epsilon (ε), minimum number of points (n-minimum) and the volume (v). The basic ideas of DBSCAN involve a number of definitions. The first step of DBSCAN is that the density represents the number of points (n), surrounding a certain point of data (p_n), within a small volume (v). The volume

can be assumed as a sphere of radius ε centred at p_n. By using n-minimum, the threshold density can be specified to make the volume v, significantly dense. The point p_n can be defined as either a dense point, known as a core point, or a non-dense point (border point or non-core point). The rules used to define the method are [12], [65]:

- If a number of points (n) contains at least a minimum number ($n \geq$ n-minimum) of points within the radius ε, centred at p_n and are included in the volume v, the point p_n is called a core point.
- p_n is called a border point if a number of points (n) contains at less than minimum number ($n <$ n-minimum) of points within the radius ε, centred at p_n and are included in the volume v.
- If point q is included in v, within the radius ε and p_n is a core point, point q is called directly-density reachable (DDR) from point p_n.
- A point r is called density reachable (DR) from p_n within volume v with respect to the radius ε, if there is a chain of objects p_1, p_2……p_k, where $p_1=p_n$, $p_k=r$ such that, p_{i+1} is DDR from p_i.
- A point s is called density-connected to p_n with respect to radius ε if there is a point t such that both points, s and p_n are density reachable from point t with respect to the radius ε.
- Any point which not belong to any group of point (p_n, q, r or s), it is considered as a noise points.

DBSCAN then checks the condition of point p_n for any given ε and n-minimum value. If the point p_n is a core point, it selects the DR and DDR points and expands the cluster by merging neighbouring dense regions together. If p_n is a border point, then no points are DR from p_n and DBSCAN visits the next point of the database. The point p_n initially can be selected randomly or resorting to the maximum or minimum weight of a selected function. Then, once the border of the first cluster is identified, DBSCAN will select another point p_n in the 3-D space which does not belong to a previous cluster and this process is a repetitive process and will terminates when no new point can be detected to add to any previous formed clusters.

4.3.2 ORDERING POINTS TO IDENTIFY CLUSTERING STRUCTURE (OPTICS)

Another density based clustering technique known as OPTICS has been used in order to reveal clusters of pulses that have similar characteristics in terms of their energy distribution. The key concept of density based clustering technique is that for each object of a cluster in a space, the neighbourhood of a given radius has to contain at least a minimum number of objects. OPTICS was found suitable for signal separation for its ability to discover clusters of arbitrary shape with different densities in n-dimensional space [110]. The OPTICS algorithm uses two important parameters, which are the radius ϵo, of the neighbourhood of each object in a data set, and the minimal number of objects considered as a cluster, k. Two definitions are needed to describe OPTICS; first is the core distance (CD) which is a distance between i^{th} object and its k neighbour, second is the reachability distance (RD) of the jth object which is a maximum of distances between the jth object and the nearest object and the core distance of the nearest object. The algorithms of OPTICS can be presented as follows [111], [112]:

1. First an object is randomly chosen known as the current object and marked as processed. Then it is plotted in the reachability plot in the first position which is an undefined value.
2. The RD was then calculated for all objects with respect to the marked current object.
3. The object with the smallest RD to the marked current object is selected and its RD was plotted in the reachability plot in the next position and this object is marked as the new processed object (new current object).
4. The RD of all the remaining not processed objects is calculated with respect to the new current object. If the current RD for any object is smaller than the previous RD for that object, replace it with the new current RD. Step 3 and 4 are repeated until all objects are processed.

Although OPTICS does not produce groups or clusters of the applied data by itself, it gives detailed information about n dimensional data structure, which can be visualized using the reachability plot. In terms of plotting, OPTICS ordered the points on the x-axis and the reachability distance on the y-axis in the reachability plot. Within the reachability plot, clusters are visible as valleys and are separated by large spikes. The higher the spikes, the more different the data will be in the clusters; and the lower the valley, the denser the cluster.

4.4 SUMMARY

In order to process and visualise the partial discharge activity, an important function of using PD analysis as a feature diagnostic tool, an overview of a number of techniques has been presented in this chapter. This chapter was divided into three main parts which are partial discharge signal decomposition, partial discharge data mining and partial discharge data clustering techniques. Wavelet transform and mathematical morphology are proposed as the signal decomposition techniques in this investigation in order to analyse the measured signals in the time and frequency domains and to decompose the signals into different regions of frequency from both measurement points. Signal decomposition techniques are used to reveal intrinsic components which are representative to the measured PD signals related to the corresponding PD sources. In order to reduce the dataset produced to the useful dataset for the visualisation and feature extraction, PCA, t-SNE and time-frequency mapping are proposed as the partial discharge data mining techniques and briefly explained in this chapter. These techniques have been employed with the objective to identify specific features of individual PD pulses with the aim of identifying pulses with similar characteristics that can be attributed to individual sources. This approach relies on the assumption that PD pulse waveforms produced by the same source generate similar characteristics and subsequently occupy a localised region of feature space, Two clustering techniques are proposed to automatically identify subsets within the data set produced from data mining techniques. The two techniques known as DBSCAN and OPTICS have been proposed and explained.

CHAPTER 5

DECOMPOSITION TECHNIQUES

A decomposition technique is a technique that is able to represent signals using different levels based on their frequency ranges. Two techniques; wavelet analysis and mathematical morphology decomposition were employed to generate a representation of an original measured PD signal into different components.

5.1 DECOMPOSITION USING WAVELET ENERGY DISTRIBUTION

Wavelet energy distribution was performed on PD measurement data obtained from the bushing tap point and neutral to earth connections. The original signal is decomposed into a user defined number of levels where at each level is half the bandwidth (sampling rate in frequency domain) and half length (number of samples in time domain) than the level from which it was derived. It effectively characterizes the original signal at various frequency ranges that are then represented by coefficients at each node of the decomposition tree.

It is assumed that the selected decomposition coefficients effectively represent the unique characteristics of PD pulses generated from different discharge sources. In order to show the percentage of energies at different composition levels for different PD signals, energy distribution histograms are used to facilitates an easy comparison between different PD pulses. Figure 5.1.1 to Figure 5.1.3 visualise the percentage energy distribution histograms generated from surface, void and floating discharge pulses using the Mother Wavelet of ‘db9’ with nine decomposition levels.

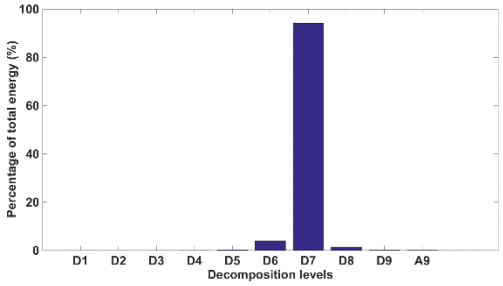

(a) Bushing tap point

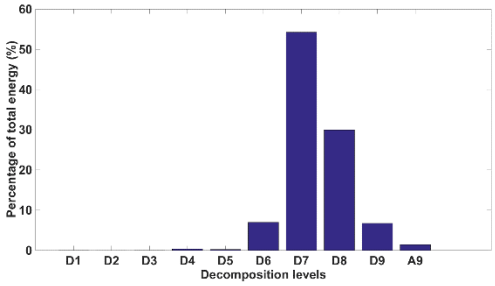

(b) Neutral to earth point

Figure 5.1.1. Histogram representing the energy distribution of signal between different decomposition coefficients of surface discharge.

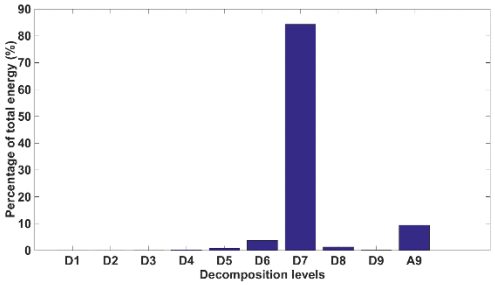

(a) Bushing tap point

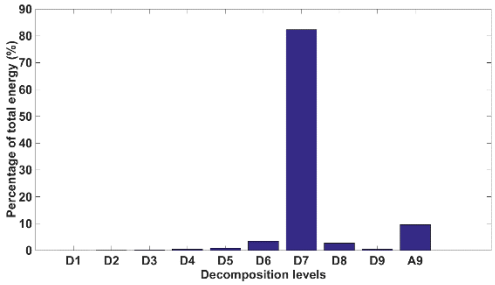

(b) Neutral to earth point

Figure 5.1.2. Histogram representing the energy distribution of signal between different decomposition coefficients of void discharge.

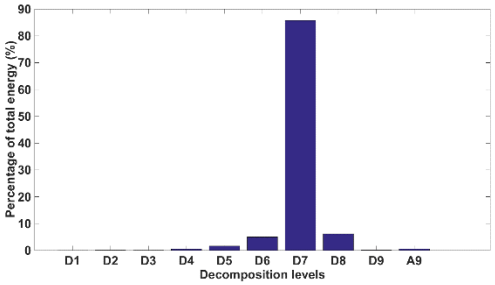

(a) Bushing tap point

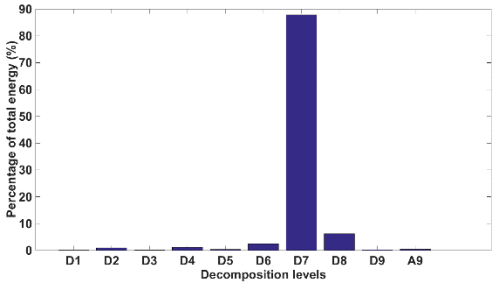

(b) Neutral to earth point

Figure 5.1.3. Histogram representing the energy distribution of signal between different decomposition coefficients of floating discharge.

A comparison of Figure 5.1.1 – Figure 5.1.3 shows that the percentage of energy distribution for both measurement points is varied at different decomposition levels. This indicates that the signal is composed of different signal components and different frequency ranges at different levels of decomposition. PD signals may carry different amounts of energy at different frequency ranges. However, as discussed in Chapter 4.1.1, this energy distribution cannot differentiate the variations in energy at different injection points.

This is due to the wavelet energy distribution being scaled to give 100 percent for both measurement points. Because of this, the absolute energy is used to reveal the variation of energy at different measurement points as well as different PD signals. Figure 5.1.4 – Figure 5.1.11 shows an example of percentage energy distribution histograms for a surface discharge source under an applied voltage of 20 kV injected into terminal 1 to terminal 8 measured at bushing and neutral to earth connections respectively.

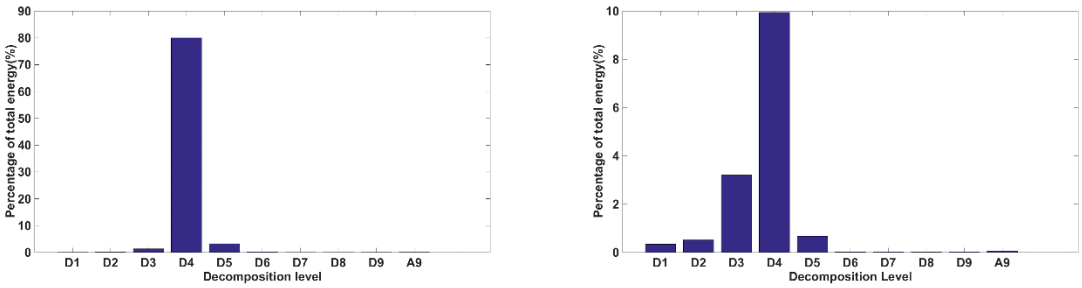

(a) Bushing tap point (b) Neutral to earth point

Figure 5.1.4. Histogram representing the energy distribution of signal between different decomposition coefficients at terminal 1

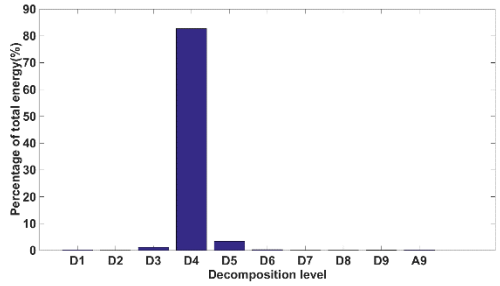

(a) Bushing tap point

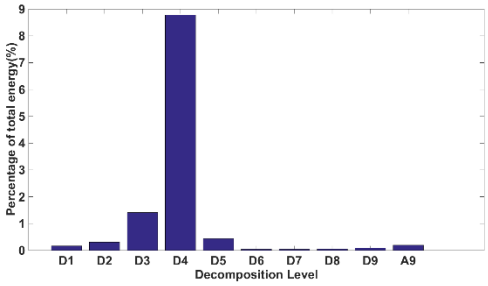

(b) Neutral to earth point

Figure 5.1.5. Histogram representing the energy distribution of signal between different decomposition coefficients at terminal 2

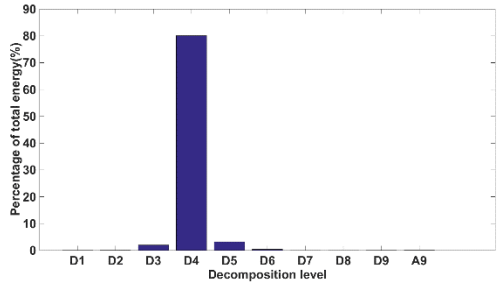

(a) Bushing tap point

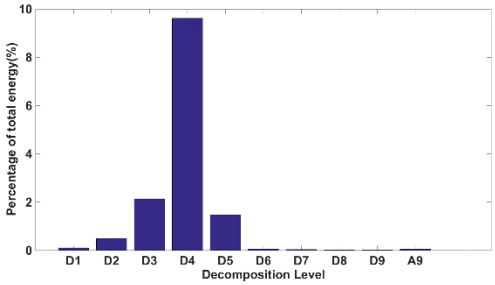

(b) Neutral to earth point

Figure 5.1.6. Histogram representing the energy distribution of signal between different decomposition coefficients at terminal 3

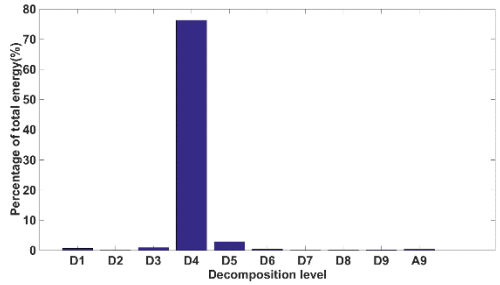

(a) Bushing tap point

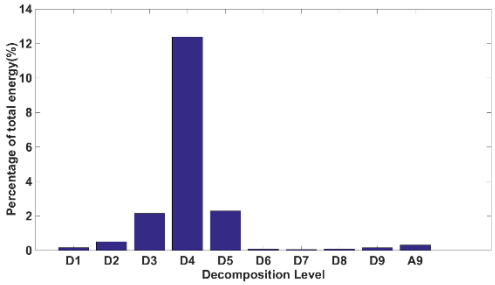

(b) Neutral to earth point

Figure 5.1.7. Histogram representing the energy distribution of signal between different decomposition coefficients at terminal 4

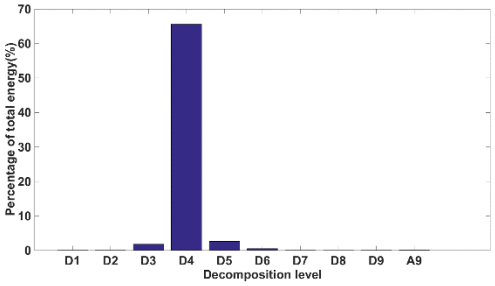

(a) Bushing tap point

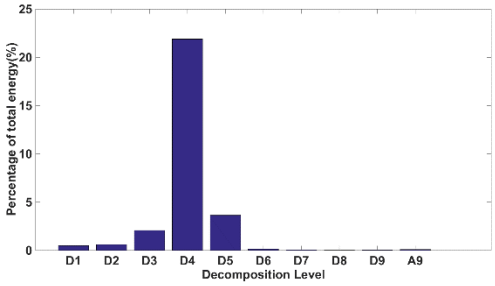

(b) Neutral to earth point

Figure 5.1.8. Histogram representing the energy distribution of signal between different decomposition coefficients at terminal 5

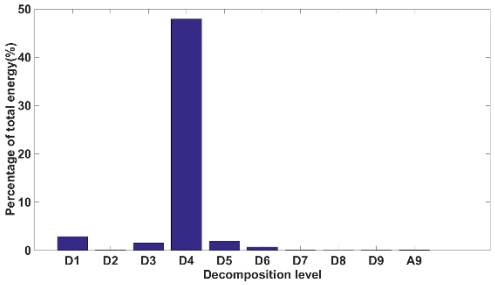

(a) Bushing tap point

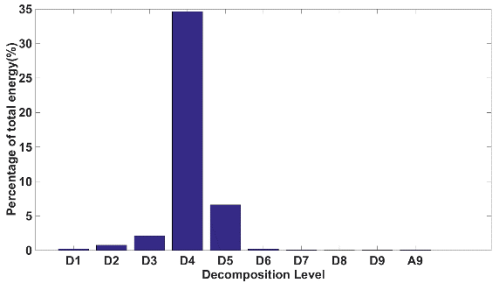

(b) Neutral to earth point

Figure 5.1.9. Histogram representing the energy distribution of signal between different decomposition coefficients at terminal 6

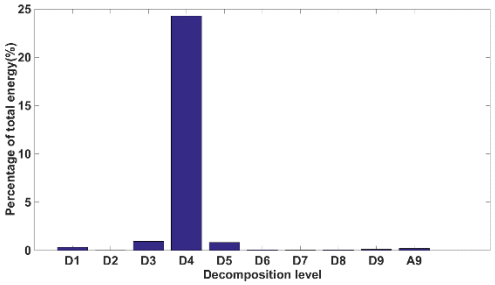

(a) Bushing tap point

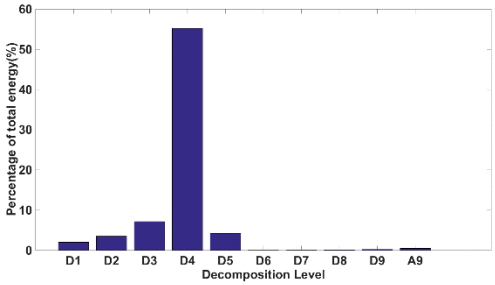

(b) Neutral to earth point

Figure 5.1.10. Histogram representing the energy distribution of signal between different decomposition coefficients at terminal 7

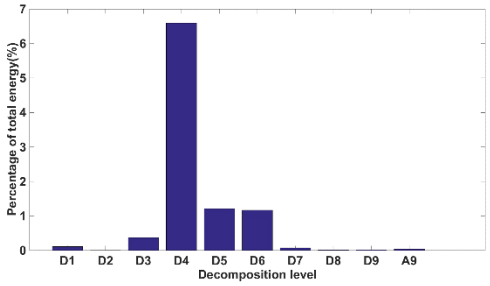

(a) Bushing tap point

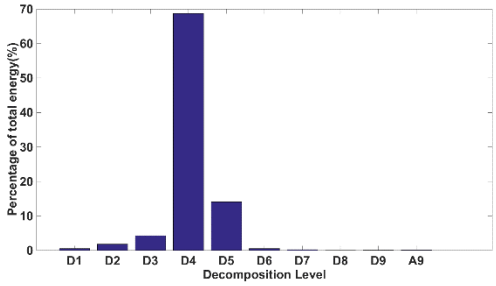

(b) Neutral to earth point

Figure 5.1.11. Histogram representing the energy distribution of signal between different decomposition coefficients at terminal 8

The difference in energy distribution seen in Figure 5.1.4 – Figure 5.1.11 shows that when absolute energy is considered, the variation of energy at different measurement points and also at different injection terminals can be calculated. Table 5.1.1 – Table 5.1.3 provides the total percentage of absolute energy for all types of PD sources seen at the bushing tap and neutral earth points.

Table 5.1.1. Percentage of total energy produced by surface discharge

Terminal	Bushing tap point	Neutral to earth point
1	89.17	10.83
2	88.47	11.53
3	85.97	14.03
4	81.84	18.16
5	70.87	29.12
6	55.19	44.81
7	26.86	73.14
8	9.61	90.39

Table 5.1.2. Percentage of total energy produced by void discharge

Terminal	Bushing tap point	Neutral to earth point
1	90.15	9.85
2	89.69	10.31
3	86.02	13.98
4	81.76	18.24
5	61.92	38.08
6	46.64	53.36
7	22.46	77.54
8	13.30	86.70

Table 5.1.3. Percentage of total energy produced by floating discharge

Terminal	Bushing tap point	Neutral to earth point
1	92.70	7.30
2	91.07	8.93
3	90.26	9.74
4	84.38	15.62
5	73.08	26.92
6	56.77	43.23
7	28.97	71.03
8	6.41	93.58

In Table 5.1.1 – Table 5.1.3, from terminal 1 to terminal 5 or terminal 6, the overall percentage of energy measured at the bushing tap point is higher than that measured at the neutral to earth connection point and vice versa from terminal 6 onwards. However, the reduction of distribution energy between a terminal to another is different for different types of PD sources. This is possibly due to the non-linear characteristics of a transformer winding. Although many assume that the winding can be considered as a linear element, the assumption does not hold on closer analysis. The inter-turn capacitance is distributed and in a function of position, there are stray terms that are unaccounted for as well as issues due to mutual coupling. This will in turn ensures that a windings response to a PD event will be a

function of the frequency features of the original discharge pulse and their interaction with specific resonances and anti-resonances along a given transmission pathway.

5.2 DECOMPOSITION USING MATHEMATICAL MORPHOLOGY

As discussed in Chapter 4, a wavelet transform can been applied to decompose and represent PD signals in the time and frequency domains. However, wavelet transform performance is dependent on the selected mother wavelet and decomposition levels. The selection of the mother wavelet is an important step in Wavelet analysis. It is assumed that a selected wavelet prototype function can be determined based on the success of the function estimation for analysing signals.

The mother wavelet needs to closely match to the original PD signal shape for better approximation of transient response of the analysed signal. Regarding decomposition levels, it needs to be carefully chosen in order to prevent unwanted loss of any PD data in the frequency region of interest. A study [16] revealed that the Daubechies (db) and Symlet (sym) Wavelet families were found to be closest mother wavelet to the PD signals. These results are supported by these mother wavelet being used in numerous studies including [12], [43].

In Mathematical Morphology, the SE lengths are set from 1 to 20 to provides 20 different frequency bands to characterise the PD pulse. In order to illustrate the MM based signal decompositions, a Gaussian signal is chosen to demonstrate the performance of MM signal decompositions. A Gaussian signal has a wide frequency spectrum, which can be used to verify the decomposition performance.

Figure 5.2.1 shows the results of MM decomposition in time and frequency domains of a Gaussian signal using MM signal decomposition method with the use of a flat structuring element.

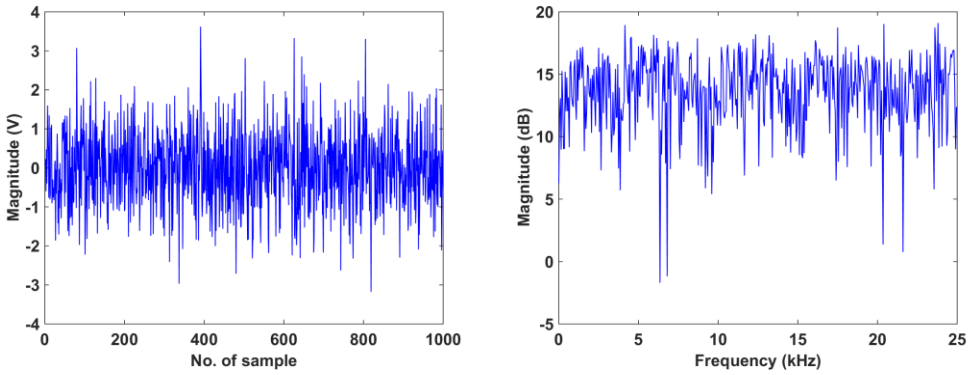
Magnitude (V)
No. of sample
Magnitude (dB)
Frequency (kHz)

(a)

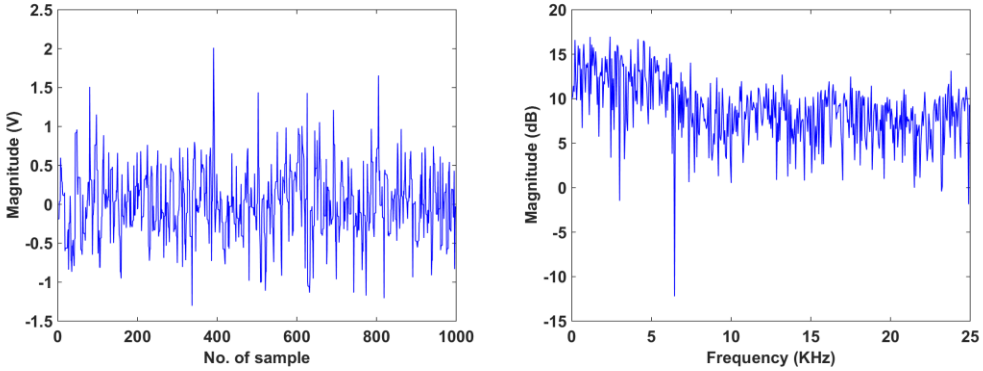
Magnitude (V)
No. of sample
Magnitude (dB)
Frequency (KHz)

(b)

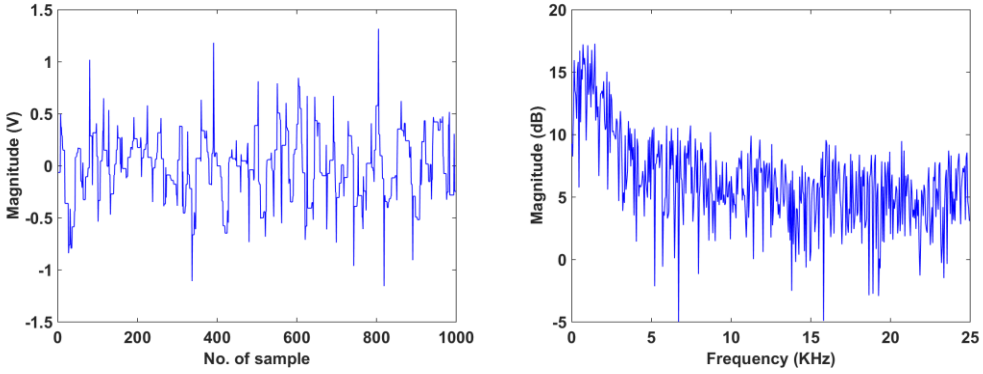
Magnitude (V)
No. of sample
Magnitude (dB)
Frequency (KHz)

(c)

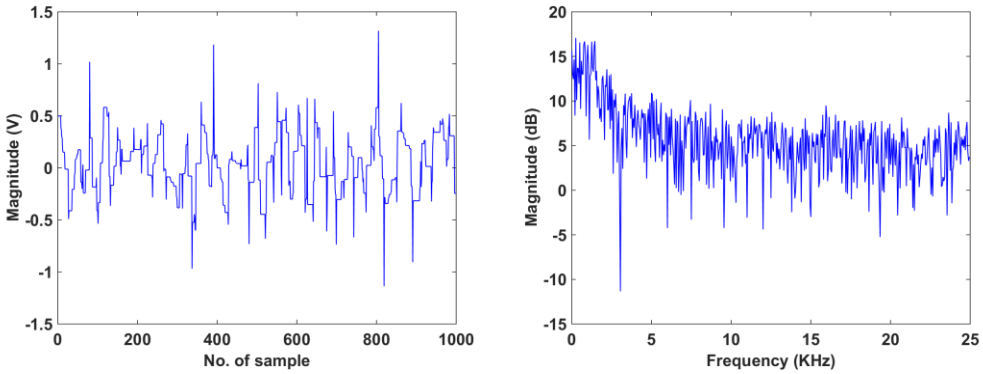

(d)

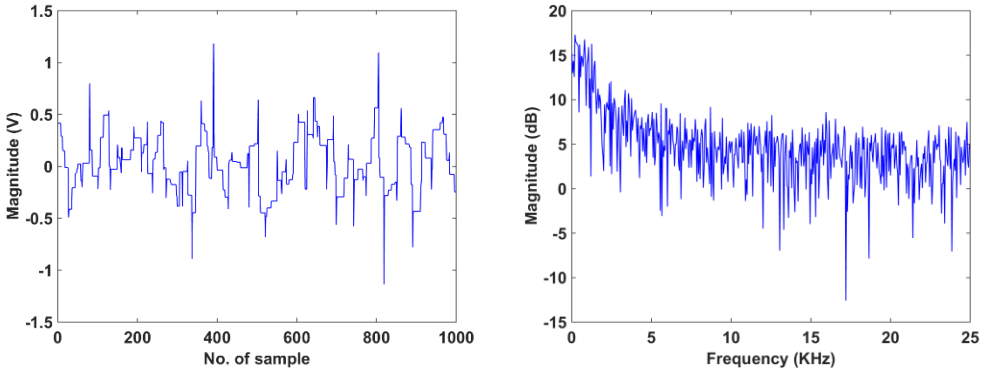

(e)

Figure 5.2.1. Decomposition results in time (left column) and frequency (right column) domains of a Gaussian signal by using MM signal decomposition method.
((a) Original signal and (b)-(e) Decomposition results for the lengths of flat SE equal to 5, 10, 15 and 20)

Figure 5.2.1 highlights that as the SE length increases, the original PD signal can be decomposed from high to low frequencies. Therefore, it can be concluded that the decomposition performance using MM with increasing the length of SE is similar to that of applying a range of low pass zero phase filters.

5.2.1 MATHEMATICAL MORPHOLOGY ENERGY

Different frequency bands of the measured signal produced from different lengths of SE contain different finite amounts of energy over their specific range of frequency. Therefore, the energy (E_L) for each length, L of SE was calculated for current pulses captured at both measurement points using:

$$E_L = \sum_{i=1}^{N} Pd_i^2(t) \tag{5.1}$$

where Pd are the signal produced from each length of SE.

However, the use of absolute energy distribution is considered rather than the individual energy from each measurement point. The use of an absolute energy distribution is based on the assumption that absolute energy can reveal the variation of energy at different measurement points and also at different terminals from different sources.

The absolute energy for bushing tap point to earth (E_{abs_B}) and for neutral to earth measurement point (E_{abs_N}) can be calculated using:

$$E_{abs_B} = \frac{E_{L_B}}{E_{L_B} + E_{L_N}} \times 100\% \tag{5.2}$$

$$E_{abs_N} = \frac{E_{L_N}}{E_{L_B} + E_{L_N}} \times 100\% \tag{5.3}$$

where E_{L_B} and E_{L_N} are the individual energies measured at the bushing tap point to earth and neutral to earth measurement point respectively.

Table 5.2.1 – Table 5.2.3 provides the total percentage of absolute energy for all types of PD sources seen at the bushing tap and neutral earth points.

Table 5.2.1. Percentage of total energy produced by surface discharge

Terminal	Bushing tap point	Neutral to earth point
1	89.98	10.02
2	88.99	11.01
3	86.35	13.65
4	81.97	18.03
5	71.42	28.58
6	52.16	47.84
7	25.69	74.31
8	9.37	90.63

Table 5.2.2. Percentage of total energy produced by void discharge

Terminal	Bushing tap point	Neutral to earth point
1	90.44	9.56
2	89.96	10.04
3	86.04	13.96
4	77.42	22.58
5	61.58	38.42
6	43.83	56.17
7	20.37	79.63
8	12.70	87.30

Table 5.2.3. Percentage of total energy produced by floating discharge

Terminal	Bushing tap point	Neutral to earth point
1	93.33	6.67
2	91.23	8.77
3	90.78	9.22
4	85.55	14.45
5	74.58	25.42
6	56.92	43.08
7	27.59	72.41
8	6.02	93.98

In Table 5.2.1 – Table 5.2.3, the overall percentage of energy measured at the bushing tap point is higher than that measured at the neutral to earth connection point and vice versa from terminal 6 to terminal 8. These results are the same with results when the absolute energy was calculated using wavelet analysis (in Table 5.1.1 – Table 5.1.3). The information from this percentage of absolute energy from either Wavelet energy analysis or MM energy analysis seems to provide an initial indication about the location of PD sources within a transformer winding. Nevertheless, further analysis such as dimensionality reduction or feature extraction on the absolute energy distribution are needed to manipulate the features and also possibly for the visualisation process which ultimately indicate PD source location.

5.2.2 MATHEMATICAL MORPHOLOGY SPARSITY

After the decomposition process, sparsity values are calculated in time and frequency domains. A signal is considered sparse if a relatively flat space is located between peaks. PD pulses are transient signals with oscillations or which oscillate around the peaks, and some space existing between two consecutive peaks of PD pulses [113]. Therefore, sparsity is adopted as a function to represent distribution of PD pulse peaks.

Sparse values are calculated in time and frequency domain after the extracted PD pulses are decomposed. Sparsity in time and frequency domain can be calculated using:

$$S(p) = \sqrt{N}\frac{\sqrt{\sum_{i=1}^{N} p^2(i)}}{\sum_{i=1}^{N}|p(i)|} \tag{5.4}$$

Where p is the decomposed PD pulse with N samples [114].

Figure 5.2.2 shows sparsity values calculated in time and frequency domains from each of the decomposed signals represented by the length of structure element for combination of floating and surface discharge using MM method measured at terminal 1 from bushing measurement point and neutral to earth measurement point respectively.

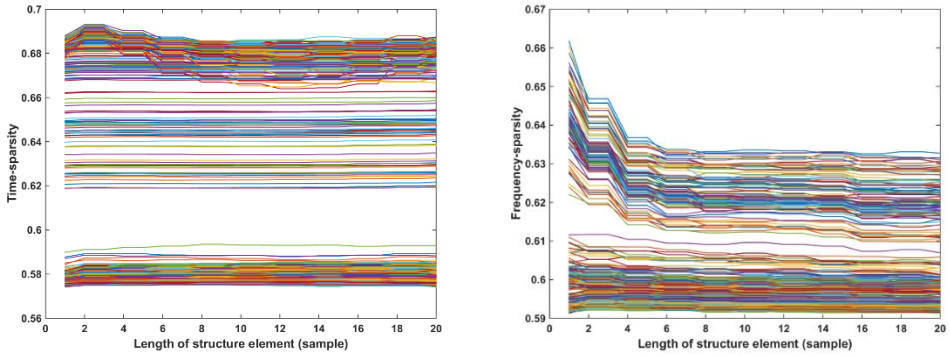

(a)

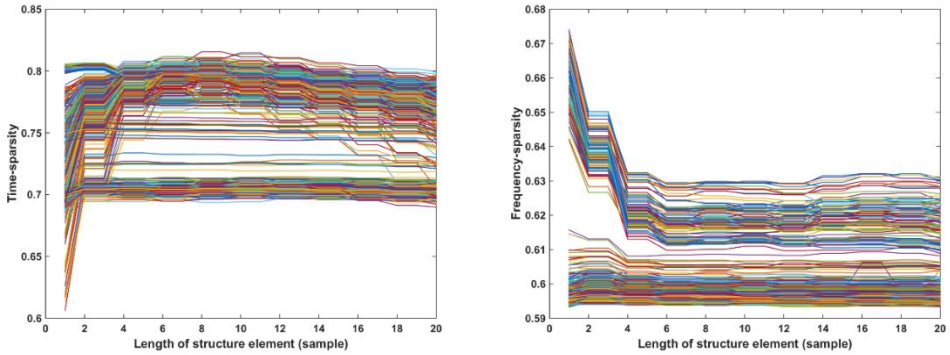

(b)

Figure 5.2.2. Sparsity trends in time (left) and frequency (right) domains of decomposed signal of terminal 1 measured at (a) bushing measurement point and (b) neutral to earth measurement point. Each line in the plots represents data for a particular captured pulse.

Figure 5.2.2 highlights that the calculated sparsity values for all decomposed signals exhibit a particular trend of sparsity values for each PD source. There are two trends of sparsity value which represent two types of PD sources that were injected into the transformer winding. However, there are some cases where the trends of sparsity value are not clear enough to represent the two sources due to the trends that may have similar tendency. Figure 5.2.3 shows that the trends of sparsity value have similar tendency when a combination of floating and surface discharges are injected at terminal 7.

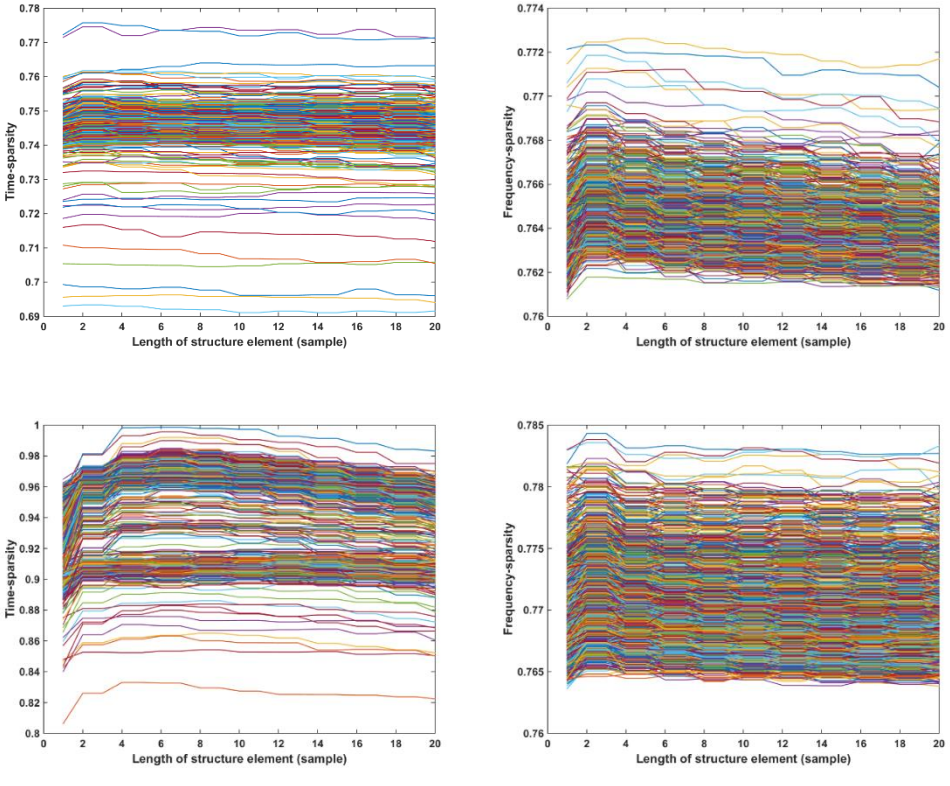

Figure 5.2.3. Sparsity trends in time (left) and frequency (right) domains of decomposed signal of terminal 7 measured at (a) bushing measurement point and (b) neutral to earth measurement point. Each line in the plots represents data for a particular captured pulse.

Figure 5.2.3 shows sparsity values calculated in the time and frequency domains of decomposed signal of terminal 7. It can be seen that sparsity values have a similar tendency especially in the frequency domains for both measurement points. Therefore, in this case, a particular type of PD source cannot be represented as there is only one trend in the plot.

5.3 SUMMARY

In this chapter, two decomposition techniques that were applied in this thesis; wavelet analysis and mathematical morphology have been discussed. The techniques have been implemented in order to analyse the measured signals from the bushing measurement point and neutral to earth measurement point in the time and frequency domains and also to decompose the signals into different regions of frequency. By using the percentage of energy distribution, Wavelet and MM energy are useful to determine the decomposition of energy inside an individual signal. However, when they are used to compare energy from two different measurement points at the same time, they cannot measure the difference between the two energies. Therefore, in this thesis, the use of absolute energy of wavelet and MM energy provides an alternative solution to this issue. Besides wavelet and MM energy, sparsity values are also calculated in time and frequency domains of the signals that had been decomposed by MM analysis. Sparsity is adopted as a function to represent the distribution of PD pulses peaks.

CHAPTER 6

DIMENSIONAL REDUCTION TECHNIQUES WITH DBSCAN

To further reduce the number of dimensions of the processed data, PCA and t-SNE have been independently applied to the data sets processed using wavelet energy and MM energy data decomposition. Time frequency mapping techniques have been applied as the dimensionality reduction technique to the data set generated from MM sparsity decomposition. These dimension reduction techniques are carried out in order to evaluate their suitability for this application and for visualisation of the data set for manual verification of the technique. This process relies on the assumption that PD pulses produced from different sources generate unique characteristics and therefore will be projected into a localised region in their specific space.

In order to compare the suitability and sensitivity of the techniques used, they were each applied to the same data set that consisted of the wavelet energy distribution or MM energy data of a set of PD pulses. The combination of floating and surface discharge generated at terminal 1 and terminal 5 respectively are used as the example in this chapter in order to compare the performances of the techniques.

At terminal 1, the differences in terms of energy between the two expected clusters are very significant. The source that was injected into terminal 1 had significantly greater energy at the bushing measurement point compared to the source that was injected in the middle of the winding (terminal 5 in this case). While at the neutral earth measurement point, the source that was injected into terminal 1 has less energy compared to the source that was injected in the middle of the winding. Therefore, at terminal 1, the differences between the two clusters at both measurement points are significant, which makes them straight forward to separate.

When the injection point moves along the transformer winding, the distance between the two clusters generated from bushing measurement point and neutral to earth measurement point

decreases. However, at terminal 5, both clusters are in almost the same space as they were both injected towards the middle of the winding. However, different types of PD sources have different types of waveforms in terms of magnitude and frequency contents. From terminal 6 onwards, the distance between the two clusters increases again but in this case, the source that was injected at terminal 1 has less energy at the bushing measurement point and more at the neutral measurement point.

All terminals create distinct outputs at both measurement points except terminal 5, as the propagation path to both measurement points are almost identical from this terminal. Hence, only data generated at terminal 1 and terminal 5 are used to verify the performance of dimension reduction techniques in terms of separating the multiple PD sources that were injected into the winding. This is because the measured output caused by PD injected into terminals 2, 3, 4, 6, 7 and 8 have equal distinct characteristics as those produced by injection into terminal 1.

In order to group the processed data obtained using dimensional reduction techniques automatically, a partitioning type clustering method was used. This was Density-based Spatial Clustering of Applications with Noise (DBSCAN). The results of the clustering technique are verified by visually inspecting the results and analysing the PD plots generated. Analysis of the performance of the technique was undertaken and used to establish the most effective technique for separation of multiple PD sources within a transformer winding.

6.1 APPLICATION OF DBSCAN ON WAVELET TRANSFORM DATA USING PCA AND T-SNE

DBSCAN was applied in this application due to its ability to recognise clusters of arbitrary shape as well as to distinguish noise in n-dimensions [12]. DBSCAN performs clustering based on the density of data points in a volume defined by a minimum number of data points (n-minimum) and neighborhood radius. Examples of the characterized 3-D representations of the wavelet energy data set using PCA and t-SNE generated from a

combination of floating (at terminal 1) and surface discharge (fixed at terminal 5) are shown in Figure 6.1.1 and Figure 6.1.2.

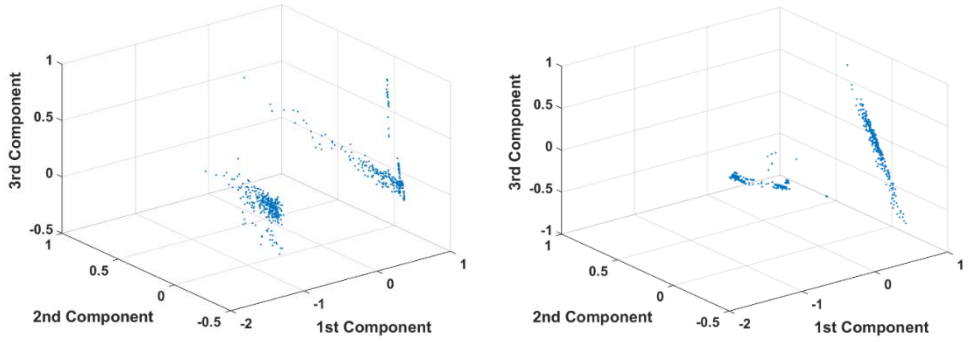

(a) (b)

Figure 6.1.1. 3-D representation of the wavelet energy data set generated using PCA at terminal 1 for (a) bushing measurement point and (b) neutral to earth measurement point.

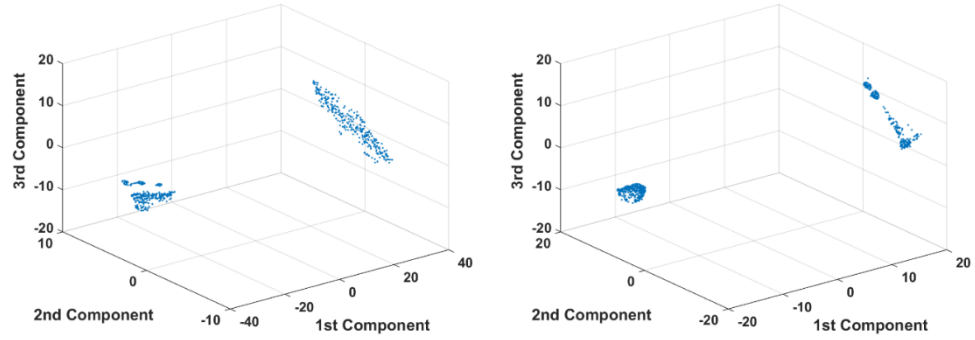

(a) (b)

Figure 6.1.2. 3-D representation of the wavelet energy data set generated using t-SNE at terminal 1 for (a) bushing measurement point and (b) neutral to earth measurement point.

Two clear clusters were identified by each method. Upon visual inspection of the plots, t-SNE is seen to produce better defined boundaries compared to clusters that were generated using PCA. There are outliers in the plot generated using PCA, which indicate that there is some data associated with a different characteristic appearing within a similar group of data. These outliers may affect the clustering process which will be discussed later.

A comparison is also made based on execution time. A non-optimized MATLAB software running on a desktop computer with a 3.4 GHz I7 processor and 16 GB RAM was used to run the two algorithms. Results show that the processing times for t-SNE are longer than the processing times for PCA. This is because t-SNE involves an iteration process within its algorithms. Execution time is important as it is predicted that greater computational efficiency will be needed when analysing more captured PD pulses on-site to accommodate the increase in data sample.

DBSCAN was then applied to the processed data with the three-dimensional representation of the clustered data using PCA and t-SNE. In this investigation, the minimum number of data points for DBSCAN was set to 2 to ensure that a small number of PD pulses belonging to the same PD source could be clustered. The results of the DBSCAN algorithms on the wavelet energy data sets processed by PCA from a combination of floating and surface discharge for terminal 1 measured at both measurement points are shown in Figure 6.1.3.

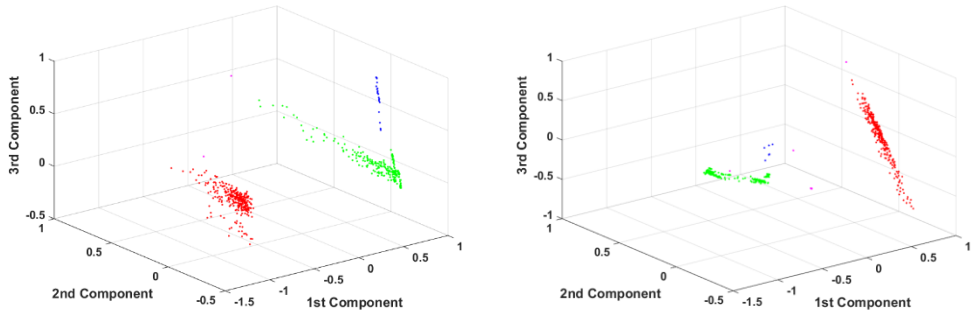

(a) (b)

Figure 6.1.3. 3-D PCA representation of wavelet energy data at terminal 1 clustered using DBSCAN for (a) bushing measurement point, (b) neutral to earth measurement point.

Analysis of the Figure 6.1.3 shows that there are outliers or misclassified points produced by DBSCAN on the data that had been processed using PCA. Throughout the analysis, clusters that have a number of points less than 1% from the total number of points are neglected as they are classified as outliers rather than a cluster. A 2-D histogram pattern and typical

individual pulses associated with the main clusters which are more than 1% from the total number of points in Figure 6.1.3(a) and Figure 6.1.3(b) are shown in Figure 6.1.4 and Figure 6.1.5 respectively.

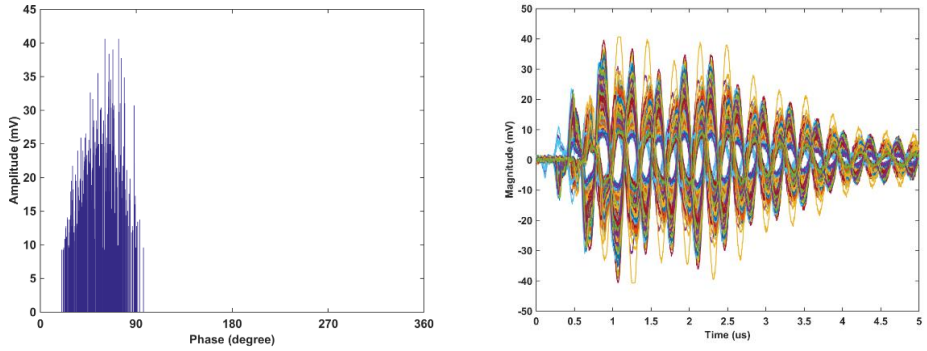

(a) Cluster 1 (in red)

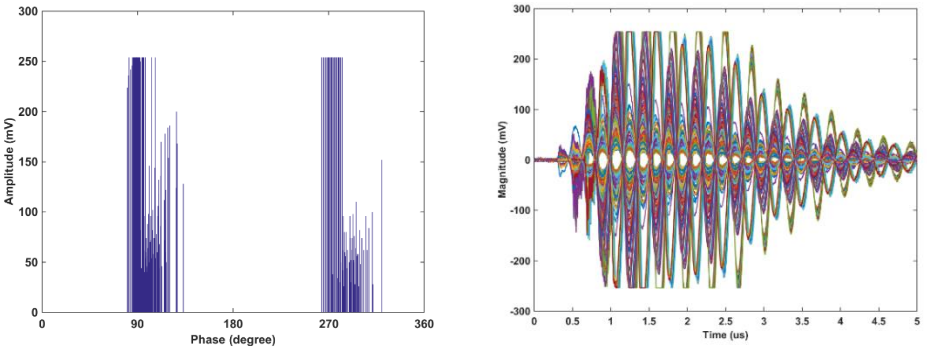

(b) Cluster 2 (in green)

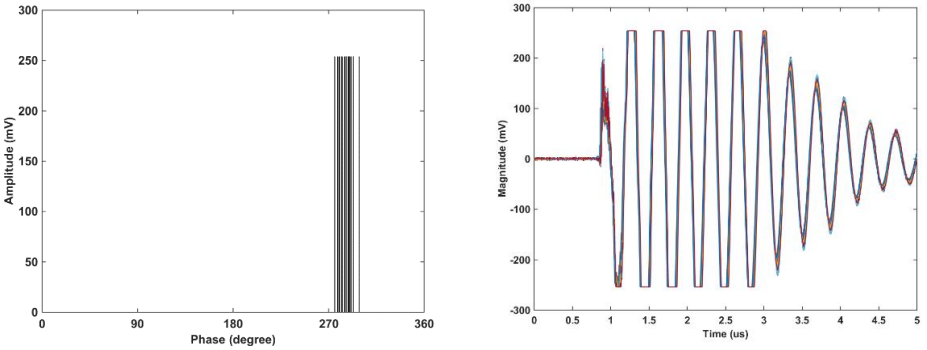

(c) Cluster 3 (in blue)

Figure 6.1.4. 2-D histogram pattern and typical individual pulses associated with the main clusters in Figure 6.1.3(a).

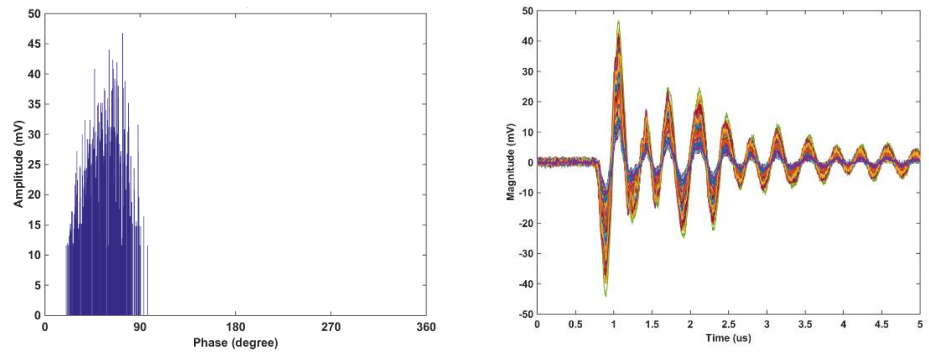

(a) Cluster 1 (in red)

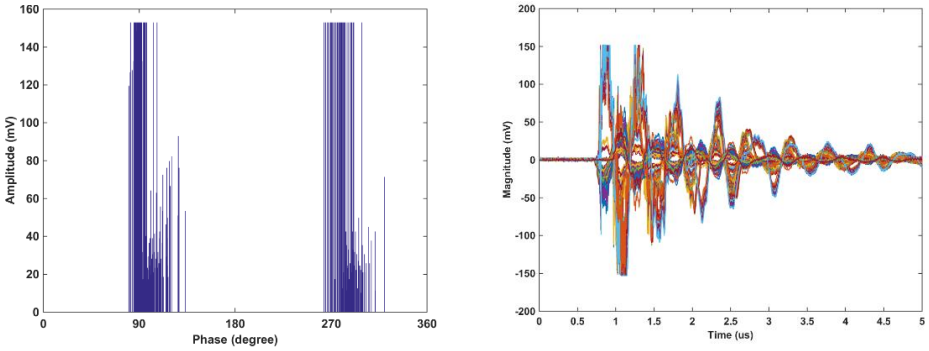

(b) Cluster 2 (in green)

Figure 6.1.5. 2-D histogram pattern and typical individual pulses associated with the main clusters in Figure 6.1.3(b).

Figure 6.1.4 shows that there are misclassified points produced by DBSCAN in the data that was processed using PCA. Based on 2-D histogram pattern and typical individual pulses in Figure 6.1.4, cluster 3 should part of cluster 2 as they have similar patterns and magnitude. However, as PCA produced scattered points in the space, DBSCAN was not able to group the points together that should be in one cluster. When compared to Figure 6.1.5, based on the 2-D histogram pattern, cluster 1 and cluster 2 are produced from the same source as cluster 1 and cluster 2 in Figure 6.1.4. In terms of magnitude, pulses from cluster 1 have almost identical magnitudes at both measurement points (in both figures) while magnitudes for cluster 2 measured at the neutral measurement point (Figure 6.1.5) are smaller than in cluster 2 measured at the bushing measurement point (in Figure 6.1.4).

This is because pulses grouped in cluster 1 are from the source that was injected in the middle of transformer winding. In this case, surface discharge was injected in the middle of the winding (terminal 5) while floating discharge was injected into terminal 1. The magnitude being smaller in cluster 2 measured at the neutral measurement point is due to the propagation path taken by the signals to the sensor.

As the signal propagates from the source location to the sensor, the signal may suffer attenuation and distortion. The longer the propagation path taken, the more attenuation and distortion will be seen by the sensors. This will reduce the magnitude of the signal which reaches the sensor. Therefore, the magnitude of the signals from the source that was injected into terminal 1 will be bigger at bushing measurement point compared to neutral to earth measurement point as they suffer less attenuation and distortion.

When t-SNE was applied to the same data, the data was segregated into two main different sub-sets by DBSCAN. Results of the DBSCAN algorithm on the wavelet energy data sets that had been processed by t-SNE for the same data set as PCA measured at both measurement points are shown in Figure 6.1.6.

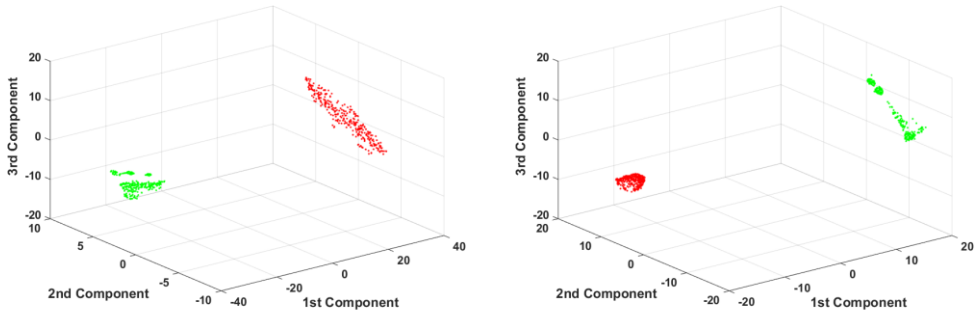

(a) (b)

Figure 6.1.6. 3-D t-SNE representation of wavelet energy data at terminal 1 using DBSCAN for (a) bushing measurement point, (b) neutral to earth measurement point.

The 2-D histogram patterns and typical individual pulses associated with the main clusters are shown in Figure 6.1.7 and Figure 6.1.8 for both measurement points.

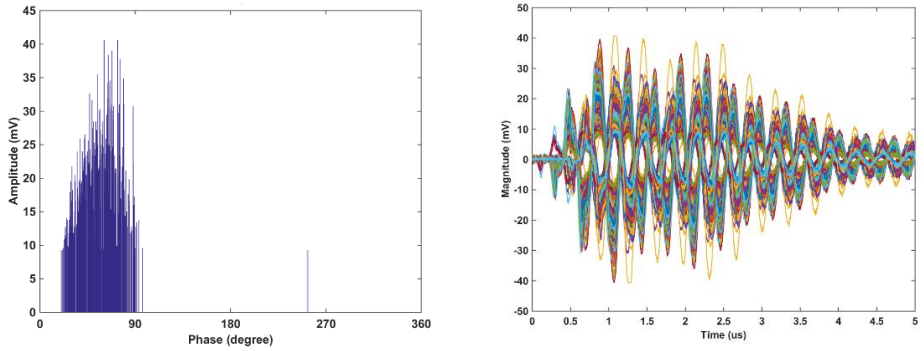

(a) Cluster 1 (in red)

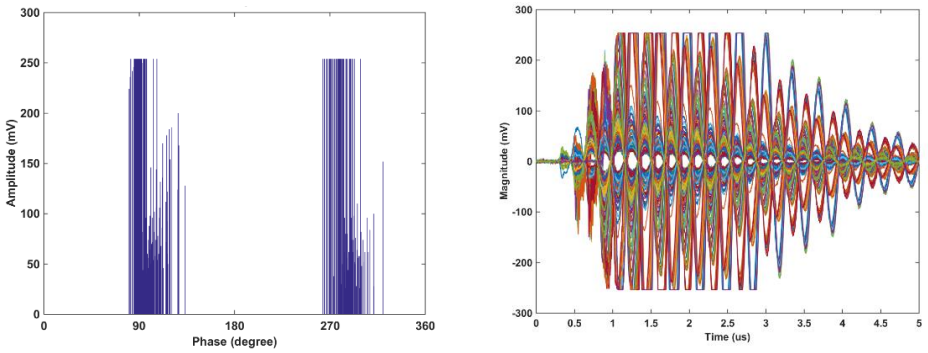

(b) Cluster 2 (in green)

Figure 6.1.7. 2-D histogram pattern and typical individual pulses associated with the main clusters in Figure 6.1.6(a)

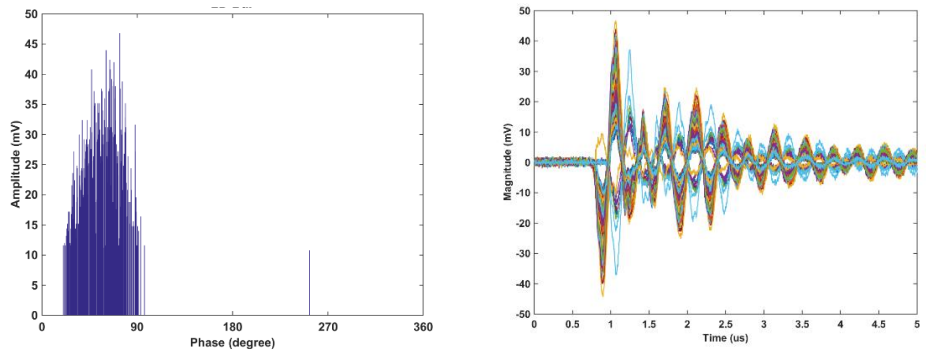

(a) Cluster 1 (in red)

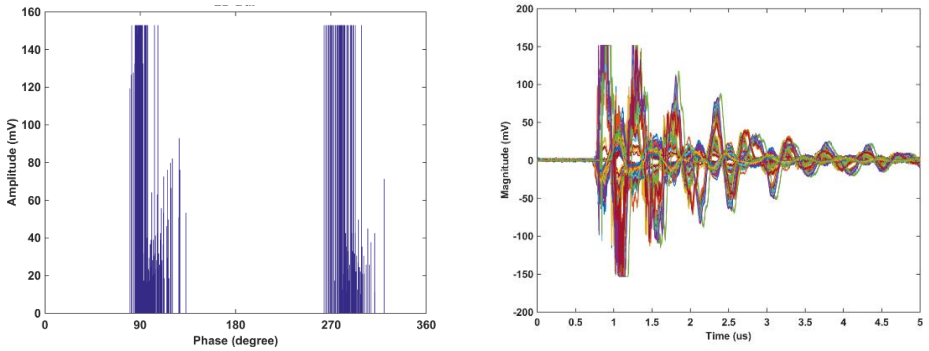

(b) Cluster 2 (in green)

Figure 6.1.8. 2-D histogram pattern and typical individual pulses associated with the main clusters in Figure 6.1.6(b)

Compared to the results of applying DBSCAN to the PCA output, Figure 6.1.6 shows that there are no misclassified clusters produced by DBSCAN in the data that had been processed using t-SNE. This is because t-SNE produces well-defined boundaries between clusters and the distinction between clusters is very high which is easier for DBSCAN to group them accordingly. It is also easier to visually verify the clusters generated by t-SNE as they form complex structures of data that are generally linearly separable. However, one disadvantage of using t-SNE as apposed to PCA is the computational time required for t-SNE takes longer than PCA. This is seen to be acceptable given its superior performance.

Another issue with PCA is that when PD signals are injected into terminal 5 or terminal 6, where the propagation path taken by the PD signals within the winding are almost similar. In

this case, PCA generates the expected two clusters in the same principle component space. Figure 6.1.9 shows the characterized 3-D representation of the wavelet energy data set of PD pulses generated using PCA when both sources; floating and surface discharge were injected into terminal 5 measured at bushing measurement point and neutral to earth measurement point respectively. While the results of the DBSCAN on 3-D representation of the wavelet energy data sets processed by PCA at both measurement points are shown in Figure 6.1.10.

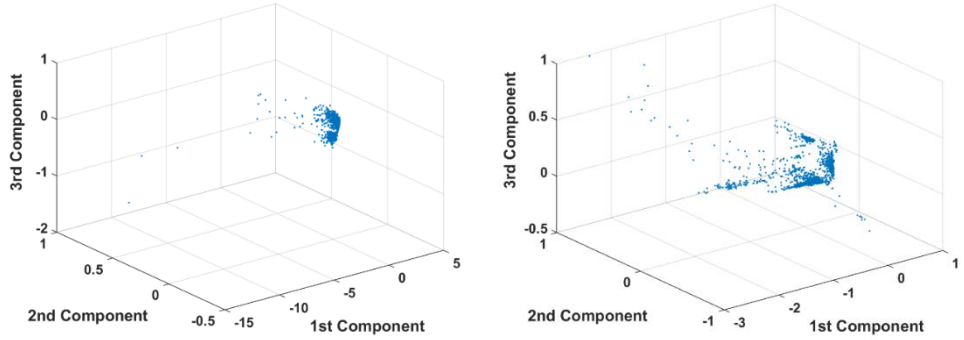

(a) (b)

Figure 6.1.9. 3-D representation of the wavelet energy data set generated using PCA at terminal 5 for (a) bushing measurement point and (b) neutral to earth measurement point.

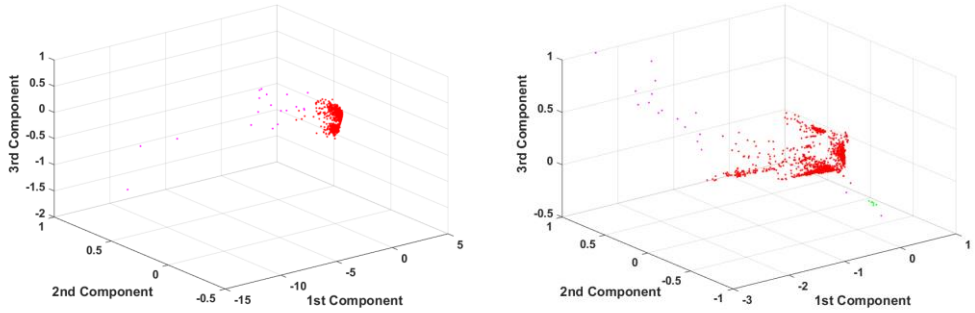

(a) (b)

Figure 6.1.10. 3-D PCA representation of wavelet energy data at terminal 5 using DBSCAN for (a) bushing measurement point, (b) neutral to earth measurement point.

In Figure 6.1.10, visual inspection of the representation generated using DBSCAN on the PCA output appear to produce a single cluster of data points. The distributions of points form a single high density of cluster within the feature space. DBSCAN is not able to separate the wavelet energy data that had been processed by PCA due to the clusters overlapping or being very close to each other in the space. Figure 6.1.11 and Figure 6.1.12 show the 2-D histogram pattern and typical individual pulses associated with the only one main cluster in Figure 6.1.10(a) and Figure 6.1.10(b) respectively.

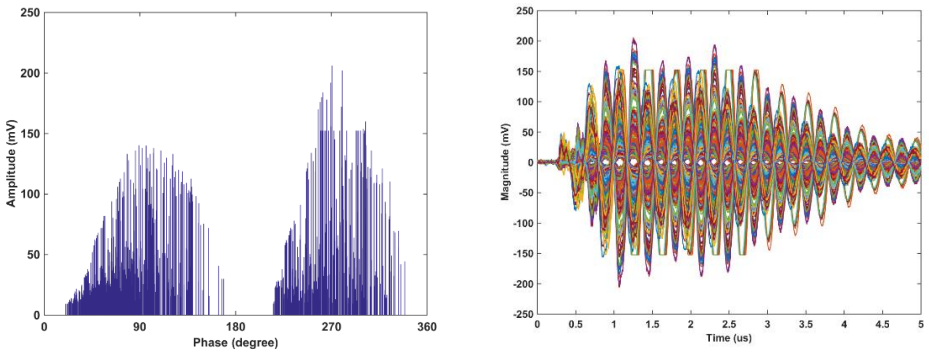

Figure 6.1.11. 2-D histogram pattern and typical individual pulses associated with the main clusters in Figure 6.1.10(a)

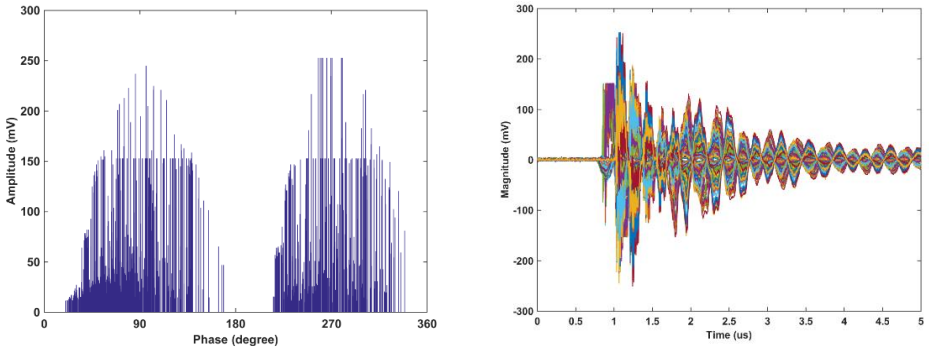

Figure 6.1.12. 2-D histogram pattern and typical individual pulses associated with the main clusters in Figure 6.1.10(b)

Figure 6.1.11 and Figure 6.1.12 show that the clusters produced from signals that were generated from the two injected PD sources are overlapping each other. This can be verified with the results obtained when t-SNE was applied to the same data set. In contrast to PCA, the t-SNE algorithm produced an intricate pattern of data points that clearly form two clusters of data. Figure 6.1.13 shows the characterized 3-D representation of the wavelet energy data set of PD pulses generated using t-SNE on the same data set for both measurement points.

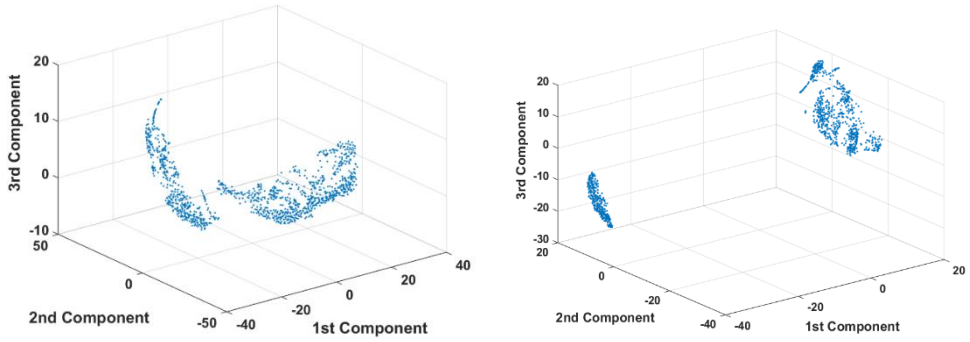

(a) (b)

Figure 6.1.13. 3-D representation of the wavelet energy data set generated using t-SNE at terminal 5 for (a) bushing measurement point and (b) neutral to earth measurement point.

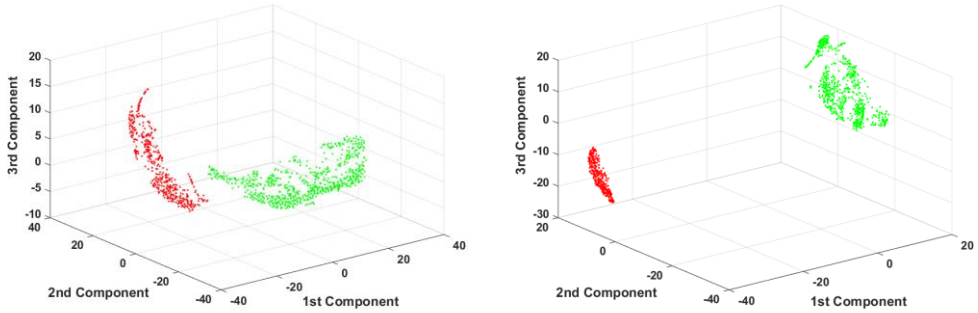

(a) (b)

Figure 6.1.14. 3-D t-SNE representation of wavelet energy data at terminal 5 using DBSCAN for (a) bushing measurement point, (b) neutral to earth measurement point.

The wavelet energy data is well separated by DBSCAN when the data are processed by t-SNE. There are clearly two clusters in the space when t-SNE was applied as shown in Figure 6.1.14. The clusters produced by t-SNE on the same wavelet energy data set not even close or overlapped each other in the space. The clusters are clearly separated with an obvious distance between them, which is easier for DBSCAN or any other clustering technique to groups them into specific clusters. The 2-D histogram pattern and typical individual pulses associated with the clusters produced in Figure 6.1.14(a) and Figure 6.1.14(b) are shown in Figure 6.1.15 and Figure 6.1.16 respectively.

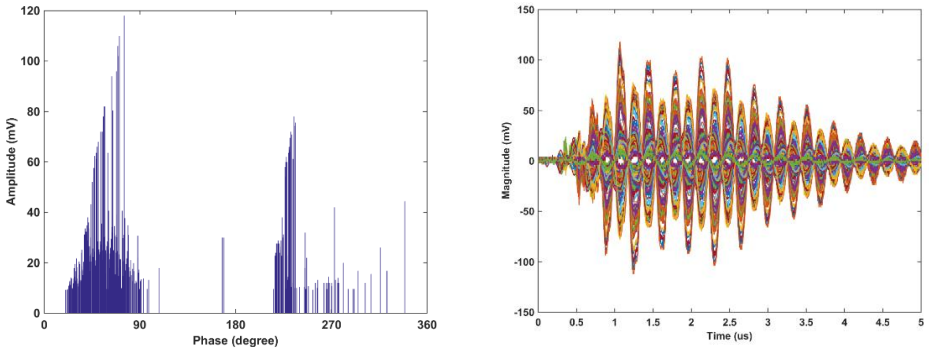

(a) Cluster 1 (in red)

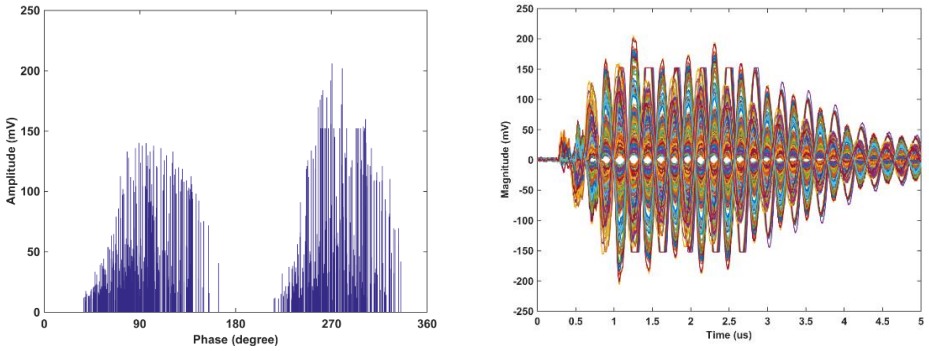

(b) Cluster 2 (in green)

Figure 6.1.15. 2-D histogram pattern and typical individual pulses associated with the main clusters in Figure 6.1.14(a)

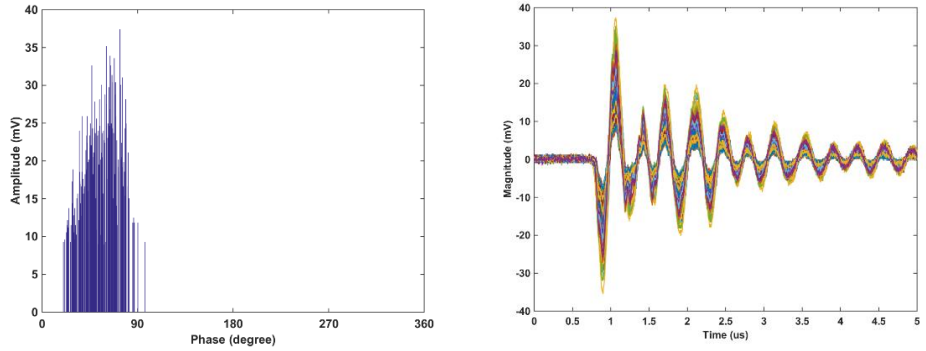

(a) Cluster 1 (in red)

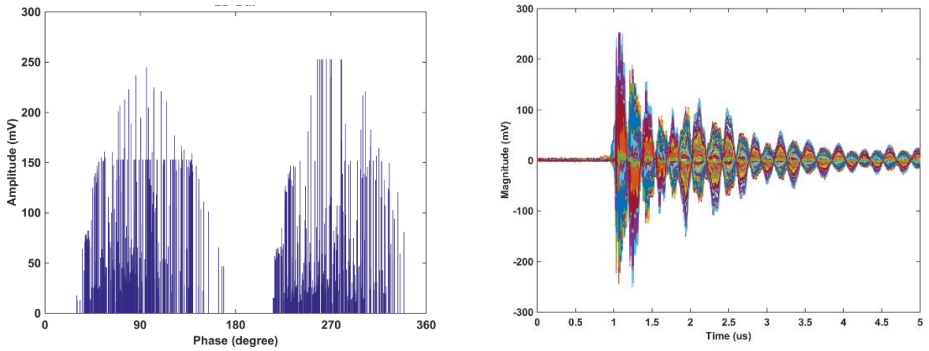

(b) Cluster 2 (in green)

Figure 6.1.16. 2-D histogram pattern and typical individual pulses associated with the main clusters in Figure 6.1.14(b)

Figure 6.1.15 and Figure 6.1.16 show that there are two clusters from different sources produced by t-SNE instead of a single cluster produced from PCA on the same wavelet energy data set. However, Figure 6.1.15(a) looks like there are some pulses in cluster 1 that belong to cluster 2. Based on the 2-D histogram patterns, some pulses in cluster 1 have the same magnitude and patterns as the pulses in cluster 2. A comparison can be made between Figure 6.1.15(a) and Figure 6.1.16(a). This is because, pulses measured at the bushing measurement point should have their own pairs at the neutral measurement point. It is believed that pulses occurred during the positive half cycle of the power cycle with magnitude of more than 40 mV and pulses occurred at negative half cycle belong to cluster 2.

These plots prove that the single cluster produced from PCA actually consists of two different signals. The cluster patterns produced from PCA on the wavelet energy data sets show similar positions and patterns in the space of principle component domain regardless of the type of PD sources. When two different PD sources were injected in the middle of transformer winding, which suffer almost identical attenuation and distortion from source location to both measurement points, the clusters produced by PCA were close to or overlapped with each other.

Unlike the representation generated using the PCA method, when t-SNE was applied, the clusters of data are clearly linearly separable which can be verified visually. The cluster identification result produced by DBSCAN on the data that had been processed using t-SNE algorithms shows accurate identification of the main clusters compared to the results produced from PCA. The outliers or scattered data produced are the drawback of PCA which makes the algorithms less robust and less effective compared to t-SNE algorithms.

Analysis of the results from application of DBSCAN on wavelet energy data processed by PCA show that, it is difficult to build confidence with the technique. The PCA algorithm was ineffective at identifying clusters when the sources were injected at the middle of the winding. Although PCA has computational advantages over t-SNE, the clear example of inability to identify multiple sources influences the selection of the technique. PCA is not sufficiently robust and did not illustrate sufficient performance. Another example will discuss the performance of PCA on another data set later on in this chapter.

6.2 APPLICATION OF DBSCAN ON MM ENERGY DATA USING PCA AND T-SNE

As discussed previously, in MM, the SE lengths are set from 1 to 20 to give 20 different frequency bands of PD pulses. Different frequency bands of the measured signal produced from different length of SE contain different finite amounts of energy within a specific range of frequencies. Energy of the measured signals are calculated for each SE lengths, which give 20 different energy elements for each signal. Then PCA and t-SNE were applied as

dimensional reduction techniques to the data set reducing the number of MM energy distribution levels from 20 to 3 element vectors for visualisation. The characterized 3-D representation of the MM energy data set of PD pulses and its representation using DBSCAN generated from a combination of floating and surface discharges at terminal 1 processed using PCA are shown in Figure 6.2.1 and Figure 6.2.2 for both measurement points respectively.

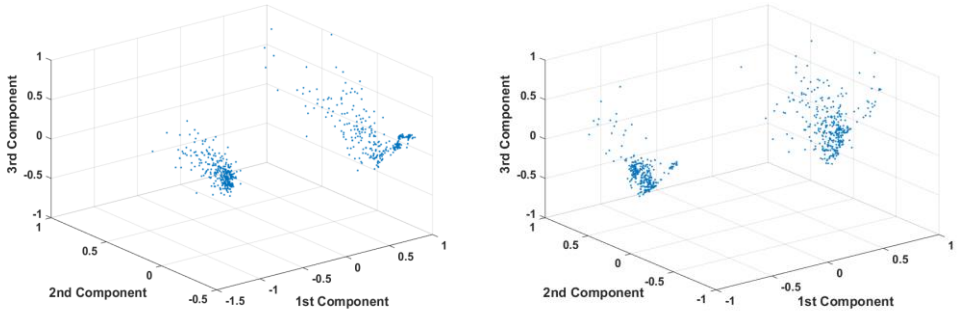

(a) (b)

Figure 6.2.1. 3-D representation of the MM energy data set generated using PCA at terminal 1 for (a) bushing measurement point and (b) neutral to earth measurement point.

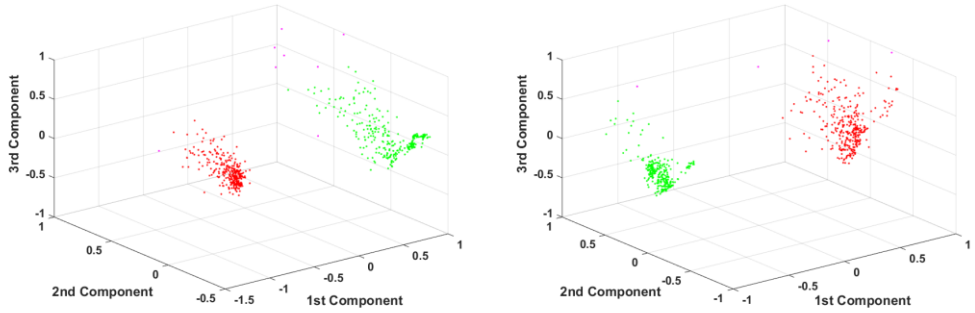

(a) (b)

Figure 6.2.2. 3-D PCA representation of MM energy data at terminal 1 using DBSCAN for (a) bushing measurement point, (b) neutral to earth measurement point.

Figure 6.2.2 shows that the clusters produced by PCA and clustered using DBSCAN are scattered with some outliers. However, it produced better results than when DBSCAN was applied to the data produced by PCA from wavelet energy data set because there are no misclassified clusters that have points more than 1% from the total points in the space. Previously, DBSCAN was not able to group the outliers that belong to one of the main cluster together. When DBSCAN was given the same parameters applied to the PCA output from MM energy data set, DBSCAN was able to group the two main clusters in principle component space. Figure 6.2.3 and Figure 6.2.4 show the 2-D histogram patterns and typical individual pulses associated with the main clusters in Figure 6.2.2 for both measurement points.

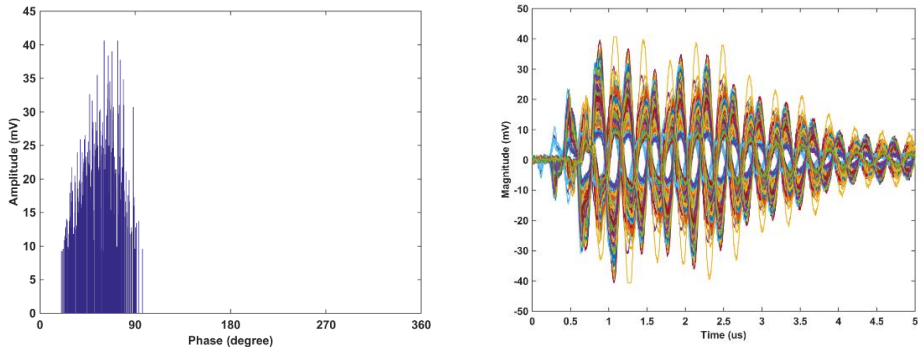

(a) Cluster 1 (in red)

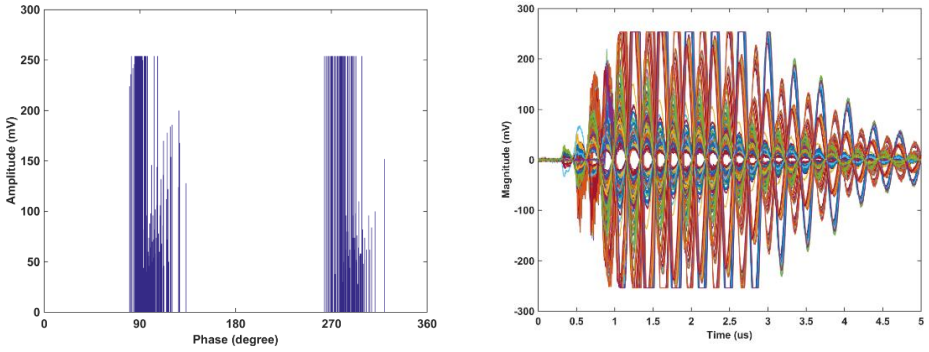

(b) Cluster 2 (in green)

Figure 6.2.3. 2-D histogram pattern and typical individual pulses associated with the main clusters in Figure 6.2.2(a)

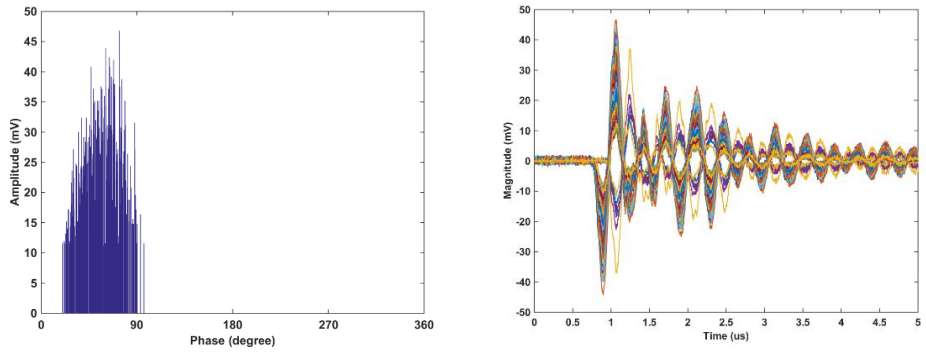

(a) Cluster 1 (in red)

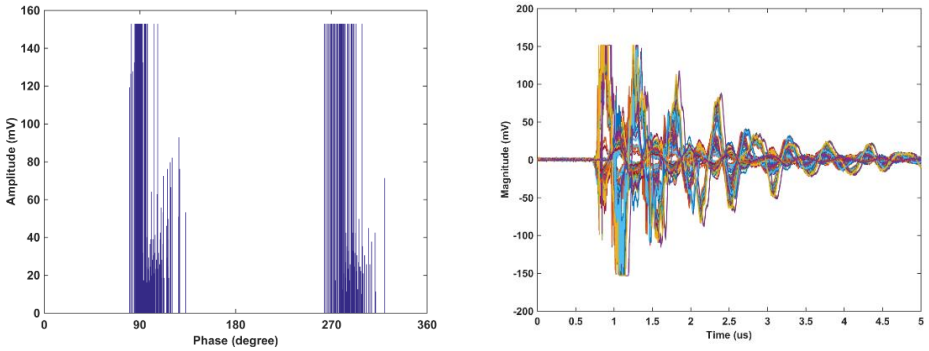

(b) Cluster 2 (in green)

Figure 6.2.4. 2-D histogram pattern and typical individual pulses associated with the main clusters in Figure 6.2.2(b)

While Figure 6.2.5 and Figure 6.2.6 show the 3-D representation and its representation when DBSCAN was applied to t-SNE output of the MM energy data set.

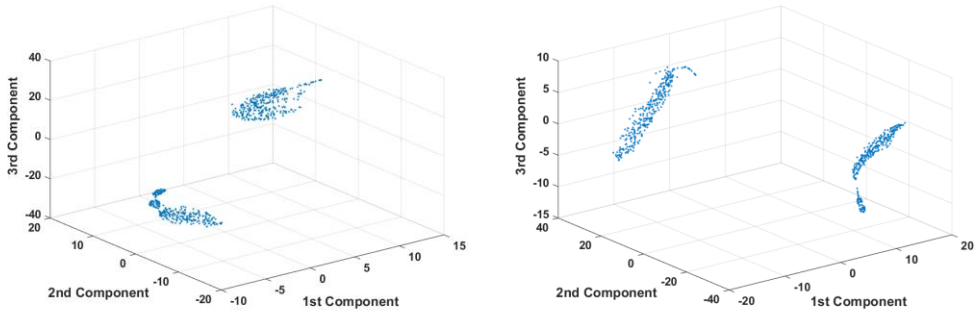

(a) (b)

Figure 6.2.5. 3-D representation of the MM energy data set generated using t-SNE at terminal 1 for (a) bushing measurement point and (b) neutral to earth measurement point.

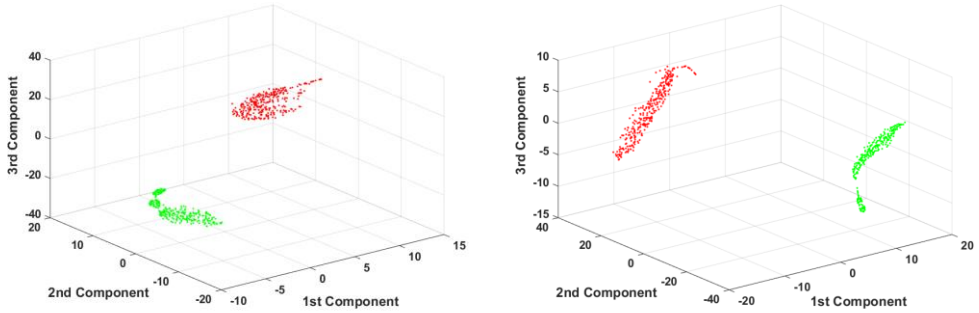

(a) (b)

Figure 6.2.6. 3-D t-SNE representation of MM energy data at terminal 1 using DBSCAN for (a) bushing measurement point, (b) neutral to earth measurement point.

Figure 6.2.6 shows that clusters that are produced when t-SNE are applied seem to have more better defined boundaries compared to clusters generated using PCA. Two linearly separable clusters have been identified using t-SNE and DBSCAN to the MM energy data set. Analysis

of the cluster identification results produced by DBSCAN on the data that had been processed using t-SNE shows accurate identification of the two clusters that were highlighted previously.

The t-SNE algorithms has demonstrated a greater sensitivity in highlighting subtle attributes of the data either when it was applied to either wavelet energy data or MM energy data. Figure 6.2.7 and Figure 6.2.8 show the 2-D histogram patterns and typical individual pulses associated with the main clusters in Figure 6.2.6.

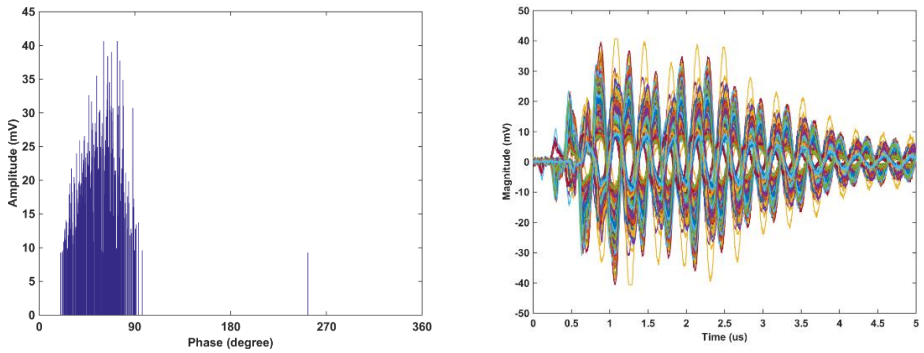

(a) Cluster 1 (in red)

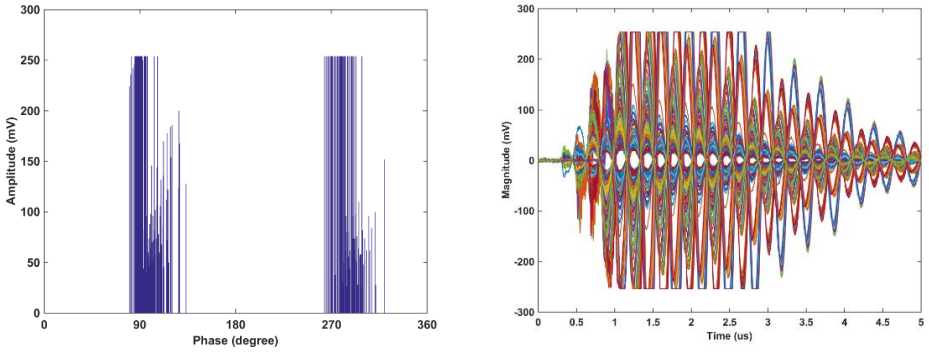

(b) Cluster 2 (in green)

Figure 6.2.7. 2-D histogram pattern and typical individual pulses associated with the main clusters in Figure 6.2.6(a)

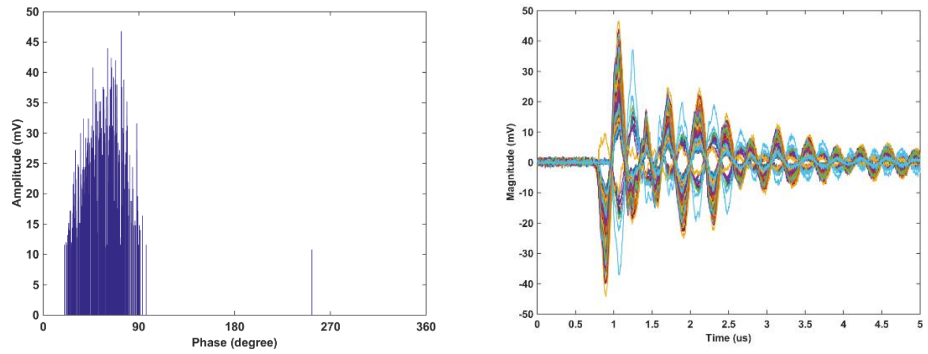

(a) Cluster 1 (in red)

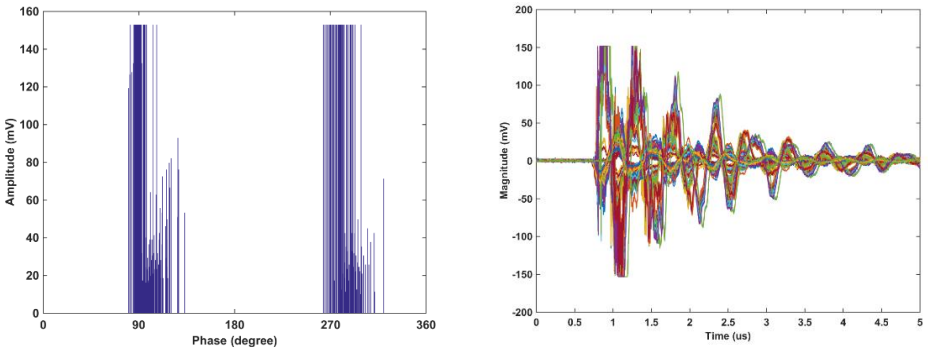

(b) Cluster 2 (in green)

Figure 6.2.8. 2-D histogram patterns and typical individual pulses associated with the main clusters in Figure 6.2.6(b)

Analysis of the 2-D histogram patterns and typical individual pulses associated with the clusters using t-SNE on the MM energy data set (Figure 6.2.7 and Figure 6.2.8) reveal exactly the same results as when t-SNE was applied to the wavelet energy data set (Figure 6.1.7 and Figure 6.1.8). This shows that the performance of MM energy analysis as a decomposition technique is similar to the performance of wavelet energy analysis. Previously, pulse injected into the middle of a transformer winding generated using DBSCAN on the PCA output from wavelet energy data set appears to produce a single cluster of data points. DBSCAN is not able to separate the wavelet energy data that had been processed by PCA due to the clusters overlapping or being very close to each other in the space. However, by using MM energy as the decomposition technique, PCA produced two clusters rather than only one cluster from

the same data set. Figure 6.2.9 shows the 3-D representation of the MM energy data set generated using PCA with PD injected into terminal 5 for both measurement points.

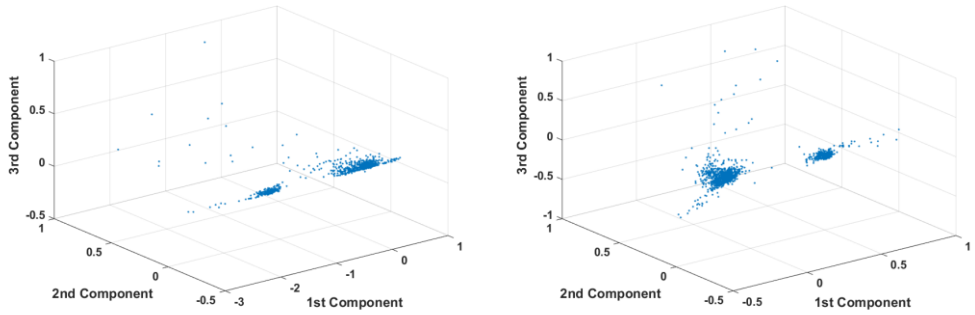

(a) (b)

Figure 6.2.9. 3-D representation of the MM energy data set generated using PCA at terminal 5 for (a) bushing measurement point and (b) neutral to earth measurement point.

While Figure 6.2.10 shows the 3-D PCA representation of MM energy data with PD injected into terminal 5 when DBSCAN was applied.

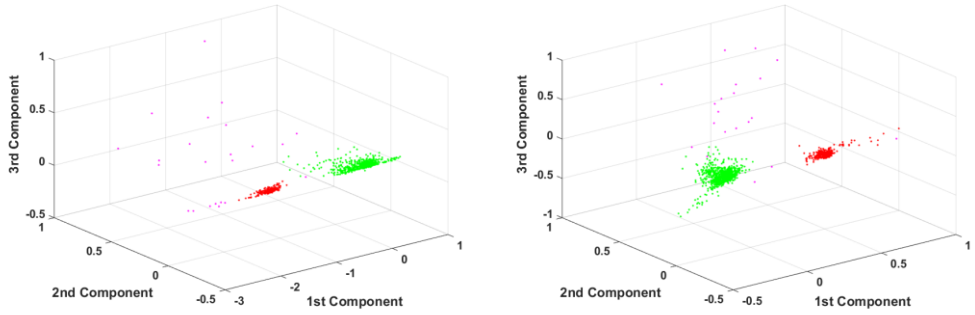

(a) (b)

Figure 6.2.10. 3-D PCA representation of MM energy data at terminal 5 using DBSCAN for (a) bushing measurement point, (b) neutral to earth measurement point.

Figure 6.2.10 shows that although there are some outliers produced in the principle component space, DBSCAN is still able to group the data into two specific classes. This is better than when the data was processed with PCA applied to the wavelet energy data set. Figure 6.2.11 and Figure 6.2.12 show the 2-D histogram patterns and typical individual pulses associated with the main clusters in Figure 6.2.10 for both measurement points.

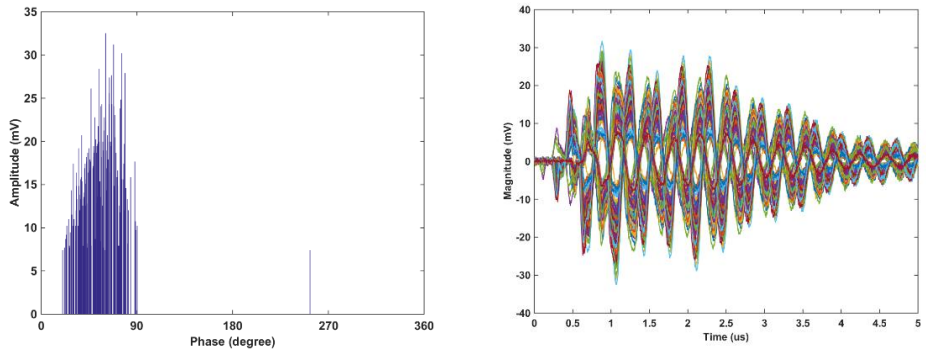

(a) Cluster 1 (in red)

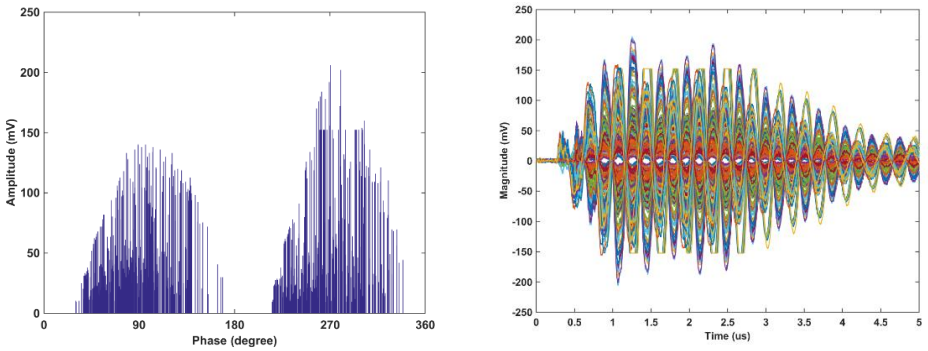

(b) Cluster 2 (in green)

Figure 6.2.11. 2-D histogram pattern and typical individual pulses associated with the main clusters in Figure 6.2.10(a)

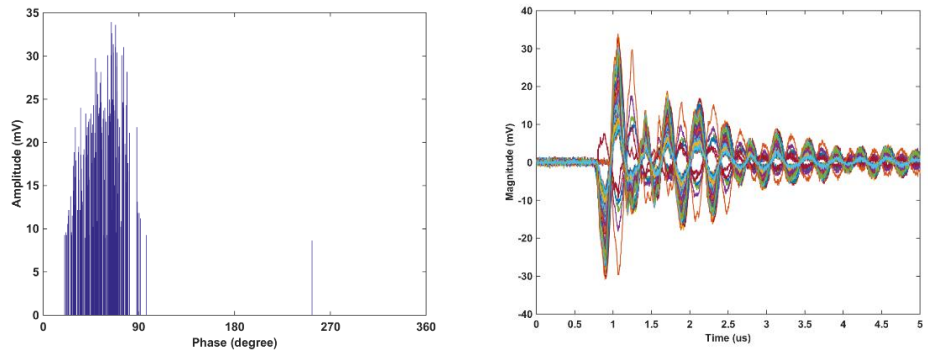

(a) Cluster 1 (in red)

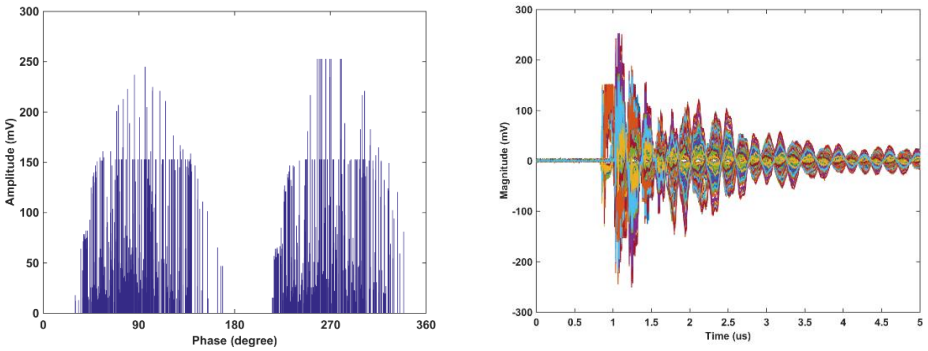

(b) Cluster 2 (in green)

Figure 6.2.12. 2-D histogram pattern and typical individual pulses associated with the main clusters in Figure 6.2.10(b)

Figure 6.2.11 and Figure 6.2.12 show that the data consist of two different pulses, which represent two different PD sources that were injected into the winding. By using MM as the decomposition technique, the data that had been considered as a single cluster when PCA was applied to wavelet energy data is now separated into two different clusters. These can be seen as different 2-D histogram patterns and different typical individual pulses for both measurement points.

The 3-D representation of MM energy data generated using t-SNE and its representation using DBSCAN when PD is injected into terminal 5 for bushing measurement point and neutral to earth measurement point are shown in Figure 6.2.13 and Figure 6.2.14.

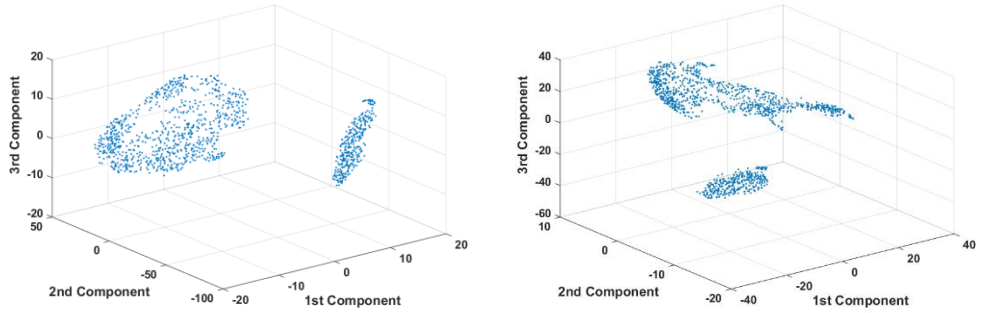

(a) (b)

Figure 6.2.13. 3-D representation of the MM energy data set generated using t-SNE at terminal 5 for (a) bushing measurement point and (b) neutral to earth measurement point.

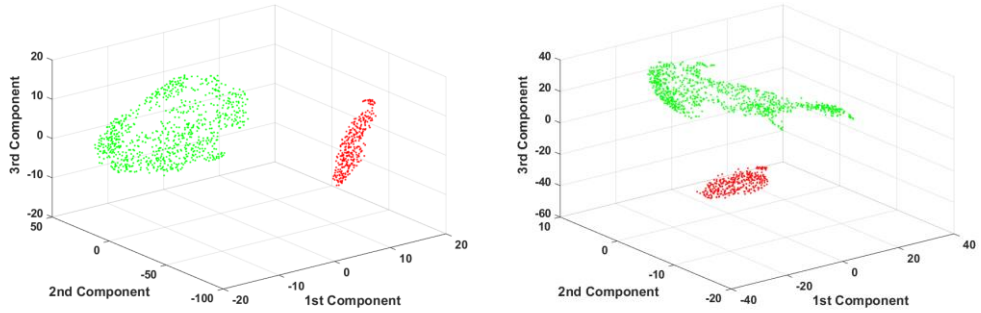

(a) (b)

Figure 6.2.14. 3-D t-SNE representation of MM energy data at terminal 5 using DBSCAN for (a) bushing measurement point, (b) neutral to earth measurement point.

Visual verification of the performance of the t-SNE algorithms to characterize the MM energy data in Figure 6.2.14 provides similar observations as the other t-SNE results. The clusters identified using t-SNE with DBSCAN in either wavelet energy data or MM energy data are linearly separable. The algorithm was very effective at identifying clusters within

complex multi-dimensional distributions. The t-SNE promises to be more effective at retaining the local characteristics of the data as well as the global ones. This is essential for visual verification of the process. The algorithm also produced a higher robustness in the data that was recognised by a higher sensitivity to subtle characteristics of the data. Figure 6.2.15 and Figure 6.2.16 show the 2-D histogram pattern and typical individual pulses associated with the main clusters in Figure 6.2.14 for both measurement points.

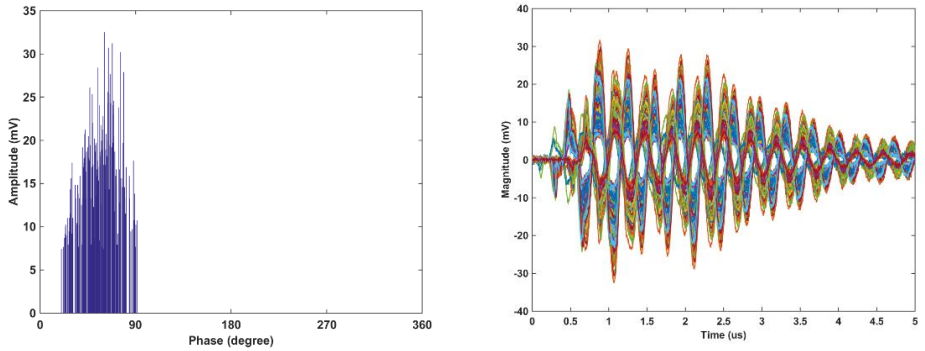

(a) Cluster 1 (in red)

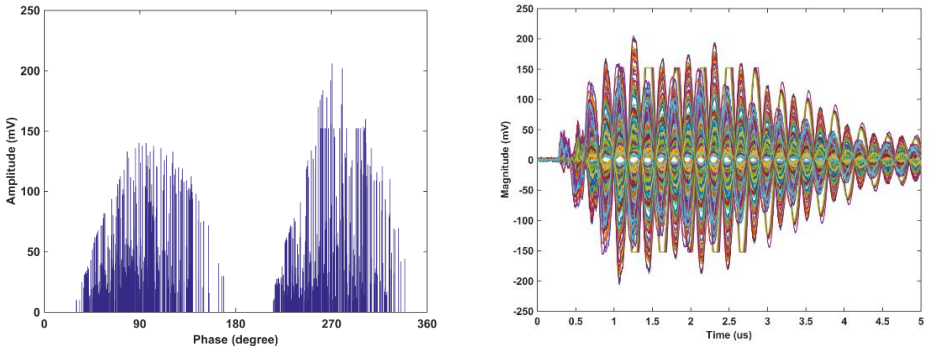

(b) Cluster 2 (in green)

Figure 6.2.15. 2-D histogram pattern and typical individual pulses associated with the main clusters in Figure 6.2.14(a)

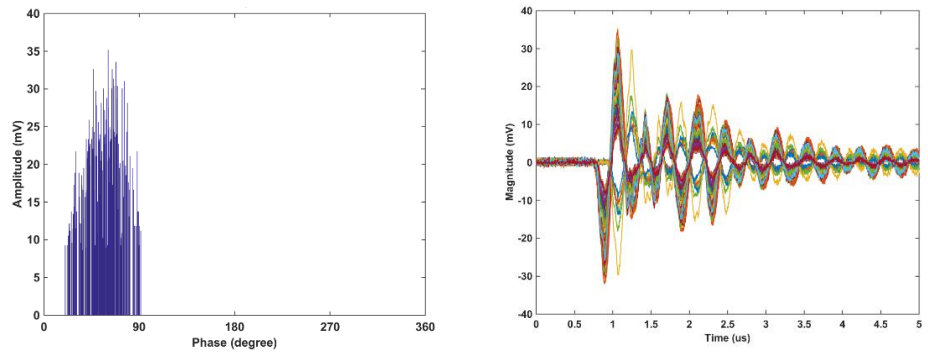

(a) Cluster 1 (in red)

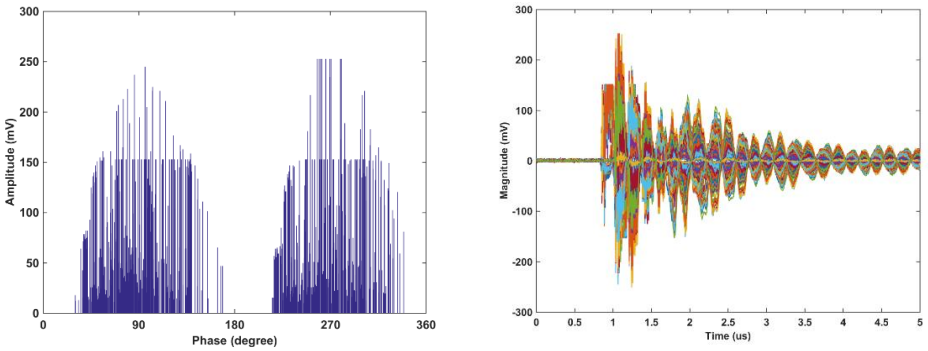

(b) Cluster 2 (in green)

Figure 6.2.16. 2-D histogram pattern and typical individual pulses associated with the main clusters in Figure 6.2.14(b)

Previously, application of DBSCAN on wavelet energy data set using t-SNE showed that there were some misclassified pulses between cluster 1 and cluster 2 at the bushing measurement point. However, Figure 6.2.15 and Figure 6.2.16 show there are no misclassified pulses, and all pulses from both measurement points are now paired between the two measurement points.

Analysis of the plots produced from MM energy using PCA or t-SNE and the application of DBSCAN show that two clusters were identified for each plot in each case. However, as discussed previously, t-SNE is seen to produce well-defined boundaries and compact clusters of the MM energy data set compared to PCA. Furthermore, the main advantage of decomposition using mathematical morphology is that the performance of MM energy does

not depend on pre-selected functions as with wavelet energy analysis. This is highly dependent on pre-selected wavelet functions and need to have high correlation with original PD pulses.

6.3 APPLICATION OF DBSCAN ON MM SPARSITY USING TIME FREQUENCY MAPPING

After sparsity values are calculated, in order to describe the variation of sparsity trends in time and frequency domains for representing PD pulses from multiple PD sources, the values of roughness are applied. Roughness is defined as the average of absolute values of the sparsity, S that can be calculated using:

$$R = \frac{1}{L}\sum_{i=1}^{N} |S(i)| \tag{5.5}$$

where S is the sparsity for each pulse and L is the number of length of SE.

By projecting roughness values of each PD pulse from time and frequency domains onto a time-frequency map, a time-frequency sparsity roughness map is obtained. Each PD pulse is represented by two roughness values calculated in the time and frequency domains. Figure 6.3.1 shows the time-frequency sparsity roughness maps for a combination of floating and surface discharge data which was produced by injecting PD into terminal 1 from bushing measurement point and neutral to earth measurement point respectively. Figure 6.3.2 shows what happens when DBSCAN is applied.

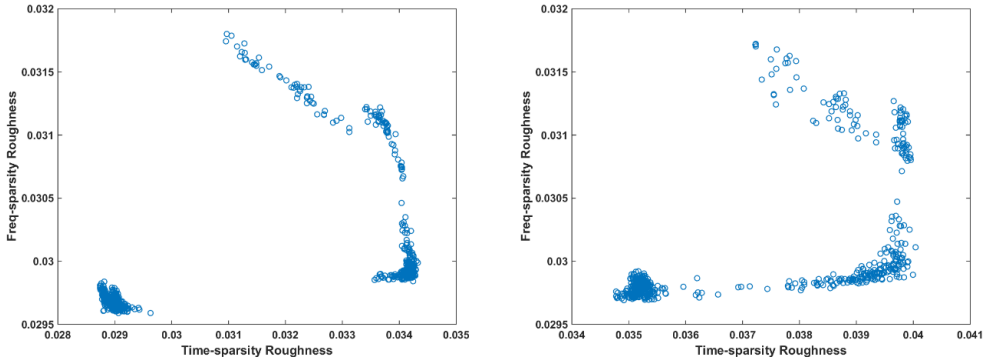

(a) (b)

Figure 6.3.1. Time-frequency sparsity roughness map measured at terminal 1 for (a) bushing measurement point, (b) neutral to earth measurement point.

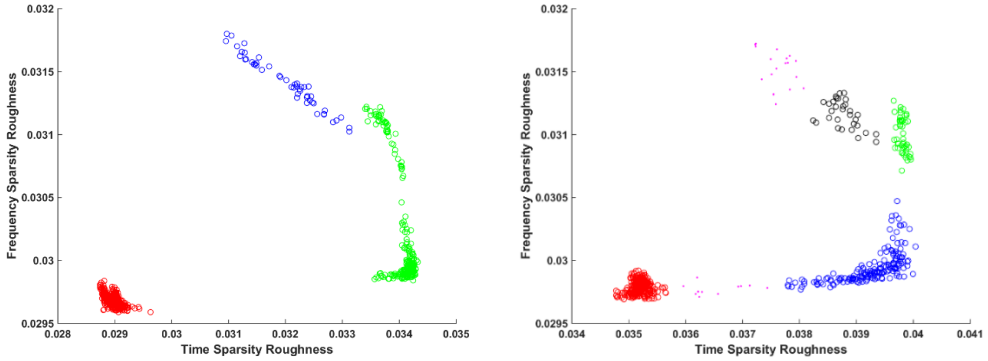

(a) (b)

Figure 6.3.2. Time-frequency sparsity roughness map using DBSCAN measured at terminal 1 for (a) bushing measurement point, (b) neutral to earth measurement point.

Figure 6.3.2(a) and Figure 6.3.2(b) are constructed by projecting roughness values calculated from sparsity values in the time and frequency domains of Figure 5.2.2(a) and Figure 5.2.2(b) with the application of DBSCAN. There are more than two main clusters in each plot, which should represent two different sources injected into the transformer winding. A comparison between the plots of PCA and t-SNE shows these sparsity roughness maps have more outliers, which will affect the clustering process.

As mentioned in Sub-chapter 5.2.2, there are some cases where the trends of sparsity value are not clear enough to represent two sources due to the trends having a similar tendency. Figure 6.3.3 shows the calculated roughness values for the sparsity that have similar tendency while Figure 6.3.4 shows its representation when using DBSCAN.

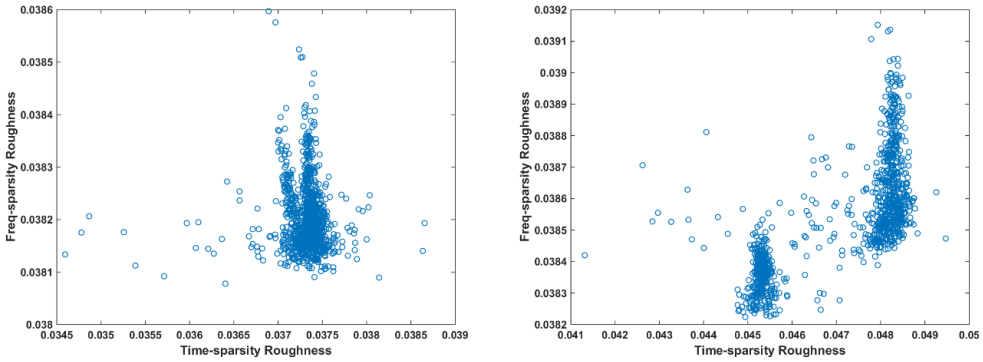

(a) (b)

Figure 6.3.3. Time-frequency sparsity roughness map measured at terminal 7 for (a) bushing measurement point, (b) neutral to earth measurement point.

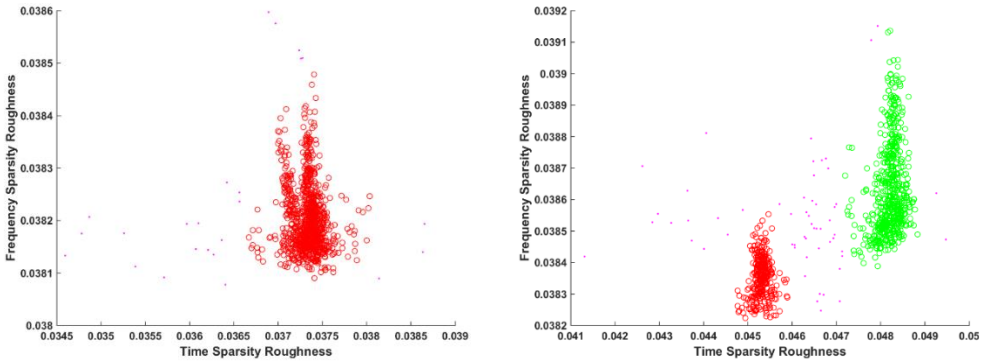

(a) (b)

Figure 6.3.4. Time-frequency sparsity roughness map using DBSCAN measured at terminal 7 for (a) bushing measurement point, (b) neutral to earth measurement point.

Figure 6.3.4(b) shows that although the trends may have a similar tendency, by combining the trends from time domain and frequency domain, a particular type of PD source still can be uniquely represented. However, in Figure 6.3.4(a), the two clusters are seen to overlap each other. This may be because the values of the sparsity trends in this case are very close and the differences are not sufficient to represent the difference between different PD sources. Even though, these two groups can be visualized, DBSCAN as the clustering methods may not be able to distinguish them and consequently multiple PD sources cannot be identified when they are too close on the map.

6.4 SUMMARY

In this chapter, the application of DBSCAN was applied to the Wavelet energy and MM energy data that was processed using PCA, t-SNE and time frequency mapping. Analysis show that MM energy analysis outperform wavelet energy analysis in separating multiple PD sources within a HV transformer winding. The main advantage of decomposition using mathematical morphology is that the performance of MM energy does not depend on pre selecting parameter as in wavelet energy analysis, which is highly, depend on pre-selected mother wavelet and need to having a high correlation with original PD pulses.

The use of PCA, t-SNE and time frequency mapping as the dimension reduction techniques to reduce the dataset is useful to aid in visualisation process and feature extraction. The t-distributed Stochastic Neighbourhood Embedding (t-SNE) algorithm was identified as performing most effectively. It proved to be more effective than PCA and time frequency mapping at retaining the local characteristics of the data as well as the global ones. However, t-SNE is inherently stochastic in nature, so it produces slightly variable results and cannot be used when accurately assessing the separation and location of clusters from multiple plots where the results must be reproducible.

CHAPTER 7

DIMENSIONAL REDUCTION TECHNIQUES WITH OPTICS

Another density based clustering algorithms for spatial data, OPTICS has been chosen as the second clustering technique as it produces clear results that are visually interpretable. In this section, OPTICS is applied to the data that had been discussed previously using DBSCAN and also directly to the data without any dimension reduction technique i.e. a wavelet energy data set and a MM energy data set in order to test the performance of OPTICS on a high dimensional data set.

The main advantages of OPTICS compared to DBSCAN is that it only requires one parameter that was found to be automatable. The only input parameter in OPTICS is MinPts. Throughout this research, a value of one percent of the number of PD signals analysed was found to be perfectly adequate, which is consistent with all the data set. Contrasted with DBSCAN, which is heavily dependent on the parameter ε which cannot be estimated for universal application. The OPTICS algorithm provides ordered points and reachability distances in its reachability plot, which is a useful way of displaying clusters that exist in the tested data set. Within this plot, data that is considered a cluster will be visible as valleys that are separated by a high spikes. The higher the spikes, the more different the data will be in the tested data set. While, the lower the valley, the denser the cluster.

Automatic cluster extraction is vital for any automated process, J. Sander [115] has suggested a means of extracting clusters automatically from the reachability plots. The method is trying to replicate a visual inspection of the data in an automatic programme by considering the rate of rise and fall, sign change ratio and difference in density between different clusters. This produces a tree like representation of the data set containing all clusters and sub-clusters of the data. However, other methods that can be used for universal application and create more compact clusters are still under investigation as these are an important prerequisites for data mining applications.

As far as the automated process is concerned, automatic cluster extraction is implemented in this application based on the data set obtained from the experiments by using the derivative and magnitude of the reachability graph. A cluster boundary is therefore defined by a large derivative of the reachability distance, coupled with a magnitude that is significantly above 80% of three maximum values from 10% to 90% of the ordered points. This is to make sure that the threshold is taken on the spikes that are situated between the two flattest or lowest valleys. If there are a few spikes that are very close together, the maximum spikes are chosen while the rest will be neglected as due to the points or outliers that are close together and connected to each other between the main clusters. The performance of OPTICS will be presented and discussed in this section.

7.1 APPLICATION OF OPTICS TO WAVELET TRANSFORM OUTPUT

In this section, OPTICS is applied directly to the wavelet energy data set without any dimensional reduction techniques. That is mean OPTICS was applied to the 10 dimensional of wavelet energy data set without application of PCA or t-SNE. Figure 7.1.1 shows the reachability plot produced by OPTICS for the wavelet energy data set generated from a combination of floating and surface discharges at terminal 1 for both measurement points.

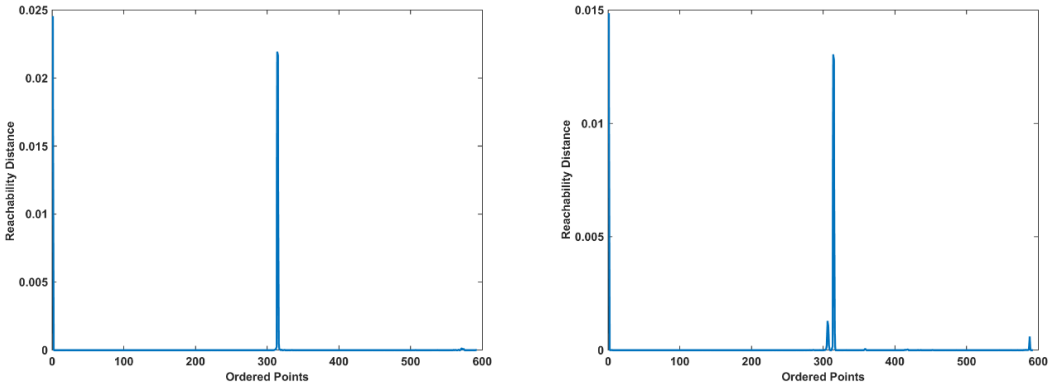

(a) (b)

Figure 7.1.1. The reachability plots of OPTICS on wavelet energy data at terminal 1 for (a) bushing measurement point, (b) neutral to earth measurement point.

The reachability plots clearly show that the clusters have been extracted correctly, as they are separated by a large spike approximately at point 320 for both measurement points. The clusters were separated at the same point for both measurement point due to the pulse pairing process that was done before the analysis. The pulse pairing process which is based on a reasonable time of flight duration is used to find and match pairs of PD pulses for both measurement points before a comparison can be made. The analysis was done on the same original pulses from the PD sources at both measurement points. The 2-D histogram patterns and typical individual pulses associated with each cluster for both measurement points are shown in Figure 7.1.2 and Figure 7.1.3.

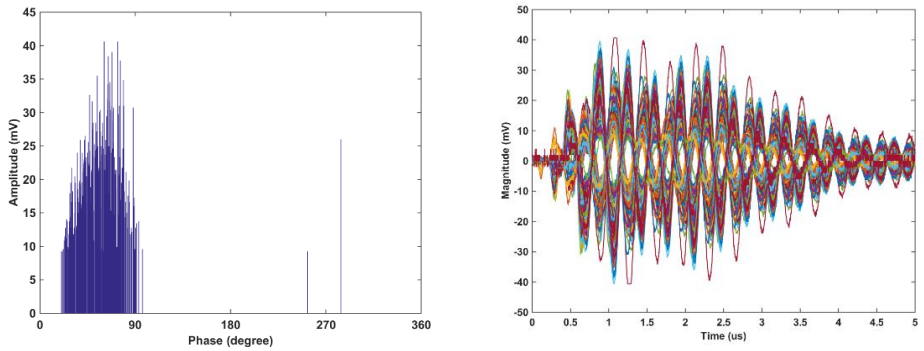

(a) Cluster 1 (left)

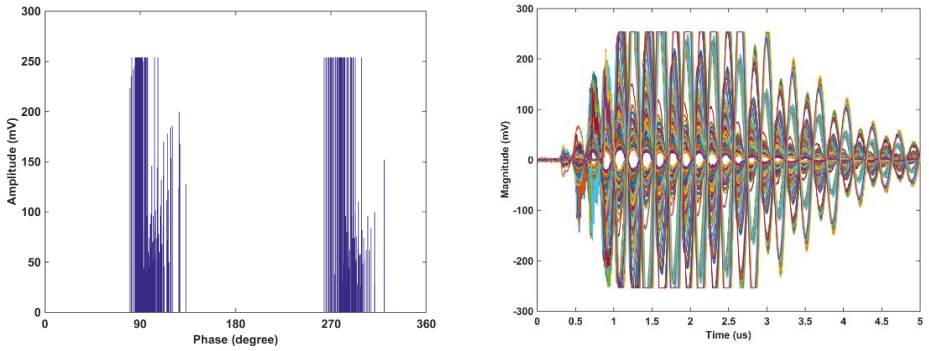

(b) Cluster 2 (right)

Figure 7.1.2. 2-D histogram pattern and typical individual pulses associated with the clusters in Figure 7.1.1(a)

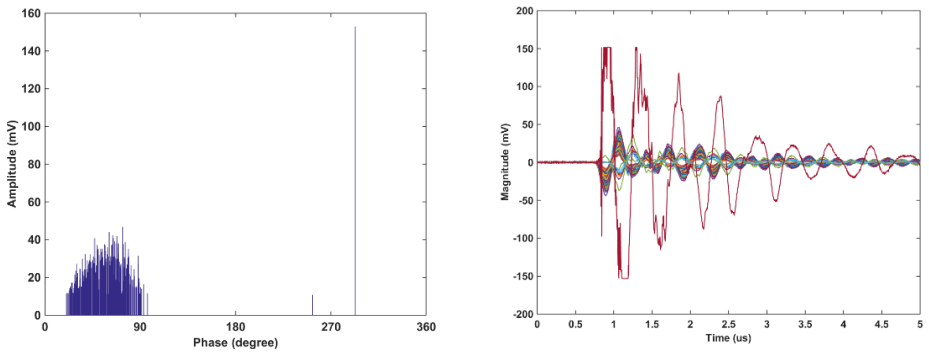

(a) Cluster 1 (left)

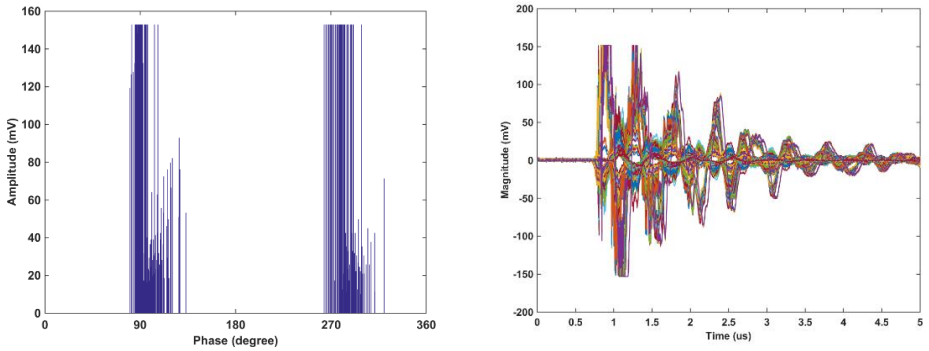

(b) Cluster 2 (right)

Figure 7.1.3. 2-D histogram pattern and typical individual pulses associated with the clusters in Figure 7.1.1(b)

There are two different pulse shapes which were clustered by OPTICS which is similar to when DBSCAN was applied to wavelet energy data using t-SNE. However, in cluster 1 of Figure 7.1.3 one additional pulse was found. This additional pulse is believed to be a misclassified pulse from cluster 2 as it has same value of magnitude as the pulses from cluster 2 as shown in Figure 7.1.3. This may be due to the fact that this point is closer to the points in cluster 1 than to cluster 2. Therefore, this point might be considered as the outlier point of cluster 2 as it is further away from the main points of cluster 2. Although some misclassifications occurred which can be neglected as the misclassified pulses do not make up more than 1% of the total number of PD pulses, OPTICS is still able to separate the two

different PD pulses without any dimensional reduction technique. This shows that OPTICS works within a high dimensional data set.

However, when it comes to terminal 5, the spikes are hidden and not clearly visual within the reachability plots. This is due to the fact that the energy that represents each pulse from both measurement points are close together as they were injected in the middle of the winding. Figure 7.1.4 shows the reachability plot produced by OPTICS on the wavelet energy data set generated from a combination of floating and surface discharge at terminal 5 for both measurement points.

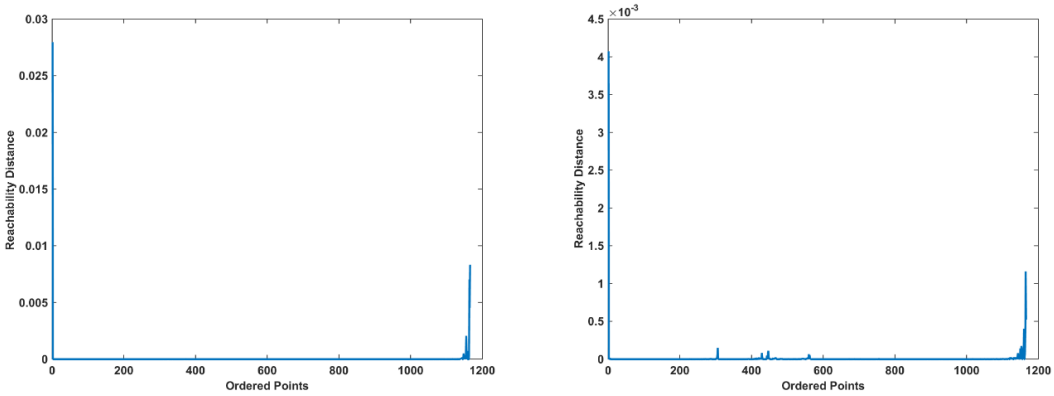

(a) (b)

Figure 7.1.4. The reachability plots of OPTICS on wavelet energy data at terminal 5 for (a) bushing measurement point, (b) neutral to earth measurement point.

Initial examination of the reachability plot produced by OPTICS clearly indicates the presence of only one cluster. However, it has been shown using previous methods that there are in fact two different main clusters in the data set. When the reachability distance was plotted from 10% to 90% of the ordered points, the spikes in the middle of the reachability plot were revealed. Figure 7.1.5 shows the reachability plots with the threshold value that was set automatically. By using the threshold value that was set automatically from 10% to 90% of the ordered points, the two expected clusters are extracted. The 2-D histogram patterns and typical individual pulses associated with each cluster for both measurement points are shown in Figure 7.1.6 and Figure 7.1.7.

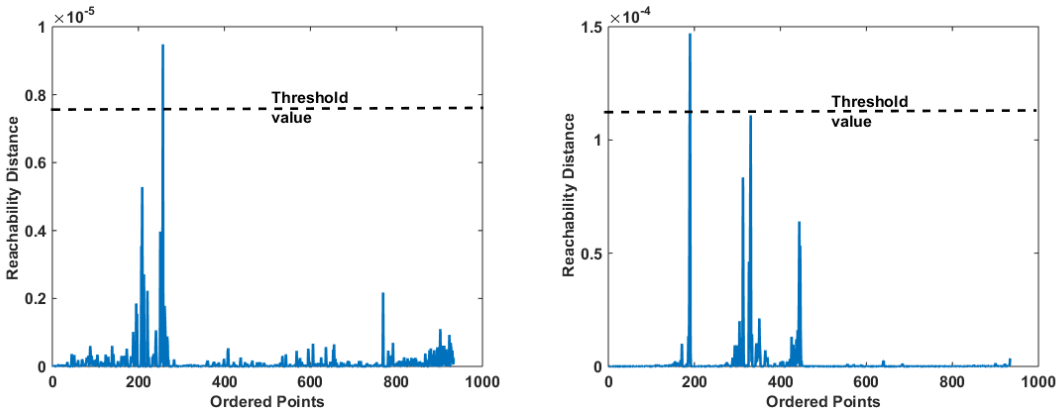

(a) (b)

Figure 7.1.5. The reachability plots from 10% to 90% of ordered points at terminal 5 for (a) bushing measurement point, (b) neutral to earth measurement point.

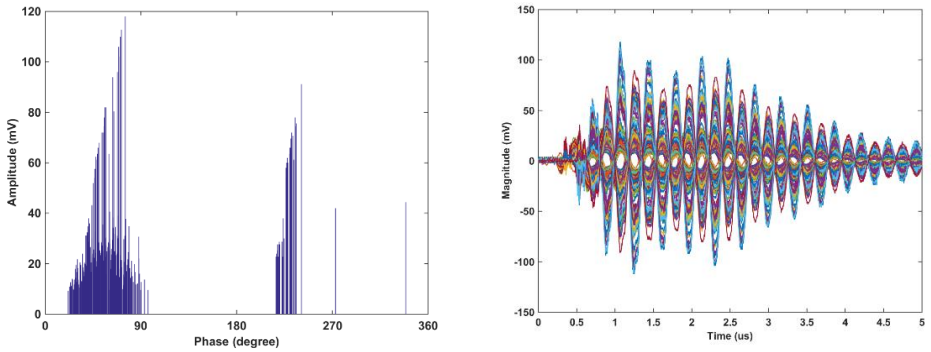

(a) Cluster 1 (left)

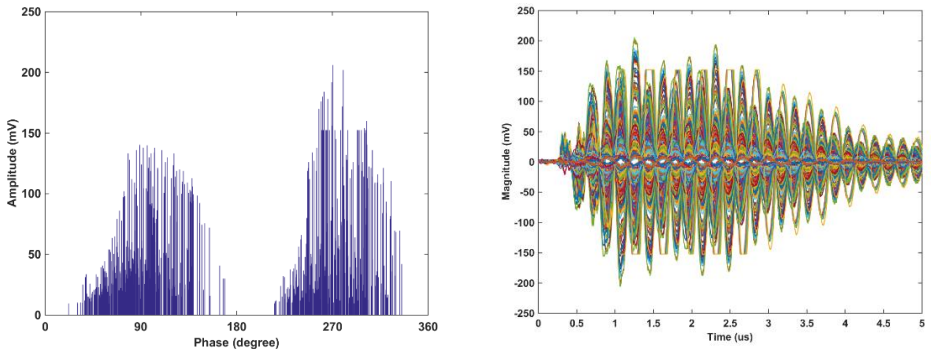

(b) Cluster 2 (right)

Figure 7.1.6. 2-D histogram patterns and typical individual pulses associated with the clusters in Figure 7.1.5(a)

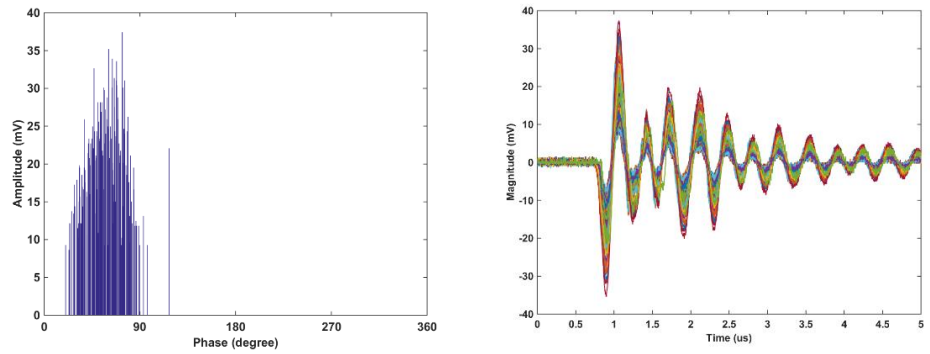

(a) Cluster 1 (left)

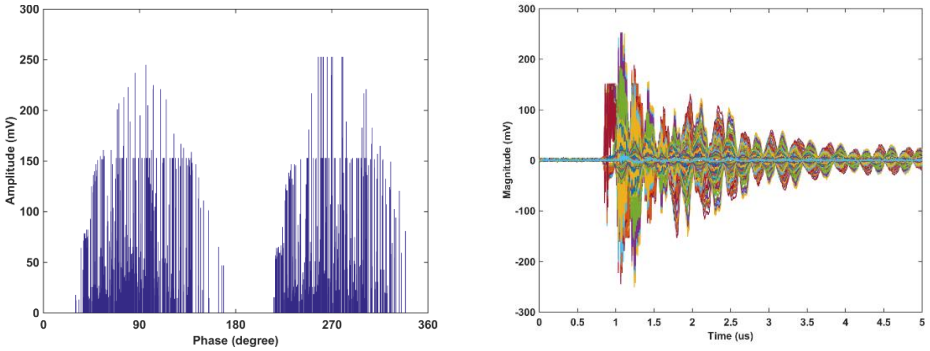

(b) Cluster 2 (right)

Figure 7.1.7. 2-D histogram patterns and typical individual pulses associated with the clusters in Figure 7.1.5(b)

In Figure 7.1.6(a), based on the 2-D histogram pattern, there are some pulses that have a similar magnitude and pattern to the pulses in cluster 2. These are not in pairs with cluster 1 in Figure 7.1.7(a). This is similar to what happened when DBSCAN was applied to the wavelet energy data set using t-SNE as discussed previously. However, as seen Figure 7.1.5 if the threshold value to extract clusters was set manually from the reachability plot, more clusters with different pulse shapes can be extracted as there might be pulses that come from external random signals or background noise picked up by measuring sensors by coincidence. Additionally, the pulses that come from the same PD sources might produce different pulse shapes, as PD events are stochastic in nature meaning that there is a variation in the time interval between discharges as well as the magnitude of discharges.

Figure 7.1.8 and Figure 7.1.9 show more clusters with different patterns of pulses which are extracted when the threshold was set according to a large derivative of the reachability distance, coupled with a magnitude that is significantly above 20% instead of 80% of three maximum values from 10% to 90% of the ordered points.

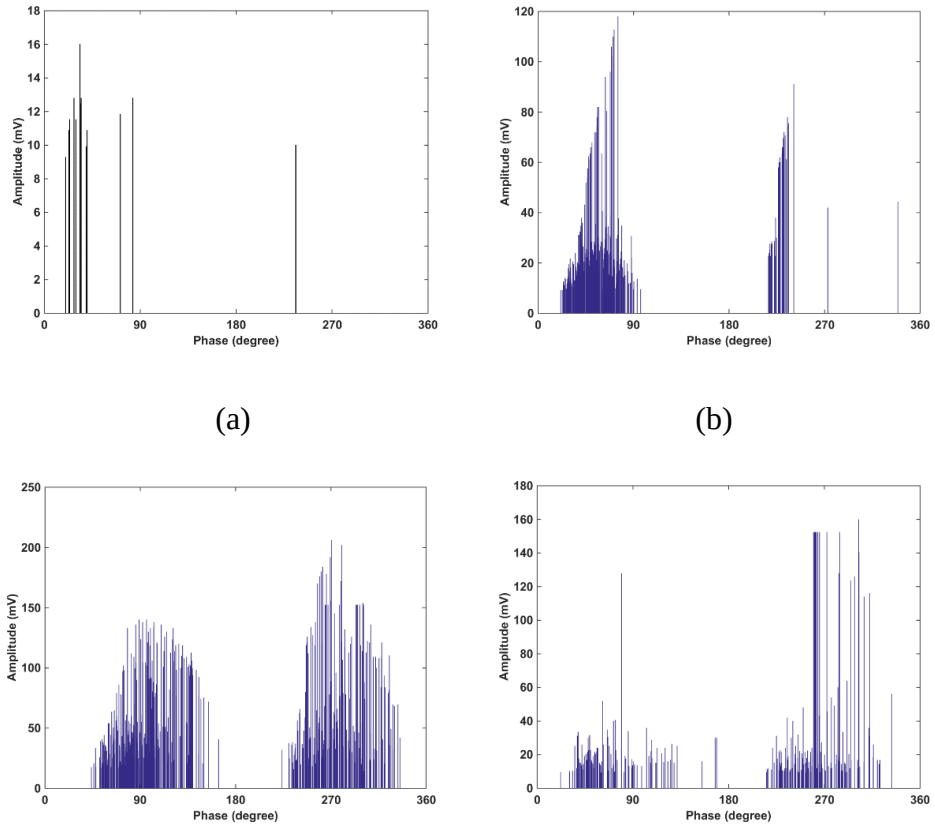

Figure 7.1.8. 2-D histogram patterns associated with the clusters in Figure 7.1.5(a) when threshold was set above 20% of three maximum values.

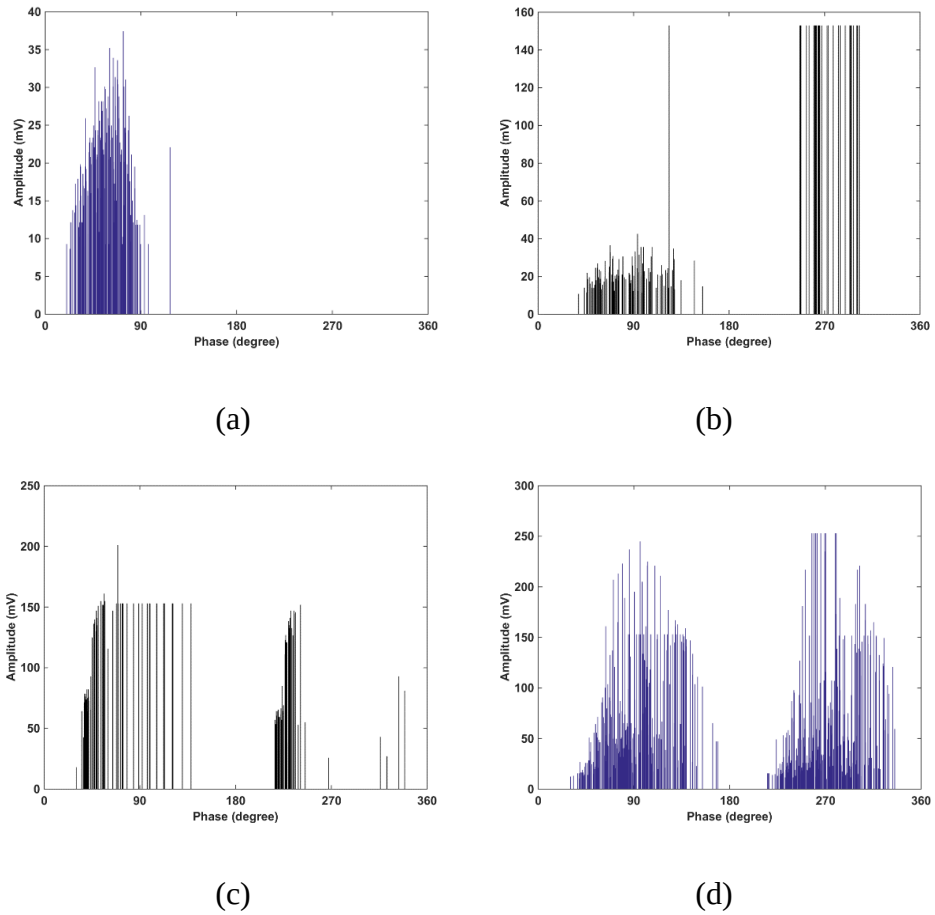

Figure 7.1.9. 2-D histogram patterns associated with the clusters in Figure 7.1.5(b) when threshold was set above 20% of three maximum values.

This shows OPTICS is useful to evaluate the performance of dimensional reduction techniques in order to find the best representation of the data that leads to reliable clustering. Therefore, OPTICS provides superior performance within research environments by giving the user the ability to manually control the threshold value and see the clustering effects and also to refine the program so that all clusters can be extracted accordingly. Analysis of OPTICS directly on the high dimension wavelet energy data set shows that OPTICS without any dimension reduction techniques is able to separate the multiple sources very well.

7.2 APPLICATION OF OPTICS ON WAVELET ENERGY USING PCA AND T-SNE

In this section, the application of OPTICS is considered with dimensional reduction techniques, from ten dimensions to three dimensions using PCA and t-SNE. As discussed previously, the use of dimensional reduction techniques are to provide the additional benefit of allowing visual examination by directly plotting the data in 3D space. However, by using OPTICS reachability plots, it also provides an easy way to visualise the performance of the dimensional reduction techniques. Figure 7.2.1 and Figure 7.2.4 show the reachability plots produced by OPTICS for wavelet energy data sets that had been processed by PCA and t-SNE algorithms generated from a combination of floating and surface discharges at terminal 1 for both measurement points. While their 2D histograms pattern and typical individual pulses are shown in Figure 7.2.2 – Figure 7.2.3 and Figure 7.2.5 – Figure 7.2.6 respectively.

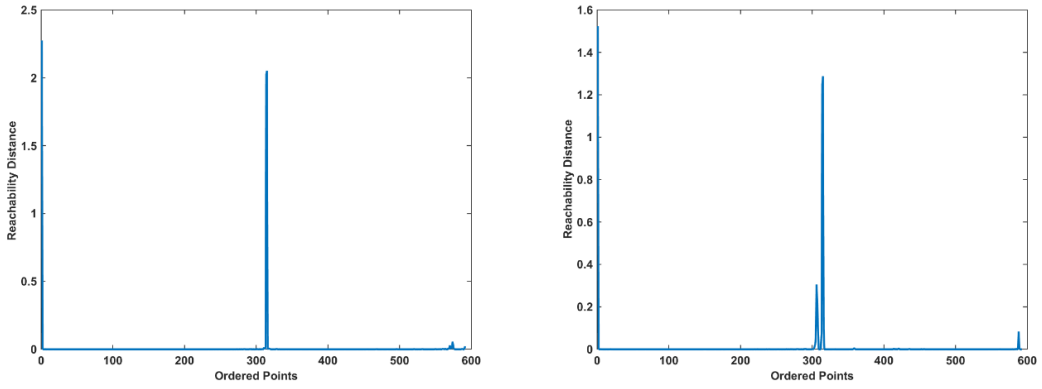

(a) (b)

Figure 7.2.1. The reachability plots of OPTICS on wavelet energy data processed by PCA at terminal 1 for (a) bushing measurement point, (b) neutral to earth measurement point.

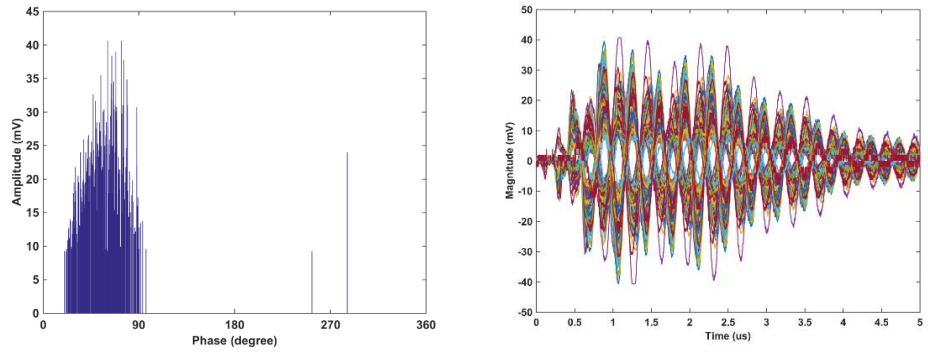

(a) Cluster 1 (left)

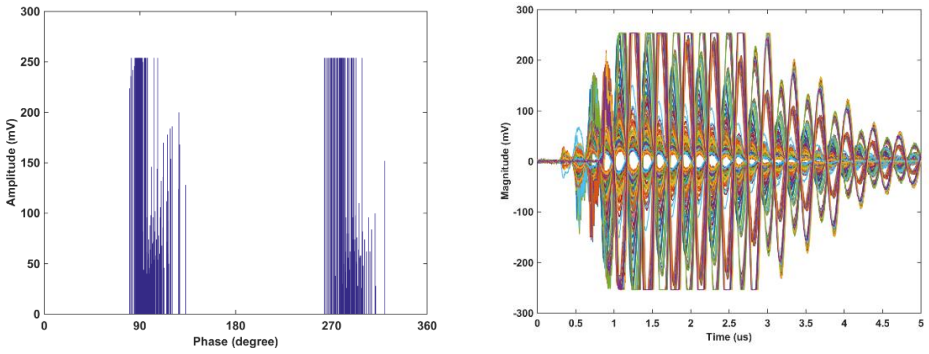

(b) Cluster 2 (right)

Figure 7.2.2. 2-D histogram pattern and typical individual pulses associated with the clusters in Figure 7.2.1(a)

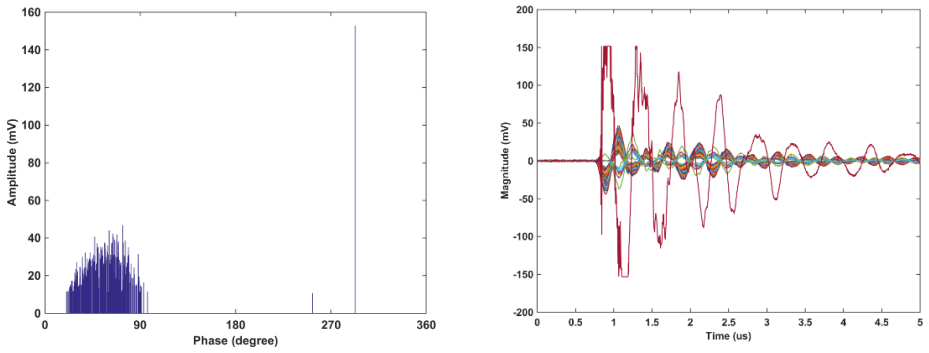

(a) Cluster 1 (left)

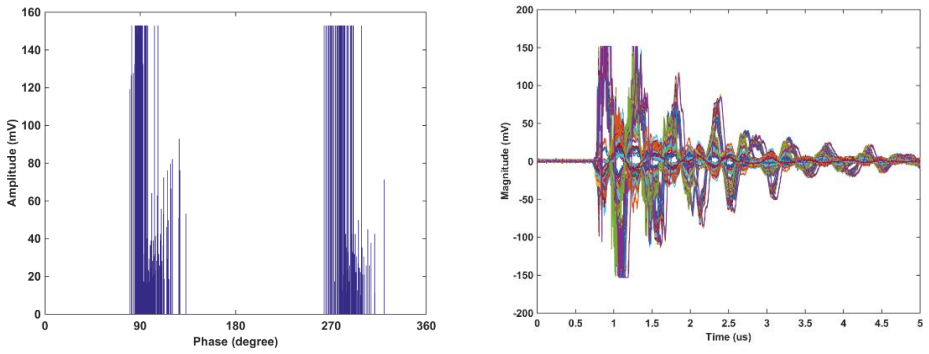

(b) Cluster 2 (right)

Figure 7.2.3. 2-D histogram pattern and typical individual pulses associated with the clusters in Figure 7.2.1(b)

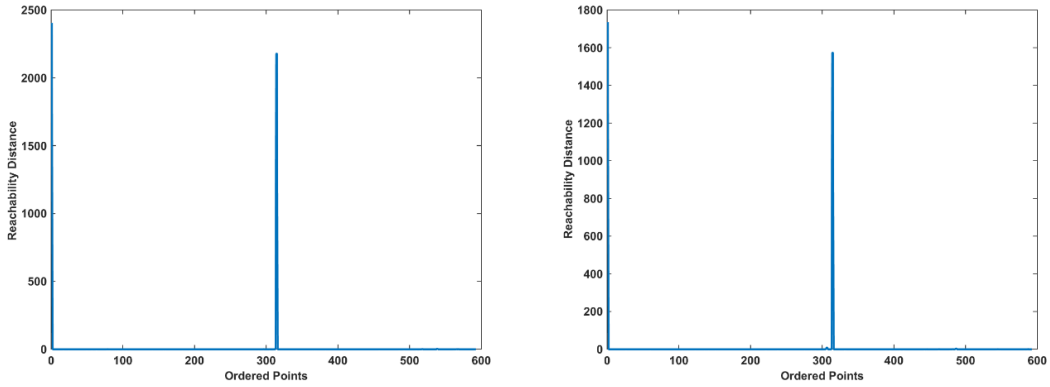

(a) (b)

Figure 7.2.4. The reachability plots of OPTICS on wavelet energy data processed by t-SNE at terminal 1 for (a) bushing measurement point, (b) neutral to earth measurement point.

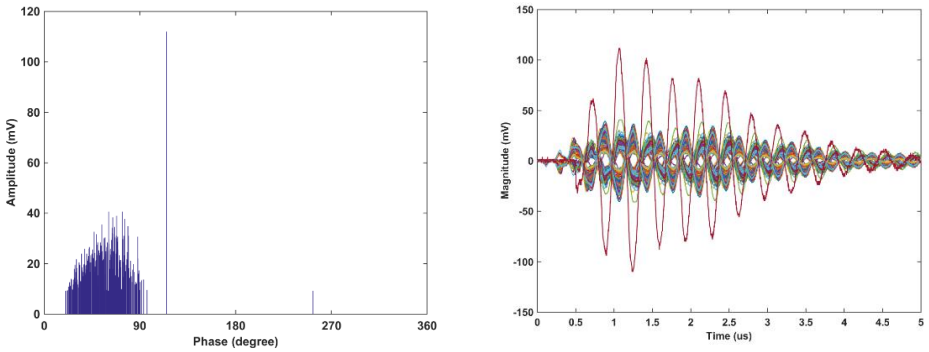

(a) Cluster 1 (left)

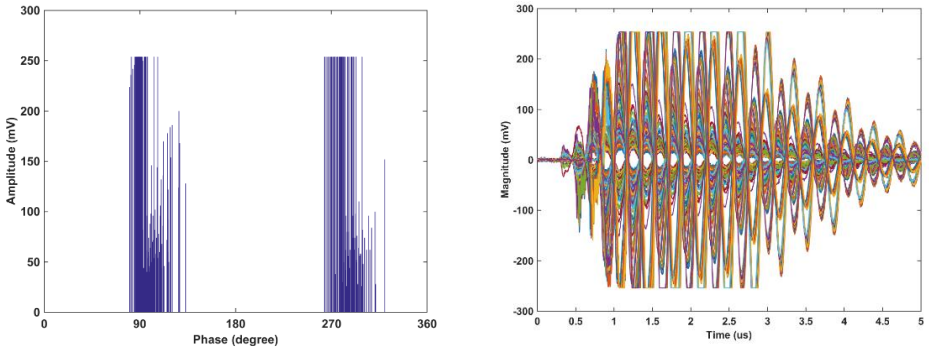

(b) Cluster 2 (right)

Figure 7.2.5. 2-D histogram pattern and typical individual pulses associated with the clusters in Figure 7.2.4(a)

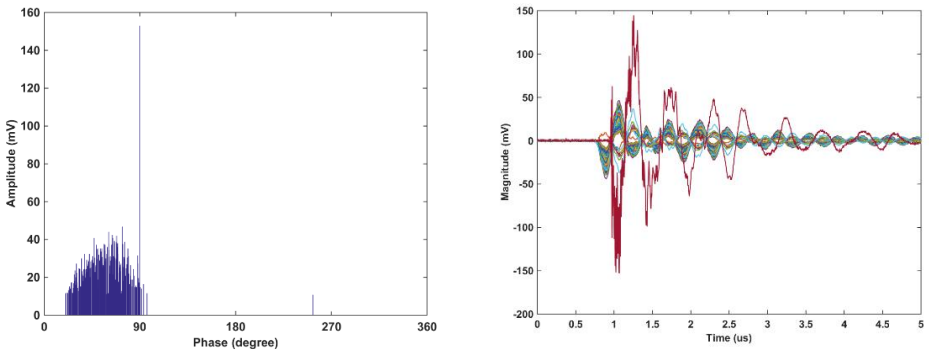

(a) Cluster 1 (left)

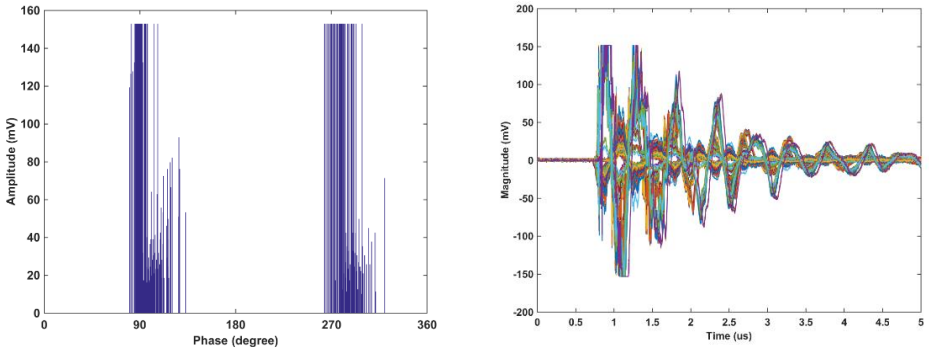

(b) Cluster 2 (right)

Figure 7.2.6. 2-D histogram pattern and typical individual pulses associated with the clusters in Figure 7.2.4(b)

Both techniques produced some misclassified pulses which can be neglected in cluster 1 as they consist of pulses less than 1% of the total points for both measurement points. The performance of OPTICS on the data that had been processed by PCA and t-SNE at this terminal are almost identical to the results when DBSCAN was used as they are able to separate the two sources easily. However, when PD is injected into terminal 5, OPTICS seems to outperform DBSCAN in separating multiple sources for both measurement points.

As discussed in sub-chapter 6.1, visual inspection of the representation generated using DBSCAN on the wavelet energy that had been processed by PCA appears to produce a single cluster of data points. DBSCAN was not able to separate the wavelet energy data that had

been processed by PCA as the clusters overlapped or were very close to each other in the space.

The main problem with DBSCAN is its inability to group data in which clusters are of different densities. Additionally, the DBSCAN clustering performance is very dependent on input parameters whose selection cannot be analytically evaluated nor assumed constant. However, by using OPTICS on the same wavelet energy data set, two clusters were extracted as expected. Figure 7.2.7 shows the reachability plots from 10% to 90% of the ordered points with the threshold value that was set automatically when OPTICS was applied to the wavelet energy data processed by PCA with PD injected into terminal 5 for both measurement points.

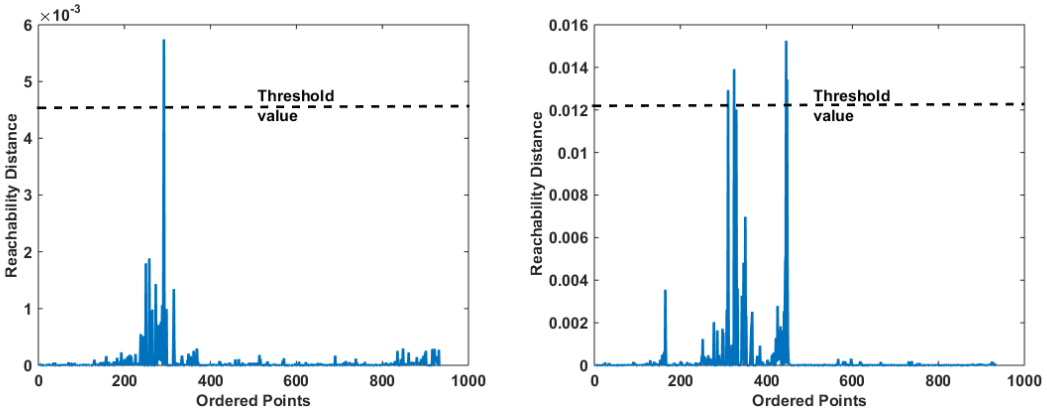

(a) (b)

Figure 7.2.7. The reachability plots of OPTICS on wavelet energy data processed by PCA at terminal 5 for (a) bushing measurement point, (b) neutral to earth measurement point.

The reachability plot of OPTICS in Figure 7.2.7 shows that the clusters were separated by the high spike. There are two separate clusters measured at the bushing measurement point, while there were three separate clusters measured at the neutral to earth measurement points.

The 2-D histogram patterns and typical individual pulses associated with the extracted clusters for both measurement points are shown in Figure 7.2.8 and Figure 7.2.9 respectively.

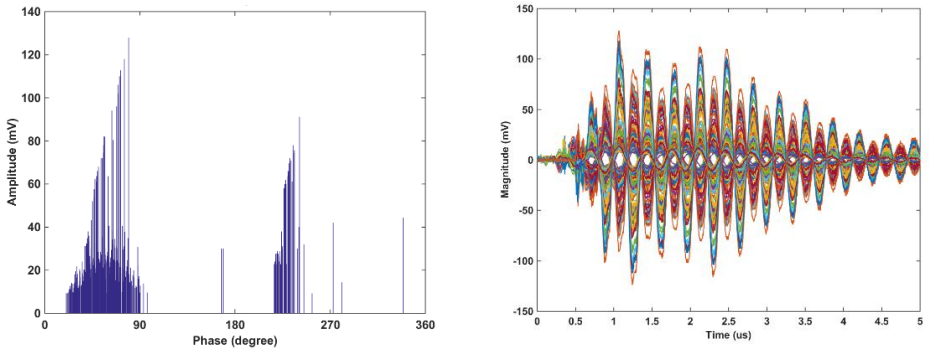

(a) Cluster 1 (left)

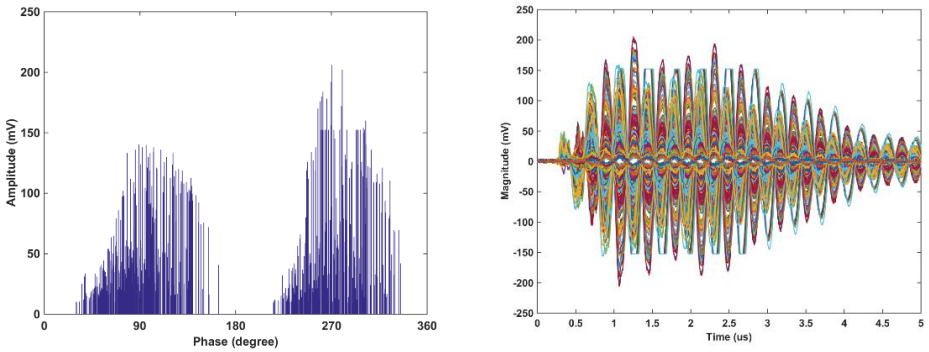

(b) Cluster 2 (right)

Figure 7.2.8. 2-D histogram pattern and typical individual pulses associated with the clusters in Figure 7.2.7(a)

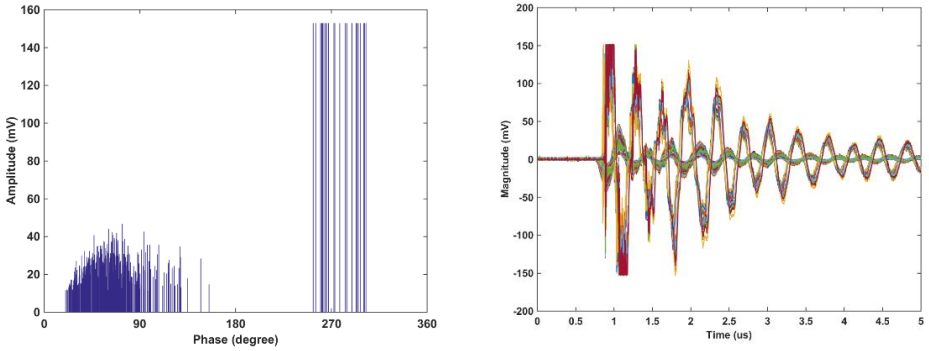

(a) Cluster 1 (left)

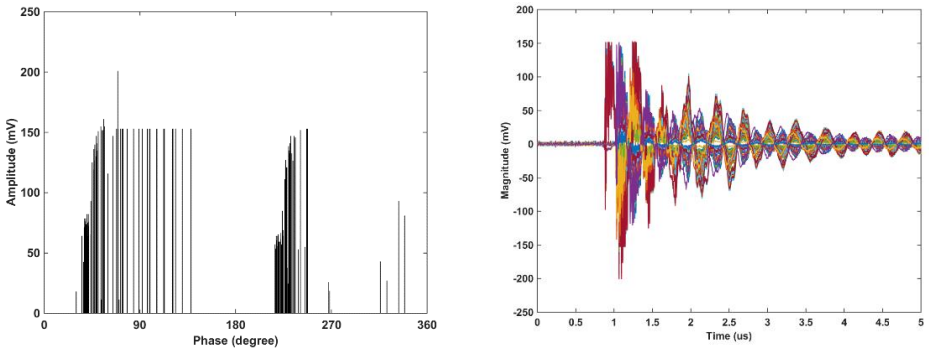

(b) Cluster 2 (middle)

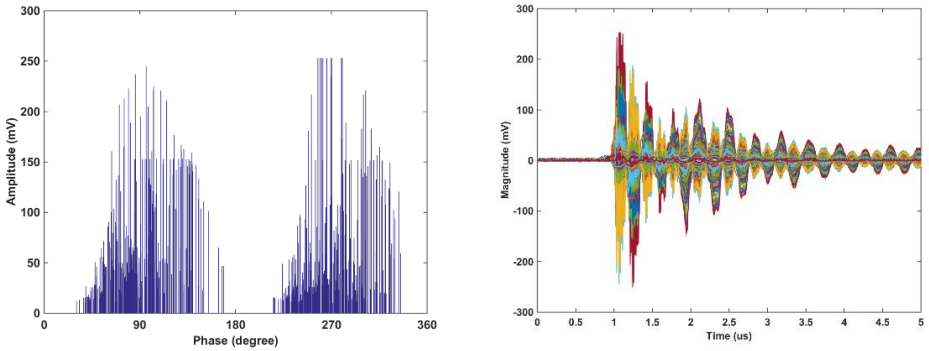

(c) Cluster 3 (left)

Figure 7.2.9. 2-D histogram pattern and typical individual pulses associated with the clusters in Figure 7.2.7(b)

Figure 7.2.8 and Figure 7.2.9 show that OPTICS is able to separate the sources by its reachability plots with the threshold that was set automatically. Even though the 2-D histogram patterns show that lots of misclassified pulses occurred, OPTICS at least provides far better results than DBSCAN on wavelet energy data that had been processed by PCA. However, as discussed previously, the threshold of OPTICS can be adjustable in order to reveal more clusters that may have different densities in the data. For a clear comparison between DBSCAN and OPTICS, Figure 7.2.10 shows the output of OPTICS created using the method used to generate clusters using DBSCAN.

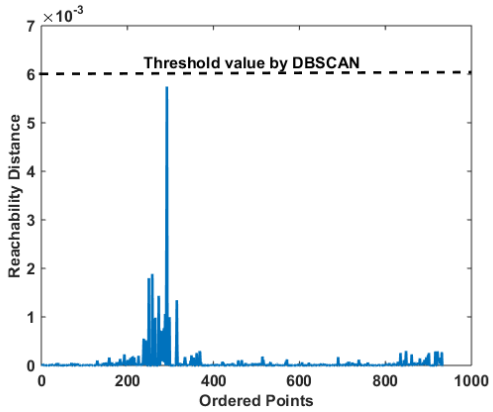

Figure 7.2.10. The output of OPTICS contracted with the method used to generate clusters using DBSCAN.

The comparison was made as both techniques use very similar density based clustering techniques. Figure 7.2.10 shows that by using its universal parameter, DBSCAN overlooked the peak and provides only one main cluster in the data. This is may be due to the clusters having significantly different densities which DBSCAN is unable to differentiate.

Figure 7.2.11 shows the reachability plots when OPTICS was applied to the wavelet energy data processed by t-SNE for both measurement points. The 2-D histogram patterns and typical individual pulses for both measurement points are shown in Figure 7.2.12 and Figure 7.2.13 respectively.

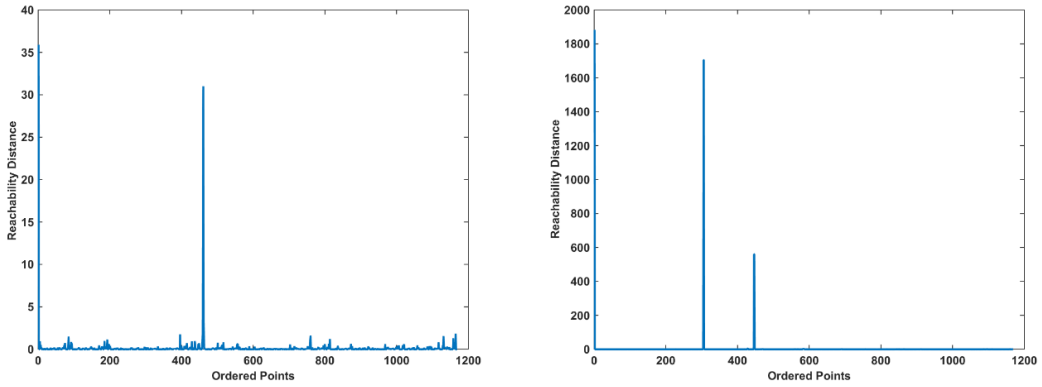

(a) (b)

Figure 7.2.11. The reachability plots of OPTICS on wavelet energy data processed by t-SNE at terminal 5 for (a) bushing measurement point, (b) neutral to earth measurement point.

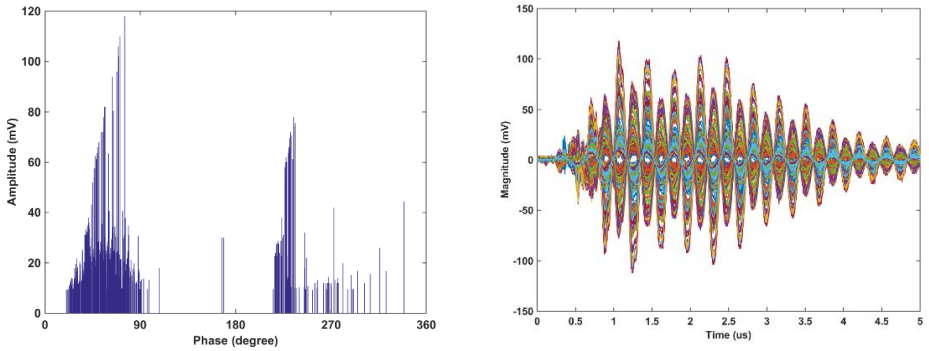

(a) Cluster 1 (left)

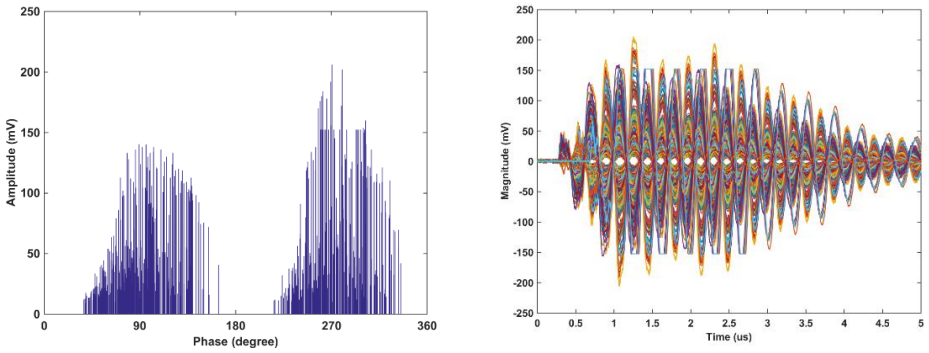

(b) Cluster 2 (right)

Figure 7.2.12. 2-D histogram pattern and typical individual pulses associated with the clusters in Figure 7.2.11(a)

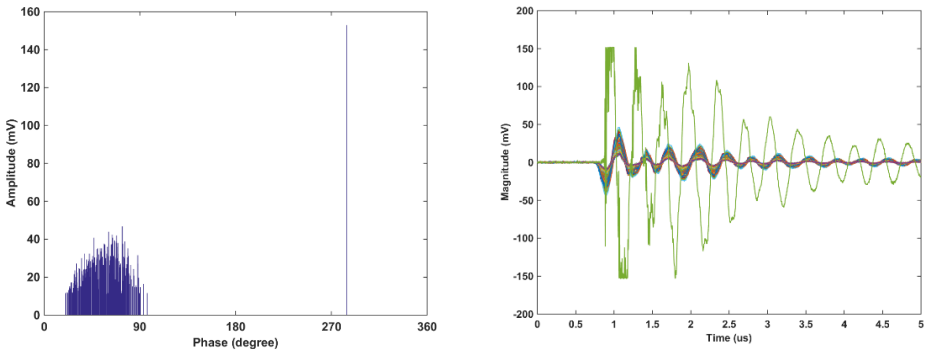

(a) Cluster 1 (left)

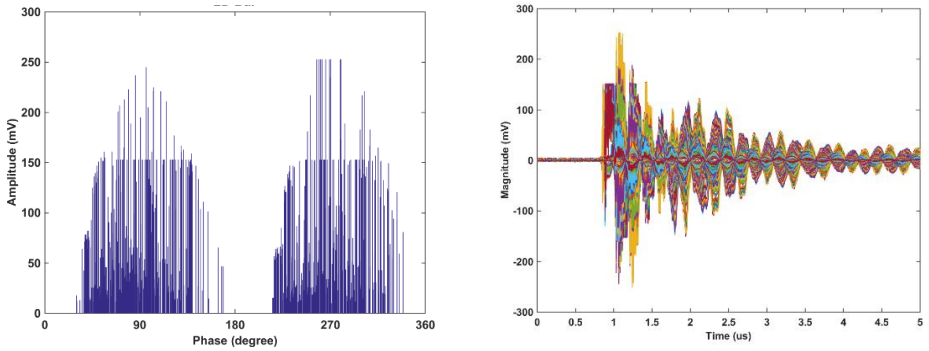

(b) Cluster 1 (right)

Figure 7.2.13. 2-D histogram pattern and typical individual pulses associated with the clusters in Figure 7.2.11(b)

The clustering of the data pre-processed by t-SNE is vastly superior to that achieved with PCA. This is apparent from the spikes on the reachability plots produced from PCA showing that the pulse shapes within each cluster do not vary much. The very large spikes in the reachability plots produced using t-SNE shows that the clusters are very separable in the three-dimensional space. Similar results were seen when OPTICS was applied to the wavelet energy data set that had been produced by PCA and t-SNE when PD was injected into terminal 7 as shown in Figure 7.2.14 and Figure 7.2.15 respectively.

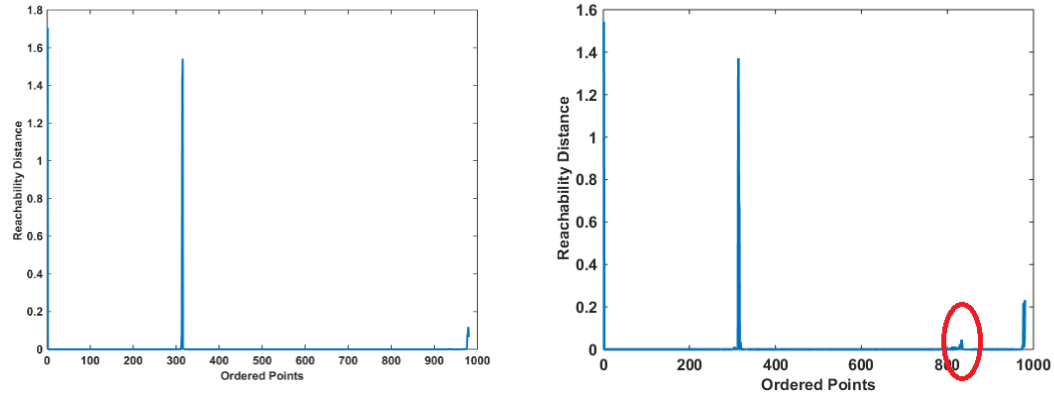

(a) (b)

Figure 7.2.14. The reachability plots of OPTICS on wavelet energy data processed by PCA at terminal 7 for (a) bushing measurement point, (b) neutral to earth measurement point.

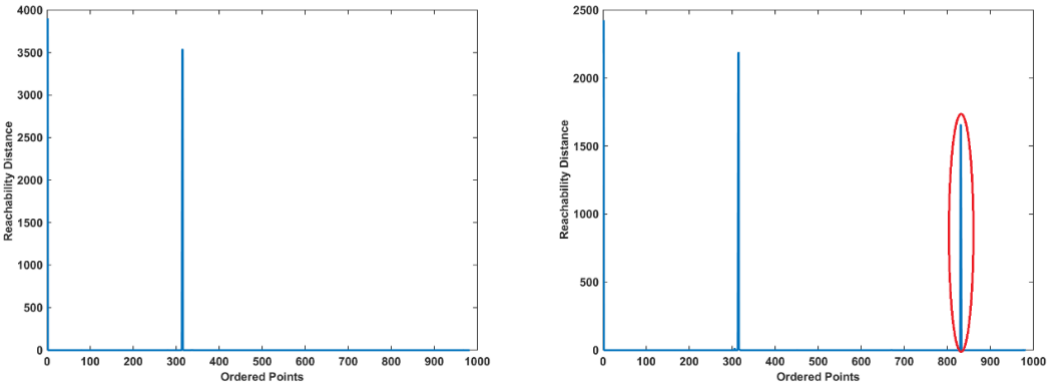

(a) (b)

Figure 7.2.15. The reachability plots of OPTICS on wavelet energy data processed by t-SNE at terminal 7 for (a) bushing measurement point, (b) neutral to earth measurement point.

Analysis of the reachability plots of OPTICS on wavelet energy data processed by PCA and t-SNE show that the distinction between clusters that had been processed by PCA are very low compared to those that had been processed by t-SNE. These are highlighted in Figure 7.2.14 and Figure 7.2.15. In terms of data representation between PCA and t-SNE,

t-SNE provides better results. Additionally, t-SNE also maintains the separation of the data points from high to low dimension space.

7.3 APPLICATION OF OPTICS ON A MM ENERGY OUTPUT

This section considers the application of OPTICS to a high dimensional data set of MM energy. As discussed previously, when SE lengths are set from 1 to 20, it gives 20 different frequency bands of PD pulses. Different lengths of SE, contain different finite amounts of energy within a specific range of frequencies. The energy of the measured signals are calculated for each SE length, which gives 20 different energy elements for each signal. The reachability plots when OPTICS was applied to the MM energy data set generated from a combination of floating and surface discharge at terminal 1 are shown in Figure 7.3.1 for both measurement points.

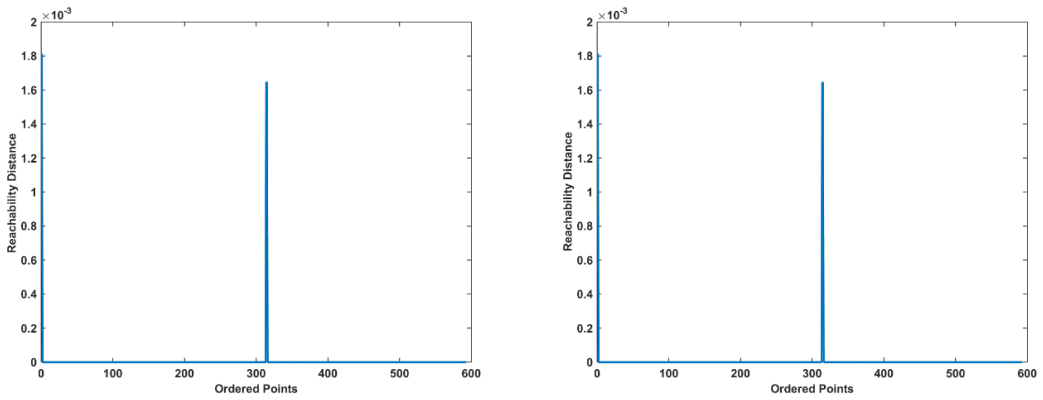

(a) (b)

Figure 7.3.1. The reachability plots of OPTICS on MM energy data at terminal 1 for (a) bushing measurement point, (b) neutral to earth measurement point.

The 2-D histogram pattern and typical individual pulses associated with each cluster for both measurement points are shown in Figure 7.3.2 and Figure 7.3.3.

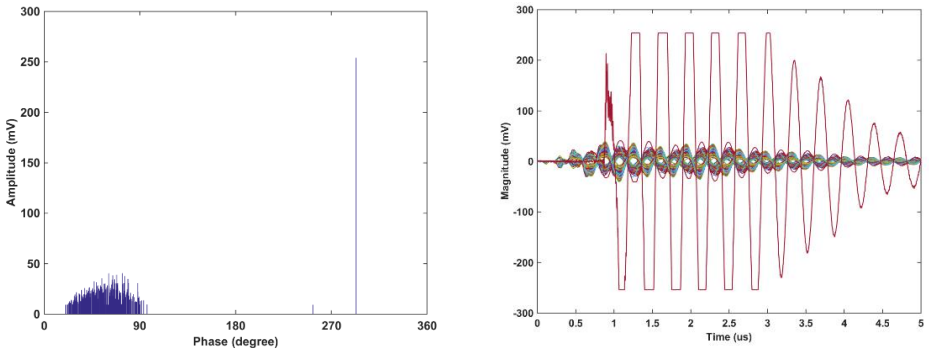

(a) Cluster 1 (left)

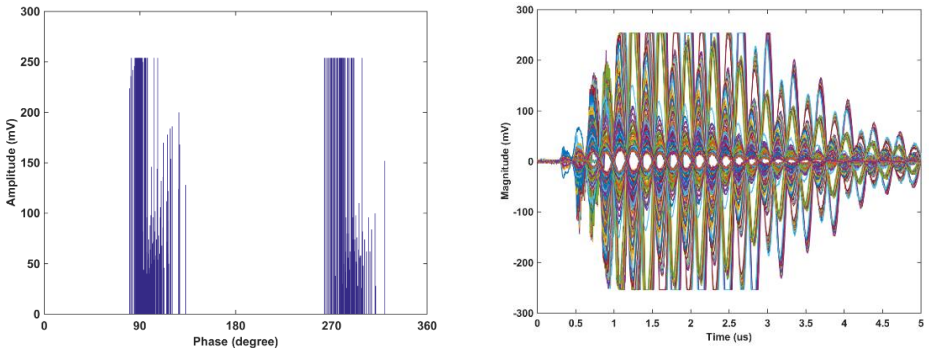

(b) Cluster 1 (right)

Figure 7.3.2. 2-D histogram pattern and typical individual pulses associated with the clusters in Figure 7.3.1(a)

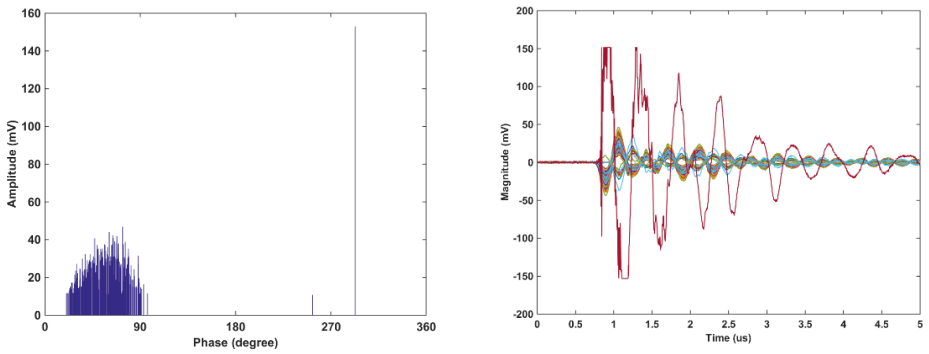

(a) Cluster 1 (left)

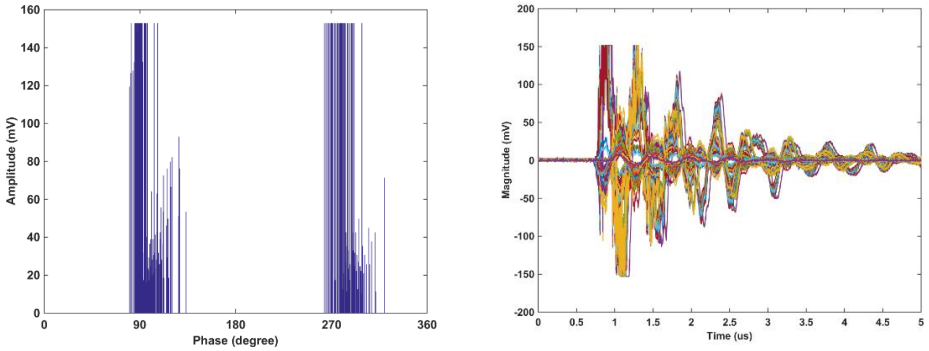

(b) Cluster 2 (right)

Figure 7.3.3. 2-D histogram pattern and typical individual pulses associated with the clusters in Figure 7.3.1(b)

Figure 7.3.2 and Figure 7.3.3 clearly show that the two PD sources were separated very well by using OPTICS on the MM energy output. There are two clusters with relatively high density as the valley is deep which can be easily noticed on the reachability plots. This is due to PD being injected into terminal 1, the difference in terms of energy between the two clusters is very significant. The source that was injected at terminal 1 has significantly greater energy at the bushing measurement point compared to the source that was injected towards the middle of the winding (terminal 5 in this case). While at the neutral earth measurement point, the source that was injected at terminal 1 had less energy than the source that was injected towards the middle of the winding. Therefore, the differences between the two clusters at both measurement points is significant large, which make them easy to separate.

In contrast to when PD was injected into terminal 1, the energy for both clusters are almost the same when they were both injected at the middle of the winding. However, different types of PD sources have different waveforms in terms of magnitude and frequency contents. Figure 7.3.4 shows the reachability plots produced by applying OPTICS on the MM energy data set when PD was injected into terminal 5.

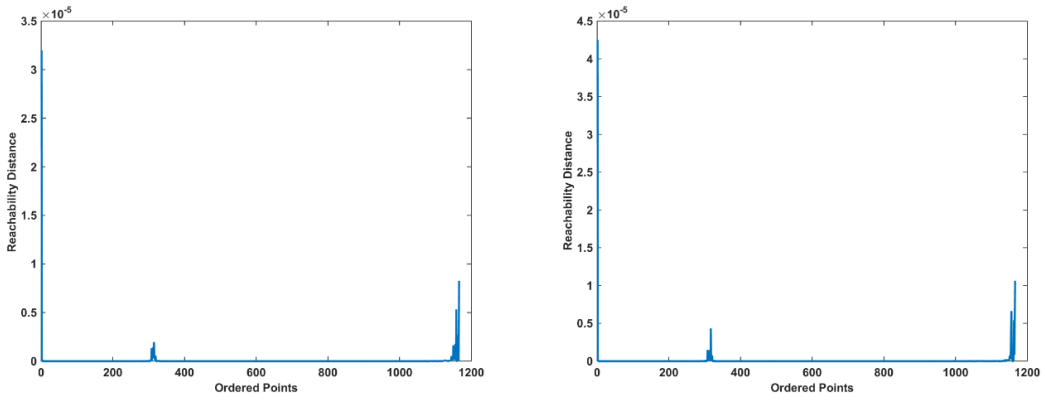

(a) (b)

Figure 7.3.4. The reachability plots of OPTICS on MM energy data at terminal 5 for (a) bushing measurement point, (b) neutral to earth measurement point.

Figure 7.3.4 shows that, the spikes of the reachability plot for this terminal are very low compared to other terminals. This is due to the energy contained within the two clusters at both measurement points being very similar as they were injected in the middle of the winding. Therefore, the reachability distance between points for both clusters are close together. However, OPTICS algorithms are still able to separate the two PD sources from the MM energy data set which are separated by a spike in the middle of both plots. Figure 7.3.5 and Figure 7.3.6 show the 2-D histogram patterns and typical individual pulses associated with each cluster for both measurement points.

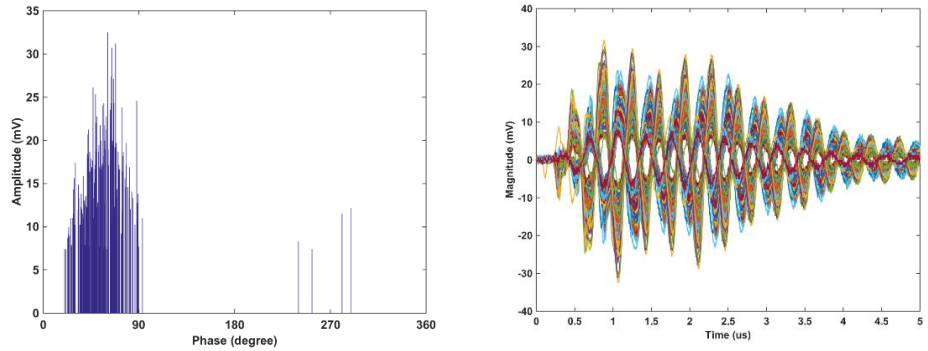

(a) Cluster 1 (left)

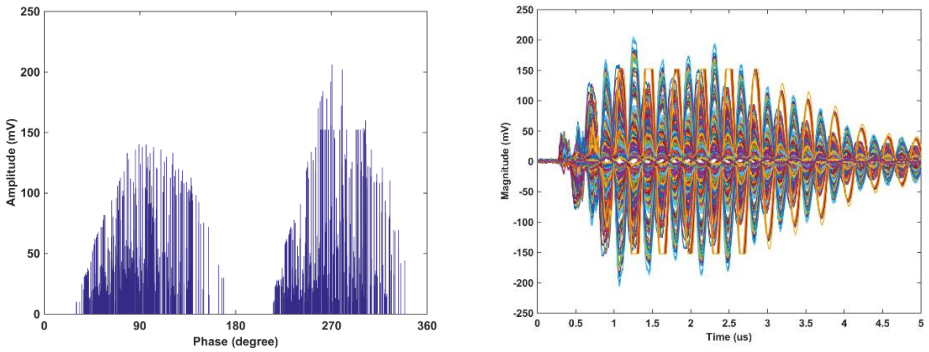

(b) Cluster 2 (right)

Figure 7.3.5. 2-D histogram pattern and typical individual pulses associated with the clusters in Figure 7.3.4(a)

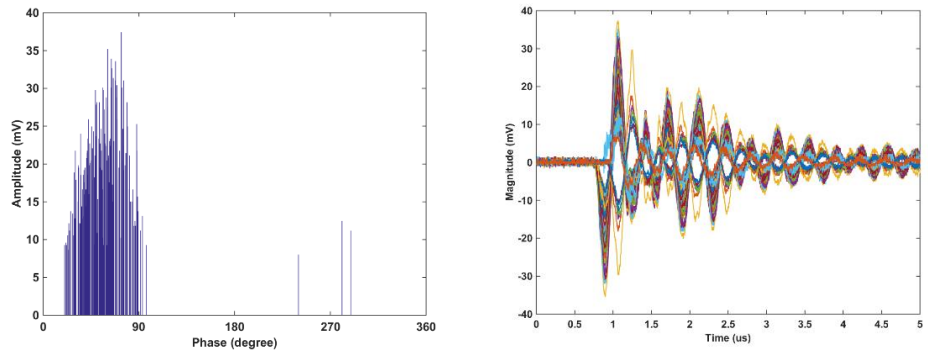

(a) Cluster 1 (left)

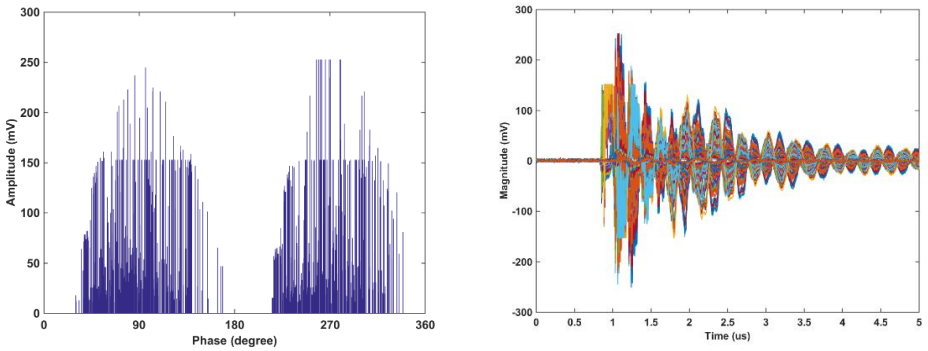

(b) Cluster 2 (right)

Figure 7.3.6. 2-D histogram pattern and typical individual pulses associated with the clusters in Figure 7.3.4(b)

This section discussed the performance of OPTICS on a high dimension data set produced from MM energy analysis. The results obtained prove the consistency of OPTICS on high dimensional data either MM energy data or wavelet energy data at all terminals. The two PD sources that were injected into the winding are clearly separated by applying OPTICS to the MM energy data set. The results obtained are almost identical to the results that were discussed previously.

7.4 APPLICATION OF OPTICS TO MM ENERGY USING PCA AND T-SNE

OPTICS has been applied to data that has already been processed using PCA and t-SNE, reducing its number of dimensions in a MM energy data set to three. These results are similar to the results obtained when DBSCAN was applied to the same data set. The results from OPTICS on MM energy data set are straight forward, two clusters are clearly separated by the highest spikes in the reachability plots. Figure 7.4.1 shows the reachability plots produced by OPTICS on the MM energy data that had been processed by PCA when PD is injected into terminal 1.

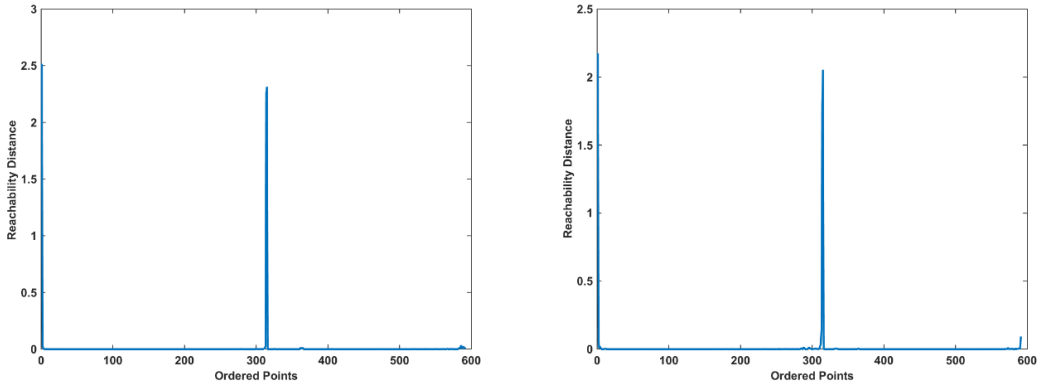

(a) (b)

Figure 7.4.1. The reachability plots of OPTICS on MM energy data processed by PCA at terminal 1 for (a) bushing measurement point, (b) neutral to earth measurement point.

The OPTICS reachability plots in Figure 7.4.1 show that there are clearly two clusters separated by the spikes. The high spikes on the plots show that the two clusters are separated by a significant separation distance, which is similar to the results when DSCAN was applied to the same data set. Figure 7.4.2 and Figure 7.4.3 show the 2-D histogram patterns and typical individual pulses associated with the main clusters in Figure 7.4.1 for both measurement points.

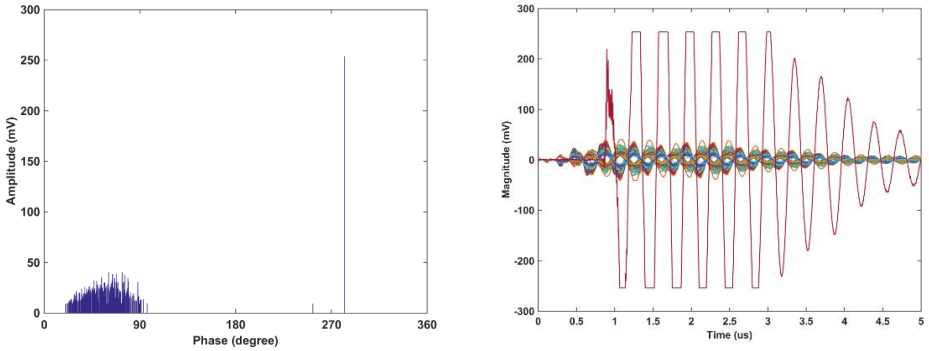

(a) Cluster 1 (left)

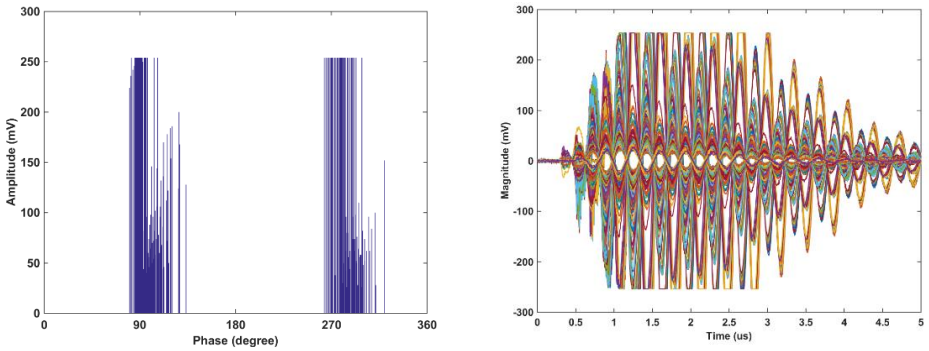

(b) Cluster 2 (right)

Figure 7.4.2. 2-D histogram pattern and typical individual pulses associated with the clusters in Figure 7.4.1(a)

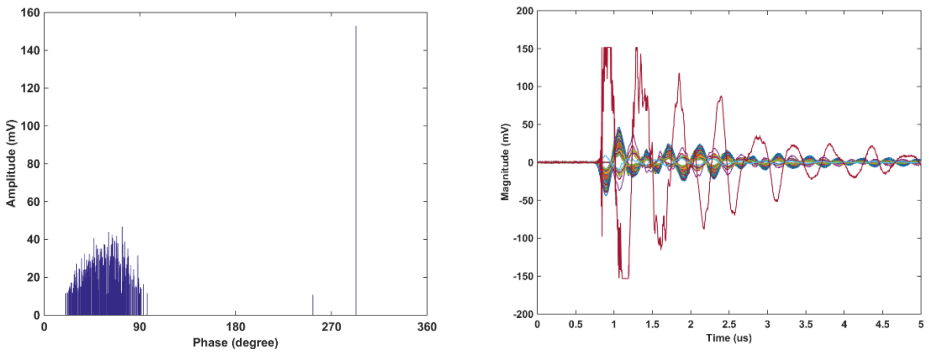

(a) Cluster 1 (left)

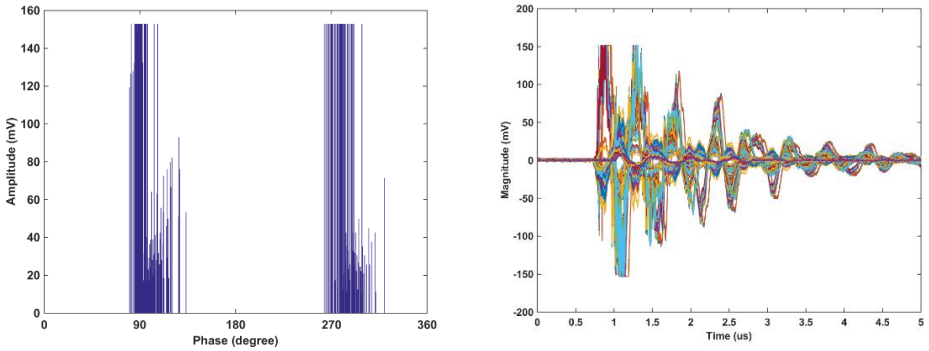

(b) Cluster 2 (right)

Figure 7.4.3. 2-D histogram pattern and typical individual pulses associated with the clusters in Figure 7.4.1(b)

While Figure 7.4.4 shows the reachability plots produced by applying OPTICS to the MM energy data that had been processed by t-SNE at terminal 1. The 2-D histogram pattern and typical individual pulses associated with the clusters are shown in Figure 7.4.5 and Figure 7.4.6 for both measurement points respectively.

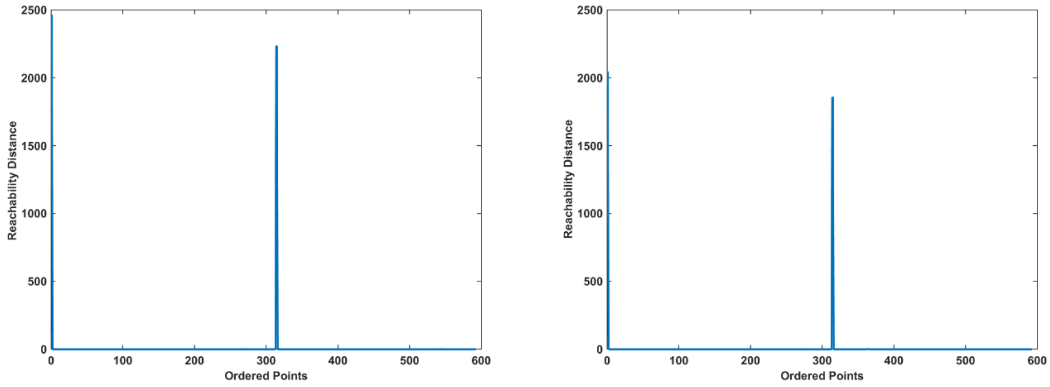

(a) (b)

Figure 7.4.4. The reachability plots of OPTICS on MM energy data processed by t-SNE at terminal 1 for (a) bushing measurement point, (b) neutral to earth measurement point.

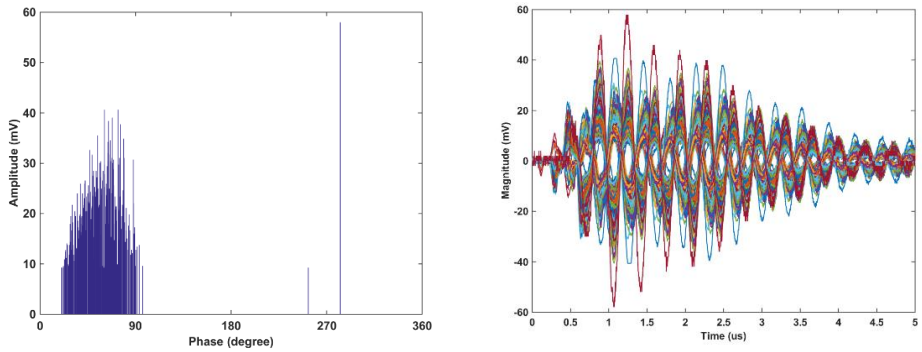

(a) Cluster 1 (left)

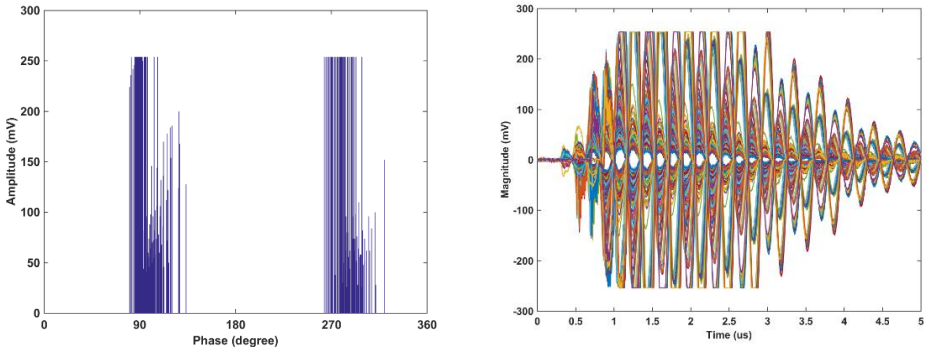

(b) Cluster 2 (right)

Figure 7.4.5. 2-D histogram pattern and typical individual pulses associated with the clusters in Figure 7.4.4(a)

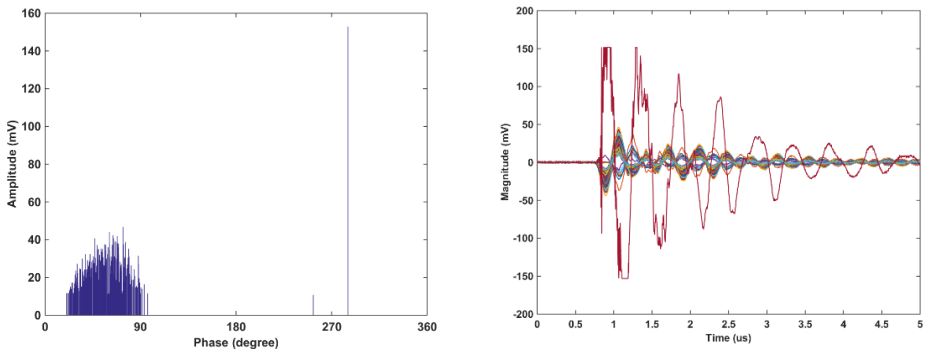

(a) Cluster 1 (left)

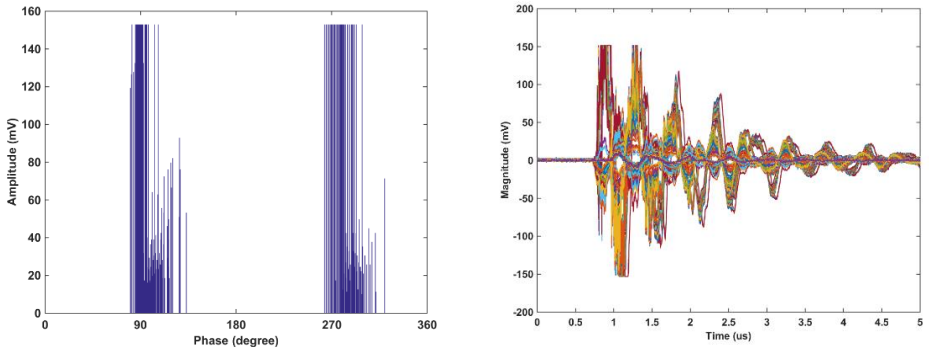

(b) Cluster 2 (right)

Figure 7.4.6. 2-D histogram pattern and typical individual pulses associated with the clusters in Figure 7.4.4(b)

The results obtained from applying OPTICS to MM energy data set using PCA and t-SNE when PD is injected into terminal 1 are similar to the results when DBSCAN was applied. Both algorithms show a good performance in terms of the ability to separate the multiple PD sources when applied to the data set that had been processed by dimensional reduction techniques. The only different between OPTICS and DBSCAN in this case is that OPTICS seems to produce one misclassified pulse, which can be neglected, as the number of misclassified pulses are not more than 1% of the total points of the data set.

Figure 7.4.7 shows the reachability plots produced by applying OPTICS to the MM energy data that had been processed by PCA when PD is injected into terminal 5.

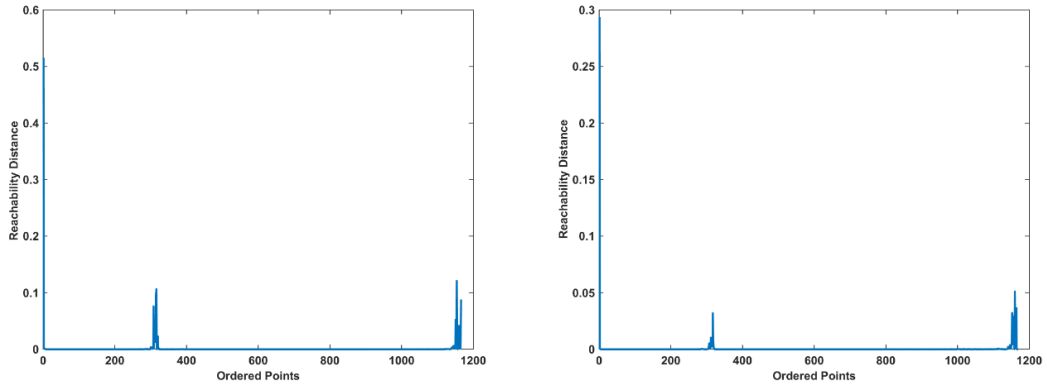

(a) (b)

Figure 7.4.7. The reachability plots of OPTICS on MM energy data processed by PCA at terminal 5 for (a) bushing measurement point, (b) neutral to earth measurement point.

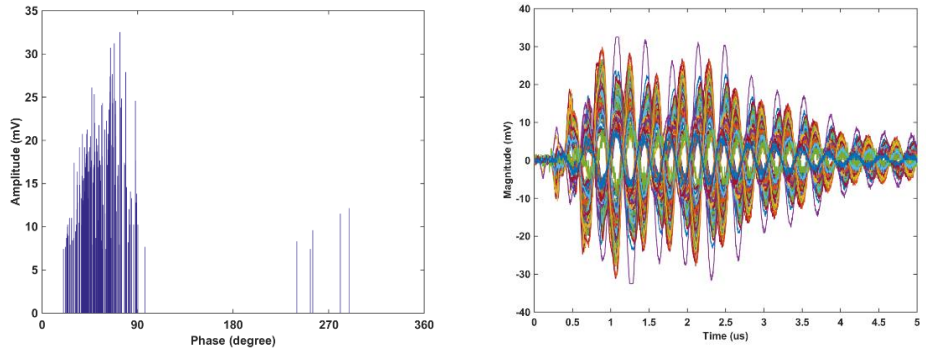

(a) Cluster 1 (left)

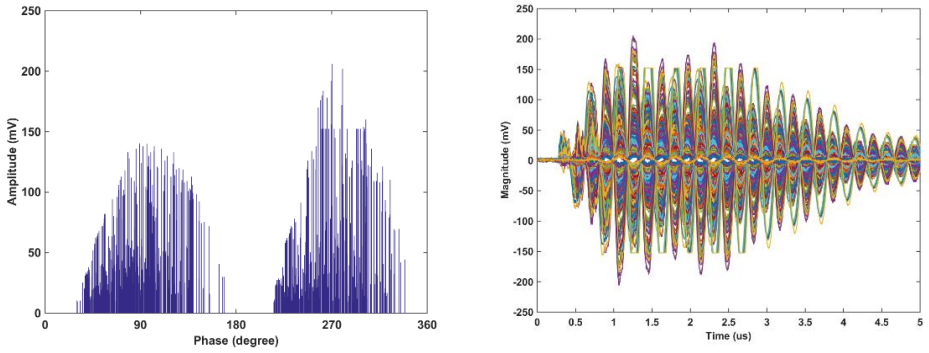

(b) Cluster 2 (right)

Figure 7.4.8. 2-D histogram pattern and typical individual pulses associated with the clusters in Figure 7.4.7(a)

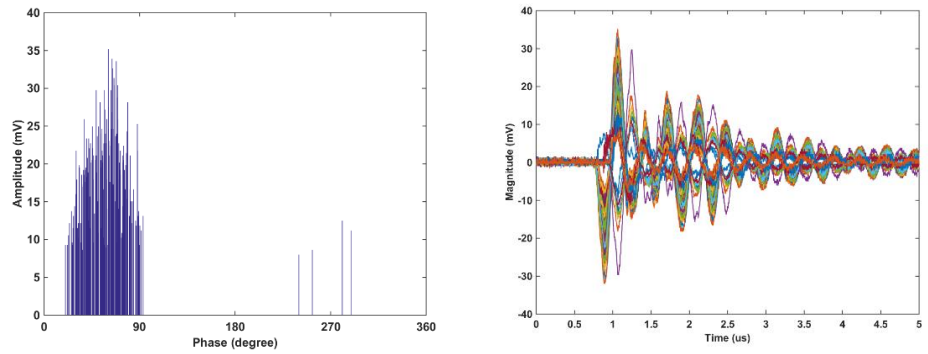

(a) Cluster 1 (left)

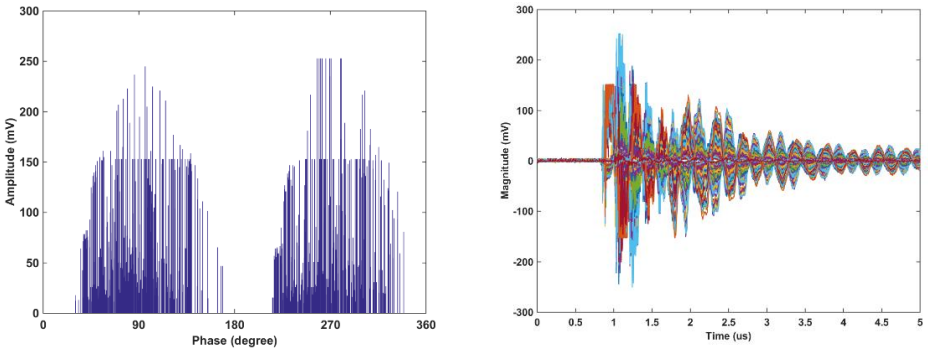

(b) Cluster 2 (right)

Figure 7.4.9. 2-D histogram pattern and typical individual pulses associated with the clusters in Figure 7.4.7(b)

Figure 7.4.7 shows that, the spikes of reachability plot for this terminal are very low for both measurement points, which means that the two clusters are close to each other. This is similar to the results when DBSCAN was applied to the same data set. However, when t-SNE was applied to the same data set, the separation distance between the two clusters are improved. Figure 7.4.10 shows the reachability plots produced by OPTICS on the MM energy data that had been processed by t-SNE at terminal 5. While the 2-D histogram patterns and typical individual pulses associated with the clusters are shown in Figure 7.4.11 and Figure 7.4.12.

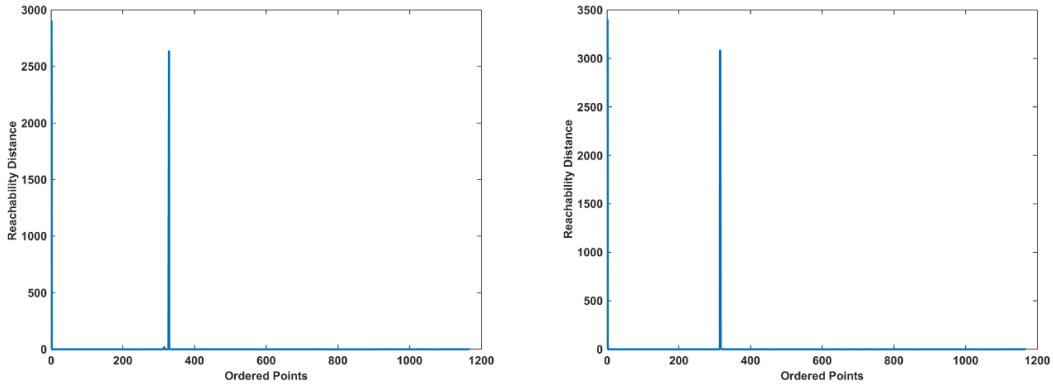

(a) (b)

Figure 7.4.10. The reachability plots of OPTICS on MM energy data processed by t-SNE at terminal 5 for (a) bushing measurement point, (b) neutral to earth measurement point.

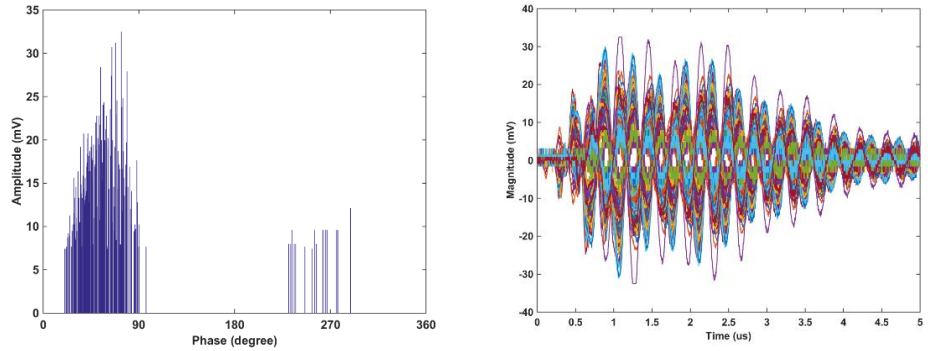

(a) Cluster 1 (left)

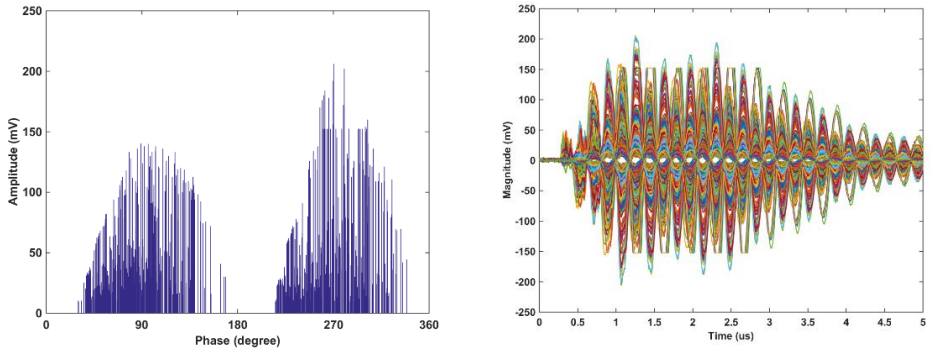

(b) Cluster 2 (right)

Figure 7.4.11. 2-D histogram pattern and typical individual pulses associated with the clusters in Figure 7.4.10(a)

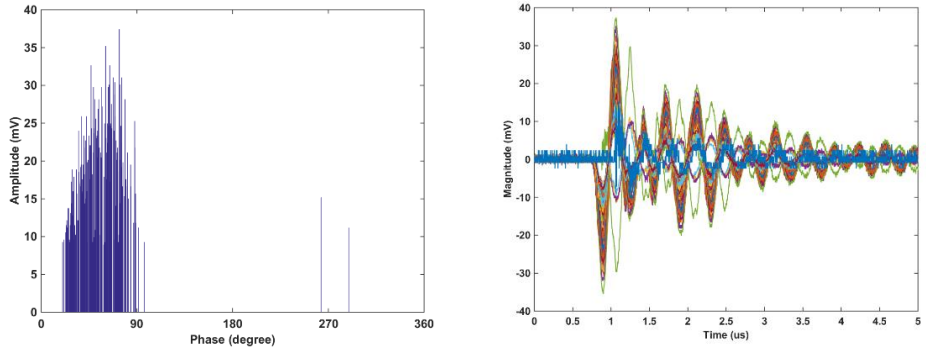

(a) Cluster 1 (left)

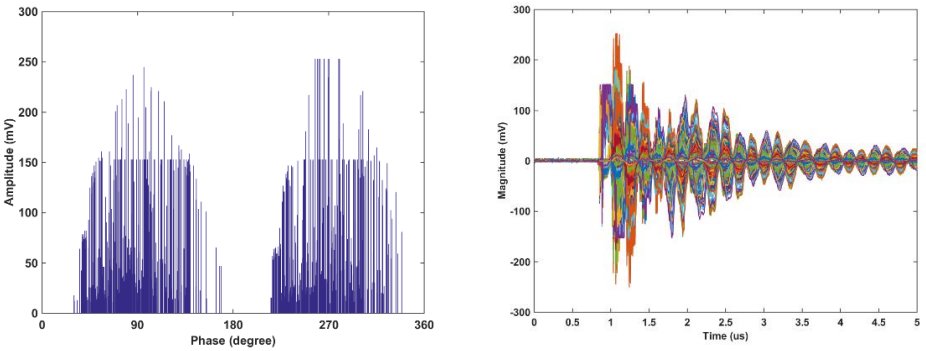

(b) Cluster 2 (right)

Figure 7.4.12. 2-D histogram pattern and typical individual pulses associated with the clusters in Figure 7.4.10(b)

The spikes in Figure 7.4.10 for both measurement points are very large indicating that the two clusters are separated by a substantial distance. Two clusters have been clearly extracted without difficulty. This shows that t-SNE was good in terms of its ability to represent the data in a way that made clustering technique far more reliable and also its ability to clearly separate data points with very similar probability density functions, thus accurately separating clusters which have similar tendency or similar energy content.

7.5 APPLICATION OF OPTICS ON TIME FREQUENCY MAPPING OUTPUT

This section considers the application of OPTICS on the time frequency mapping output. Figure 7.5.1 and Figure 7.5.2 show the reachability plots produced when OPTICS was applied to the time frequency mapping output data when PD was injected into terminal 1 and terminal 7 for both measurement points. The reachability plot for terminal 1 was plot as normal while the reachability plot for terminal 7 was plot from 10% to 90% of the ordered points for comparison purposes.

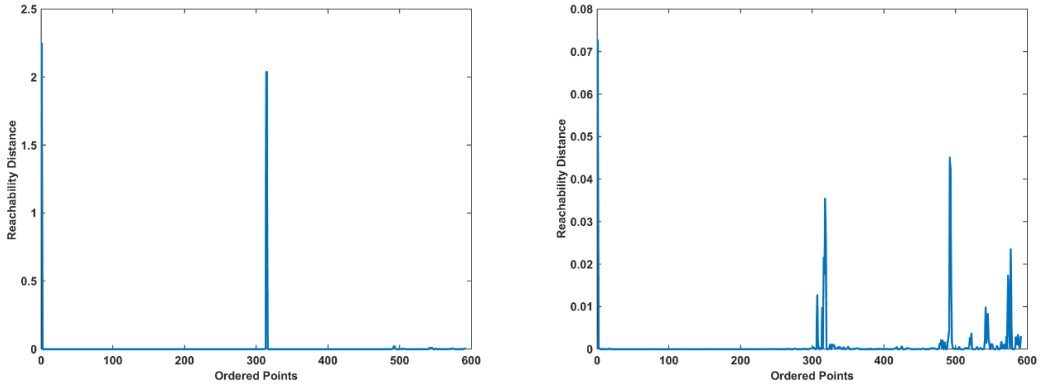

(a) (b)

Figure 7.5.1. The reachability plots of OPTICS on time frequency output at terminal 1 for (a) bushing measurement point, (b) neutral to earth measurement point.

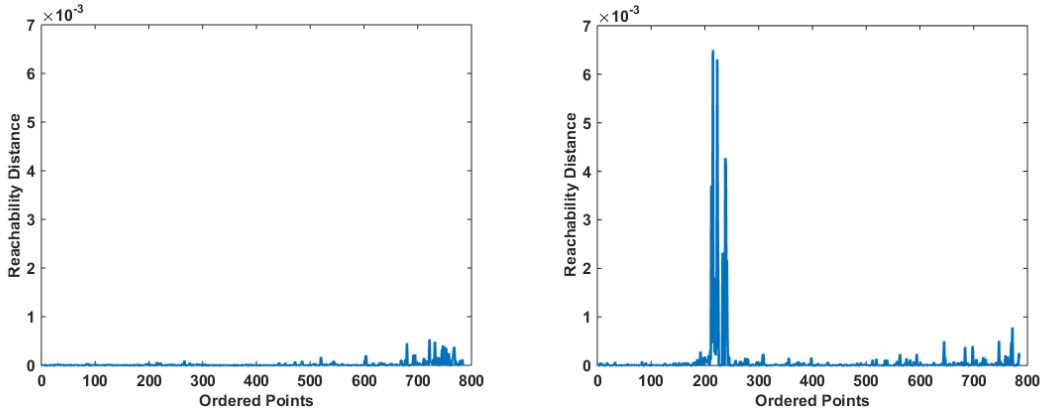

(a) (b)

Figure 7.5.2. The reachability plots of OPTICS on time frequency output at terminal 7 for (a) bushing measurement point, (b) neutral to earth measurement point.

Figure 7.5.1 shows that the two clusters were separated at the bushing measurement point. However, at the neutral earth measurement point there are around 5 clusters were produced by OPTICS. While, in Figure 7.5.2 shows that the trends of MM sparsity have a similar tendency, there are no clusters produced on the bushing measurement point, which is similar to the results when DBSCAN was applied. Therefore, these show that time frequency mapping based on the MM sparsity roughness value in time and frequency domains are not robust enough to be used in separating multiple PD sources in this application.

7.6 SUMMARY

The performance of OPTICS was discussed in this chapter. OPTICS have been applied to the data that had been discussed in Chapter 6 using DBSCAN and also directly to the data without any dimension reduction technique i.e. a wavelet energy data set and a MM energy data set. The operation of both algorithms rely on the assumptions that the PD waveforms produced from different sources are fundamentally different and that frequency dependent properties of the pulses propagation path from the source location to the measurement sensors are consistent within the timescale of the experiments. Analysis showed that the OPTICS clustering algorithms proved to be more robust than DBSCAN clustering. It was shown that DBSCAN was heavily dependent on the parameter ε which is a uniform parameter meaning that in some cases it was impossible to cluster the data set correctly. By contrast, OPTICS only needs one input parameter known as the minimal number of objects considered as a cluster, which should be defined by the user.

CHAPTER 8

LOCALISATION OF MULTIPLE PARTIAL DISCHARGE SOURCES

This chapter aims to demonstrate the developed approach for localisation of multiple PD sources based on PD signals and their characteristics. Localisation of PD is an important aspect for condition monitoring assessment when applied to a large HV transformer. It can be a complicated process when a winding is involved. The approach is based on the assumption that PD pulses propagating towards the different ends of the winding contain different information due to factors such as different propagation paths inside the winding with different levels of dispersion and attenuation.

8.1 SINGLE SOURCE LOCALISATION

In order to develop multiple PD source localisation, single source localisation was initially undertaken. The approach used is based on the published technique in [16]. Generally, the main idea is to use energy distributions from wavelet analysis of captured PD pulses. However, the use of distribution energy is not very helpful to aid a visualisation process due to the large dimension of the data. Therefore, PCA was implemented as a dimensional reduction technique in order to transform the correlated data into uncorrelated data with different principle components. The principle component values generated from the process are related to the original data based on the eigenvectors of the original dataset and explain the relation of each of the objects in the dataset to the principle component.

There are two main groups of clusters in each plot representing different sets of measurement data. The blue cluster represents signals measured at the bushing measurement tap while the red cluster represents signals measured at the neutral to earth terminal signals. Figure 8.1.1 – Figure 8.1.3 show cluster plots for surface, void and floating discharge for an applied voltage of 20 kV.

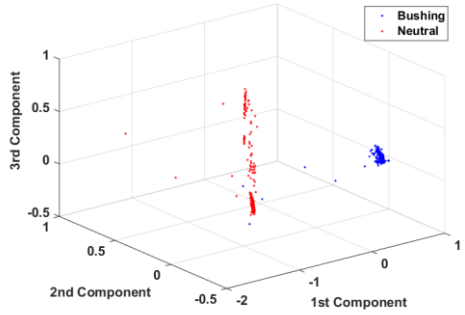

(a) Terminal 1

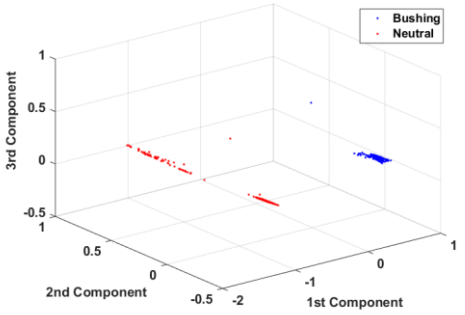

(b) Terminal 2

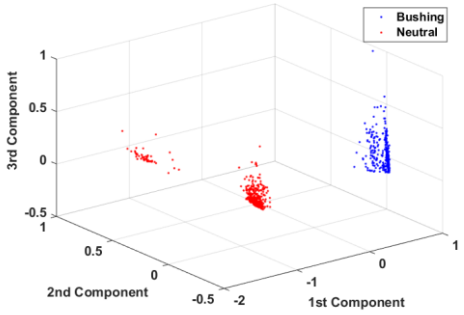

(c) Terminal 3

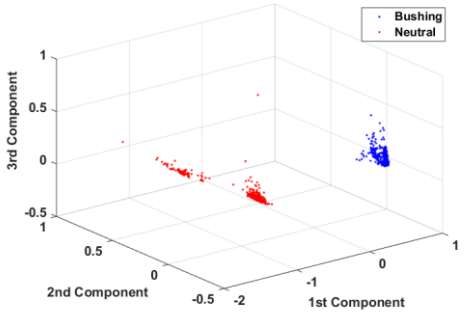

(d) Terminal 4

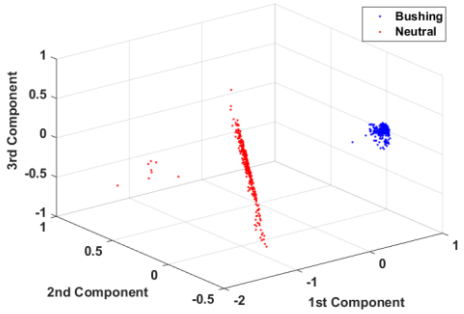

(e) Terminal 5

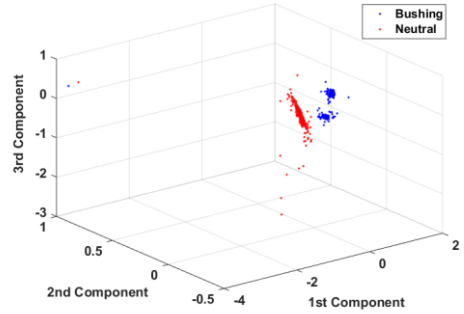

(f) Terminal 6

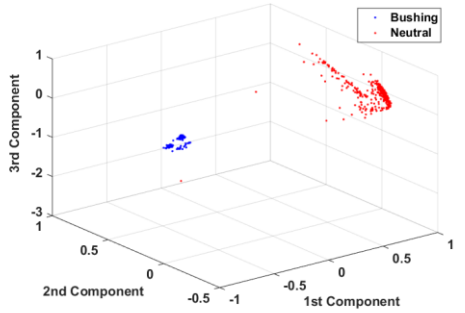

(g) Terminal 7

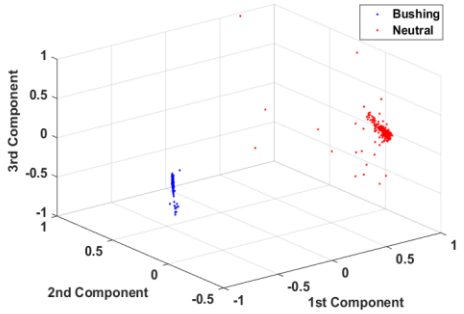

(h) Terminal 8

Figure 8.1.1. Clusters plot for surface discharge.

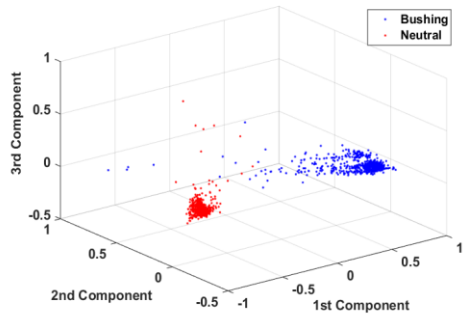

(a) Terminal 1

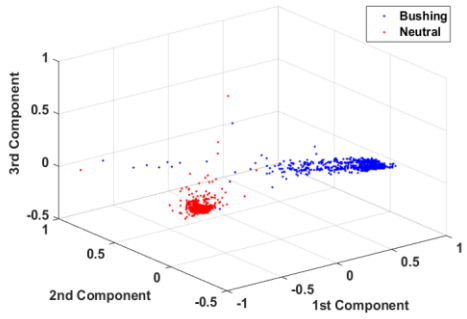

(b) Terminal 2

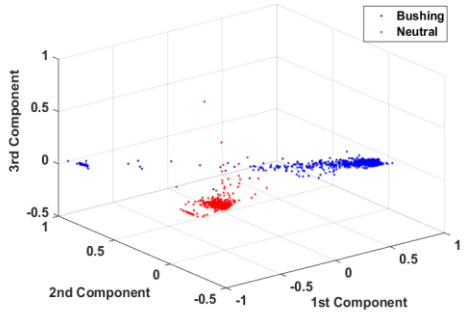

(c) Terminal 3

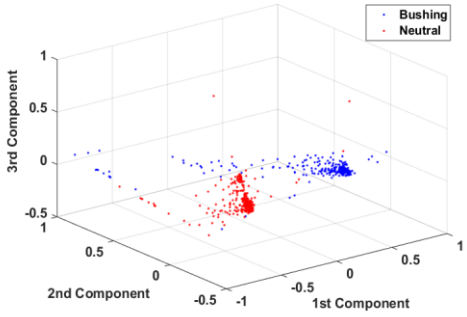

(d) Terminal 4

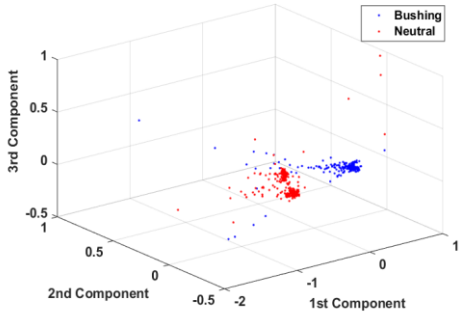

(e) Terminal 5

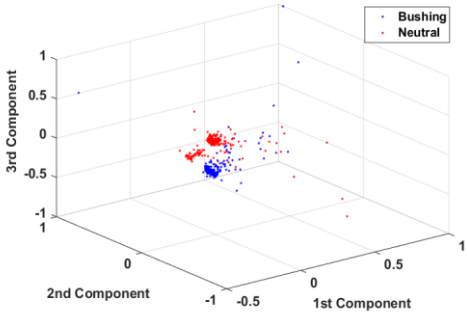

(f) Terminal 6

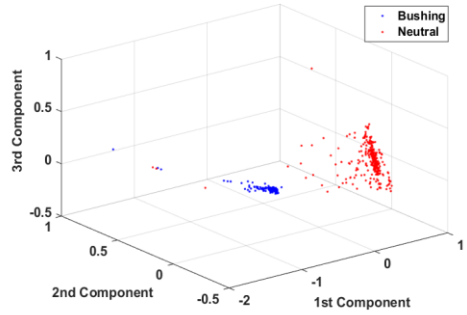

(g) Terminal 7

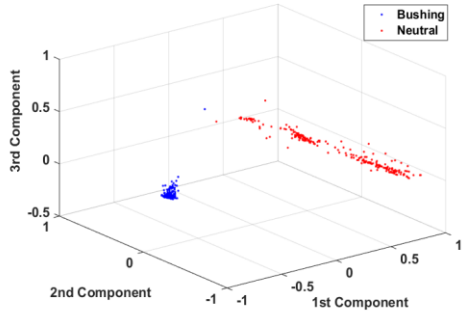

(h) Terminal 8

Figure 8.1.2. Clusters plot for void discharge.

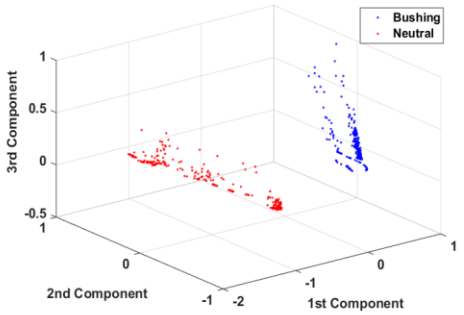

(a) Terminal 1

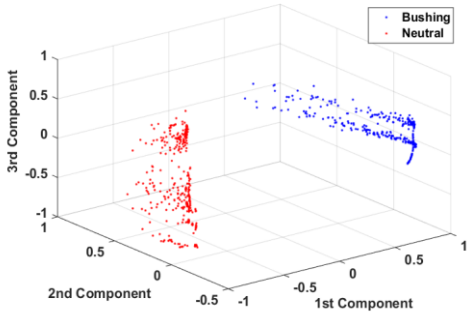

(b) Terminal 2

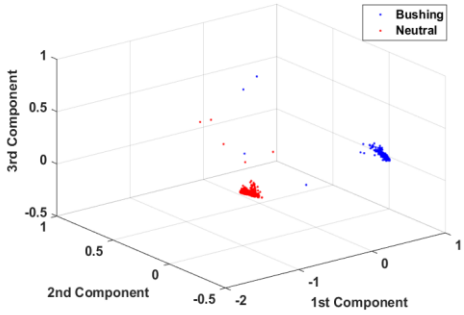

(c) Terminal 3

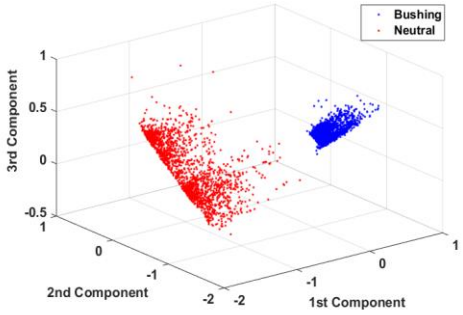

(d) Terminal 4

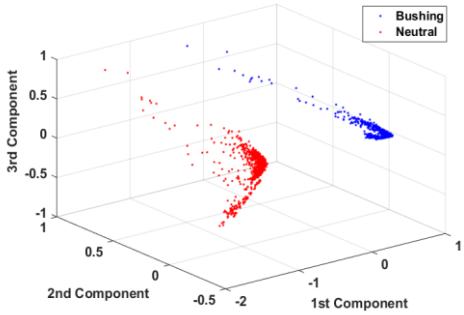

(e) Terminal 5

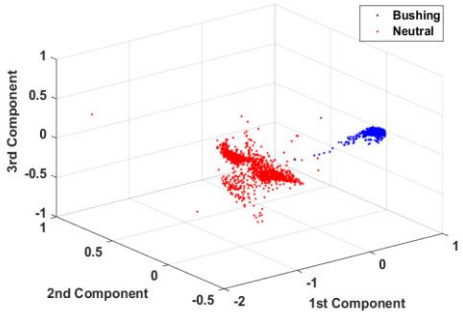

(f) Terminal 6

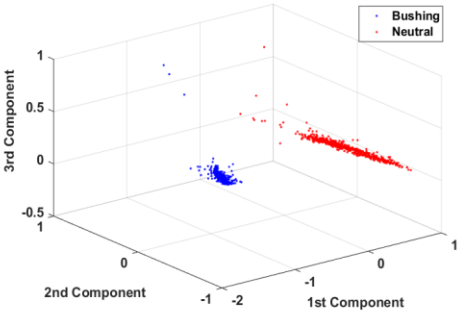

(g) Terminal 7

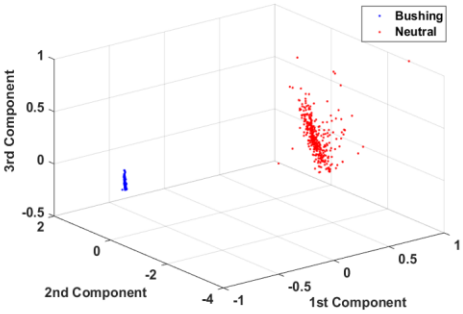

(h) Terminal 8

Figure 8.1.3. Clusters plot for floating discharge.

According to all plots, the position of blue and red clusters are located differently in the principle component spaces. The data are clustered differently when each of the PD source was injected at different terminals along the winding. The two clusters have a clear separation between each other when the PD source was injected at terminal 1. However, the clusters are seen to come closer towards each other when the PD source was injected at terminal 2 onwards. After a point where the signals travels in a more or less similar length of propagation path which usually in the middle of the winding (terminal 5 or terminal 6), the separation between the two clusters are seen to be increased again and these clusters rotate in a different position within the principle component space.

Based on the observation from Figure 8.1.1 – Figure 8.1.3, the position of the clusters in the 3-D principle component space vary when produced from measurement data sets which are obtained at different injection points along the transformer winding; Terminal 1-Terminal 8. The clusters are separated by a distance between them in the space. Therefore, it may be useful to measure the separation distance between clusters in order to determine the variation occurs from Terminal 1 to Terminal 8, which then can be used to identify the location of multiple PD sources within the transformer winding.

Thus, the distance between centroid of clusters are used in order to measure the separation distance between the two clusters. The centroid of a cluster is a centre point of the cluster which can be calculated by taking the average of all points in the cluster using:

$$\mathrm{C_x} = 1/\mathrm{N_p}\,(\sum_{\mathrm{i=1}}^{\mathrm{N}} \mathrm{x_i})$$

$$C_y = 1/N_p\,(\sum_{i=1}^{N} y_i) \tag{8.1}$$

$$C_z = 1/N_p\,(\sum_{i=1}^{N} z_i)$$

where x, y and z represent first, second and third principle component while N_p is the number of points in clusters.

The magnitude, P with respect to each principle component and Euclidean distance, D(x,y,z) between them in three dimensions are calculated using:

$$Px = (Cx_1 - Cx_2)^2$$

$$Py = (Cy_1 - Cy_2)^2 \quad (8.2)$$

$$Pz = (Cz_1 - Cz_2)^2$$

$$D(x,y,z) = \sqrt{(Px + Py + Pz)^2} \quad (8.3)$$

where number 1 and 2 in the equations represent the first cluster and second cluster in the 3-D space of the principle component.

Clusters produced from bushing tap point to earth measurement are considered as the first cluster, while clusters produced from neutral to earth point measurement are considered as second cluster. Table 8.1.1 – Table 8.1.3 show the separation distance between the two clusters produced in the 3-D principle component space for surface, void and floating discharge respectively.

Table 8.1.1. Separation distance of clusters for surface discharge.

Terminal	D(x,y,z)
1	0.7439
2	0.7599
3	0.7208
4	0.6304
5	0.4367
6	0.0939
7	-0.4626
8	-0.7576

Table 8.1.2. Separation distance of clusters for void discharge.

Terminal	D(x,y,z)
1	0.7045
2	0.6956
3	0.6032
4	0.3655
5	0.1996
6	0.1549
7	-0.3712
8	-0.6085

Table 8.1.3. Separation distance of clusters for floating discharge.

Terminal	D(x,y,z)
1	0.8302
2	0.8267
3	0.7921
4	0.7013
5	0.4859
6	0.1820
7	-0.3410
8	-0.7225

According to the Table 8.1.1 – Table 8.1.3, the value of separation distance for all PD sources lie within the same range for terminal 1 to terminal 8 respectively. Therefore, it emphasises that this approach is robust to different type of PD sources which will have different frequency and time characteristics when compared with each other. The positive and negative values indicate the direction of the measurement from cluster 1 to cluster 2. In this work, the sign negative and positive was calculated by subtraction of the energy of the pulses from bushing measurement data to the pulses from neutral to earth measurement data. This is due

to the events which occur at Terminal 7 and Terminal 8 because of the percentage of energy detected at the bushing tap point signal is lesser than the neutral to earth connection at these terminals. Therefore, with the combination of both magnitude and vector elements, either the positive or negative distance based on clusters position can be established which enhances the ability of this approach to locate PD sources. The separation distance can also be plotted against the winding terminal, Figure 8.1.4 show the separation distance plot for Table 8.1.1 – Table 8.1.3.

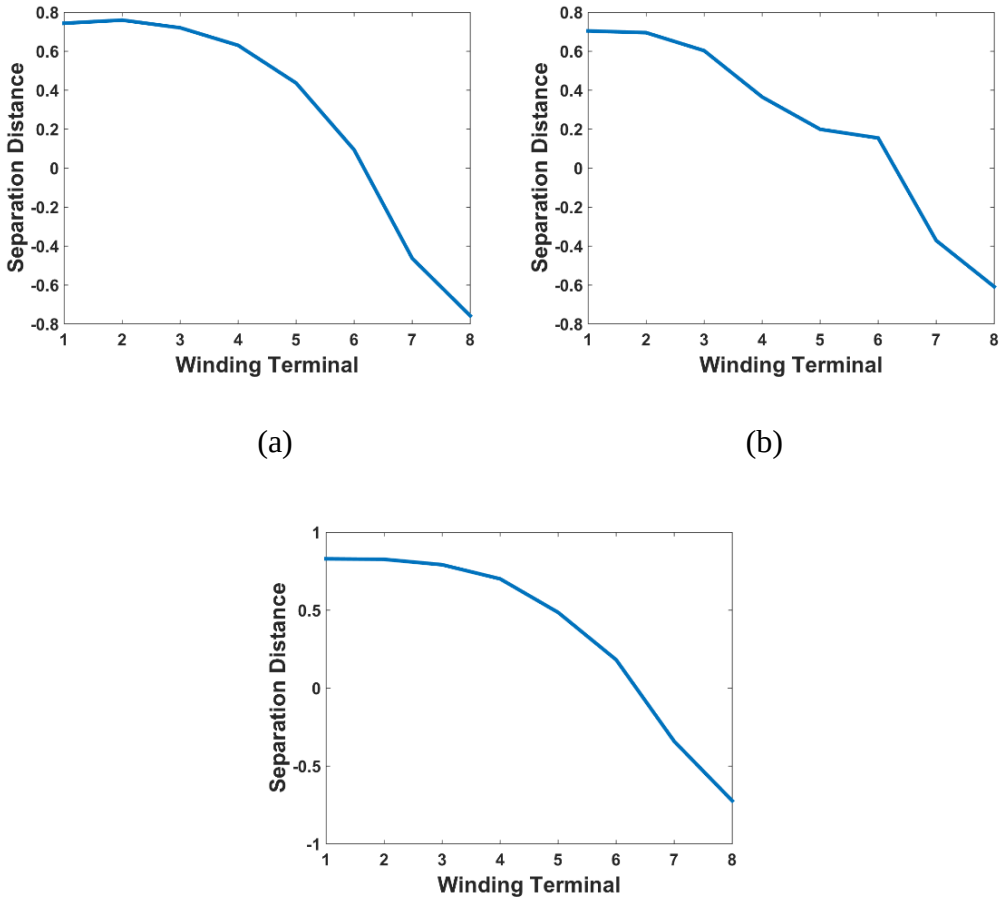

Figure 8.1.4. Separation distance for (a) surface discharge, (b) void discharge and (c) floating discharge.

Between Terminal 1 and Terminal 2, the differences in the separation distance are very small. This is due to the electrical connections which connect both terminals are very close to each other. However, the clusters are seen to come closer towards each other when the PD source was injected from Terminal 2 to Terminal 6. Then, the clusters are seen to part and swap position from each other at Terminal 7 onwards.

8.2 MULTIPLE SOURCE LOCALISATION

Generally, there are two clusters either in the 3-D space or in the reachability plots for each measurement data, which represent two types of PD signals injected into the winding. Before any separation distance calculation can be made, clusters that belong to the same source need to be determine first. PD pulses generated from the same source have similar characteristics. As the analysis of the pulse shapes of the PD signals revealed that there are differences in accordance to the type of the PD defects [112], [116], this works uses the cross correlation method in order to find the cluster pairs (same source types) from both measurement data.

8.2.1 SIGNAL CROSS CORRELATION TECHNIQUE

According to [117], each consecutive pulse from a given source is related to the previous pulse. Therefore, time relation between each pulse is exploited to develop a technique that can match the clusters produced in order to determine which clusters belong to which sources. The pulses from each cluster produced from application of OPTICS on the MM energy output are reconstructed back to their original stream, where the presence of a pulse is represented by a series of ones while the absence is represented by a series of zeros. Figure 8.2.1 shows the example of the streams for combination of floating and surface discharges at Terminal 1.

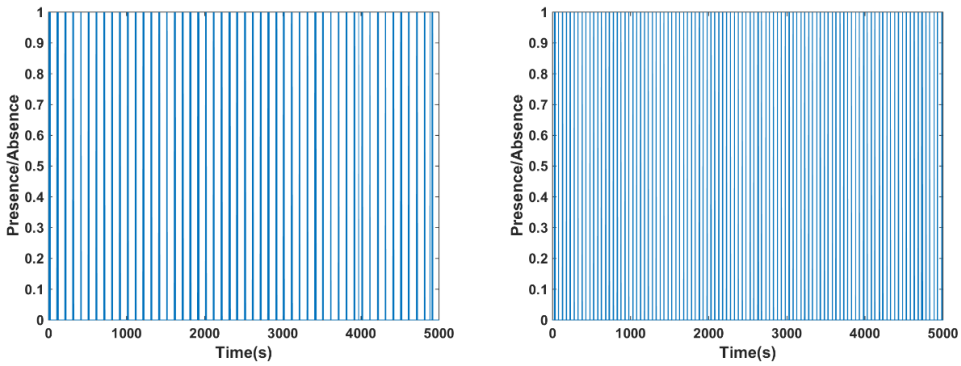

(a) Bushing cluster 1

(b) Bushing cluster 2

(c) Neutral cluster 1

(d) Neutral cluster 2

Figure 8.2.1. Reconstructed streams for each cluster produced from combination of floating and surface discharges at terminal 1

By visual inspection, the pattern of the reconstructed stream for cluster 1 and cluster 2 from bushing measurement point is nearly identical with the pattern of the reconstructed stream for cluster 1 and cluster 2 produced from neutral to earth measurement point. The pairing process is based on which pair of stream gives the highest cross correlation percentage. Table 8.2.1 shows the stream similarity percentage for Terminal 1.

Table 8.2.1. Stream similarity percentage for Terminal 1.

Neutral / Bushing	Cross correlation percentage (%)	
	Cluster 1	Cluster 2
Cluster 1	97.63	2.37
Cluster 2	2.35	86.26

In Table 8.2.1, the cross correlation between cluster 1 from the bushing measurement point with cluster 1 from the neutral to earth measurement point produced a higher percentage than the cross correlation between cluster 1 from the bushing measurement point with cluster 2 from neutral to earth measurement point. Therefore, it shows that cluster 1 from both measurement points are very likely to belong to the same source. Similarly, cluster 2 from the bushing measurement point, had a higher percentage of cross correlation with cluster 2 from the neutral to earth measurement point.

8.2.2 SEPARATION DISTANCE BETWEEN CLUSTERS IN 3 PRINCIPLES COMPONENT SPACE

Once the pairs of clusters between both measurements points have been identified, a localisation technique can be applied. Generally, the main idea in this technique is to use the energy distributions from mathematical morphology. The mathematical energy from paired clusters are combined together. Then, in order to aid a visualisation process, PCA was implemented in this study as a dimensional reduction tool to the combined data. PCA generates the principle component values of the data, which is representative of the original data in the principle component space. These values are related to the original data based on the eigenvectors of the original data set and explain the relation of each of the objects in the dataset to the component. In each plot, there will be two groups of clusters representing different sets of clusters from different PD injection points along the winding. Hence, the variation of the clusters relative position in the principle component space may be used as an indicator of partial discharge location within a transformer winding. Table 8.2.2 shows the three combination of the sources as a reference. Figures 8.2.2 – Figure 8.2.7 show the characterized 3-D (using PCA) representation of the mathematical morphology energy data generated for combination of floating-surface discharges, surface-void discharges and void-floating discharges for Terminal 1 – Terminal 8.

Table 8.2.2

Combination	Terminal 1 – Terminal 8	Terminal 5
1	Floating discharge	Surface discharge
2	Surface discharge	Void discharge
3	Void discharge	Floating discharge

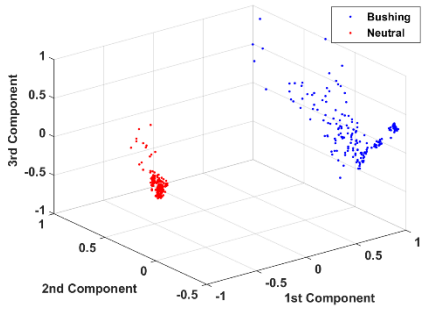

(a) Terminal 1

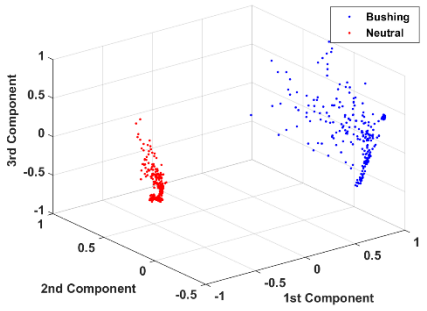

(b) Terminal 2

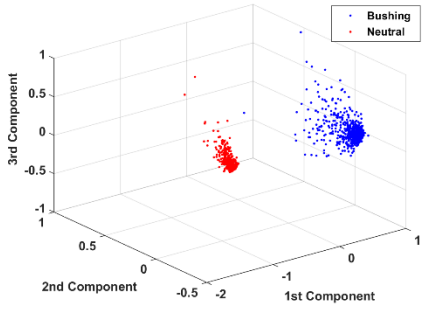

(c) Terminal 3

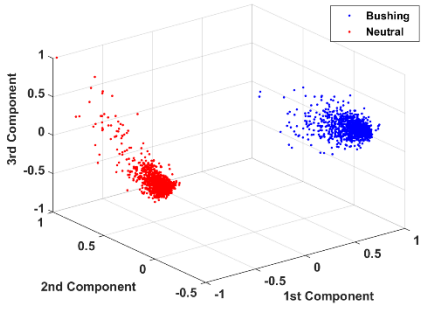

(d) Terminal 4

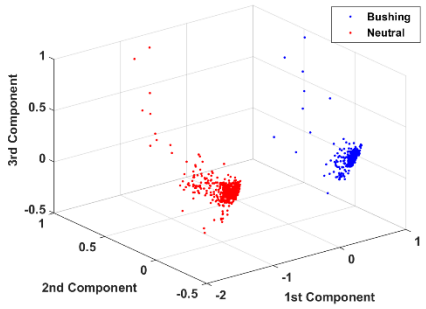

(e) Terminal 5

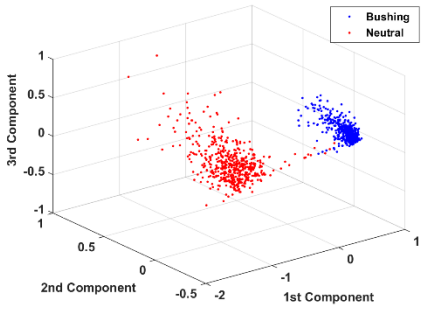

(f) Terminal 6

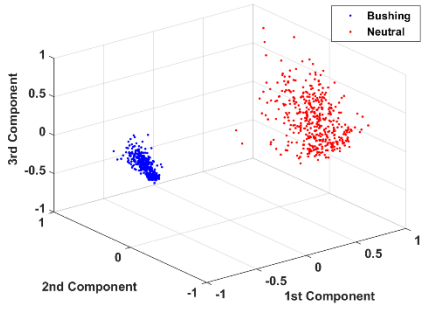

(g) Terminal 7

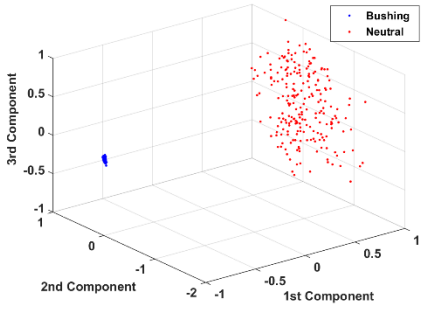

(h) Terminal 8

Figure 8.2.2. Clusters plot for floating discharge from combination 1.

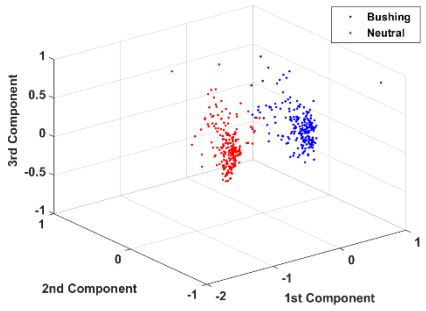

(a) Terminal 1

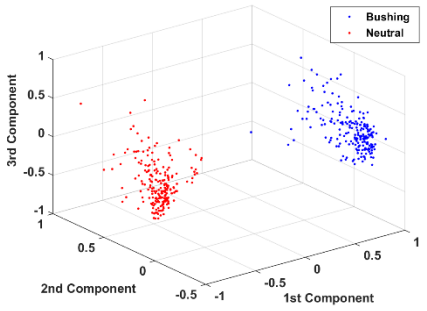

(b) Terminal 2

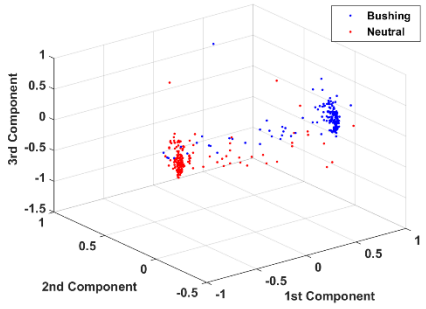

(c) Terminal 3

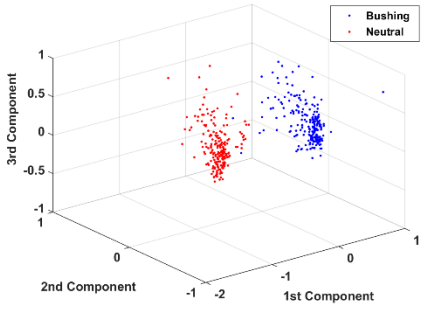

(d) Terminal 4

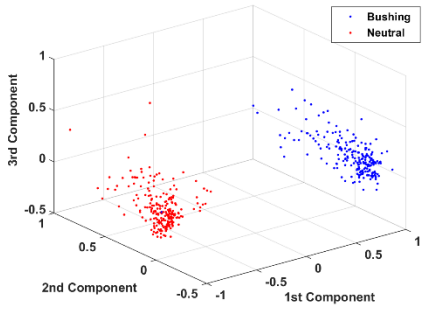

(e) Terminal 5

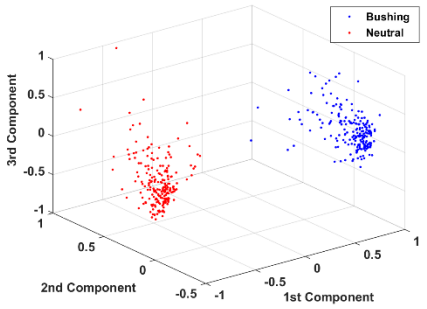

(f) Terminal 6

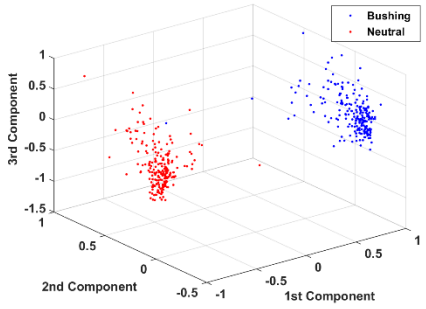

(g) Terminal 7

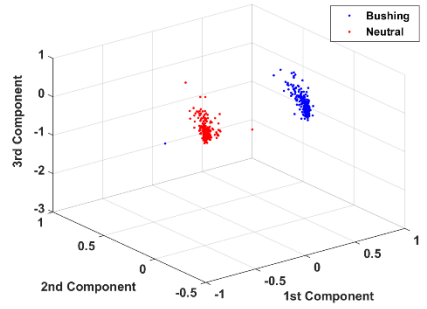

(h) Terminal 8

Figure 8.2.3. Clusters plot for surface discharge from combination 1.

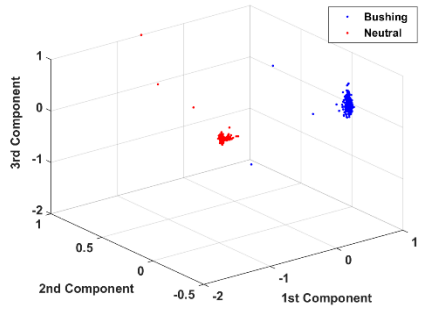

(a) Terminal 1

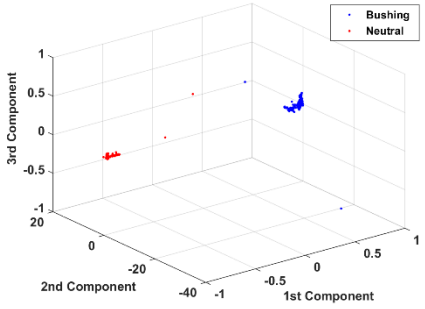

(b) Terminal 2

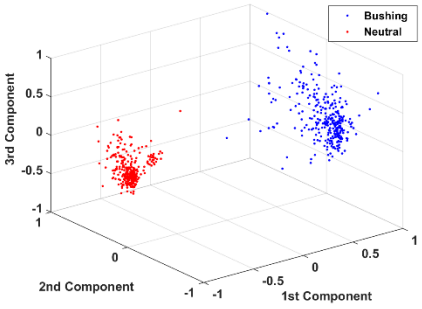

(c) Terminal 3

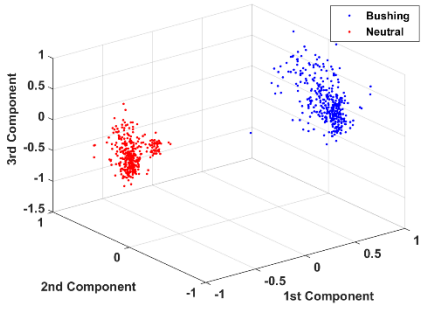

(d) Terminal 4

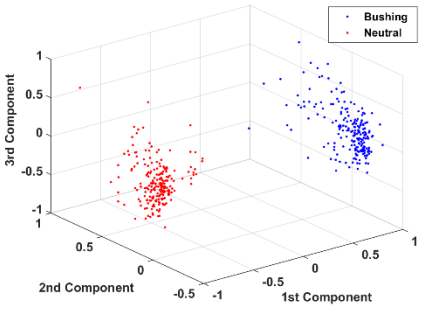

(e) Terminal 5

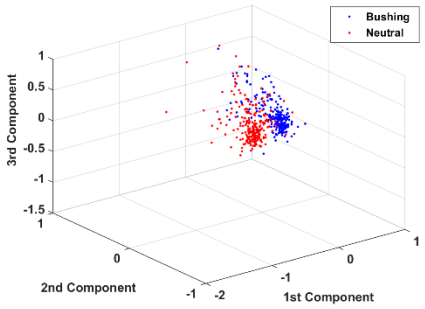

(f) Terminal 6

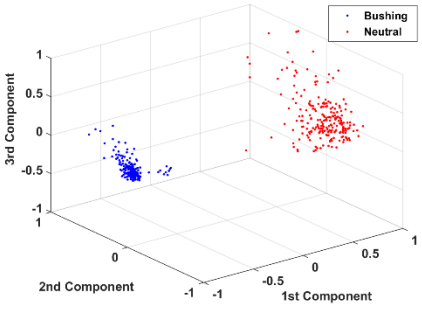

(g) Terminal 7

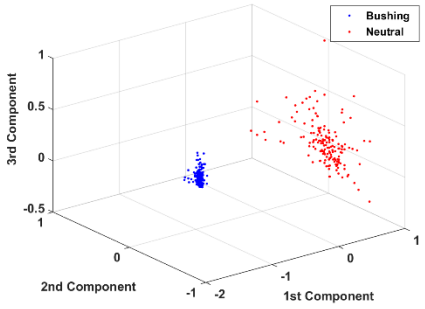

(h) Terminal 8

Figure 8.2.4. Clusters plot for surface discharge from combination 2.

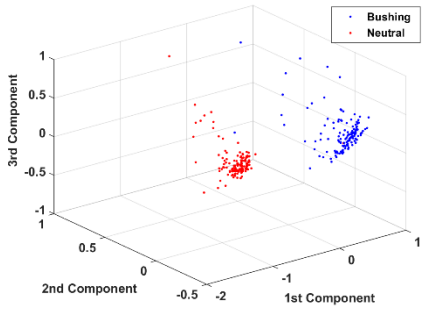

(a) Terminal 1

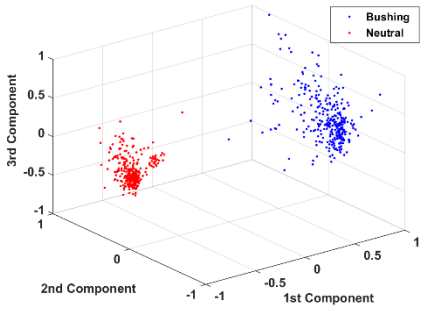

(b) Terminal 2

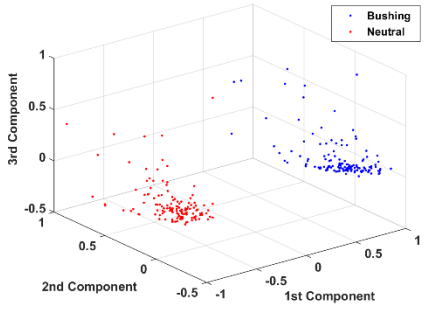

(c) Terminal 3

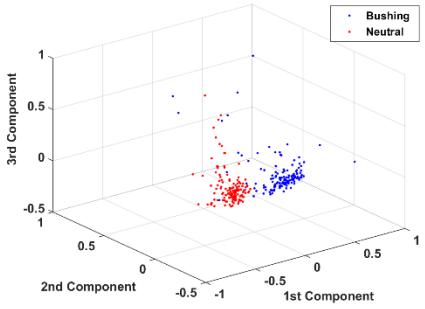

(d) Terminal 4

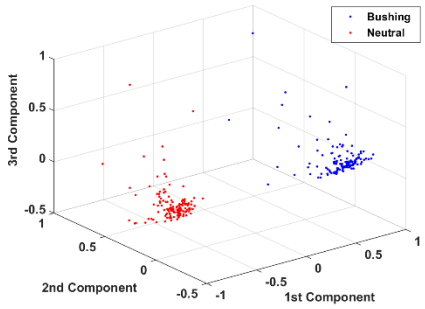

(e) Terminal 5

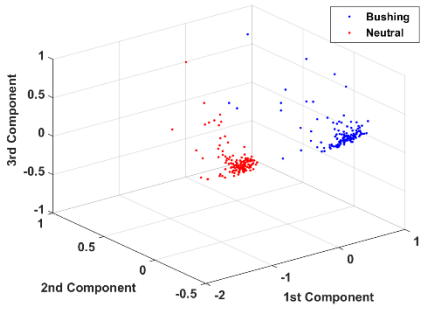

(f) Terminal 6

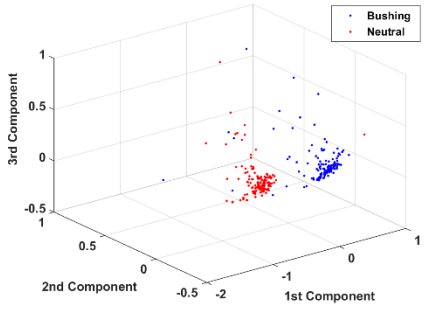

(g) Terminal 7

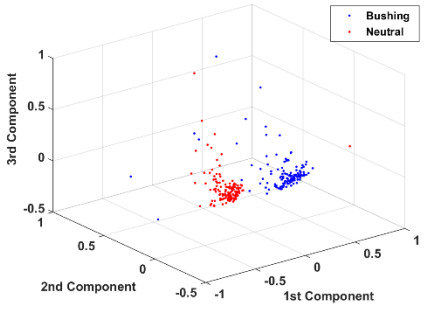

(h) Terminal 8

Figure 8.2.5. Clusters plot for void discharge from combination 2.

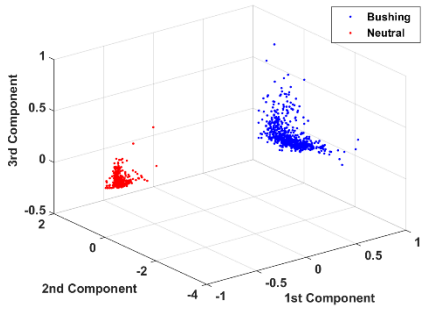

(a) Terminal 1

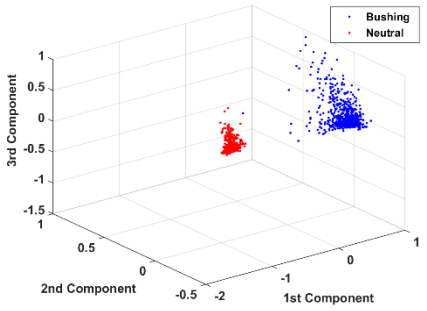

(b) Terminal 2

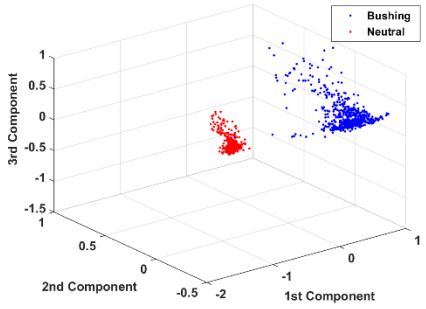

(c) Terminal 3

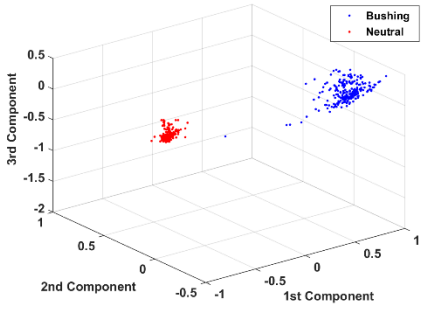

(d) Terminal 4

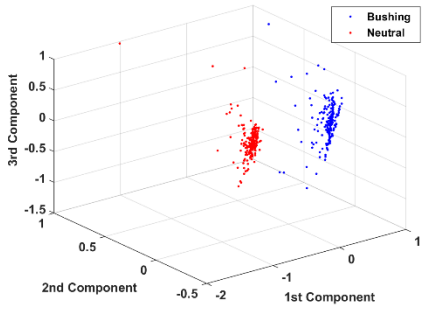

(e) Terminal 5

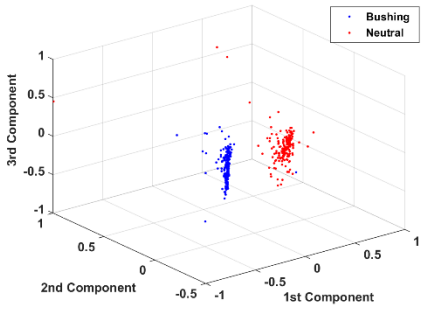

(f) Terminal 6

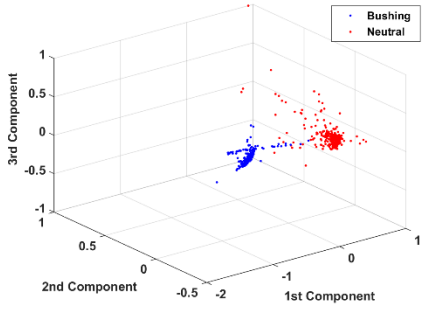

(g) Terminal 7

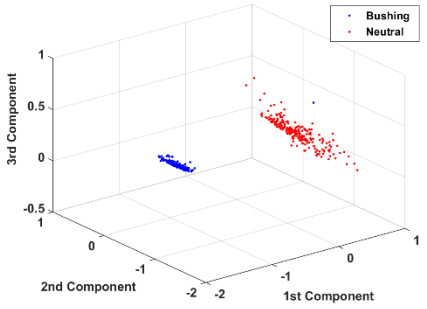

(h) Terminal 8

Figure 8.2.6. Clusters plot for void discharge from combination 3.

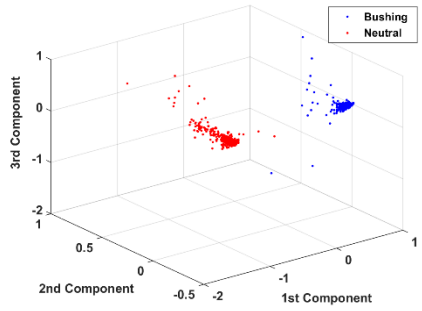

(a) Terminal 1

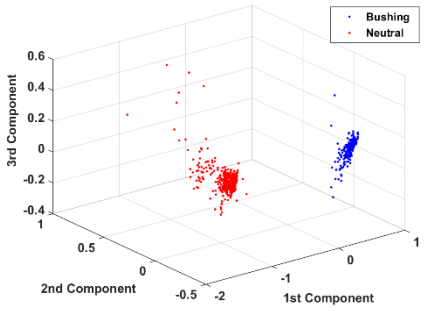

(b) Terminal 2

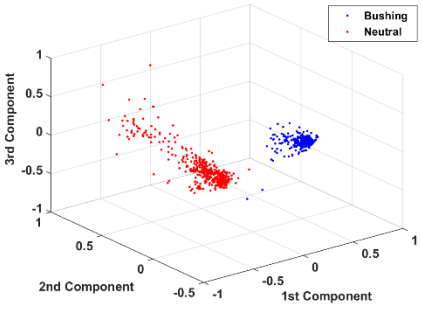

(c) Terminal 3

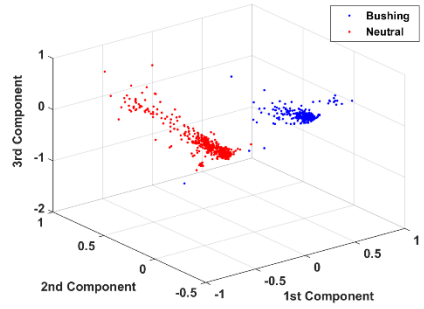

(d) Terminal 4

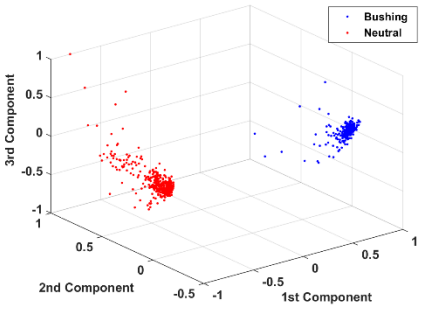

(e) Terminal 5

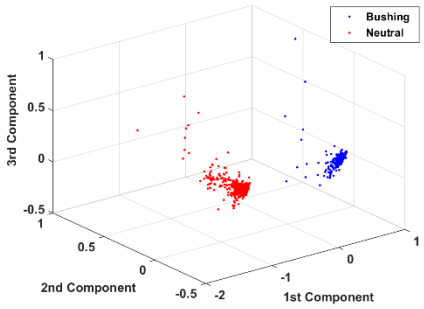

(f) Terminal 6

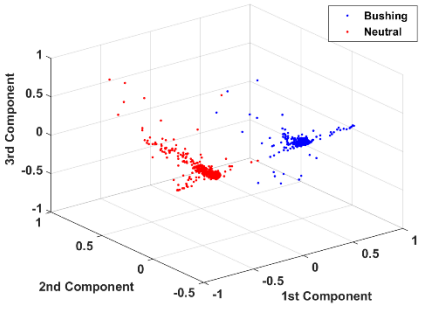

(g) Terminal 7

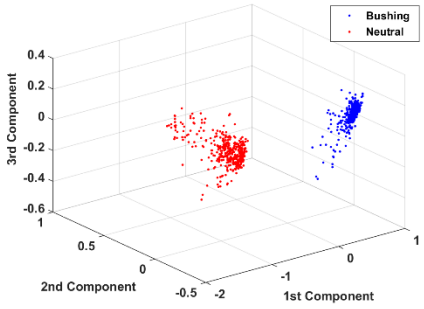

(h) Terminal 8

Figure 8.2.7. Clusters plot for floating discharge from combination 3.

According to Figure 8.2.2, Figure 8.2.4 and Figure 8.2.6, the position of the blue and red clusters is in a different position when the source was injected into different terminals along the winding. The clusters injected at terminal 1 have a clear separation between each other. However, when the PD signal was injected at terminal 2 onwards both of the clusters might be seen to come closer towards each other. It is anticipated that the separation of the clusters will be increased again after a point where the signals travel along a similar length of propagation path, which is normally at terminal 5 or 6. It is also observed that after this point, these clusters are seen to split away and swap position with each other within the principal component space.

While based on the Figure 8.2.3, Figure 8.2.5 and Figure 8.2.7, the position of the blue and red clusters is in an almost the same position and there is no relative swapping of position. This is because the source injection point was always fixed at terminal 5 at all the times. In this case, the signals travel along a similar length of a propagation path from the injection point to both ends of the transformer winding.

Both clusters for either source 1 or source 2 are separate and there is a variation in the gap between the paired clusters. The position of the clusters in the principal component space are varied for source 1 and almost the same position for source 2 when they are produced from measurement data sets which are obtained at different injection points along a transformer winding from terminal 1 to terminal 8. Therefore, it may be useful to measure the separation distance between clusters in order to precisely determine how much the variation occurs at each terminal along a transformer winding. As in single source localisation, this work used distance between centroid of clusters in order to measure the separation distance between cluster groups. The separation distance can be calculated using a centroid of the clusters using the Equation 8.1 – Equation 8.3. The details of the separation distance measured using the cluster plots for all PD sources is shown in Table 8.2.2 – Table 8.2.4.

Table 8.2.3. Separation distance for combination of floating and surface discharges

Terminal	D(x,y,z) for source 1	D(x,y,z) for source 2
1	0.4357	0.3555
2	0.4375	0.3548
3	0.4143	0.3533
4	0.3606	0.3555
5	0.2488	0.3537
6	0.0688	0.3536
7	-0.2240	0.3525
8	-0.4474	0.3492

Table 8.2.4. Separation distance for combination of surface and void discharges.

Terminal	D(x,y,z) for source 1	D(x,y,z) for source 2
1	0.4270	0.3518
2	0.4303	0.3563
3	0.4041	0.3563
4	0.3502	0.3613
5	0.2344	0.3568
6	0.0170	0.3555
7	-0.2884	0.3486
8	-0.4559	0.3410

Table 8.2.5. Separation distance for combination of void and floating discharges.

Terminal	D(x,y,z) for source 1	D(x,y,z) for source 2
1	0.455	0.3498
2	0.4507	0.3502
3	0.4156	0.3616
4	0.3154	0.3563
5	0.1389	0.3510
6	-0.0685	0.3512
7	-0.3373	0.3565
8	-0.4236	0.3512

Most of the terminal 1 and terminal 2 for all PD sources show a small difference regarding the separation distance. This is because the electrical connection that connects to both terminals is very close to each other. The separation distance can also be plotted against the winding terminals where Figure 8.2.8 shows the separation distance plot for Table 8.2.2 – Table 8.2.4 respectively.

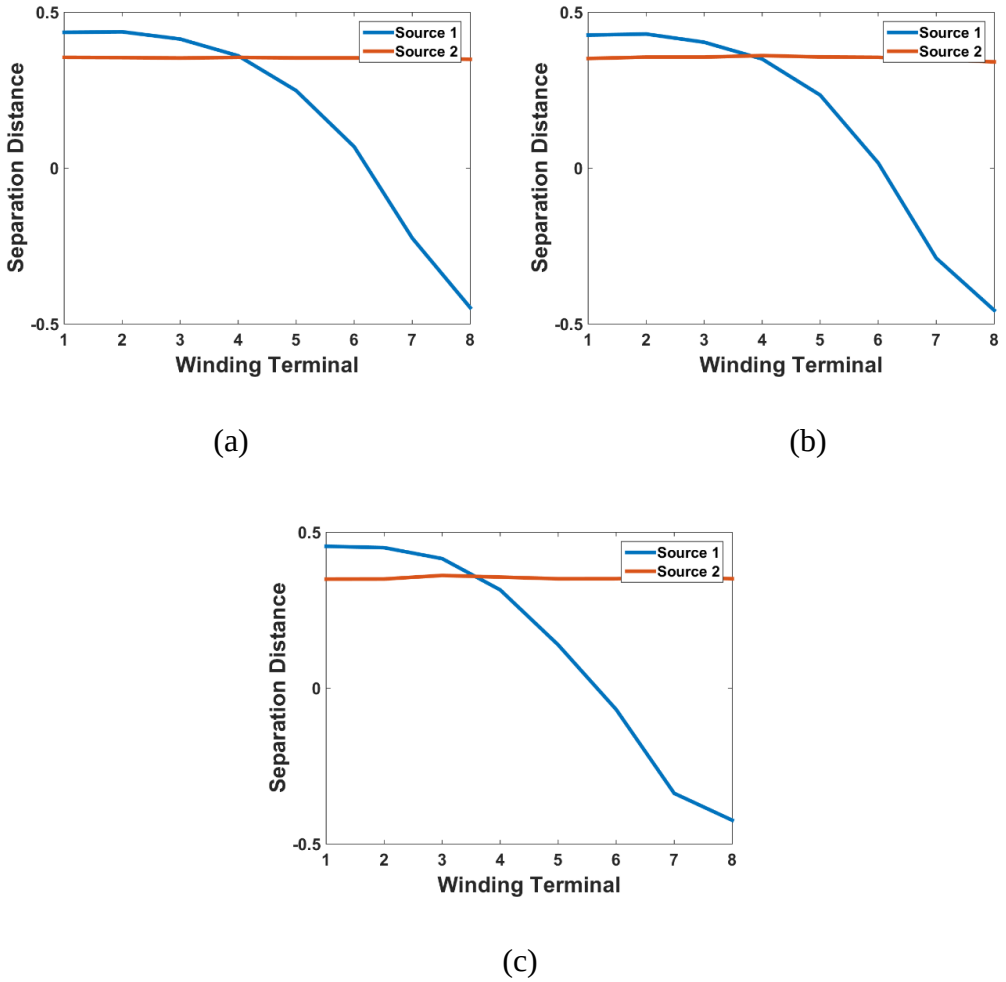

Figure 8.2.8. Separation distance plots of clusters for combination of (a) floating and surface discharges (b) surface and void discharges and (c) void and floating discharges.

Observation from Figure 8.2.8 shows that a more or less similar pattern of separation distance plots between two groups of clusters from both measurement points can been seen. The separation distance of clusters from source 1 are seen to come closer towards each other when

the source was injected from Terminal 2 to Terminal 6. Then, the clusters are seen to split away and swap positions from each other at Terminal 7 onwards. This is due to the fact that the propagation distance of the signals is closer to the neutral to earth point measurement and farther away from bushing tap point to earth measurement at Terminal 1 to Terminal 6 and vice versa for Terminal 7 onwards. While, for source 2, the separation distance is almost the same for all terminals as the source injection point was fixed at Terminal 5.

8.2.3 SEPARATION DISTANCE BETWEEN CLUSTERS IN HIGH DIMENSIONAL SPACE

OPTICS was applied directly to the high dimension of MM energy data set and the results were promising as discussed in Chapter 7. Therefore, the separation distance was directly calculated in the 20 dimensions of MM energy data set without the need for further dimension reduction. The details of the separation distance in 20 dimensions for all PD sources is shown in Table 8.2.5 – Table 8.2.7.

Table 8.2.6. Separation distance in 20 dimensions for combination of floating and surface discharges.

Terminal	D(x,y,z) for source 1	D(x,y,z) for source 2
1	0.4354	0.3559
2	0.4373	0.3540
3	0.4143	0.3548
4	0.3607	0.3559
5	0.2492	0.3544
6	0.0686	0.3533
7	-0.2239	0.3510
8	-0.4475	0.3488

Table 8.2.7. Separation distance in 20 dimensions for combination of surface and void discharges.

Terminal	D(x,y,z) for source 1	D(x,y,z) for source 2
1	0.4274	0.3554
2	0.4298	0.3544
3	0.4040	0.3548
4	0.3504	0.3632
5	0.2343	0.3549
6	0.0167	0.3583
7	-0.2884	0.3462
8	-0.4560	0.3403

Table 8.2.8. Separation distance in 20 dimensions for combination of void and floating discharges.

Terminal	D(x,y,z) for source 1	D(x,y,z) for source 2
1	0.4473	0.3498
2	0.4435	0.3506
3	0.4084	0.3616
4	0.3560	0.3563
5	0.1365	0.3510
6	-0.0673	0.3512
7	-0.3315	0.3565
8	-0.4201	0.3510

Figures 8.2.9 shows the separation distance plot for Table 8.2.5 – Table 8.2.7 plotted against the winding terminals.

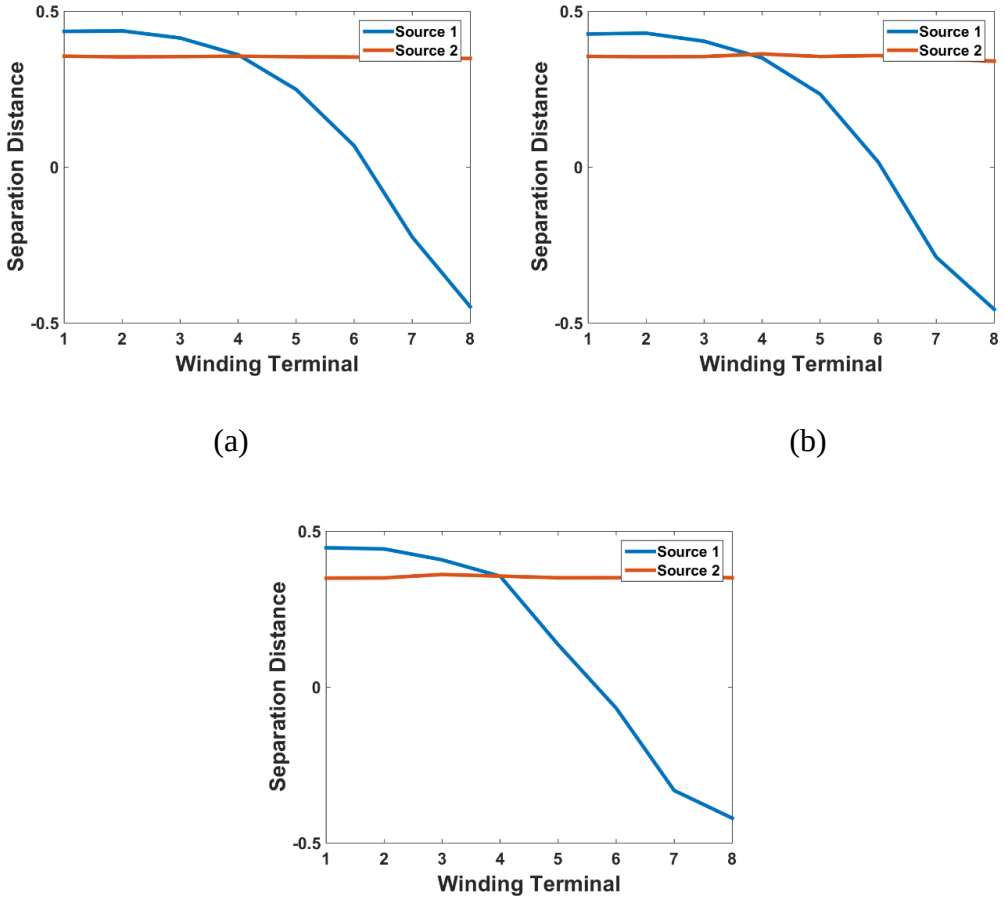

(a) (b)

(c)

Figure 8.2.9. Separation distance plots of clusters in 20D for combination of (a) floating and surface discharges (b) surface and void discharges and (c) void and floating discharges.

The results of separation distance calculated from 20 dimensions of MM energy data set are similar to the results of separation distance calculated between clusters within the three principle component space. It is believed that the pattern depends on the geometrical structure of the winding itself. Thus, it is believed if the approach is undertaken on a large transformer, the separation distance plot will be significantly steeper than the patterns illustrated in this

thesis. The advantages of this approach are that there is no need for dimensional reduction techniques used in order to calculate the separation distance between the clusters. Moreover, the time taken to calculate the separation distance without dimensional reduction technique is significantly shorter. This is because in PCA algorithms, the calculation of eigenvalues and eigenvectors requires significant processing time whereas a calculation directly in 20 dimensions is more efficient.

8.2.4 SEPARATION DISTANCE USING HEIGHT OF SPIKES OF OPTICS REACHABILITY PLOTS

Effectively, the height of the spikes of the OPTICS reachability plots represent the separation distance between each data set. The higher the peak of these spikes the more separate the data will be in the clusters. The idea is to use the variation of height of the spikes to estimate the location of the PD source. It is assume that the separation distance between each data produced from the OPTICS reachability plots are similar to those separations calculated in either 3 or 20 dimensions. However, the variation of the height of the spikes of OPTICS reachability plots were found not to be an effective approach to estimate the location of the source. This is due to unexpected events such as either excessive noise or stochastic variation of PD pulses that can cause a decrease in separation distance between clusters, and thus also decrease the height of the spikes of OPTICS reachability plots.

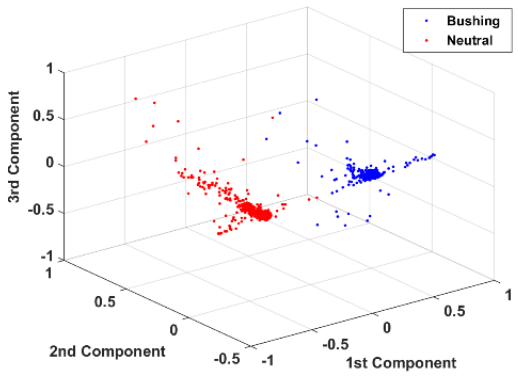

Figure 8.2.10. An example of variation on PD pulses which cause a decrease in separation distance between clusters.

8.2.5 LOCATION ESTIMATION

A reference length is needed in order to determine the location of the PD sources in the winding. Signals can be also injected at bushing core bar and measured at the bushing tap point and neutral to earth connection. It must be assumed that this approach represents the greatest difference in terms of percentage of energy distribution for bushing tap and neutral to earth measurement data due to the maximal distance between both measurement points, which includes the length of a transformer winding. Figure 8.2.11 shows a cluster plot for pulses injected into the bushing core bar of the experiment, which is selected as a reference point.

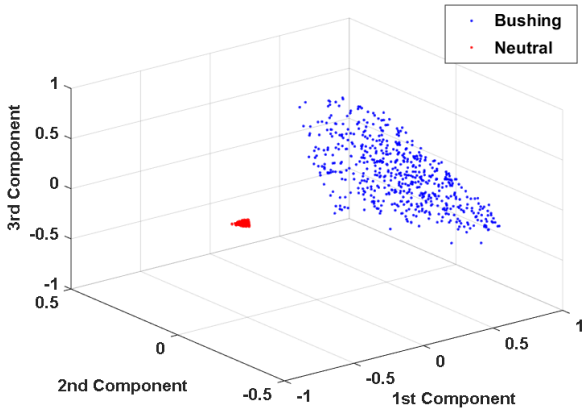

Figure 8.2.11. 3-D plots representing the three principal components derived from the mathematical morphology energies of pulses at reference point.

The length of the separation produced from the bushing core bar measurement data is expected to be the biggest compared to the other when PD signals were injected at terminals along a winding. This is due to the fact that the signal from bushing core bar reaches the bushing tap point more easily compared to the neutral to earth connection point, thus the signal energies measured from the bushing tap point will always have higher frequency content than a signal that measured at the neutral to earth connection.

The separation value when the PD signals were injected at the bushing core bar is 0.55 which show that it is the greatest separation values can be obtained from all the cluster plots derived from the mathematical morphology energies. Thus, by using the ratio of separation length of the terminal, $D_{terminal}$, with respect to the bushing core bar separation length, $D_{reference}$, the location of PD sources along the winding can be estimated. The ratio, R_D can be calculated by using:

$$R_D = \frac{D_{terminal}}{D_{reference}} \tag{8.4}$$

The interpretation of this value will give a broad indication of the location of the PD source along a transformer winding where the value near to 1 will indicate that the location of PD is near to the bushing tap point while if the value is near to zero means near to center of winding. On the other hand, if the value is near to -1 will indicate that the location of PD is near to the neutral to earth tap point.

This is useful when considering unknown transformer windings due to the fact that different transformer windings do have a different number of sections, different layers and numbers of discs i.e. length. Moreover, it may be possible to access a bushing externally thus the same measurement can be done on other high voltage transformers. Thus, a reference length is needed in order to determine what is the maximum separation distance could be for a particular winding so the location of PD in other sections can be estimated.

In order to validate the approach, some "blind tests" have been undertaken. The multiple PD source data have been randomly selected and have been go through the proposed approach. From the calculated value of R_D, an interpretation can be made which will give an estimation of the location of the PD source along the transformer winding. Table 8.2.8 – Table 8.2.10 show the interpretation of the obtained results from the blind tests for all combination of PD discharges.

Table 8.2.9. Interpretation of the obtained results from the blind tests for combination of floating and surface discharges.

Random selected data	**Obtained value of R_D**	**Interpretation of R_D value**	**Exact answer**
Data A	0.7533	This value is near to 1. Therefore, it can be concluded that the location of the PD source is near to the bushing measurement point.	Terminal 3
Data B	0.1251	This value is near zero. Therefore, it can be concluded that the location of the PD source is near to the center of the transformer winding.	Terminal 6
Data C	0.7955	This value is near to 1. Therefore, it can be concluded that the location of the PD source is near to the bushing measurement point.	Terminal 2
Data D	0.6556	This value is between 0 and 1. It is not near to 1 or either 0. Therefore, it can be concluded that the location of the PD source is between the center of the winding and the bushing measurement point.	Terminal 4

Table 8.2.10. Interpretation of the obtained results from the blind tests for combination of surface and void discharges.

Random selected data	**Obtained value of R_D**	**Interpretation of R_D value**	**Exact answer**
Data A	-0.5244	This value is between 0 and -1. It is not near to -1 or either 0. Therefore, it can be concluded that the location of the PD source is between the center of the winding and the neutral to earth measurement point.	Terminal 7
Data B	0.7764	This value is near to 1. Therefore, it can be concluded that the location of the PD source is near to the bushing measurement point.	Terminal 1
Data C	0.0309	This value is near zero. Therefore, it can be concluded that the location of the PD source is near to the center of the transformer winding.	Terminal 6
Data D	-0.8289	This value is near to -1. Therefore, it can be concluded that the location of the PD source is near to the neutral to earth measurement point.	Terminal 8

Table 8.2.11. Interpretation of the obtained results from the blind tests for combination of void and floating discharges.

Random selected data	**Obtained value of R_D**	**Interpretation of R_D value**	**Exact answer**
Data A	0.2525	This value is near zero. Therefore, it can be concluded that the location of the PD source is near to the center of the transformer winding.	Terminal 5
Data B	-0.7702	This value is near to -1. Therefore, it can be concluded that the location of the PD source is near to the neutral to earth measurement point.	Terminal 8
Data C	-0.1245	This value is negative value and also near to zero. Therefore, it can be concluded that the location of the PD source is between the center of the winding and the neutral to earth measurement point.	Terminal 6
Data D	0.8273	This value is near to 1. Therefore, it can be concluded that the location of the PD source is near to the bushing measurement point.	Terminal 1

From the Table 8.2.8 – Table 8.2.10, it can be concluded that the interpretation of the obtained R_D value can give a broad estimation of the location of the PD source along a transformer winding either near to the bushing measurement point, at the center of the winding or near to the neutral to earth measurement point.

8.3 SUMMARY

The localisation process of multiple partial discharge within a transformer winding in this work is focused on the PD signals that have been detected and measured from the bushing tap point and neutral to earth measurement point. In order to process the data and to extract some useful features, this work involved advanced digital signal processing methods. The techniques is based on the vector of distribution of energy at the bushing tap point and neutral to earth measurement point. Experiments reveal that different injection terminals along the transformer winding produced different locations of clusters either in 3D space or 20D space. Therefore, in this work, the separation distance between clusters was exploited in order to estimate the location of the PD sources. However, before any separation distance can be calculated, clusters that belong to the same source need to be determined first. This work used the cross correlation technique in order to find the clusters that generated from the same source from both measurement points.

Three techniques have been discussed in this chapter to calculate the separation distance between the paired clusters from both measurement points. The first approach is to use the separation distance between the centroid of two clusters in the 3D principle component space. While the second approach is to use the separation distance between two clusters in 20D MM energy data set. This approach had similar results with the first approach and the advantages of this approach is there is no need for addition dimensional reduction calculations. The third approach is to use the height of the spikes in OPTICS reachability plots. However, this approach cannot be used reliably as the height of the spikes can be distorted by events such as either excessive noise or variation within PD pulses, which cause a decrease in the height of the spikes of OPTICS reachability plots.

Finally, apart from the winding terminal, PD signals can be also injected at bushing core bar and measured at the bushing tap point and neutral to earth connection. The length of the separation produced from the bushing core bar measurement data is largest compared to where PD signals are injected at terminals along a winding. Therefore, by using the ratio of separation length of the terminal with respect to the bushing core bar separation length, the location of PD sources along the winding can be estimated.

CHAPTER 9

DISCUSSION, CONCLUSION AND FUTURE WORK

9.1 DISCUSSION

The main objective of this research is to study approaches that facilitate identification and localisation of multiple PD sources within a HV transformer winding. This thesis includes a literature review, reports of undertaken experiments and PD signal data processing. The literature review includes some basic information regarding HV power transformers, power transformer condition monitoring as well as previous on-going research regarding the identification and localisation of multiple PD sources within a HV transformer winding.

A set of experiments have been completed in order to generate data representing PD activities within a transformer winding, which can be used in this research. Three types of artificial PD sources namely; surface discharge, void discharge and floating were generated using different experimental arrangements. The sources were used in this research in order to study the activities and propagation characteristics of multiple PD sources within a transformer winding. Two approaches were studied i.e. by using artificial discharge sources and using an impulse signal generated from pulse generator. The result of the experiment using a pulse generator was compared to the experiments when artificial PD sources signal were injected into the terminals of the transformer winding. It is assumed that the characteristics of the signal propagation from the pulse generator with constant rise time, amplitude and pulse duration can be assumed to be similar to the characteristics of the signal from artificial discharge sources that produce non-uniform signals in terms of amplitude and frequency.

Two measurement sensors were placed at both ends of the winding, which were at bushing tap point to earth and neutral to earth point. This is because according to the fundamental theory using the theory of travelling waves along passive transmission lines by L.V. Bewley [15], the produced PD signals can be considered as travelling waves and will propagate from a source location towards both ends of the transformer winding. The

propagated electrical signals were measured by the two RFCTs which can be used for development of identification and localisation of multiple PD sources within a HV transformer winding. Meanwhile detection and evaluation of PD events were performed using a Mtronix PD measurement system.

This research presents the analysis of identification and localisation of multiple PD sources within a HV transformer winding mainly based on two decomposition techniques, which are Wavelet analysis and Mathematical Morphology. These decomposition techniques are useful signal processing technique producing feature vectors that represent the distribution of signal energy in both time domain and frequency domain. The high dimension data set produced from the decomposition techniques can be further reduced to three dimensions using PCA and t-SNE or to two dimensions using time frequency mapping in order to allow for visualisation of the data. The results show the formation of two main clusters produced from each measurement point represent two PD sources that were injected into different terminals along the transformer winding. Phase resolved PD patterns were used in order to comprehensively describe the PD pattern for each cluster.

However, in order to estimate the location of the each PD source, clusters that are belong to the same PD source from both measurement points need to be determined first. Therefore, this thesis used pulse cross correlation techniques to find the clusters that are belong to the same PD source. This technique is based on the analysis of the time delay between consecutive pulses. An approach for localisation can be developed once the pair of each cluster between both measurements points were identified. The main idea of this technique is to use the differences in energy distributions of each cluster.

The results show the formation of clusters when a PD source was injected into different terminals along the transformer winding. Therefore, the separation of the groups of clusters were exploited to indicate the location of the PD source. There are three approaches used to calculate the separation distance between two clusters in this thesis. Firstly is by calculating the separation distance between clusters in principle component space. Secondly is by calculating the separation distance between clusters in 20 dimensions of MM energy. Thirdly is by calculating the height of spikes of OPTICS reachability plots. Only the separation

distance in principle component space and separation distance in 20 dimensions of MM energy data set show very promising results.

Apart from the winding terminal, PD-like signals can be also injected at bushing core bar to create the largest separation distance between clusters from both measurement points compared to when PD signals were injected at terminals along a winding. Therefore, by using the ratio of separation length of the terminal with respect to the bushing core bar separation distance, the location of PD sources along the winding can be estimated.

9.2 CONCLUSIONS

A bespoke experiment has been designed and developed to enable the representative of a transformer winding. PD data was recorded using two radio frequency current transducers located at both ends of the winding parallel with a commercial PD detector from OMICRON Mtronix with a MPD600 acquisition unit. The produced measurement data were used to assess different approaches to HV transformer condition monitoring, which involve PD identification and localisation within HV transformer windings.

PD discrimination algorithms were developed and successfully applied to the measured data and the performance of each algorithm were presented in this thesis. The techniques rely on the independent signal energy frequency profile exhibited by pulses from different sources. The process involves plotting the clusters either in three or two dimensions to represent each pulse's signal energy distribution. The assumption that pulses produced by different source will occupy different localised region of feature space has been proved accurately. This finding allows for an automated clustering system to identify pulses attributed to unique sources. Analysis of the PD activity produced by each PD source could be used in future condition monitoring systems.

Cluster plots have been produced and their energy can be used in order to identify the location of multiple PD sources within a transformer winding. There are two successful techniques have been discussed in order to calculate the separation distance between the paired clusters from both measurement points. The use of ratio of separation length of the terminal with

respect to the bushing core bar separation length allow the estimation of the location of PD sources along the winding. To conclude a potential future condition monitoring tool that uses pulse waveform information for classification and localization of multiple PD sources within high voltage transformer winding has been developed.

9.3 FUTURE WORKS

In this research, the measurement data was taken from two radio frequency current transducers located at both ends of the transformer winding. For further investigation, the techniques that have been proposed in this thesis can be tested on PD measurement data measured from different type of sensors such as UHF sensors. This is because different type of sensor have different measurable frequency ranges.

It is important to remove the noise in order to extract PD pulses with confidence. As this investigation have been carried out in a controlled laboratory conditions which have a low noise level, a method known as hard-thresholding was used for de-noising the raw signals as well as to extract PD pulses. Therefore, future work should investigate how to develop better techniques for de-noising the raw signals, which is believed to provide improvements to the cluster patterns that can ultimately improve the localisation technique of PDs within transformer winding.

As far as the automated process is concerned, automatic cluster extraction has been implemented in this thesis based on the data set obtained from the experiments by using the derivative and magnitude of the OPTICS reachability graph. However, this approach is not necessary applicable for all applications. Therefore, automatic cluster extraction methods suitable for universal application need to be investigate, as these are important prerequisites for data mining applications.

It was mentioned in this thesis that by using the ratio of separation length of the terminal with respect to the bushing core bar separation length is an approach when considering unknown transformer windings due to the fact that different transformer windings do have a different number of sections, different layers and numbers of discs. Therefore, this research can

proceed with further work on the experiments regarding partial discharge activities, identification and localisation in different high voltage transformer windings, which allows further investigation of validation on the techniques that have been proposed in this thesis.

In a typical field environment, partial discharges within power transformers can be divided into two different types: internal and external discharges. External discharges usually take place at the bushings of the transformer and are either corona or surface discharges. Internal discharges are due to voids, solid contamination, floating or exposed conductors occur within the transformer tank. However, partial discharge may also occur somewhere within the transformer windings. Therefore, it is useful to apply and validate the proposed technique on the measurement data taken from on-field high voltage transformers in order to test whether identification and localisation processes can be achieved successfully.

In the context of PD analysis for condition monitoring, variations in the conditions at the PD source location is very useful for the operator about the condition of dielectrics at the PD source. The development of the PD discrimination technique proposed in this thesis will now facilitate this. Clearly, further investigation is required in this area in order to quantify of PD activities within transformer windings based on the approaches in terms of estimating the severity of the identified PDs at the source of the PD activity.

APPENDIX A – TRANSFORMER MODEL CONSTRUCTION

The transformer winding model was constructed by Alstom transformer and National Grid Company in 2004. It was then further redesigned into experimental model in the Tony Davies High Voltage Laboratory, University of Southampton. The windings of the transformer are connected for a pair of disc from outside via metal terminals. Table A1 shows the physical dimensions of the transformer winding model.

Table A1: Physical dimensions

Parameters	Dimensions
Number of disc per winding	14
Number of turns per disc	14
Total number of turns per winding	24
Mean length per turn	1810 mm
Width of spacers	40 mm
Radial depth of disc	85 mm
Physical axial length of per winding	150 mm
Width of the conductor	3 mm
Height of the conductor	7 mm
Duct dimension between two adjacent discs	3 mm
Thickness between the end disc and static ring	3 mm
Thickness of static ring	5 mm
Turn insulation thickness	1 mm
Inside diameter of winding	475 mm
Outside diameter of winding	650 mm
Distance from winding to the outer wall of tank	100 mm
Distance from winding to the inner core	50 mm
Distance from upper static ring to bottom	50 mm
Distance from lower static to top pressure plate	50 mm
Total mass	730 Kg

APPENDIX B – EXPERIMENTAL APPARATUS

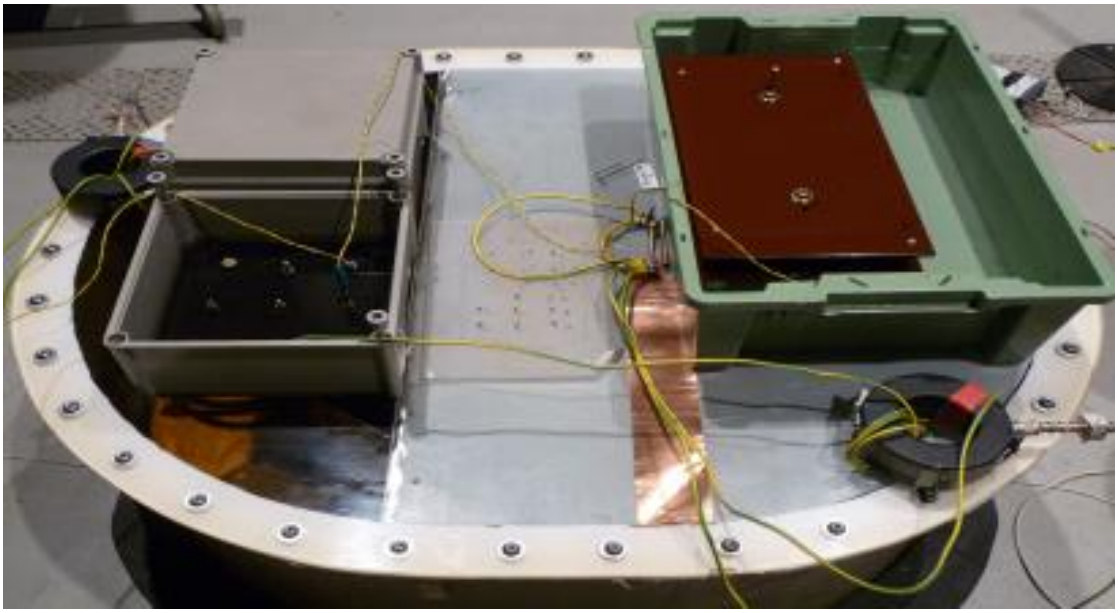

Figure B1. Transformer winding model.

Figure B2. A 60 kV transformer bushing.

Figure B3. RFCT measuring sensor.

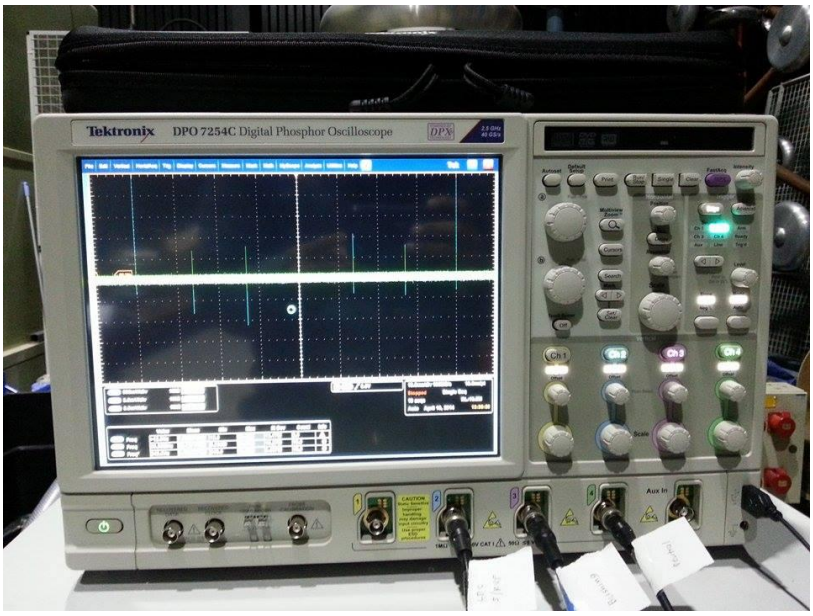

Figure B4. Textronix digital oscilloscope.

Figure B5. Frequency response measurement of the RFCT with a network analyser.

APPENDIX C – ENERGY DISTRIBUTION UNDER AN APPLIED VOLTAGE OF 20 KV

C.1 VOID DISCHARGE

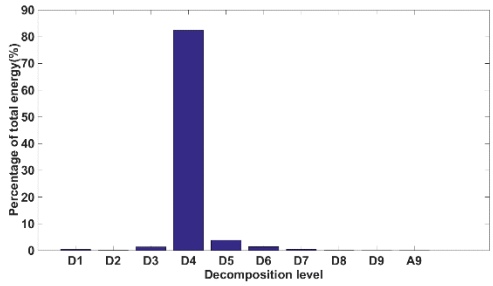

(a) Bushing tap point

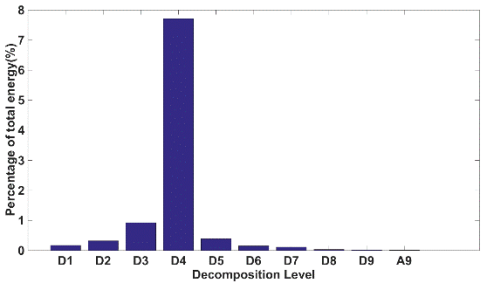

(b) Neutral to earth point

Figure C.1.1 Histogram representing the energy distribution of signal between different decomposition coefficients at terminal 1

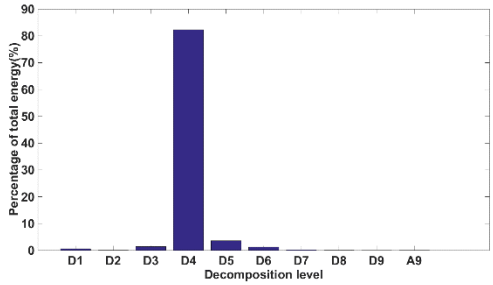

(a) Bushing tap point

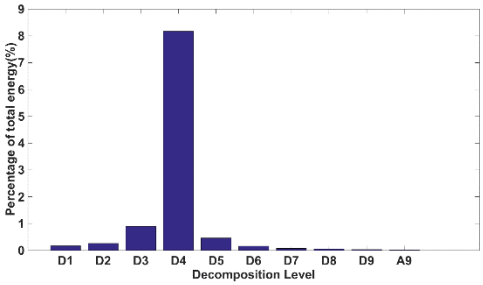

(b) Neutral to earth point

Figure C.1.2 Histogram representing the energy distribution of signal between different decomposition coefficients at terminal 2

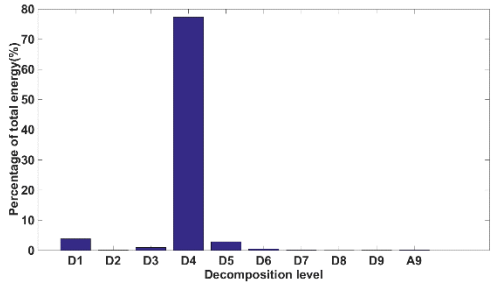

(a) Bushing tap point

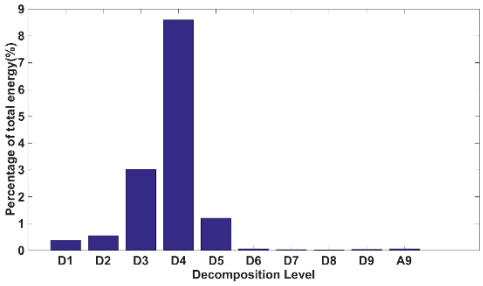

(b) Neutral to earth point

Figure C.1.3 Histogram representing the energy distribution of signal between different decomposition coefficients at terminal 3

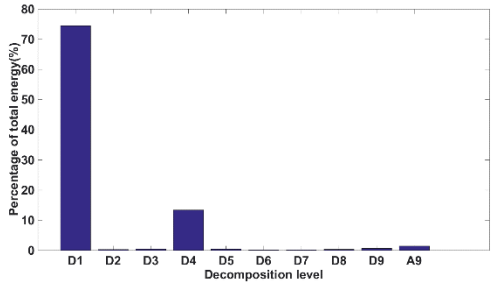

(a) Bushing tap point

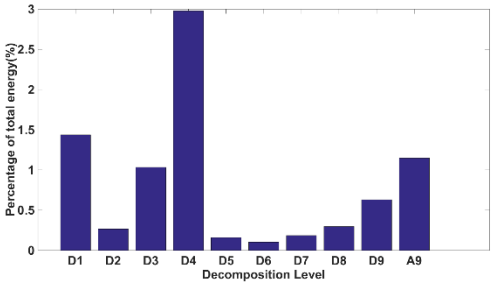

(b) Neutral to earth point

Figure C.1.4 Histogram representing the energy distribution of signal between different decomposition coefficients at terminal 4

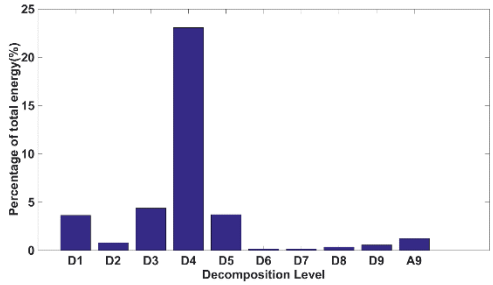

(a) Bushing tap point

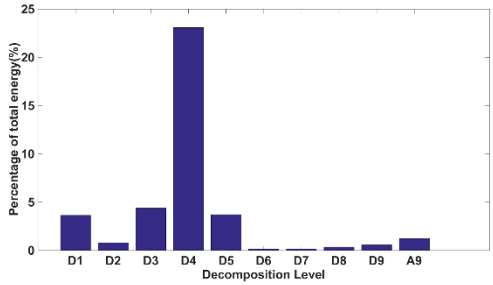

(b) Neutral to earth point

Figure C.1.5 Histogram representing the energy distribution of signal between different decomposition coefficients at terminal 5

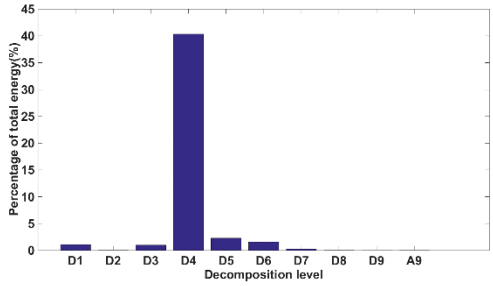

(a) Bushing tap point

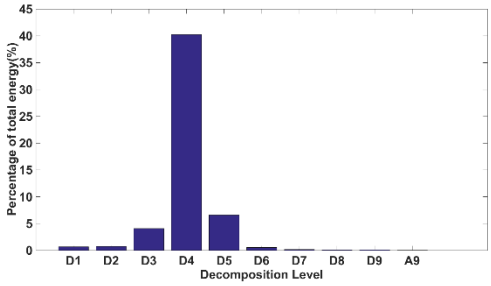

(b) Neutral to earth point

Figure C.1.6 Histogram representing the energy distribution of signal between different decomposition coefficients at terminal 6

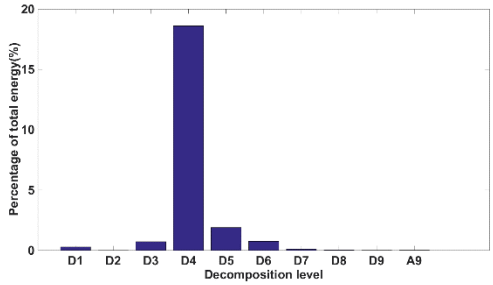

(a) Bushing tap point

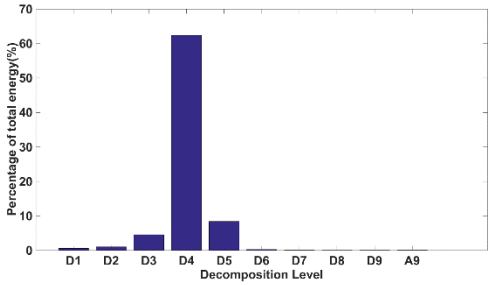

(b) Neutral to earth point

Figure C.1.7 Histogram representing the energy distribution of signal between different decomposition coefficients at terminal 7

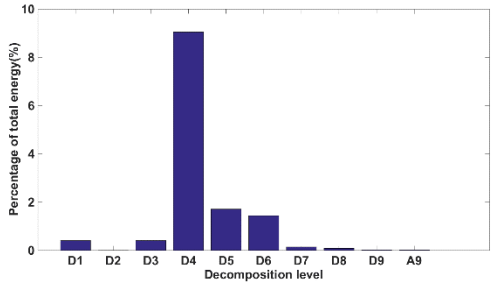

(a) Bushing tap point

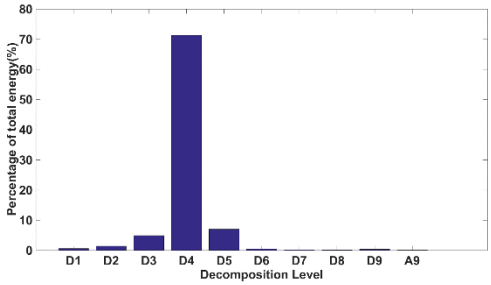

(b) Neutral to earth point

Figure C.1.8 Histogram representing the energy distribution of signal between different decomposition coefficients at terminal 8

C.2 FLOATING DISCHARGE

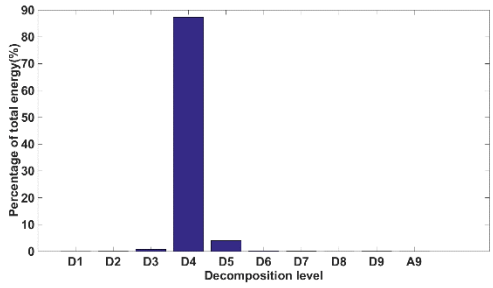

(a) Bushing tap point

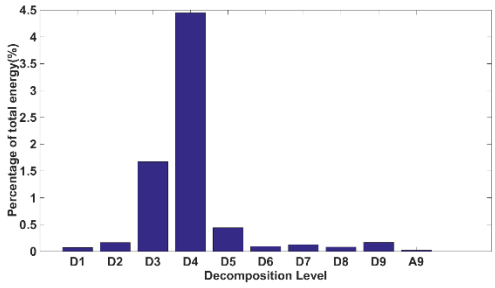

(b) Neutral to earth point

Figure C.2.1 Histogram representing the energy distribution of signal between different decomposition coefficients at terminal 1

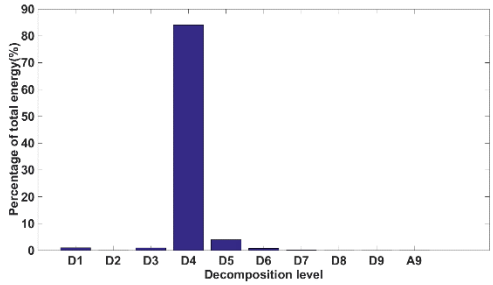

(a) Bushing tap point

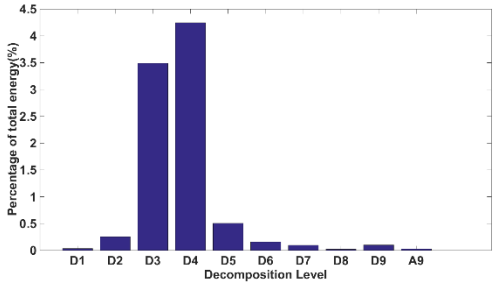

(b) Neutral to earth point

Figure C.2.2 Histogram representing the energy distribution of signal between different decomposition coefficients at terminal 2

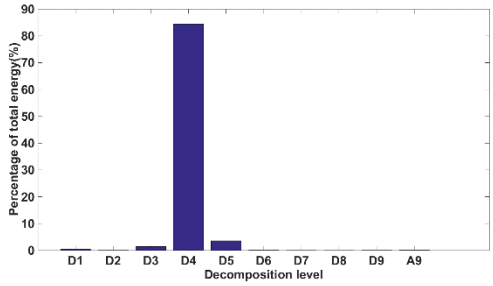

(a) Bushing tap point

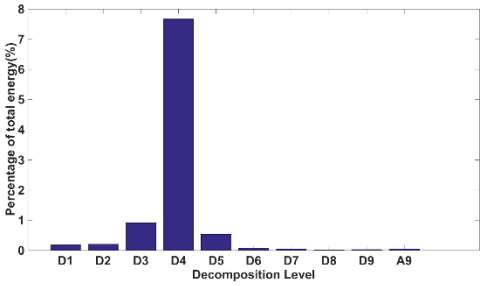

(b) Neutral to earth point

Figure C.2.3 Histogram representing the energy distribution of signal between different decomposition coefficients at terminal 3

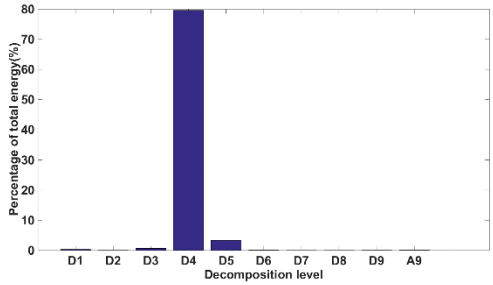

(a) Bushing tap point

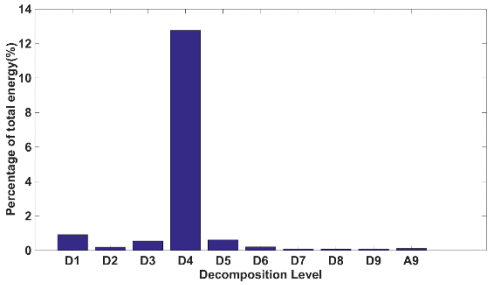

(b) Neutral to earth point

Figure C.2.4 Histogram representing the energy distribution of signal between different decomposition coefficients at terminal 4

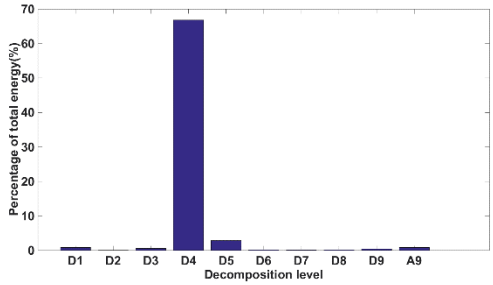

(a) Bushing tap point

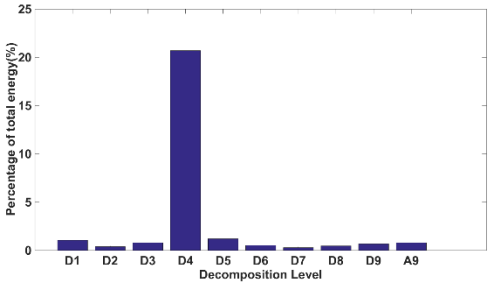

(b) Neutral to earth point

Figure C.2.5 Histogram representing the energy distribution of signal between different decomposition coefficients at terminal 5

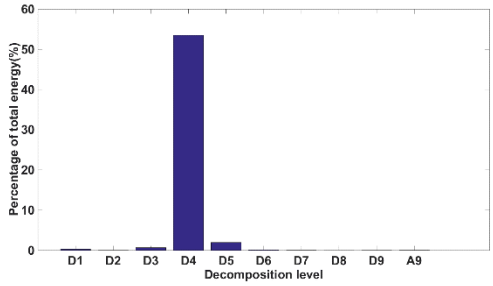

(a) Bushing tap point

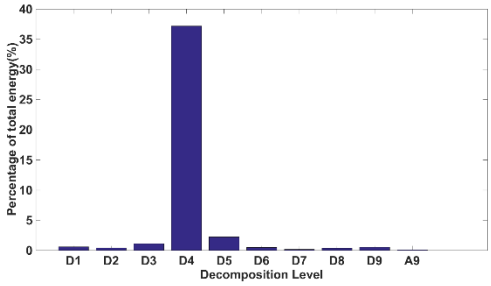

(b) Neutral to earth point

Figure C.2.6 Histogram representing the energy distribution of signal between different decomposition coefficients at terminal 6

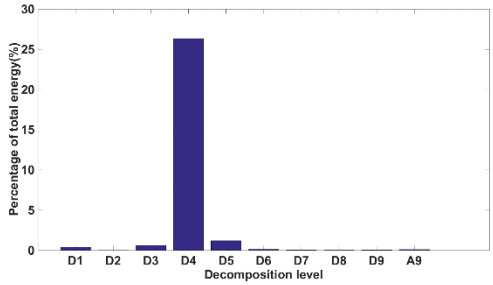

(a) Bushing tap point

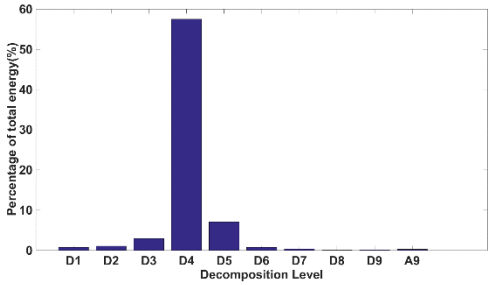

(b) Neutral to earth point

Figure C.2.7 Histogram representing the energy distribution of signal between different decomposition coefficients at terminal 7

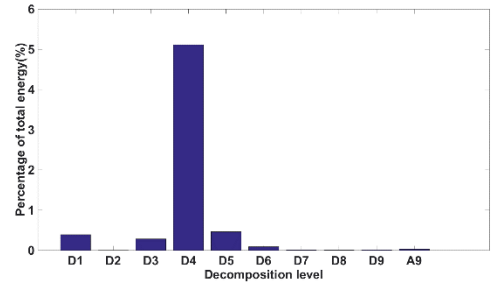

(a) Bushing tap point

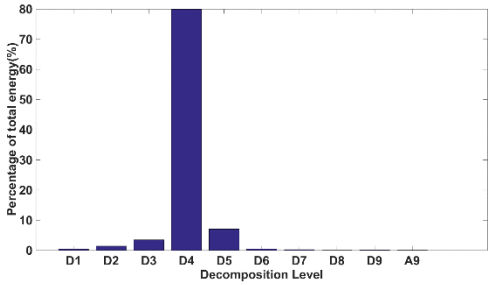

(b) Neutral to earth point

Figure C.2.8 Histogram representing the energy distribution of signal between different decomposition coefficients at terminal 8

REFERENCES

[1] H. A. Homaei, M. Moosavian, S.M., Illias, "Partial Discharge Localization in Power Transformers Using Neuro-Fuzzy Technique," in *IEEE Transactions on Power Delivery*, 2014, vol. 29, no. 5, pp. 2066–2076.

[2] M. Wang, a. J. Vandermaar, and K. D. Srivastava, "Review of condition assessment of power transformers in service," *IEEE Electr. Insul. Mag.*, vol. 18, no. 6, pp. 12–25, Nov. 2002.

[3] A. Akbari, P. Werle, H. Borsi, and E. Gockenbach, "Transfer function-based partial discharge localization in power transformers: a feasibility study," *IEEE Electr. Insul. Mag.*, vol. 18, no. 5, pp. 22–32, Sep. 2002.

[4] S. N. Rotby, A. H. El-Hag, M. M. a. Salama, and R. Bartnikas, "Partial discharge detection and localization inside the winding of power transformer," *2012 Annu. Rep. Conf. Electr. Insul. Dielectr. Phenom.*, pp. 84–87, Oct. 2012.

[5] C. Bengtsson, "Status and trends in transformer monitoring," *IEEE Trans. Power Deliv.*, vol. 11, no. 3, pp. 1379–1384, 1996.

[6] E. Gockenbach and H. Borsi, "Condition Monitoring and Diagnosis of Power Transformers," in *International Conference on CMD*, 2008, pp. 894–897.

[7] A. E. B. Abu-Elanien and M. M. a. Salama, "Survey on the Transformer Condition Monitoring," *2007 Large Eng. Syst. Conf. Power Eng.*, pp. 187–191, Oct. 2007.

[8] J. Singh, Y. Sood, and R. Jarial, "Condition monitoring of power transformers-bibliography survey," *Electr. Insul. Mag. ...*, vol. 24, no. 3, pp. 11–25, 2008.

[9] T. K. Saha, "Review of Modern Diagnostic Techniques for Assessing Insulation Condition in Aged Transformers," in *IEEE Transactions on Dielectrics and Electrical Insulation*, 2003, vol. 10, no. 5, pp. 903–917.

[10] B. Fruth and L. Niemeyer, "The importance of statistical characteristics of partial discharge data," *IEEE Trans. Electr. Insul.*, vol. 27, no. 1, pp. 60–69, 1992.

[11] E. Gulski, "Digital analysis of partial discharges," *Dielectr. Electr. Insul. IEEE Trans.*, vol. 2, no. 5, pp. 822–837, 1995.

[12] L. Hao, P. L. Lewin, J. A. Hunter, and D. J. Swaffield, “Discrimination of Multiple PD Sources Using Wavelet Decomposition and Principal Component Analysis,” no. September 2010, pp. 1702–1711.

[13] A. Contin and S. Pastore, “Classification and separation of partial discharge signals by means of their auto-correlation function evaluation,” *IEEE Trans. Dielectr. Electr. Insul.*, vol. 16, no. 6, pp. 1609–1622, Dec. 2009.

[14] A. Cavallini and G. C. Montanari, “A new methodology for the identification of PD in electrical apparatus: properties and applications,” *IEEE Trans. Dielectr. Electr. Insul.*, vol. 12, no. 2, pp. 203–215, Apr. 2005.

[15] L. V. Bewley, “Traveling Waves on Transmission Systems,” *Trans. Am. Inst. Electr. Eng.*, vol. 50, no. 2, pp. 532–550, 1931.

[16] M. S. A. Rahman, “Identification of Partial Discharge Sources and Their Location within High Voltage Transformer Windings,” PhD Thesis, University of Southampton, 2014.

[17] H. Zainuddin, “Study of Surface Discharge Behaviour at the Oil-pressboard Interface,” PhD Thesis, University of Southampton, 2013.

[18] V. P. Darabad, M. Vakilian, T. R. Blackburn, and B. T. Phung, “An efficient PD data mining method for power transformer defect models using SOM technique,” *Int. J. Electr. Power Energy Syst.*, vol. 71, no. November, pp. 373–382, 2015.

[19] D. J. Allan and A. White, “Transformer Design for High Reliability,” in *Second International Conference on the Reliability of Transmission and Distribution Equipment*, 1995, pp. 66–72.

[20] V. Sokolov, Z. Berler, and V. Rashkes, “Effective Methods of Assessment of Insulation System Conditions in Power Transformers: a View Based on Practical Experience,” *Proc. Electr. Insul. Conf. Electr. Manuf. Coil Wind. Conf. (Cat. No.99CH37035)*, pp. 659–667, 1999.

[21] William H Bartley P.E., “Analysis of Transformer Failures,” *Int. Assoc. Eng. Insur. 36th Annu. Conf. – Stock.*, pp. 1–5, 2003.

[22] A. J. and E. G. R. Jongen, P. Morshuis, J. Smit, “A Statistical Approach to Processing

Power Transformer Failure Data," *19th Int. Conf. Electr. Distrib. Vienna*, pp. 21–24.

[23] W. Young, "Transformer life management - condition monitoring," *IEE Colloq. Transform. Life Manag.*, vol. 1998, pp. 2–2, 1998.

[24] R. Mohamed, "Partial Discharge Signal Propagation Modelling and Estimation in High Voltage Transformer Windings," *PhD Thesis, Univ. Southampt.*, 2010.

[25] C. H. and T. Leibfried, "Practical Experience on Transformer Insulation Condition Assessment," *Int. Conf. Prop. Appl. Dielectr. Mater.*, pp. 238–241, 2006.

[26] A. Nesbitt and B. Stewart, "Condition monitoring of power transformers through partial discharge measurement: Problems associated with pulse distortion in the windings," *IEEE Trans. Power Deliv.*, vol. 10, pp. 1171–1176, 1997.

[27] M. S. A. S. A. Minhas, J. P. P. Reynders, and P. J. J. de Klerk, "Failures in power system transformers and appropriate monitoring techniques," *High Volt. Eng. 1999. Elev. Int. Symp. {(Conf.} Publ. No. 467)*, vol. 1, no. 467, pp. 94--97 vol.1, 1999.

[28] D. H. and M. Saravolac, "Condition monitoring in power transformers," *IEE Colloq. Cond. Monit. Large Mach. Power Transform. (Digest No 1997/086)*, p. 7/1-7/3, 1997.

[29] S. Tenbohlen, T. Stirl, G. Bastos, J. Baldauf, P. Mayer, and M. Stach, "Experienced based evaluation of economic benefits of on-line monitoring systems for power transformers," *CIGRE Sess. 2002;2002*, pp. 12–110, 2002.

[30] J. A. Lapworth, P. N. Jarman, and I. R. Funnell, "Condition assessment techniques for large power transformers," *Second Int. Conf. Reliab. Transm. Distrib. Equip.*, no. 406, pp. 85–90, 1995.

[31] J. Lapworth and T. McGrail, "Transformer failure modes and planned replacement," *IEE Colloq. Transform. Life Manag.*, vol. (Ref. No., p. 9/1 –9/7, 1998.

[32] Y. Han and Y. H. Song, "Condition monitoring techniques for electrical equipment-a literature survey," *IEEE Trans. Power Deliv.*, vol. 18, no. 1, pp. 4–13, 2003.

[33] T. Krieg and M. Napolitano, "Techniques and experience in on-line transformer condition monitoring and fault diagnosis in ElectraNet SA," *Int. Conf. Power Syst. Technol. Proc.*, pp. 1019–1024, 2000.

[34] H. C. Lin CE, Ling JM, "An expert system for transformer fault diagnosis using

dissolved gas analysis," *Power Deliv. IEEE Trans.*, vol. 8, no. 1, pp. 231–238, 1993.

[35] B. J. Wang P, Raghuveer MR, McDermid W, "A Digital Technique for the On-line Measurement of Dissipation Factor and Capacitance," *Dielectr. Electr. Insul. IEEE Trans*, vol. 8, no. 2, pp. 228–232, 2001.

[36] M. D. Judd, L. Yang, and I. B. B. Hunter, "Partial discharge monitoring for power transformers using UHF sensors part 1: Sensors and signal interpretation," *IEEE Electr. Insul. Mag.*, vol. 21, no. 2, pp. 5–14, 2005.

[37] S. R. Allan D, Blackburn TR, "Methodologies and Models to Improve the Reliability of service Aged Electrical Insulation," *Present. CIGRÉ, Paris*, 2002.

[38] J. L. Kirtley, W. H. Hagman, and B. C. L. et Al., "Monitoring the health of power transformers," *IEEE Comput. Appl. Power*, pp. 18–23, 1996.

[39] S. Figel and F.Tenbohlen, "On-line Condition Monitoring of Power Transformers," *IEEE Power Eng. Soc. Winter Meet.*, vol. 3, pp. 2211–2216, 2000.

[40] T. Leibfried, "Online monitors keep transformers in service," *IEEE Comput. Appl. Power*, pp. 36–42, 1996.

[41] E. Kuffel, W. S. Zaengl, and J. Kuffel, *High Voltage Engineering - Fundamentals (Second Edition)*. 2000.

[42] H. a Illias, G. Chen, and P. L. Lewin, "The influence of spherical cavity surface charge distribution on the sequence of partial discharge events," *J. Phys. D. Appl. Phys.*, vol. 44, no. 24, p. 245202, 2011.

[43] X. Ma, C. Zhou, and I. J. Kemp, "Interpretation of wavelet analysis and its application in partial discharge detection," *IEEE Trans. Dielectr. Electr. Insul.*, vol. 9, no. 3, pp. 446–457, 2002.

[44] S. Sriram, S. Nitin, K. M. M. Prabhu, and M. J. Bastiaans, "Signal denoising techniques for partial discharge measurements," *IEEE Trans. Dielectr. Electr. Insul.*, vol. 12, no. 6, pp. 1182–1191, 2005.

[45] X. Zhou, C. Zhou, and I. J. Kemp, "An improved methodology for application of wavelet transform to partial discharge measurement denoising," *IEEE Trans. Dielectr. Electr. Insul.*, vol. 12, no. 3, pp. 586–594, 2005.

[46] M. Ghaffarian, M. Vakilian, V. Parvin, and a Ghaedi, “Investigation of online detected partial discharges in power transformer,” *Power Eng. Conf. 2008. AUPEC ’08. Australas. Univ.*, pp. 1–6, 2008.

[47] G. C. Stone, “Partial discharge diagnostics and electrical equipment insulation condition assessment,” *IEEE Trans. Dielectr. Electr. Insul.*, vol. 12, no. 5, pp. 891–904, 2005.

[48] I. A. Soomro and M. N. Ramdon, “Study on different techniques of partial discharge (PD) detection in power transformers winding : Simulation between paper and EPOXY resin using UHF method,” *Int. J. Conceptions Electr. Electron. Eng.*, vol. 2, no. 1, pp. 57–61, 2014.

[49] a. S. Kumar, R. P. Gupta, K. Udayakumar, and A. Venkatasami, “Online partial discharge detection and location techniques for condition monitoring of power transformers: A review,” *Int. Conf. Cond. Monit. Diagnosis*, pp. 927–931, 2008.

[50] B. H. Ward, “A survey of new techniques in insulation monitoring of power transformers,” *IEEE Electr. Insul. Mag.*, vol. 17, pp. 16–23, 2001.

[51] J. Ramírez-Niño and a Pascacio, “Acoustic measuring of partial discharge in power transformers,” *Meas. Sci. Technol.*, vol. 20, no. 11, p. 115108, 2009.

[52] L. Hao, P. L. Lewin, Y. Tian, J. S. Wilkinson, S. G. Swingler, and S. J. Sutton, “Application of Electro-optic Modulation Technique for PD Monitoring of Power Transformers,” *Conf. Rec. 2006 IEEE Int. Symp. Electr. Insul.*, pp. 412–415, 2006.

[53] Z. B. Shen and E. F. El-Saadany, “Localization of Partial Discharges Using UHF Sensors in Power Transformers,” *IEEE Power Eng. Soc. Gen. Meet.*, pp. 1–6, 2006.

[54] M. D. Judd and L. Yang, “Recognising multiple partial discharge sources in power transformers by wavelet analysis of UHF signals,” *IEE Proc. - Sci. Meas. Technol.*, vol. 150, no. 3, pp. 119–127, 2003.

[55] M. D. Judd and T. Pinpart, “Differentiating between partial discharge sources using envelope comparison of ultra-high-frequency signals,” *IET Sci. Meas. Technol.*, vol. 4, no. 5, pp. 256–267, Sep. 2010.

[56] M. D. Judd, O. Farish, J. S. Pearson, T. Breckenridge, and B. M. Pryor, “Power

transformer monitoring using UHF sensors: installation and testing," *Conf. Rec. 2000 IEEE Int. Symp. Electr. Insul.*, pp. 373–376, 2000.

[57] M. S. A. Rahman, P. Rapisarda, and P. L. Lewin, "Construction of Finite Impulse Wavelet Filter for Partial Discharge Localisation inside a Transformer Winding," *Electr. Insul. Conf.*, no. June, pp. 30–34, 2013.

[58] C. Dodds, "Condition Assessment of HV Cables - Guest Blog by EA Technology." [Online]. Available: http://www.cablejoints.co.uk/blog/article/condition-assessment-of-hv-cables.

[59] J. A. Hunter, "An investigation into partial discharge activity within three-phase belted cables," *PhD Thesis, Univ. Southampt.*, 2013.

[60] P. Werle, H. Borsi, and E. Gockenbach, "A new method for partial discharge location on power transformers based on a system theoretical approach," *Prop. Appl. Dielectr. Mater. 2000. Proc. 6th Int. Conf.*, vol. 2, pp. 831–834 vol.2, 2000.

[61] Z. Zheng, Y. Yang, C. Li, S. Liu, and J. Ma, "Characteristics of partial discharge during its evolution in transformer winding," *Conf. Rec. IEEE Int. Symp. Electr. Insul.*, pp. 1–4, 2010.

[62] Y. Yuan, C. Li, Z. Zheng, S. Liu, and J. Ma, "Lab investigation of PD development in transformer winding," *Conf. Rec. 2010 IEEE Int. Symp. Electr. Insul.*, pp. 1–4, 2010.

[63] P. L. Lewin, I. O. Golosnoy, and R. Mohamed, "Locating partial discharge sources in high voltage transformer windings," in *2011 Electrical Insulation Conference, EIC 2011*, 2011, no. June, pp. 196–200.

[64] A. L. Kupershtokh *et al.*, "Stochastic models of partial discharge activity in solid and liquid dielectrics," *Sci. Meas. Technol. IET*, vol. 1, no. 6, pp. 303–311, 2007.

[65] N. H. Nik Ali, J. A. Hunter, P. Rapisarda, and P. L. Lewin, "Identification of Multiple Partial Discharge Sources in High Voltage Transformer Windings," *IEEE Conf. Electr. Insul. Dielectr. Phenom.*, pp. 188–191, 2014.

[66] N. H. Nik Ali, W. Goldsmith, J. A. Hunter, and P. L. Lewin, "Comparison of Clustering Techniques of Multiple Transformer Windings," *IEEE 11th Int. Conf. theProperties Appl. Dielectr. Mater.*, pp. 256–259, 2015.

[67] W. Gao and K. Tan, “Study on the influence of pulse propagation in transformer winding on partial discharge pattern recognition,” *Proc. 6th Int. Conf. Prop. Appl. Dielectr. Mater.*, vol. 1, pp. 125–128, 2000.

[68] C. Heitz, “A generalized model for partial discharge processes based on a stochastic process approach,” *J. Phys. D. Appl. Phys.*, vol. 32, no. 9, p. 1012, 1999.

[69] J. C. Chan, T. K. Saha, and C. Ekanayake, “Pattern recognition techniques and their applications for automatic classification of artificial partial discharge sources,” *IEEE Trans. Dielectr. Electr. Insul.*, vol. 20, no. 2, pp. 468–478, Apr. 2013.

[70] T. R. Blackburn, B. T. Phung, and H. H. Sinaga, “Recognition of single and multiple partial discharge sources in transformers based on ultra-high frequency signals,” *IET Gener. Transm. Distrib.*, vol. 8, no. 1, pp. 160–169, Jan. 2014.

[71] H. C. Chen, “Partial discharge identification system for high-voltage power transformers using fractal feature-based extension method,” *IET Sci. Meas. Technol.*, vol. 7, no. 2, pp. 77–84, 2013.

[72] D. Evagorou, A. Kyprianou, G. E. Georghiou, L. Hao, P. L. Lewin, and A. Stavrou, “Multisource PD identification based on phase synchronous and asynchronous data,” *Annu. Rep. Conf. Electr. Insul. Dielectr. Phenom.*, pp. 460–463, Oct. 2011.

[73] J. Li, R. Liao, S. Grzybowski, and L. Yang, “Oil-paper aging evaluation by fuzzy clustering and factor analysis to statistical parameters of partial discharges,” *IEEE Trans. Dielectr. Electr. Insul.*, vol. 17, no. 3, pp. 756–763, 2010.

[74] M. A. Fard, A. Akbari, R. Shojaee, H. R. Mirzaei, and P. Naderi, “Partial discharge defects classification using neuro-fuzzy inference system,” *Solid Dielectr. (ICSD), 2010 10th IEEE Int. Conf.*, pp. 1–4, 2010.

[75] A. Contin, G. C. Montanari, and C. Ferraro, “PD source recognition by Weibull processing of pulse height distributions,” *IEEE Trans. Dielectr. Electr. Insul.*, vol. 7, no. 1, pp. 48–58, 2000.

[76] a. Contin, a. Cavallini, G. C. Montanari, G. Pasini, and F. Puletti, “Digital detection and fuzzy classification of partial discharge signals,” *IEEE Trans. Dielectr. Electr. Insul.*, vol. 9, no. 3, pp. 335–348, Jun. 2002.

[77] P. Werle, E. Gockenbach, and H. Borsi, “Partial discharge measurements on power transformers using transfer function for detection and localisation,” *Proc. 7th Int. Conf. Prop. Appl. Dielectr. Mater.*, vol. 3, pp. 1154–1157, 2003.

[78] A. M. Jafari and A. Akbari, “Partial discharge localization in transformer windings using multi-conductor transmission line model,” *Electr. Power Syst. Res.*, vol. 78, pp. 1028–1037, 2008.

[79] R. a. Jongen, P. Morshuis, S. Meijer, and J. J. Smit, “Identification of partial discharge defects in transformer oil,” *CEIDP ’05. 2005 Annu. Rep. Conf. Electr. Insul. Dielectr. Phenomena, 2005.*, pp. 565–568, 2005.

[80] T. Zhiguo, L. Chengrong, H. Xingquan, L. Zhili, and F. Shangying, “The feasibility of locating PD source in transformer using the UHF technology,” *Annu. Rep. Conf. Electr. Insul. Dielectr. Phenomena, CEIDP*, pp. 477–480, 2004.

[81] Z. Tang, C. Li, X. Cheng, W. Wang, J. Li, and J. Li, “Partial discharge location in power transformers using wideband RF detection,” *IEEE Trans. Dielectr. Electr. Insul.*, vol. 13, no. 6, pp. 1193–1199, Dec. 2006.

[82] M. a. Eldery, T. K. Abdel-Galil, E. F. El-Saandany, and M. M. a Salama, “Identification of partial discharge locations in transformer winding using PSD estimation,” *IEEE Trans. Power Deliv.*, vol. 21, no. 2, pp. 1022–1023, 2006.

[83] M. G. Niasar, “Partial Discharge Signatures of Defects in Insulation Systems Consisting of Oil and Oil-impregnated Paper,” PhD Thesis, KTH School of Electrical Engineering, 2012.

[84] L. Kebbabi and A. Beroual, “Optical and electrical characterization of creeping discharges over solid/liquid interfaces under lightning impulse voltage,” *IEEE Trans. Dielectr. Electr. Insul.*, vol. 13, no. 3, pp. 565–571, 2006.

[85] Y. Nakao, H. Itoh, Y. Sakai, and H. Tagashira, “Studies of impulse creepage discharge in transformer oil,” *IEEE Trans. Electr. Insul.*, vol. 26, no. 4, pp. 732–738, 1991.

[86] O. Lesaint and G. Massala, “Transition to fast streamers in mineral oil in the presence of insulating solids,” *Conf. Rec. 1996 IEEE Int. Symp. Electr. Insul.*, pp. 737–740, 1996.

[87] R. L. R. Liu and A. Jaksts, “Breakdown processes in transformer insulation under LI voltages,” *IEEE Int. Conf. Dielectr. Liq. 2005. ICDL 2005.*, pp. 75–78, 2005.

[88] K. Firuzi, V. Parvin, and M. Vakilian, “Identification of free conducting particles in transformer oils using PD signals,” *IEEE 11th Int. Conf. Prop. Appl. Dielectr. Mater.*, pp. 724–727, 2015.

[89] P. Kang and D. Birtwhistle, “Condition Assessment of Power Transformer on-Load Tap-Changers Using Wavelet Analysis and Self-Organizing Map: Field Evaluation,” *IEEE Power Eng. Rev.*, vol. 22, no. 8, pp. 69–69, 2002.

[90] S. K. Pandey; L. Satish, “Multiresolution signal decomposition: a new tool for fault detection in power transformers during impulse tests,” *IEEE Trans. Power Deliv.*, vol. 13, no. 4, pp. 1194–1200, 1998.

[91] W. a. Wilkinson and M. D. Cox, “Discrete wavelet analysis of power system transients,” *IEEE Trans. Power Syst.*, vol. 11, no. 4, pp. 2038–2044, 1996.

[92] G. T. Heydt; A. W. Galli, “Transient power quality problems analyzed using wavelets,” *IEEE Trans. Power Deliv.*, vol. 12, no. 2, pp. 908–915, 1997.

[93] P. L. Mao and R. K. Aggarwal, “A novel approach to the classification of the transient phenomena in power transformers using combined wavelet transform and neural network,” *Power Deliv. IEEE Trans.*, vol. 16, no. 4, pp. 654–660, 2001.

[94] J. Jang, S. Kim, Y. Lee, and J. Kim, “Classification of Partial Discharge Electrical signals Using Wavelet Transforms,” pp. 552–555, 1999.

[95] N. G. Nikolaou and I. a. Antoniadis, “Application of Morphological Operators As Envelope Extractors for Impulsive-Type Periodic Signals,” *Mech. Syst. Signal Process.*, vol. 17, no. 6, pp. 1147–1162, Nov. 2003.

[96] L. Zhang, J. Xu, J. Yang, D. Yang, and D. Wang, “Multiscale morphology analysis and its application to fault diagnosis,” *Mech. Syst. Signal Process.*, vol. 22, no. 3, pp. 597–610, Apr. 2008.

[97] J. Wang, G. Xu, Q. Zhang, and L. Liang, “Application of improved morphological filter to the extraction of impulsive attenuation signals,” *Mech. Syst. Signal Process.*, vol. 23, no. 1, pp. 236–245, 2009.

[98] Y. Dong, M. Liao, X. Zhang, and F. Wang, “Faults diagnosis of rolling element bearings based on modified morphological method,” *Mech. Syst. Signal Process.*, vol. 25, no. 4, pp. 1276–1286, May 2011.

[99] I. Pitas, “Morphological signal decomposition,” *Proc. 1990 IEEE Conf. Acoust. Speech, Signal Process.*, vol. 4, pp. 2169–2192, 1990.

[100] J. Chan, H. Ma, T. Saha, and C. Ekanayake, “Self-adaptive partial discharge signal de-noising based on ensemble empirical mode decomposition and automatic morphological thresholding,” *IEEE Trans. Dielectr. Electr. Insul.*, vol. 21, no. 1, pp. 294–303, Feb. 2014.

[101] N. H. Nik Ali, M. S. Abd Rahman, J. A. Hunter, P. Rapisarda, and P. L. Lewin, “Wavelet and Mathematical Morphology as the de-noising methods for PD analysis of high voltage transformer windings,” *IEEE Electr. Insul. Conf.*, pp. 214–217, 2015.

[102] J. C. Chan, H. Ma, and T. K. Saha, “Time-frequency sparsity map on automatic partial discharge sources separation for power transformer condition assessment,” *IEEE Trans. Dielectr. Electr. Insul.*, vol. 22, no. 4, pp. 2271–2283, 2015.

[103] T. Babnik, R. K. Aggarwal, and P. J. Moore, “Principal Component and Hierarchical Cluster Analyses as Applied to Transformer Partial Discharge Data With Particular Reference to Transformer Condition Monitoring,” *IEEE Trans. Power Deliv.*, vol. 23, no. 4, pp. 2008–2016, Oct. 2008.

[104] G. E. and A. D. S. N. Hettiwatte, Z. D. Wang, P. A. Crossley, P. Jarman, “An electrical PD location method applied to a continuous disc type transformer winding,” *Proc. 7th Int. Conf. Prop. Appl. Dielectr. Mater.*, pp. 471–474, 2003.

[105] L. Van Der Maaten and G. Hinton, “Visualizing Data using t-SNE,” vol. 9, pp. 2579–2605, 2008.

[106] a. Gisbrecht, B. Mokbel, and B. Hammer, “Linear basis-function t-SNE for fast nonlinear dimensionality reduction,” *Proc. Int. Jt. Conf. Neural Networks*, pp. 10–15, 2012.

[107] A. Cavallini, X. Chen, G. C. Montanari, and F. Ciani, “Diagnosis of EHV and HV transformers through an innovative partial-discharge-based technique,” *IEEE Trans. Power Deliv.*, vol. 25, no. 2, pp. 814–824, 2010.

[108] A. Cavallini, G.Montanari, A. Contin, and F. Puletti, “A New Approach to the Diagnosis of Solid Insulation Systems Based on PD Signal Inference,” *IEEE Electr. Insul. Mag.*, vol. 19, no. 2, pp. 23–30, 2003.

[109] J. C. Chan, H. Ma, and T. K. Saha, “Time-frequency sparsity map on automatic partial discharge sources separation for power transformer condition assessment,” *IEEE Trans. Dielectr. Electr. Insul.*, vol. 22, no. 4, pp. 2271–2283, 2015.

[110] A. Contin, S. Pastore, and R. Paganin, “Evaluation of Spaces for the Separation of Signals Due to Multiple PD Sources,” *Electr. Insul. Conf. (EIC), 2015 IEEE*, no. June, pp. 7–10, 2015.

[111] M. Daszykowski, B. Walczak, and D. L. Massart, “Looking for natural patterns in analytical data. 2. Tracing local density with OPTICS,” *J. Chem. Inf. Comput. Sci.*, vol. 42, no. 3, pp. 500–507, 2002.

[112] N. H. Nik Ali, M. Giannakou, R. D. Nimmo, P. Rapisarda, and P. L. Lewin, “Classification and Localisation of Multiple Partial Discharge Sources Within a High Voltage Transformer Winding,” in *IEEE Electrical Insulation Conference (EIC)*, 2016, pp. 519–522.

[113] L. Wei, L. Hua-Ming, and Q. Pei-Wen, “Sparsity enhancement for blind deconvolution of ultrasonic signals in nondestructive testing application,” *Rev. Sci. Instrum.*, vol. 79, no. 1, 2008.

[114] N. H. N. Ali, P. Rapisarda, and P. L. Lewin, “Separation of Multiple Partial Discharge Sources Within a High Voltage Transformer Winding using Time Frequency Sparsity Roughness Mapping,” in *Condition Monitoring and Diagnosis (CMD)*, 2016, pp. 230–233.

[115] J. Sander, X. Qin, Z. Lu, N. Niu, A. Kovarsky, and C. Tg, “Automatic Extraction of Clusters from Hierarchical Clustering Representations,” in *7th Pacific-Asia Conferece on Advances in Knowledge Discovery and Data Mining, Berlin*, 2003, pp. 1–12.

[116] R. Patsch, F. Berton, and D. Benzerouk, “PD-Source identification and characterization on the basis of pulse shape analysis,” in *Annual Report Conference on Electrical Insulation and Dielectric Phenomena (CEIDP)*, 2002, pp. 728–731.

[117] J. M. B. G.C. Stone, H.G. Sedding, N. Fujimoto, “Practical Implementation of

Ultrawideband Partial Discharge Detectors," *IEEE Trans. Electr. Insul.*, vol. 27, no. 1, pp. 70–81, 1992.